

Aldehyde Oxidase Drug Metabolism: Evaluation of Drug Interaction Potential and
Allometric Scaling Methods to Predict Human Pharmacokinetics

By

Rachel Denise Crouch

Dissertation

Submitted to the Faculty of the
Graduate School of Vanderbilt University
in partial fulfillment of the requirements
for the degree of

DOCTOR OF PHILOSOPHY

in

Pharmacology

December, 2016

Nashville, Tennessee

Approved:

J. Scott Daniels, Ph.D.

Joey V. Barnett, Ph.D.

Colleen M. Niswender, Ph.D.

C. David Weaver, Ph.D.

Neil Osheroff, Ph.D.

Wendell S. Akers, Pharm.D., Ph.D.

For Mom, Dad, and Robby

Colossians 3:17

ACKNOWLEDGEMENTS

The research described herein was supported by the NIGMS Vanderbilt Training Program in Pharmacological Sciences, the PhRMA Pre-Doctoral Fellowship Program in Pharmacology/Toxicology, and the NIH Division of Loan Repayment Program in Clinical Research. The commitment of these organizations to the development of young scientists in biomedical, pharmaceutical, and translational research is vital to the discovery and advancement of disease diagnosis, treatment, and prevention, and I would like to thank them for the financial provisions they have provided to me throughout my Ph.D. training.

In addition, I would like to thank the Lipscomb University College of Pharmacy/Vanderbilt University Department of Pharmacology Pharm.D./Ph.D. Degree Partnership Program for providing me the opportunity to train in an environment of exceptional scientists and a program dedicated to high-quality education. Most notably, I want to express my gratitude toward the individuals who created this program, Drs. Joey Barnett and Scott Akers, for the countless avenues of support they have provided to me. I would not be in the position to present this work today without their support and encouragement—no one, perhaps, is owed more credit for me taking the step toward this achievement than Dr. Akers.

Likewise, several prior teachers and mentors at Lipscomb have contributed to my interest in science and my ultimate decision to pursue a career in research. From my undergraduate professors and mentors Drs. Kent Clinger and Ronnie Boone, to my pharmacy school professors and mentors Drs. Michael Fowler and

Susan Mercer, I am thankful for the instruction, mentoring, and encouragement I received from these individuals. Likewise, I would not have made it through pharmacy school to reach this point without the support and encouragement of my pharmacy classmates Drs. Katie Black and Chris Stokes.

In addition to Drs. Barnett and Akers, I am grateful for the others who have graciously served on my dissertation committee. Insightful suggestions from Dr. Colleen Niswender have been an essential contribution to improving the quality and focus of my studies, as have fresh perspectives and ideas from Dr. Neil Osheroff. I am also very appreciative of Dr. Dave Weaver for stepping in to serve as my co-chair alongside Dr. Niswender. Each member of my committee has been tremendously supportive and encouraging, and it has been a pleasure to work with them and gain from their expertise. I would also like to take this time to thank Dr. Matthew Hutzler, who has generously served as an additional mentor to me and a critical contributor to completion of this work.

In addition to my committee members, I am especially thankful for the opportunity to work with my mentor, Dr. Scott Daniels, who has been more than just a research advisor, but a life coach, in support of my research, my career aims, as well as my personal well-being. I am appreciative to Dr. Daniels for granting me the freedom to take ownership of my research and for always encouraging me to explore my own ideas. At the same time, I have been fortunate for the opportunity to learn from his expertise and build a foundation for my career. Dr. Daniels has always been my advocate, and I am eternally grateful for his dedicated commitment to my

success. It has truly been a privilege to train with Dr. Daniels and likewise to have gained a lifelong mentor, colleague, and friend.

As for the DMPK lab members, past and present, I am thankful for their friendship and for all that they have graciously taught me. I am especially grateful to Dr. Tom Bridges, who I could always count on to take time to answer a question, Frank Byers for that all he taught and assisted me with and, especially, for making the lab a fun place to be, Jay Foster for always being willing to help and for keeping me entertained in the lab, and Dr. Annie Blobaum and Dr. Chuck Locuson for all their assistance and encouragement. I undoubtedly owe my gratitude to Ryan Morrison for the hours of time he generously dedicated to teaching me everything I know about LC/MS/MS, among countless other concepts and techniques relating to DMPK. His instruction was essential to me reaching this point, as was his friendship. I also thank Sichen Chang, Katrina Brewer, and several other past labmates for all they have done to aid me.

Thanks as well to those in the Lindsely Lab, especially Craig Lindsley, who aided in facilitating the completion of my research. I am also particularly thankful to Matt Mulder for the many ways in which he has assisted me, as well as being a great desk neighbor, and Jeanette Bertron for being a fun, supportive, and encouraging friend. Thanks to everyone else in Cool Springs for all their help, especially Nathan Kett for keeping the place up and running, as well as many others for creating a fun environment in which to work. There are many others who are owed my gratitude for various means of support in the Department of Pharmacology and VCND. I specifically want to thank Karen Gieg, Donna Johnson, and Kristin Riggs for all their

assistance, as well as Dr. Jeffrey Conn and his research group, many members of which have aided me in one way or another.

Of course, I must also thank my friends and family, who are too many to name, for all the moral support provided to me over the past several years. I most certainly could not have made it through this challenging time without their support and encouragement. My Mom and Dad have always supported me in whatever I chose to pursue and always believed I could achieve anything I set out to do. I could never repay them for all they have done for me, and I am forever indebted to them for all their love and support. I also want to thank my brother Matt for his love and encouragement, as well as my mother and father-in-law, Bob and Martha, who have treated me like their own daughter. I lastly am infinitely grateful for my husband and best friend, Robby, who has supported me through eight years of pharmacy school and graduate school without complaint. He makes me laugh, makes me think, makes me strong, makes me happy, and I could not make it through life without him.

Finally, for all these blessings I have received, I am eternally grateful to God, who already knows the answer before we even conceive the question.

TABLE OF CONTENTS

	Page
DEDICATION.....	ii
ACKNOWLEDGEMENTS.....	iii
LIST OF TABLES.....	xiii
LIST OF FIGURES.....	xvii
LIST OF EQUATIONS.....	xxii
LIST OF ABBREVIATIONS.....	xxiii
Chapter	
I. INTRODUCTION TO ALDEHYDE OXIDASE.....	1
Aldehyde Oxidase Structure.....	1
Aldehyde Oxidase Substrate Specificity and Reactions.....	2
Aldehyde Oxidase Catalytic Mechanism.....	3
Known Clinical Aldehyde Oxidase Substrates.....	4
Known Clinical Aldehyde Oxidase Inhibitors.....	7
Aldehyde Oxidase Expression.....	8
Single human aldehyde oxidase isoform.....	8
Species-specific aldehyde oxidase isoforms.....	9
Age-dependent aldehyde oxidase expression.....	11
Regulation of aldehyde oxidase expression.....	11
Species-Specific Aldehyde Oxidase Activity.....	12
Sex Differences in Aldehyde Oxidase Activity.....	13
Endogenous Aldehyde Oxidase Substrates and Physiological Relevance.....	15
Human Aldehyde Oxidase Single Nucleotide Polymorphisms.....	16
Identification of Aldehyde Oxidase Metabolism.....	17
Failed Clinical Aldehyde Oxidase Substrates.....	20
Challenges in Predicting Human Pharmacokinetics of Aldehyde Oxidase.....	21

II. MATERIALS AND METHODS.....	23
Materials	23
In Vitro Biotransformation and Clearance of VU0409106.....	24
Biotransformation in hepatic microsomal and recombinant human P450 incubations.....	24
Metabolite formation in hepatic S9 fractions	25
Intrinsic clearance in hepatic S9 fractions.....	25
In Vivo Metabolism and Disposition of VU0409106 in Sprague-Dawley Rats	26
Intravenous or intraperitoneal administration of VU0409106.....	27
Hepatic portal vein or mesenteric ileal vein administration of VU0409106.....	28
In Vitro Biotransformation and Clearance of Zaleplon, O ⁶ -Bezylguanine, Zoniporide, BIBX1382, and SGX523	29
Biotransformation in hepatic S9 incubations	29
Intrinsic clearance and estimated hepatic clearance from hepatic S9 incubations	29
Estimation of fraction metabolized by AO ($F_{m,AO}$) in hepatic S9.....	30
Multispecies Determination of Pharmacokinetic Parameters of Zaleplon, O ⁶ -Benzylguanine, Zoniporide, BIBX1382, and SGX523	31
Intravenous cassette administration of zaleplon, O ⁶ -benzylguanine, zoniporide, BIBX1382, and SGX523.....	31
Liquid Chromatography-Mass Spectrometry Methods	32
Quantitation from hepatic S9 incubations	32
Quantitation from plasma.....	34
Metabolite detection in hepatic microsomal, S9, and rhP450 incubations and in rat plasma.....	35
Data Analysis.....	38
In vitro clearance measurements	38
In vitro estimation of fraction metabolized by aldehyde oxidase ($F_{m,AO}$)	41
Pharmacokinetic parameters.....	43
Area under the plasma concentration-time curve (AUC).....	43
Plasma clearance (CL_p)	44
Half-life ($t_{1/2}$)	44
Mean residence time (MRT)	45
Volume of distribution and steady state (V_{ss}).....	46
Maximum plasma concentration (C_{max})	46
Multispecies allometry (MA)	46
Single-species scaling (SSS)	49
Success criteria for prediction of human clearance by MA or SSS.....	49
Statistical Analysis	51

Pharmacokinetic analysis of VU0409106 and metabolites.....	51
Calculation of intrinsic clearance from incubations with hepatic S9	52
SSS Correlation with F_m or E	52
III. EVALUATING THE DISPOSITION OF A MIXED ALDEHYDE OXIDASE/CYTOCHROME P450 SUBSTRATE IN RATS WITH ATTENUATED P450 ACTIVITY.....	55
INTRODUCTION.....	55
RESULTS	59
A Mixed AO:P450 Metabolism Phenotype of VU0409106 In Vitro.....	59
Metabolism of VU0409106 in rat and human hepatic microsomes and recombinant human P450s.....	59
LC/MS/MS characterization of VU0409106 metabolite M6.....	62
Intrinsic Clearance of VU0409106 and Relative Formation of M1 in Rat and Human S9 Fractions Implicate a Metabolic Shunting Mechanism Mediated by Aldehyde Oxidase.....	66
M1 formation in hepatic S9.....	66
Concentration-dependence of total, NADPH-dependent, and NADPH- independent hepatic S9 intrinsic clearance (CL_{int}) of VU0409106	68
ABT Pretreatment Results in Increased Exposure to Parent VU0409106 and the AO Metabolite M1 In Vivo in SD Rats	70
VU0409106	70
M1	73
M4-M6	77
Pretreatment of SD Rats with Hydralazine Mildly Increased Exposure to P450 Metabolites M4-M6.....	77
M4, but not M6, was decreased in pooled plasma samples of rats pretreated with ABT.....	79
Similar Trends in VU0409106 and Metabolite Disposition in Response to Inhibitors in a Crossover Experiment of Rats Receiving 1 mg/kg VU0409106 via Mesenteric Vein Administration	81
Mean pharmacokinetics of VU0409106 and metabolites	82
Individual pharmacokinetics of VU0409106 and metabolites.....	83
DISCUSSION.....	86

IV. ALLOMETRIC SCALING OF IN VITRO HEPATIC CLEARANCE OF DRUGS POSSESSING AND ALDEHYDE OXIDASE CLEARANCE PATHWAY IN HUMAN.....	93
INTRODUCTION	93
RESULTS	98
Intrinsic Clearance in Hepatic S9 Fractions	98
Estimation of $F_{m,AO}$ in Hepatic S9 Fractions.....	101
Zaleplon $F_{m,AO}$	102
O ⁶ -benzylguanidine $F_{m,AO}$	103
Zoniporide $F_{m,AO}$	104
BIBX1382 $F_{m,AO}$	105
SGX523 $F_{m,AO}$	107
Prediction of Human Hepatic S9 Clearance by Multi- or Single-Species Allometry	109
Multispecies allometry (MA) of CL_{int}	110
Single-species scaling (SSS) of CL_{int}	116
Multispecies allometry (MA) of CL_{HEP}	118
Single-species scaling (SSS) of CL_{HEP}	122
SSS Correlation with F_m or E	124
Sex Differences in Intrinsic Clearance.....	128
Male and female rat S9 CL_{int}	129
Male and female mouse S9 CL_{int}	130
Male and female cynomolgus S9 CL_{int}	131
Male and female rhesus S9 CL_{int}	132
Male and female guinea pig S9 CL_{int}	134
Male and female minipig S9 CL_{int}	135
Single-species scaling (SSS) of female CL_{int}	136
Multispecies allometry (MA) with female minipig CL_{int} substitution for male minipig CL_{int}	139
Multispecies Biotransformation	142
Zaleplon	143
O ⁶ -benzylguanidine.....	153
Zoniporide	163
BIBX1382	171
SGX523	188
DISCUSSION	209

V. ALLOMETRIC SCALING OF IN VIVO HEPATIC CLEARANCE OF DRUGS POSSESSING AN ALDEHYDE OXIDASE PATHWAY IN HUMAN	219
INTRODUCTION	219
RESULTS	222
Pharmacokinetic Parameters in Preclinical Species.....	222
In vitro-in vivo correlation (IVIVC)	229
Single-Species Scaling (SSS) of Plasma Clearance	232
Multispecies Simple Allometry (MA) of Plasma Clearance	235
In Vitro Allometry to Guide Species Selection for In Vivo PK Anyalsis	237
Zaleplon	238
O ⁶ -benzylguanine.....	241
Zoniporide	243
BIBX1382	247
SGX523	249
DISCUSSION	256
 VI. CONCLUSIONS AND FUTURE DIRECTIONS	 264
Drug Interaction Liability Associated with AO-Mediated Drug Clearance.....	264
Summary and conclusions.....	264
Future directions.....	265
Multispecies Allometry to Predict Human Clearance of Drugs Metabolized by Aldehyde Oxidase	267
Summary and conclusions.....	267
Future directions.....	269
Application of In Vitro Intrinsic Clearance to Allometric Scaling	270
Summary and conclusions.....	270
Future directions.....	271
Influence of $F_{m,AO}$ and E on SSS Prediction Accuracy	273
Summary and conclusions.....	273
Future directions.....	274
Interspecies evaluation of metabolism, clearance, and SSS to predict human clearance of AO substrates.....	274
Summary and conclusions.....	274
Future directions.....	278
Commentary	279

REFERENCES.....281

LIST OF TABLES

Chapter I

Table	Page
I.1. Example AO inhibitors	8
I.2. Aldehyde oxidase genes expressed in liver and other tissues of humans and experimental animals.....	10
I.3. Distinctive characteristics of cytochrome P450s versus aldehyde oxidase.....	19
I.4. Drugs that have failed in clinical trials due to unidentified/underpredicted human AO-mediated metabolism	21

Chapter II

II.1. HPLC gradients and ion transitions monitored (multiple reaction monitoring) during LC/MS/MS quantitative analysis	34
II.2. Tune settings for ion trap mass spectrometers used in LC/UV/MS/MS analysis of biotransformation.....	36
II.3. HPLC gradients for LC/UV/MS/MS analysis of biotransformation.....	37
II.4. Species-specific hepatic scaling factors	40
II.5. Species-specific hepatic blood flow	41
II.6. Standard body weights used for multispecies allometry and single-species scaling of in vitro S9 intrinsic clearance	48

Chapter III

III.1. LC/MS detection of metabolites in vivo (SD rat) or in vitro in SD rat and human microsomes or recombinant human P450 enzymes	61
III.2. Exposure of M1 Formed from human or rat hepatic S9 incubations of VU0409106 in the presence or absence of NADPH.....	67
III.3. Total, NADPH-dependent, and NADPH-independent rat and human hepatic S9 intrinsic clearance of VU0409106	68
III.4. Pharmacokinetic parameters of VU0409106 following the IV (1 mg/kg) or IP (3 mg/kg) administration of VU0409106 to control rats or rats pretreated with ABT.....	72
III.5. Pharmacokinetic parameters of metabolites M1, M2, and M4-M6 following an IP administration of VU0409106 (3 mg/kg) to control	

	rats or rats pretreated with ABT	74
III.6	Systemic exposure of metabolites M1 and M2 following an IP administration of VU0409106 (10 mg/kg) to control rats or rats pretreated with ABT, allopurinol, or allopurinol + ABT.....	76
III.7.	Pharmacokinetic parameters of VU0409106 and metabolites M1, M2, and M4-M6 following an IP administration of VU0409106 (10 mg/kg) to control rats or rats pretreated with ABT or hydralazine.	79
III.8.	Exposure of VU0409106 in SD rats receiving VU0409106 via the hepatic portal vein or the mesenteric ileal vein	82
III.9.	Mean pharmacokinetic parameters of VU0409106 and metabolites M1, M2, and M4-M6 following an administration of VU0409106 (1 mg/kg) via the mesenteric vein to control rats or rats pretreated with ABT or hydralazine	83
III.10.	Individual pharmacokinetic parameters of VU0409106 and metabolites M1, M2, and M4-M6 following an administration of VU0409106 (1 mg/kg) via the mesenteric vein to rats A, B, and C when pretreated with either vehicle (control), ABT, or hydralazine.....	85

Chapter IV

IV.1.	Multispecies intrinsic clearance of zaleplon, O ⁶ -benzylguanine, zoniporide, BIBX1382, and SGX523 in incubations with hepatic S9.....	99
IV.2.	Multispecies hepatic clearance of zaleplon, O ⁶ -benzylguanine, zoniporide, BIBX1382, and SGX523 in incubations with hepatic S9.....	100
IV.3.	Substrate rank order of intrinsic clearance obtained from incubations with multiple species' hepatic S9	101
IV.4	Multispecies estimated fraction metabolized by AO ($F_{m,AO}$) of zaleplon	102
IV.5.	Multispecies estimated fraction metabolized by AO ($F_{m,AO}$) of O ⁶ -benzylguanine	103
IV.6.	Multispecies estimated fraction metabolized by AO ($F_{m,AO}$) of Zoniporide.....	104
IV.7.	Multispecies estimated fraction metabolized by AO ($F_{m,AO}$) of BIBX1382.....	105
IV.8.	Multispecies estimated fraction metabolized by AO ($F_{m,AO}$) of SGX523.....	107
IV.9.	AAFE, AFE, and percentage of compounds predicted within 2 or 3 fold-error of observed human S9 CL_{int} , as predicted by multispecies allometry.....	112
IV.10.	Multispecies allometry of zaleplon CL_{int}	114
IV.11.	Multispecies allometry of O ⁶ -benzylguanine CL_{int}	114
IV.12.	Multispecies allometry of zoniporide CL_{int}	115

IV.13. Multispecies allometry of BIBX1382 CL_{int}	115
IV.14. Multispecies allometry of SGX523 CL_{int}	116
IV.15. AAFE, AFE, and percentage of compounds predicted within 2 or 3 fold-error of observed human S9 CL_{int} , as predicted by SSS.....	118
IV.16. SSS of zaleplon, O ⁶ -benzylguanine, zonisporide, BIBX1382, and SGX523 CL_{int}	118
IV.17. AAFE, AFE, and percentage of compounds predicted within 2 or 3 fold-error of observed human S9 CL_{HEP} , as predicted by multispecies allometry.....	121
IV.18. Multispecies allometry of zaleplon, O ⁶ -benzylguanine, zonisporide, BIBX1382, and SGX523 CL_{HEP}	122
IV.19. AAFE, AFE, and percentage of compounds predicted within 2 or 3 fold-error of observed human S9 CL_{HEP} , as predicted by SSS.....	123
IV.20. SSS of zaleplon, O ⁶ -benzylguanine, zonisporide, BIBX1382, and SGX523 CL_{HEP}	124
IV.21. Female SSS of zaleplon, O ⁶ -benzylguanine, zonisporide, BIBX1382, and SGX523 CL_{int}	137
IV.22. Multispecies allometry of zaleplon, O ⁶ -benzylguanine, zonisporide, BIBX1382, and SGX523 CL_{int} using female minipig.....	140
IV.23. Peak area ratio of M1 (presence of NADPH/ absence of NADPH) detected in multispecies S9	160
IV.24. Summary of AAFE, AFE, and percentage of compounds predicted within 2 or 3 fold-error of observed human S9 CL_{int} , as predicted by MA or SSS.....	210
IV.25. Summary of AAFE, AFE, and percentage of compounds predicted within 2 or 3 fold-error of observed human S9 CL_{HEP} , as predicted by MA or SSS.....	210

Chapter V

V.1. Pharmacokinetic parameters of zaleplon, O ⁶ -benzylguanine, zonisporide, and SGX523 obtained from a cassette IV bolus dose to mouse, rat, guinea pig and minipig.....	228
V.2. In vitro-in vivo correlation (IVIVC) of S9 hepatic clearance and plasma clearance in preclinical species for zaleplon, O ⁶ -benzylguanine, zonisporide, BIBX1382, and SGX523	231
V.3. SSS of zaleplon, O ⁶ -benzylguanine, zonisporide, and BIBX1382 plasma clearance (CL_p)	233
V.4. SSS of SGX523 plasma clearance (CL_p).....	234
V.5. Multispecies allometry of zaleplon, O ⁶ -benzylguanine, zonisporide, and	

	BIBX1382 plasma clearance (CL _p).....	236
V.6.	Multispecies allometry of SGX523 plasma clearance (CL _p).....	237
V.7.	In vitro-to-in vivo comparison of zaleplon human CL (CL _{int} or CL _p) predictions by multispecies allometry.....	240
V.8.	In vitro-to-in vivo comparison of O ⁶ -benzylguanine human CL (CL _{int} or CL _p) predictions by multispecies allometry	243
V.9.	In vitro-to-in vivo comparison of zonisporide human CL (CL _{int} or CL _p) predictions by multispecies allometry.....	246
V.10.	In vitro-to-in vivo comparison of BIBX1382 human CL (CL _{int} or CL _p) predictions by multispecies allometry.....	249
V.11.	In vitro-to-in vivo comparison of SGX523 human CL (CL _{int} or CL _p) predictions by multispecies allometry.....	253
V.12.	<i>In vitro-to-in vivo</i> comparison of allometric exponents (<i>b</i>) obtained from multispecies allometry.....	255

LIST OF FIGURES

Chapter I

Figure	Page
I.1. An illustration of the aldehyde oxidase homodimer	2
I.2. Example reactions catalyzed by aldehyde oxidase	3
I.3. Proposed mechanism and catalytic cycle of aldehyde oxidase-mediated oxidation of an aromatic azaheterocycle	4
I.4. Example marketed drugs or intermediate metabolites of marketed drugs metabolized by aldehyde oxidase	6

Chapter II

II.1. Representative plot of the natural log of the percent remaining substrate versus incubation time for the determination of in vitro half-life	39
II.2. Representative plot of CL vs Body Weight to obtain the allometric coefficient and exponent used to calculate a predicted human CL with the simple allometric equation	48

Chapter III

III.1. Metabolism of VU0409106 in vitro and in vivo in Sprague-Dawley rats and in vitro in human.....	59
III.2. The AO inhibitor hydralazine inhibited the formation of M1 in incubations of VU0409106 with rat hepatic microsomes	62
III.3. LC/MS/MS and proposed structure of metabolite, M6, detected in SD rat and human hepatic microsomes and recombinant human P450 incubations.....	63
III.4. LC/MS ³ and proposed structure of metabolite, M6, detected in SD rat and human hepatic microsomes and recombinant human P450 incubations.....	64
III.5. Description of a full scan LC/MS deuterium exchange experiment	65
III.6. Full scan LC/MS deuterium exchange experiment of M6.....	66
III.7. Formation of M1 in incubations of VU0409106 with human hepatic S9 or SD rat hepatic S9 in the presence or absence of NADPH.....	67
III.8. Mean plasma concentration-time profiles of VU0409106, M1, M4-M6, and M2 following administration of VU0409106 to control or ABT pretreated SD rats	71

III.9.	Mean plasma concentration-time profiles of M2 or M1 after IP administration of VU0409106 (10 mg/kg) to rats with or without an inhibitor	76
III.10.	Mean plasma concentration-time profiles of VU0409106 , M1, M4-M6, and M2 following administration of VU0409106 to control, ABT pretreated, or hydralazine pretreated SD rats.....	78
III.11.	Relative abundance of M4 and M6 detected in extracts of pooled plasma from rats receiving 10 mg/kg of VU0409106 alone or pretreated with 50 mg/kg ABT or 50 mg/kg hydralazine	80
III.12.	Individual plasma concentration-time profiles of VU0409106 following administration of VU0409106 via the hepatic portal vein or the mesenteric ileal vein to SD rats.....	81
III.13.	Individual plasma concentration-time profiles of VU0409106, M1, M4-M6, and M2 following MV administration of VU0409106 to control ABT, or hydralazine pretreated SD rats.....	84
III.14.	Increase in M1 formation observed in rats following ABT inhibition of P450.....	86

Chapter IV

IV.1.	Structures of AO substrates subjected to in vitro allometric scaling	97
IV.2.	Plots of observed human S9 CL _{int} vs that predicted from multispecies allometry.....	111
IV.3.	Plots of observed human S9 CL _{int} vs that predicted from SSS.....	117
IV.4.	Plots of observed human S9 CL _{HEP} vs that predicted from multispecies allometry.....	120
IV.5.	Plots of observed human S9 CL _{HEP} vs that predicted from SSS.....	123
IV.6.	Correlation of CL _{int} SSS fold-error and animal/human ratios of F _{m, AO} or E.....	126
IV.7.	Correlation of CL _{HEP} SSS fold-error and animal/human ratios of F _{m, AO} or E.....	127
IV.8.	Correlation of SSS fold-error and animal/human ratios of F _{m, UGT} or CL _p as a percentage of liver blood flow for in vivo data of UGT substrates	128
IV.9.	Intrinsic clearance in male and female rat hepatic S9	130
IV.10.	Intrinsic clearance in male and female mouse hepatic S9	131
IV.11.	Intrinsic clearance in male and female cynomolgus monkey hepatic S9.....	132
IV.12.	Intrinsic clearance in male and female rhesus monkey hepatic S9.....	133
IV.13.	Intrinsic clearance in male and female guinea pig hepatic S9.....	134
IV.14.	Intrinsic clearance in male and female minipig hepatic S9	135
IV.15.	Predicted human CL _{int} of zaleplon, O ⁶ -benzylguanine, zoniporide,	

BIBX1382, or SGX523 from SSS with male and female hepatic S9	138
IV.16. Predicted human CLint of zaleplon , O ⁶ -benzylguanine, zoniporide, or SGX523 from MA using all male data or male data for all species except minipig.....	141
IV.17. Proposed multi-species metabolism of zaleplon in hepatic S9	145
IV.18. Representative LC-UV chromatograms depicting principal metabolite(s) from multispecies S9 extracts incubated with zaleplon in the absence of NADPH	146
IV.19. Representative LC-UV chromatograms depicting principal metabolite(s) from multispecies S9 incubations with zaleplon in the presence of NADPH.....	147
IV.20. LC/MS/MS spectra of zaleplon	148
IV.21. LC/MS/MS spectra of zaleplon metabolite M1.....	149
IV.22. LC/MS/MS spectra of zaleplon metabolite M2.....	150
IV.23. LC/MS/MS spectra of zaleplon metabolite M3.....	151
IV.24. LC/MS/MS spectra of zaleplon metabolite M4.....	152
IV.25. Proposed multispecies metabolism of O ⁶ -benzylguanine in hepatic S9	156
IV.26. Representative LC-UV chromatograms depicting principal metabolite from multispecies S9 incubations with O ⁶ -benzylguanine in the absence of NADPH	158
IV.27. Representative LC-UV chromatograms depicting principal metabolite from multispecies S9 incubations with O ⁶ -benzylguanine in the presence of NADPH.....	157
IV.28. Extracted ion chromatograms of m/z 242 and m/z 258 revealing elution times of 11.54 min and 11.60 min, respectively, for the parent O ⁶ -benzylguanine and the AO metabolite M1.....	159
IV.29. Chromatograms representing the total ion current of fragment ions produced by m/z 258 (M1) from multispecies S9 incubations with O ⁶ -benzylguanine in the absence of NADPH.....	161
IV.30. Chromatograms representing the total ion current of fragment ions produced by m/z 258 (M1) from multispecies S9 incubations with O ⁶ -benzylguanine in the presence of NADPH.....	160
IV.31. LC/MS/MS spectra of O ⁶ -benzylguanine	161
IV.32. LC/MS/MS spectra of O ⁶ -benzylguanine metabolite M1.....	162
IV.33. Proposed multispecies metabolism of zoniporide in hepatic S9	165
IV.34. Representative LC-UV chromatograms depicting principal metabolite from multispecies S9 incubations with zoniporide in the absence of NADPH.....	166
IV.35. Representative LC-UV chromatograms depicting principal metabolite from multispecies S9 incubations with zoniporide in the	

	presence of NADPH.....	167
IV.36.	LC/MS/MS spectra of zoniporide	168
IV.37.	LC/MS/MS spectra of zoniporide metabolite M1.....	169
IV.38.	LC/MS/MS spectra of zoniporide metabolite M2.....	170
IV.39.	Proposed multispecies metabolism of BIBX1382 in hepatic S9	175
IV.40.	Representative LC-UV chromatograms depicting principal metabolite from multispecies S9 incubations with BIBX1382 in the absence of NADPH.....	176
IV.41.	Representative LC-UV chromatograms depicting principal metabolite from multispecies S9 incubations with BIBX1382 in the presence of NADPH.....	177
IV.42.	LC/MS/MS spectra of BIBX1382.....	178
IV.43.	LC/MS/MS spectra of BIBX1382 metabolite M1	179
IV.44.	LC/MS/MS spectra of BIBX1382 metabolite M2	180
IV.45.	LC/MS/MS spectra of BIBX1382 metabolite M3	181
IV.46.	LC/MS/MS spectra of BIBX1382 metabolite M4	182
IV.47.	LC/MS/MS spectra of BIBX1382 metabolite M5	183
IV.48.	LC/MS/MS spectra of BIBX1382 metabolite M6	184
IV.49.	LC/MS/MS spectra of BIBX1382 metabolite M7	185
IV.50.	LC/MS/MS spectra of BIBX1382 metabolite M.....	186
IV.51.	LC/MS/MS spectra of BIBX1382 metabolite M9	187
IV.52.	Proposed multi-species metabolism of SGX523 in hepatic S9	191
IV.53.	Representative LC-UV chromatograms depicting principal metabolite(s) from multispecies S9 incubations with SGX523 in the absence of NADPH.....	192
IV.54.	Representative LC-UV chromatograms depicting principal metabolite(s) from multispecies S9 incubations with SGX523 in the presence of NADPH.....	193
IV.55.	Representative extracted ion chromatograms (XIC, m/z 376, 392, 346, and 362) depicting principal metabolites from S9 extracts of human incubated with SGX523 in the presence of NADPH	194
IV.56.	LC/MS/MS spectra of SGX523	195
IV.57.	LC/MS/MS spectra of SGX523 metabolite M1.....	196
IV.58.	LC/MS/MS spectra of SGX523 metabolite M2.....	197
IV.59.	LC/MS/MS spectra of SGX523 metabolite M3	198
IV.60.	LC/MS/MS spectra of SGX523 metabolite M4.....	199
IV.61.	LC/MS/MS spectra of SGX523 metabolite M5.....	200
IV.62.	LC/MS/MS spectra of SGX523 metabolite M6.....	201
IV.63.	LC/MS/MS spectra of SGX523 metabolite M7	202
IV.64.	LC/MS/MS spectra of SGX523 metabolite M8.....	203

IV.65.	LC/MS/MS spectra of SGX523 metabolite M9.....	204
IV.66.	LC/MS/MS spectra of SGX523 metabolite M10	205
IV.67.	LC/MS/MS spectra of SGX523 metabolite M11	206
IV.68.	LC/MS/MS spectra of SGX523 metabolite M12	207

Chapter V

V.1.	Plasma concentration-time curves obtained from mouse plasma following an IV cassette dose of zaleplon, SGX523, and O ⁶ -benzylguanine	224
V.2.	Plasma concentration-time curves obtained from rat plasma following an IV cassette dose of zaleplon, SGX523, and O ⁶ -benzylguanine	225
V.3.	Plasma concentration-time curves obtained from guinea pig plasma following an IV cassette dose of zaleplon, SGX523, and O ⁶ -benzylguanine	226
V.4.	Plasma concentration-time curves obtained from minipig plasma following an IV cassette dose of zaleplon, SGX523, O ⁶ -benzylguanine, and zonisporide.....	227
V.5.	Evaluation of in vitro data to select a preclinical species for in vivo PK of zaleplon and subsequent SSS to predict human CL _p	239
V.6.	Evaluation of in vitro data to select a preclinical species for in vivo PK of O ⁶ -benzylguanine and subsequent SSS to predict human CL _p	242
V.7.	Evaluation of in vitro data to select a preclinical species for in vivo PK of zonisporide and subsequent SSS to predict human CL _p	245
V.8.	Evaluation of in vitro data to select a preclinical species for in vivo PK of BIBX1382 and subsequent SSS to predict human CL _p	248
V.9.	Evaluation of in vitro data to select a preclinical species for in vivo PK of SGX523 and subsequent SSS to predict human CL _p	251

LIST OF EQUATIONS

Chapter II

Equation	Page
II.1. Determination of hepatic intrinsic clearance by the in vitro half-life method	39
II.2. Determination of CL_{HEP}	40
II.3. Determination of hepatic extraction (E).....	41
II.4. Estimation of $F_{m, AO}$ in hepatic S9 by method A	42
II.5. Estimation of $F_{m, AO}$ in hepatic S9 by method B	42
II.6. Estimation of AUC by the linear trapezoidal rule.....	44
II.7. Estimation of AUC by the logarithmic trapezoidal rule	44
II.8. Estimation of CL_p by noncompartmental analysis.....	44
II.9. Estimation of the terminal half-life.....	45
II.10. Estimation of AUMC by noncompartmental analysis.....	45
II.11. Estimation of MRT by noncompartmental analysis.....	45
II.12. Estimation of V_{ss} by noncompartmental analysis	46
II.13. Simple allometric equation for the prediction of human clearance by multispecies allometry.....	48
II.14. Prediction of human clearance by single-species scaling.....	49
II.15. Determination of fold-error in the prediction of CL_{int} , CL_{HEP} , or CL_p	50
II.16. Determination of absolute average fold-error.....	51
II.17. Determination of average fold-error	51
II.18. Determination of plasma clearance as a percentage of liver blood flow.....	53

Chapter III

III.1. Relationship between Michaelis-Menten parameters, V_{max} and K_m , and intrinsic clearance.....	88
III.2. Well stirred model of hepatic clearance.....	91

LIST OF ABBREVIATIONS

AAFE	absolute average fold error
ABT	1-aminobenzotriazole
AFE	average fold error
AO	aldehyde oxidase
AUC	area under the concentration-time curve
AUMC	area under the first moment curve
°C	degrees Celcius
CL _{HEP}	in vitro hepatic clearance
CL _{int}	in vitro intrinsic clearance
C _{max}	maximum plasma concentration
CL _p	plasma clearance
DDI	drug-drug interaction
DME	drug-metabolizing enzyme
DMPK	drug metabolism and pharmacokinetics
E	hepatic extraction ratio
ESI	electrospray ionization
FAD	Flavin adenine dinucleotide
FDA	food and drug administration
F _m	fraction metabolized
F _{m, AO}	fraction metabolized by aldehyde oxidase
F _{m, UGT}	fraction metabolized by uridine diphosphate gluruonosyl transferase
g	gram
HPLC	high performance liquid chromatography
HPV	hepatic portal vein
IP	intraperitoneal
IV	intravenous
kg	kilogram
k _{is}	dissociation constant of the enzyme-inhibitor complex
K _m	Michaelis constant
LC/MS	liquid chromatography mass spectrometry
LC/MS/MS	liquid chromatography tandem mass spectrometry
MA	multispecies simple allometry
mg	milligram
MgCl ₂	magnesium chloride
mL	milliliter
mM	millimolar

μM	micromolar
MoCo	molybdenum-containing tetracyclic pteridine complex
MRT	mean residence time
MV	mesenteric ileal vein
NADPH	nicotinamide adenine dinucleotide phosphate
NCA	noncompartmental analysis
NCE	new chemical entity
ng	nanogram
nM	nanomolar
P450	cytochrome P450
pmol	picomol
Q_H	hepatic blood flow
rhP450	recombinant human P450
PK	pharmacokinetics
S9	subcellular supernatant fraction resulting from 9000 g centrifugation
SAR	structure activity relationship
SD	Sprague-Dawley
SSS	single-species scaling
$t_{1/2}$	half-life
TIC	total ion current
T_{max}	time at maximum plasma concentration
UGT	uridine diphosphate glucuronosyltransferase
UV	ultraviolet
V_{max}	maximum reaction velocity
V_{ss}	volume of distribution at steady state
XIC	extracted ion chromatogram
XO	xanthine oxidase

CHAPTER I

INTRODUCTION TO ALDEHYDE OXIDASE

Aldehyde Oxidase Structure

Aldehyde oxidase (AO) is a cytosolic enzyme and member of the molybdo-flavoenzyme family, functioning as a homodimer with two identical subunits of approximately 150 kDa. Each subunit is composed of a 20 kDa N-terminal domain that binds two iron-sulfur clusters, a 40 kDa central domain containing a flavin-adenine dinucleotide (FAD), and an 85 kDa C-terminal domain housing a molybdenum-containing tetracyclic pteridine complex (MoCo) adjacent to the substrate binding pocket, all of which are required for catalytic activity (Figure I.1) (Terao et al., 2016). Two unstructured hinge regions link domains I and II and domains II and III (Coelho et al., 2015). Crystal structures of mouse AOX3 and human AOX1 (AO isoenzymes) have been solved, revealing high overall similarity (65% sequence identity), but important differences, within the MoCo active site and tunnel leading to the substrate binding site (Coelho et al., 2012; Coelho et al., 2015). The deep substrate tunnel present in both structures is wide at the protein surface and narrows approaching the active site and contains flexible gates that influence substrate entry and product release.

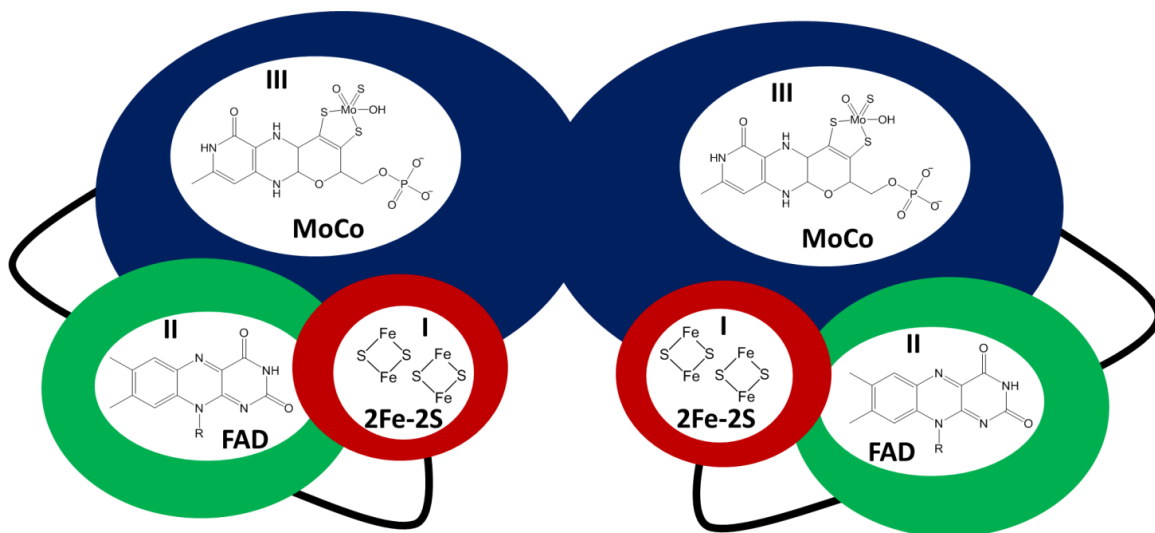


Figure I.1. An illustration of the aldehyde oxidase homodimer. Adapted from Terao et al. (Terao et al., 2016).

Aldehyde Oxidase Substrate Specificity and Reactions

As the nomenclature implies, aldehydes are among the functional groups metabolized by AO, which are oxidized to carboxylic acids (Pryde et al., 2010). The most commonly identified biotransformation catalyzed by AO, however, is oxidation of nitrogen-containing aromatic heterocycles such as pyridines and pyrimidines, which are the AO-susceptible moieties most frequently encountered in drugs or drug-like molecules (Pryde et al., 2010; Garattini and Terao, 2012). In addition, AO is capable of oxidizing iminium ions, as well as reducing amine-oxides (N-oxide) or sulfoxides (S-oxide), nitro groups and aromatic heterocycles (Pryde et al., 2010). A recent study has also demonstrated AO-mediated amide hydrolysis (Sodhi et al., 2015). Example biotransformations catalyzed by AO are depicted in Figure I.2.

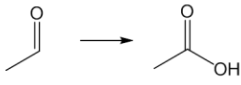
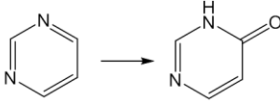
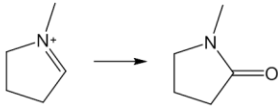
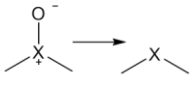
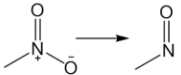
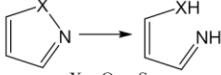
Oxidation	 <p style="text-align: center;">aldehydes</p>	 <p style="text-align: center;">aromatic azaheterocycles</p>	 <p style="text-align: center;">iminium ions</p>
Reduction	 <p style="text-align: center;">X = N or S</p> <p style="text-align: center;">N- or S-oxides</p>	 <p style="text-align: center;">nitro groups</p>	 <p style="text-align: center;">X = O or S</p> <p style="text-align: center;">heterocycles</p>

Figure I.2. Example reactions catalyzed by aldehyde oxidase.

Aldehyde Oxidase Catalytic Mechanism

The catalytic mechanism of AO used to oxidize aromatic azaheterocycles has been proposed and is depicted in Figure I.3 (Alfaro and Jones, 2008). The oxidation of an electrophilic carbon (typically located adjacent to a nitrogen) is believed to proceed via a concerted nucleophilic attack and hydride transfer to the sulfur of the MoCo, resulting in reduction of the molybdenum from Mo(VI) to Mo(IV). The reaction intermediate is hydrolyzed, releasing the oxidized product, and the reducing equivalents are shuttled from the MoCo to FAD via the iron-sulfur clusters. FADH₂ is then reoxidized by molecular oxygen, generating H₂O₂.

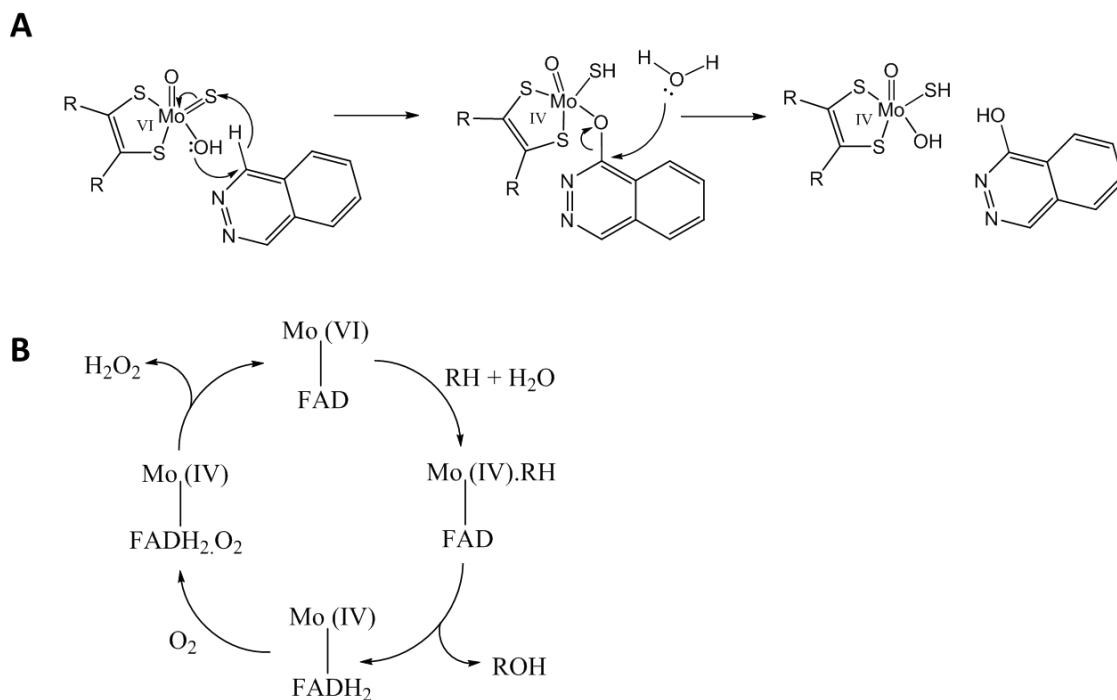


Figure I.3. Proposed mechanism (A) and catalytic cycle (B) of aldehyde oxidase-mediated oxidation of an aromatic azaheterocycle.

Known Clinical Aldehyde Oxidase Substrates

The number of drugs currently on the market known to be metabolized by AO is relatively few (Pryde et al., 2010), but the list is comprised of drugs with a variety of therapeutic targets. Both oxidative and reductive mechanisms are represented among these drugs, with most undergoing oxidation of an aromatic azaheterocycle (Pryde et al., 2010). The nonbenzodiazepine sedative hypnotic zaleplon, for example, is extensively cleared via AO-mediated oxidation of the pyrimidine ring (Lake et al., 2002a), while the second generation antipsychotic ziprasidone is metabolized by AO via reduction of the thiazole ring (Beedham et al.,

2003). In some cases, AO catalyzes secondary metabolism of an intermediate P450 metabolite, where an aldehyde (e.g., citalopram) or iminium ion (e.g., nicotine) has been generated, as well as intermediates produced by other drug metabolizing enzymes (Pryde et al., 2010). Famciclovir, for example, is a prodrug requiring activation by AO to penciclovir, proceeding through an ester hydrolysis intermediate, 6-deoxy-penciclovir (Clarke et al., 1995; Rashidi et al., 1997). Figure I.4 displays examples of marketed drugs with a primary or secondary AO-mediated metabolite (Pryde et al., 2010). A 2010 report by Pryde et al. determined that approximately 10% of drugs on the market contained structural components expected to be potentially susceptible to AO metabolism, while an examination of drugs in research and development revealed that 45% had the potential to be AO substrates based on their structural components (i.e., nitrogen-containing aromatic rings) (Pryde et al., 2010). The rise in AO-susceptible compounds encountered in drug discovery programs has been attributed to aromatic azaheterocycle inclusion in chemical scaffolds to achieve requisite target interactions (e.g. kinases) and/or as a medicinal chemistry strategy to mitigate P450 metabolism (Pryde et al., 2010). The most recent AO substrate to reach the market is the phosphoinositide-3-kinase inhibitor, idelalisib (Figure I.4), which is cleared by both AO and P450 pathways and was approved for the treatment of chronic lymphocytic leukemia (Ramanathan et al., 2016).

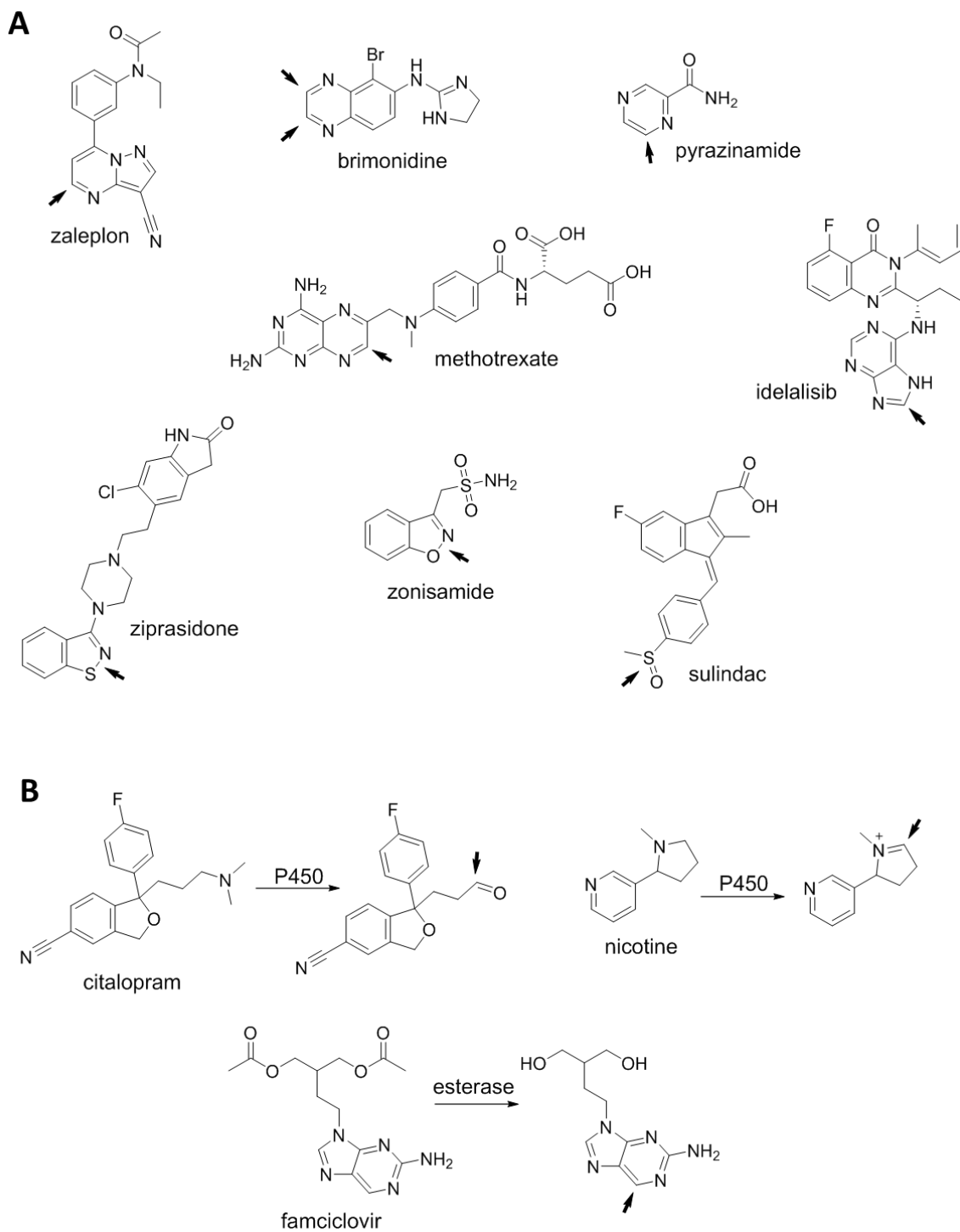


Figure I.4. Example marketed drugs (A) or intermediate metabolites of marketed drugs (B) metabolized by aldehyde oxidase. Arrows indicate the site of oxidation or reduction (ziprasidone, zonisamide, and sulindac).

Known Clinical Aldehyde Oxidase Inhibitors

A report by Obach, et al. identified 36 drugs exhibiting greater than 80% inhibition of AO-mediated phthalazine oxidation at 50 μM in human liver cytosol (Obach et al., 2004). The majority of these were compounds that target the central nervous system (e.g. antipsychotics) or were estrogen-related drugs. Table I.1 depicts examples of commonly used AO inhibitors, which illustrate a diversity of structural features. The selective estrogen receptor modulator raloxifene is the most potent known inhibitor of human AO ($\text{IC}_{50} = 2.9 \text{ nM}$) (Obach, 2004; Obach et al., 2004). Menadione is also known to potently inhibit AO ($\text{IC}_{50} = 200 \text{ nM}$) and is commonly used to assess AO-mediated metabolism (Zientek and Youdim, 2015). Hydralazine is reported to be the most selective AO inhibitor; however, there are reports suggesting that hydralazine may also inhibit cytochrome P450 2D6 (Johnson et al., 1985; Strelevitz et al., 2012; Zientek and Youdim, 2015). Of the AO inhibitors with known modes of inhibition, most exhibit a mixed-mode type of inhibition with both uncompetitive and competitive behavior, including menadione (Barr and Jones, 2011). However, studies with raloxifene suggest that the mode of AO inhibition may be substrate-dependent, as Barr et al. demonstrated raloxifene to be a purely competitive inhibitor of DACA oxidation, while Obach et al. observed only uncompetitive inhibition with respect to phthalazine oxidation (Obach, 2004; Barr and Jones, 2011). Hydralazine has been demonstrated to act as both a competitive and time-dependent inhibitor of AO (Critchley et al., 1994; Strelevitz et al., 2012). To date, the only clinical drug interaction that has been reported between a drug metabolized by AO and a recognized AO inhibitor is a moderate interaction between

the AO substrate zaleplon and cimetidine; however, cimetidine inhibits not only AO, but also the secondary clearance pathway for zaleplon, P450 3A4 (Renwick et al., 2002).

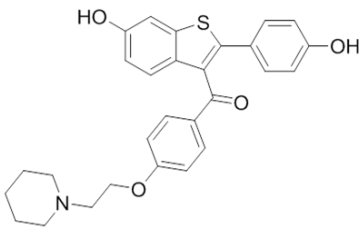
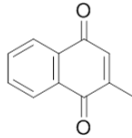
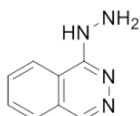
Inhibitor	Structure	IC ₅₀ (μM)
Raloxifene		0.0029
Menadione		0.2
Hydralazine		5

Table I.1. Example AO inhibitors. IC₅₀ values represent inhibitory potencies toward human liver aldehyde oxidase. Potency of raloxifene and menadione obtained from Obach et al (Obach et al., 2004). Hydralazine potency obtained from Zientek et al (Zientek and Youdim, 2015).

Aldehyde Oxidase Expression

Single human aldehyde oxidase isoform

Only a single functional AO isoform is expressed in human and is encoded by the gene *AOX1* (Garattini and Terao, 2012). Human *AOX1* expression is widely

distributed, with high levels of mRNA found in the liver, adrenal gland, prostate and adipose tissue (Terao et al., 2016). It has been detected in many other tissues as well, including highly perfused organs such as the lung and kidney (Terao et al., 2016). Although liver has been identified as the richest source of AOX1 protein (Moriwaki et al., 2001), the enzyme's broad tissue distribution presents the potential for AO-susceptible drugs to undergo extra-hepatic metabolism *in vivo*. Hutzler et al., for example, demonstrated metabolism of the AO substrate BIBX1382 in S9 fractions of human adrenal gland, kidney, and lung, possibly explaining the rapid clearance observed in patients, which exceeded hepatic blood flow (Hutzler et al., 2014a).

Species-specific aldehyde oxidase isoforms

AO expression is highly variable across species, with humans and most primates expressing only a single AO enzyme (AOX1), while others express as many as 4 isoforms (AOX1, AOX2, AOX3, and AOX4) (Garattini and Terao, 2012; Terao et al., 2016). Table I.2 reveals the variability in expression of AO isoforms in species commonly used for drug metabolism and pharmacokinetics (DMPK) and toxicology studies (Garattini and Terao, 2012; Terao et al., 2016). Importantly, rat and mouse express two liver isoforms (AOX1 and AOX3), while dog expresses no functional liver isoform at all. Furthermore, AOX3 is the predominant isoform expressed in mouse liver, bearing only 65% sequence identity with human AOX1 (Coelho et al., 2015)(in contrast to 85% homology between human and mouse AOX1). Tissue distribution of AO isoforms is also species-specific (Terao et al., 2016). AOX1 and AOX3 mRNA, for example, has been detected in many tissues in humans and/or

mice (Terao et al., 2016). The mouse AOX2 isoform, however, is specifically expressed in the nasal mucosa (Terao et al., 2000). Furthermore, the tissues expressing the highest levels of AOX1 mRNA in mice do not overlap with those in human except for the liver, and mouse AOX1 and AOX3 expression is not as widely distributed as human AOX1 (Terao et al., 2016). Challenges in predicting human clearance of drugs metabolized by AO have been attributed to these species differences in AO expression, in addition to other factors, discussed later.

Species	Liver Isoenzymes	Other Isoenzymes	Pseudogenes
Human	AOX1	---	<i>AOX2, AOX3</i>
Chimpanzee	AOX1	---	<i>AOX2, AOX3</i>
Rhesus monkey	AOX1	AOX2, AOX4	<i>AOX3</i>
Guinea pig	AOX1	AOX2, AOX4	---
Cat	---	AOX2	<i>AOX1, AOX3, AOX4</i>
Dog	---	AOX2, AOX4	<i>AOX1, AOX3</i>
Pig	AOX1	AOX2, AOX4	<i>AOX3</i>
Rabbit	AOX1, AOX3	AOX2, AOX4	---
Mouse	AOX1, AOX3	AOX2, AOX4	---
Rat	AOX1, AOX3	AOX2, AOX4	---

Table I.2. Aldehyde oxidase isoenzymes expressed in liver and other tissues of humans and experimental animals. Inactive pseudogenes are also listed. Adapted from Garattini and Terao (Garattini and Terao, 2012).

Age-dependent aldehyde oxidase expression

From a developmental perspective, AOX1 activity and protein levels have been found to be low in liver cytosol of human infants under 4 months of age, reaching adult levels by age 2 (Tayama et al., 2012). Likewise, AOX1 protein and activity has been demonstrated to be low in rats until 4 weeks of age (Tayama et al., 2007) and in mice until adulthood, while AOX3 plateaus in mice by 5 days (Terao et al., 2016).

Regulation of aldehyde oxidase expression

Studies indicate that mouse (Hu et al., 2006), rat (Maeda et al., 2012), and human (Shintani et al., 2015) *AOX1/Aox1* gene expression is regulated by the transcription factor Nrf2, which has been demonstrated to bind antioxidant responsive elements (ARE) located in the 5'-upstream region of the rat *AOX1* gene, resulting in activation of gene expression (Maeda et al., 2012). Nrf2 is also associated with regulating expression of other drug-metabolizing enzymes as well as drug transporters (Huang et al., 2015). In addition, studies in rabbits (Johnson et al., 1984), rats (Ohkubo et al., 1983), and mice (Rivera et al., 2005) suggest AO is an inducible enzyme. Induction of mouse AOX1 and AOX3 in the presence of dioxin, along with an absence of induction in cells lacking the aryl hydrocarbon receptor (AHR) or aryl hydrocarbon receptor nuclear translocator (ARNT) proteins, indicate that AO induction proceeds through the AHR pathway (Rivera et al., 2005). However, another AHR ligand, 3-methylcholanthrene, has been shown to have no inductive effect on mouse AO, indicating the possibility that other elements may influence the AO inductive mechanism (Sugihara et al., 2001). Upregulation of

human *AOX1* has also been observed in a human bronchial epithelial cell line (16HBE cells) treated with the corticosteroid dexamethasone, which was found to be associated with increased airway epithelial barrier integrity (Shintani et al., 2015).

Species-Specific Aldehyde Oxidase Activity

As might be expected due to variation in the number of AO isoforms expressed across species, differences in hepatic AO activity have been observed, with human and monkey generally exhibiting higher activity than rats, and no activity in dog (Pryde et al., 2010). However, with the exception of dog, the relative activity between species is substrate-dependent and does not exclusively abide by this trend. For example, while rat underpredicted the oral bioavailability of AO substrates BIBX1382 (Dittrich et al., 2002) and FK3453 (Akabane et al., 2011), metabolism of VU0409106 (Morrison et al., 2012) and zoniporide (Dalvie et al., 2010) in Sprague Dawley (SD) rat were comparable to or greater than human. Monkey has demonstrated similar AO-mediated metabolism to human for several substrates (Kawashima et al., 1999; Itoh et al., 2006; Diamond et al., 2010a; Morrison et al., 2012; Hutzler et al., 2014a), which is not surprising considering monkeys, like humans, express only the *AOX1* isoform (in the liver) (Garattini and Terao, 2012), which bears 96% sequence identity to human *AOX1* (Hoshino et al., 2007). However, cynomolgus monkey failed to predict human clearance of the p38 kinase inhibitor RO1 (Zhang et al., 2011), and rhesus monkey cytosol exhibited 20-

fold higher intrinsic clearance of pthalazine versus human cytosol (Choughule et al., 2013a), again reiterating the substrate dependency of AO metabolism across species. Analysis of human AOX1 and mouse AOX3 crystal structures revealed differences in the MoCo active site and substrate channel, helping to explain differences in AO activity observed between species (Coelho et al., 2015). Likewise, homology modeling of the four mouse AO isoforms also indicated differences in the substrate-binding region (Terao et al., 2016). Accordingly, of the select substrates evaluated in a report by Vila et al, most exhibited a higher intrinsic clearance by mouse AOX1 relative to AOX3 (Vila et al., 2004).

Sex Differences in Aldehyde Oxidase Activity

Differences in AO activity have been reported in male and female nonclinical species, albeit in a substrate and species-specific manner (Beedham, 1985; Klecker et al., 2006; Akabane et al., 2011; Dalvie et al., 2013). For example, AO-mediated metabolism of zoniporide measured in hepatic S9 fractions revealed higher activity in males for some species (e.g., SD rat), while female activity was higher in other species (e.g., Gottingen minipig) (Dalvie et al., 2013). Differences in zoniporide metabolism were even noted across different strains of rat, with females exhibiting elevated AO activity versus males in Wistar and Fischer rat strains in contrast to SD rat (Dalvie et al., 2013). In addition to the species-dependent differences in AO activity between the sexes, substrate-dependent differences have also been noted. For example, while a 6-fold increase in the AO-mediated intrinsic clearance (CL_{int}) of

zoniporide (Dalvie et al., 2013) was observed in liver S9 of male CD-1 mice relative to female, a 50-fold difference was observed in the AO-mediated metabolism of zebularine (Klecker et al., 2006) between male and female CD-1 mouse liver cytosol. Alternatively, in SD rat liver fractions, male exhibited a 2-fold higher intrinsic clearance of zoniporide versus female (Dalvie et al., 2013), while no difference was observed for zebularine (Klecker et al., 2006). Furthermore, intrinsic clearance of FK3453 was found to be 11-fold greater in female SD rats over males (Akabane et al., 2011). Human, however, has been consistently reported to exhibit no differences in AO activity between males and females (Al-Salmy, 2001; Klecker et al., 2006; Dalvie et al., 2013). Studies in mice demonstrated that growth hormone and testosterone increased hepatic AO activity, while it was decreased by estradiol (Yoshihara and Tatsumi, 1997). Likewise, testosterone increased AOX1 and AOX3 mRNA and protein in mouse liver (Kurosaki et al., 1999) (Terao et al., 2000). Conversely, testosterone was shown to decrease expression of AOX4 in the Harderian gland of mice (Terao et al., 2009). Interestingly, despite no differences observed between male and female AOX1 expression or activity in human liver, estradiol, ethinyl estradiol, and estrogen-related drugs raloxifene and tamoxifen were found to inhibit human AO *in vitro* (Obach et al., 2004). Estradiol, however, was reported to inhibit AO predominantly through an uncompetitive mode of inhibition, and although it exhibited some degree of competitive inhibition, plasma concentrations in women are predicted to be well-below the estimated K_{is} (dissociation constant for the enzyme-inhibitor complex) value, precluding the likelihood of a significant inhibitory effect *in vivo* (Barr and Jones, 2011).

Endogenous Aldehyde Oxidase Substrates and Physiological Relevance

While several endogenous compounds have been identified as AO substrates, including but not limited to retinaldehyde, indol, pyridoxal, and nicotinamide, the physiological role of AO (aside from xenobiotic metabolism) remains poorly understood (Garattini et al., 2008; Sanoh et al., 2015; Terao et al., 2016). The differences in AO expression across species further complicate the elucidation of the enzyme's role in human physiology. For example, it is possible that AOX4 and AOX2 have species specific functions not carried out by AOX1 in humans, as AOX4 is predominantly expressed in the Harderian gland (absent in humans) in the eye, and AOX2 is exclusively expressed in the nasal cavity, possibly serving a role in olfaction for mammals expressing this isoform (Terao et al., 2016). Many potential physiological contributions of AOX1 have been proposed, including, but not limited to, maintenance of airway epithelial barrier integrity, adipogenesis, myocyte differentiation, and nitric oxide production under hypoxic conditions (Terao et al., 2016), as well as metabolism of an endogenous DNA adduct following excision and repair (Otteneder et al., 2006). However, studies are limited, and extrapolation of data available on endogenous AO substrates across species and even interpretation of physiological relevance within a single species is difficult due to a lack of data on relative specificity of identified endogenous substrates for the different inter- and intra-species AO isoforms.

The most data available regarding an endogenous role for AO surrounds vitamin A metabolism. All-trans retinoic acid (ATRA) is the active form of vitamin A,

which is involved in development of many tissues and organs in vertebrate embryos, as well as vision and growth/differentiation of skin epithelial and hematopoietic cells in adult organisms (Terao et al., 2016). All-trans retinaldehyde (RAL) has been identified as a substrate of rabbit liver AOX (Tomita et al., 1993; Huang et al., 1999) as well as all four mouse AOX isoforms (Huang et al., 1999; Kurosaki et al., 2004; Vila et al., 2004; Terao et al., 2009; Terao et al., 2016), with the enzymes demonstrating conversion of RAL to ATRA. Furthermore, *Aox4* knockout mice exhibited decreased levels of ATRA in skin and Harderian gland and downregulation of retinoid-dependent genes, as well as perturbations in lipid homeostasis and thickening of the epidermis (Terao et al., 2009). However, kinetic studies revealed that mouse liver AOX1 and AOX3 are unlikely to contribute substantially to the formation of ATRA due to high levels of aldehyde dehydrogenases exhibiting much higher affinity and activity towards RAL relative to AOX1 and AOX3 (Garattini et al., 2008; Terao et al., 2009). As AO activity is only detectable in mice after birth, a role for AO-mediated involvement of vitamin A in developing mouse embryos is unlikely (Terao et al., 2016).

Human Aldehyde Oxidase Single Nucleotide Polymorphisms

Multiple single nucleotide polymorphisms (SNPs) have been identified for the human AOX1 gene. The clinical significance of these SNPs in drug metabolism, however, remains unclear. One study of a cohort of 180 Italian patients reported three nonsynonymous SNPs associated with poor (rs56199635) and fast

(rs55754655 and rs3731722) metabolizers, determined using enzymes purified after heterologous expression in *Escherichia coli* (Hartmann et al., 2012). Accordingly, the two fast metabolizer variants have been associated with poor response to the immunosuppressant azathioprine, which is inactivated by AO (Smith et al., 2009). However, another study evaluating human hepatocytes from 75 donors reported no statistically significant differences in the intrinsic clearance measured in hepatocytes from wild-type donors versus those with either the rs55754655 or rs3731722 variants (Hutzler et al., 2014b). In addition, patients treated with the topoisomerase II β inhibitor XK469 exhibited a wide range of clearance values, which were not explained by the SNPs identified in these patients; however, a significant decrease in clearance was associated with the rs10931910 variant when a cohort of patients with solid tumors was considered in isolation (Ramirez et al., 2014). A recent report by Foti et al. identified two AOX1 mutations resulting in the inability to synthesize a stable protein due to loss of FeSII insertion (C44W) and another resulting in a stable protein but complete loss of activity (G1269R) (Foti et al., 2016).

Identification of Aldehyde Oxidase Metabolism

Strategies to identify AO-mediated metabolism have been established that involve a variety of *in vitro* techniques. The structure of a compound offers an initial indication as to the potential for AO metabolism, particularly the presence of an aromatic nitrogen-containing heterocycle, as previously noted. In fact, an evaluation

by Pryde et al. found no correlation between AO-mediated metabolism and physiochemical properties such as cLogP and polar surface area, but rather concluded that the presence of an unsubstituted aromatic carbon adjacent to the nitrogen of an aromatic ring is more likely to indicate a potential for AO susceptibility (Pryde et al., 2010). In addition, AO exhibits several characteristics that can be utilized to distinguish AO-mediated metabolism from that catalyzed by other enzymes, particularly P450-mediated metabolism (Table I.3). First of all, AO is a cytosolic enzyme, whereas P450s are localized to the endoplasmic reticulum. Consequently, metabolism occurring in the cytosolic subcellular (liver) fraction, but not the microsomal fraction, indicates the possibility of AO-mediated metabolism (Dalvie and Zientek, 2015). Likewise, the S9 fraction, which contains both the cytosolic and microsomal fractions, can be employed in the absence and presence of NADPH to differentiate between AO and P450-mediated metabolism, respectively, since, unlike cytochrome P450s, AO does not require the co-factor NADPH for catalytic activity (Dalvie and Zientek, 2015). Accordingly, the recognition of NADPH-independent metabolism indicates the potential involvement of AO, even when the metabolism occurs in microsomes, which at times may be contaminated with small amounts of cytosol (Diamond et al., 2010a; Dalvie and Zientek, 2015). Because the closely related molybdo-flavoenzyme xanthine oxidase (XO) is also localized to the cytosol and can catalyze NADPH-independent oxidation of aromatic azaheterocycles, the use of AO and/or XO-specific inhibitors are required to confirm AO metabolism (Dalvie and Zientek, 2015). As previously discussed, common AO inhibitors include menadione, raloxifene, and hydralazine, the latter of which is

believed to be the most AO-specific (Obach et al., 2004; Strelevitz et al., 2012; Dalvie and Zientek, 2015). Allopurinol is frequently used to identify XO-mediated metabolism and is clinically marketed as an XO inhibitor (Kitamura et al., 2006). Hepatocytes are commonly employed in drug metabolism assessments, as they contain the full complement of hepatic drug-metabolizing enzymes and co-factors. Hepatocytes, therefore, may also be employed to identify the involvement of AO via the utilization of AO-specific inhibitors (Dalvie and Zientek, 2015). Finally, the catalytic mechanism of molybdenum hydroxylases can also be exploited to isolate AO/XO metabolism. Because P450s utilize molecular oxygen as their source for oxidative metabolism (Guengerich, 2001), in contrast to AO/XO which derive their oxygen from water (Alfaro and Jones, 2008), substrate incubation with hepatocytes or S9/cytosol in the presence of ^{18}O -labeled water will result in ^{18}O -incorporation into the metabolite if AO (or XO) is involved (Diamond et al., 2010a; Hutzler et al., 2012; Morrison et al., 2012).

	Cytochrome P450s	Aldehyde Oxidase
Subcellular Localization	Endoplasmic reticulum (microsomal fraction)	Cytosol (S9 and cytosolic fractions)
Substrates	Diverse Range	Aldehydes; Aromatic Azaheterocycles
NADPH-dependent	Yes	No
Source of Oxygen	O_2	H_2O

Table I.3. Distinctive characteristics of cytochrome P450s versus aldehyde oxidase.

Failed Clinical Aldehyde Oxidase Substrates

Several drug candidates have failed in clinical trials in recent years due to unexpectedly rapid clearance or toxicity related to an AO-mediated metabolite that went unrecognized in preclinical development (Table I.4) (Kaye et al., 1985; Dittrich et al., 2002; Diamond et al., 2010a; Zhang et al., 2011; Lolkema et al., 2015). In these cases, inappropriate use of microsomes (lacking cytosol, thus lacking AO) for *in vitro* intrinsic clearance estimates resulted in the underprediction of human hepatic clearance, and employment of preclinical species with decreased (e.g., rat and mouse) or absent (dog) AO activity towards the candidate drug relative to humans resulted in an overestimation of human oral exposure. Carbazeran, BIBX1382, R01, and FK3453 were all terminated during clinical assessment due to poor exposure (Dittrich et al., 2002; Akabane et al., 2011). Two other clinical candidates, c-Met inhibitors SGX523 and JNJ-38877605, were recently terminated not because of unexpected rapid clearance, but due to renal toxicity associated with a poorly soluble AO metabolite (Diamond et al., 2010a). Again, preclinical species (rat and dog) employed in toxicology assessments produced lower quantities of the AO metabolite relative to human, thus preventing occurrence of the AO metabolite-associated renal toxicity in these animals (Diamond et al., 2010a; Lolkema et al., 2015).

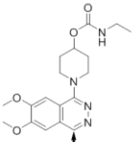
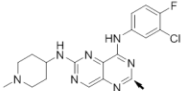
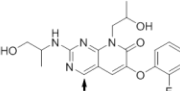
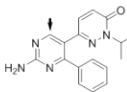
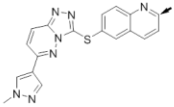
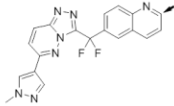
Drug	Structure	Therapeutic Target	Pre-clinical data used for human PK prediction	Clinical outcome	Reference
Carbazeran		PDE 2/3 inhibitor	Dog PK	Oral bioavailability < 5%	Kaye et al, 1984
BIBX1382		EGFR inhibitor	Liver microsomes; rat, mouse, and dog PK	Oral bioavailability 5%	Dittrich et al, 2002
RO1		p38 kinase inhibitor	Rat, dog, monkey PK	< 1 hour half-life	Zhang et al, 2011
FK3453		adenosine A1/2 inhibitor	Liver microsomes; rat and dog PK	Low exposure	Akabane et al, 2011
SGX523		c-MET inhibitor	Liver microsomes; rat and dog PK	Acute renal toxicity (poorly soluble metabolite)	Diamond et al, 2010
JNJ-38877605		c-MET inhibitor	Rat and dog PK	Acute renal toxicity (poorly soluble metabolite)	Lolkema et al, 2015

Table I.4. Drugs that have failed in clinical trials due to unidentified/underpredicted human AO-mediated metabolism. Arrows indicate the site of AO oxidation. Adapted from Hutzler et al. (Hutzler et al., 2013).

Challenges in Predicting Human Pharmacokinetics of Aldehyde Oxidase

Substrates

It is clear from the recent failures in clinical trials that traditional methods for predicting human PK are often unsuitable for AO substrates. In addition to the species differences in AO activity and expression, broad tissue distribution (i.e.,

potential for extra-hepatic metabolism), and AOX1 single nucleotide polymorphisms, several other factors may contribute to the difficulty in predicting the human disposition of drugs metabolized by AO. Several reports, for example, have found that scaled *in vitro* estimates of intrinsic clearance for AO substrates using human hepatic S9/cytosol or fresh/cryopreserved hepatocytes under-predict the clearance observed *in vivo* (Zientek et al., 2010; Akabane et al., 2012; Hutzler et al., 2012). In addition, a wide range in variability has been reported for *in vitro* clearance estimates of AO substrates (Hutzler et al., 2014b). Uncertainty remains as to which factor(s) are responsible for these observations. While polymorphisms may contribute, it has also been proposed that the processing of liver tissue for preparation of hepatocytes and liver fractions may destabilize the protein (e.g., dimer dissociation) or a deficiency of the MoCo may play a role (Fu et al., 2013). Furthermore, two laboratories have reported a 50-fold difference in levels of AOX1 quantified by LC-MS from pooled human liver cytosol (21-40 pmol/mg)(Barr et al., 2013) or cytosol of individual donors (0.74-2.3 pmol/mg) (Fu et al., 2013). Finally, environmental factors and disease states may also influence AO expression and activity, but at present are poorly understood (Fu et al., 2013; Hutzler et al., 2014b; Terao et al., 2016). The recent increase in AO metabolism of compounds in drug discovery and development (Pryde et al., 2010) highlights the importance of continued attention to the study of AO function and regulation, and particularly to improved methods for predicting human PK and disposition of AO substrates.

CHAPTER II

MATERIALS AND METHODS

Materials

VU0409106 was prepared and characterized by the Department of Medicinal Chemistry within the Vanderbilt Center for Neuroscience Drug Discovery. Potassium phosphate, ammonium formate, formic acid, magnesium chloride, dimethyl sulfoxide, 1-aminobenzotriazole (ABT), hydralazine hydrochloride, allopurinol, carbamazepine, O⁶-benzylguanine, and zaleplon were purchased from Sigma-Aldrich (St. Louis, MO). Nicotinamide adenine dinucleotide phosphate (NADPH) tetrasodium salt was purchased from VWR (Radnor, PA). Zoniporide dihydrochloride, BIBX1382 dihydrochloride, and SGX523 were purchased from Tocris Bioscience (R&D Systems, Minneapolis, MN). Pooled human (150-donor, mixed gender) or male Sprague-Dawley (SD) rat hepatic microsomes and S9 were obtained from BD Biosciences (San Diego, CA). Pooled male CD-1 mouse, cynomolgus monkey, and SD rat hepatic S9 were obtained from Corning Inc. (Tewksbury, MA). Pooled male rhesus monkey and Hartley guinea pig hepatic S9 were purchased from XenoTech (Lenexa, KS), and pooled male Gottingen minipig hepatic S9 was purchased from BioreclamationIVT (Baltimore, MD). Pooled female SD rat, Gottingen minipig, Hartley guinea pig, and cynomolgus monkey hepatic S9 were purchased from BioreclamationIVT, pooled female rhesus monkey hepatic S9 was purchased from XenoTech, and pooled female CD-1 mouse hepatic S9 was

purchased from Corning Inc. Male SD rat, CD-1 mouse, Hartley guinea pig, and Gottingen minipig plasma was purchased from BioreclamationIVT. Bacterial membranes (*Escherichia coli*) containing human cytochrome P450 enzymes (1A2, 2C9, 2C19, 2D6, and 3A4) co-expressed with human NADPH-cytochrome P450 reductase were obtained from Cypex Ltd (Dundee DD2 1NH, United Kingdom). All solvents used for bioanalysis were purchased from Sigma-Aldrich or Fisher Scientific (Waltham, MA) and were of high-performance liquid chromatography (HPLC) grade.

***In Vitro* Biotransformation and Clearance of VU0409106**

Biotransformation in hepatic microsomal and recombinant human P450 incubations

The *in vitro* metabolism of VU0409106 was investigated in rat and human hepatic microsomal fractions and recombinant human P450 enzymes (rhP450; 1A2, 2C9, 2C19, 2D6, and 3A4). A potassium phosphate-buffered reaction (100 mM, pH 7.4) of VU0409106 (10 μ M), hepatic microsomes (1 mg/mL) or rhP450 (0.2 nmol/mL), MgCl₂ (3 mM) and NADPH (2 mM) was incubated at 37°C in borosilicate glass test tubes under ambient oxygenation for 60 minutes with or without pre-incubation with the AO inhibitor hydralazine (25 μ M). The total incubation volume was 0.5 mL. Reactions were initiated by the addition of VU0409106, terminated with the addition of 2 volumes of acetonitrile, and subsequently centrifuged at 3500 rcf for 10 min. The resulting supernatant was dried under a stream of nitrogen and reconstituted in 85:15 (v/v) water:acetonitrile in preparation for LC/MS analysis.

Metabolite formation in hepatic S9 fractions

Experiments in hepatic S9 were designed to measure formation of the VU0409106 AO metabolite M1 in the presence and absence of P450 activity. Formation of M1 was measured in incubations of VU0409106 (1 μ M) with rat and human hepatic S9 fractions (2.5 mg/mL) containing potassium phosphate buffer (100 mM, pH 7.4), and MgCl₂ (3 mM), with or without NADPH (1 mM). Total incubation volume was 200 μ L. Reactions were initiated with addition of VU0409106, and at designated times (t = 0, 7, 15, 30, 45, and 60 minutes), aliquots were removed and precipitated with ice-cold acetonitrile containing an internal standard (carbamazepine, 50 nM). The mixture was centrifuged at 3500 rcf for 5 min and resulting supernatants diluted with water in preparation for LC/MS/MS analysis. Experiments were performed in triplicate.

Intrinsic clearance in hepatic S9 fractions

Intrinsic clearance (CL_{int}) of VU0409106 was determined in rat and human S9 fractions at three different concentrations of VU0409106, using NADPH and hydralazine to isolate the NADPH-dependent (P450), NADPH-independent (AO), and total (P450 + AO) hepatic S9 CL_{int} for each species. For measurement of a) total, b) NADPH-independent, and c) NADPH-dependent S9 CL_{int} , VU0409106 (0.1 μ M, 1 μ M, or 10 μ M) was incubated in rat or human S9 fractions (2.5 mg/mL) containing potassium phosphate buffer (100 mM, pH 7.4), and MgCl₂ (3 mM), a) in the presence of NADPH, b) in the absence of NADPH, or c) in the presence of NADPH after pre-incubation with the AO-specific inhibitor hydralazine (50 μ M), respectively. Total

incubation volume was 200 μ L. Reactions were initiated with addition of VU0409106, and at designated times ($t = 0, 7, 15, 20, 30,$ and 45 minutes), aliquots were removed and precipitated with ice-cold acetonitrile containing an internal standard (carbamazepine, 50 nM). The mixture was centrifuged at 3500 rcf for 5 min and resulting supernatants diluted with water in preparation for LC/MS/MS analysis of substrate depletion, by monitoring the analyte/internal standard ratio. Experiments were performed in triplicate. Calculation of CL_{int} (mL/min/kg) was estimated using the substrate depletion method (see Figure II.1 and Equation II.1).

***In Vivo* Metabolism and Disposition of VU0409106 in Sprague-Dawley Rats**

Animal studies were approved by the Vanderbilt University Medical Center Institutional Animal Care and Use Committee. To evaluate the pharmacokinetics of VU0409106, 8-12 week old male SD rats ($n = 2$) weighing between 250 and 325 g were purchased from Harlan (Indianapolis, IN) with catheters surgically implanted in the carotid artery and jugular vein for intravenous administration of 1 mg/kg VU0409106. SD rats weighing between 350 and 415 g receiving 1 mg/kg VU0409106 via the mesenteric ileal vein or the hepatic portal vein were surgically implanted with catheters in either the mesenteric ileal vein or the hepatic portal vein and the jugular vein. The cannulated animals were acclimated to their surroundings for approximately 1 week before dosing and provided food and water *ad libitum*. Similarly, in-life studies in SD rats receiving an intraperitoneal dose of 3 mg/kg ($n =$

3 for control group and n = 4 for ABT group) or 10 mg/kg (n = 2 for all groups) of VU0409106 were conducted at Frontage Laboratories (Exton, PA).

Intravenous or intraperitoneal administration of VU0409106

Inhibitors of P450 (ABT), aldehyde oxidase (hydralazine), or xanthine oxidase (allopurinol) were administered orally to male SD rats at 50 mg/kg at a dose volume of 5 mL/kg (ABT, 1% methylcellulose), 2.5 mL/kg (allopurinol, 1% methylcellulose), or 20 mL/kg (hydralazine, water). Two hours following inhibitor administration, a dose of VU0409106 (10% ethanol/70% PEG400/20% saline) was administered at 3 or 10 mg/kg intraperitoneally (IP), or intravenously (IV) at 1 mg/kg. Blood (200 µL) was collected via the carotid artery at 0.0833, 0.25, 0.5, 1, 2, 4, 6, 8, 10, 12 and 24 hours post administration of VU0409106. Samples were collected in chilled, EDTA-fortified tubes and centrifuged for 5 min (1700 rcf, 4°C), and the resulting plasma was stored at - 80°C until LC/MS/MS analysis. The resulting plasma samples were protein precipitated with ice-cold acetonitrile containing internal standard (carbamazepine, 50 nM), centrifuged (3500 rcf for 5 min) and the resulting supernatants diluted with water in preparation for LC/MS/MS analysis. For individual analysis of M4 and M6, plasma aliquots (samples collected at 1, 2, 4, and 6 hours) from rats receiving 10 mg/kg VU0409106 were pooled and precipitated with acetonitrile, then centrifuged at 3500 rcf for 10 min. Supernatants were dried under a stream of nitrogen, and resulting residues reconstituted in 85:15 (v/v) water:acetonitrile in preparation for LC/MS analysis.

Hepatic portal vein or mesenteric ileal vein administration of VU0409106

Studies were also conducted with VU0409106 dosed via the mesenteric ileal vein, which drains into the hepatic portal vein. Vehicle (1% methylcellulose), ABT (50 mg/kg) or hydralazine (10 mg/kg) was administered orally at a dose volume of 5 mL/kg, 2 hours prior to administration of 1 mg/kg VU0409106 (dose volume of 5 mL/kg, 10% EtOH 70% PEG400 20% saline) via the mesenteric ileal vein. The study was conducted in a crossover fashion, with rats (n =3) receiving vehicle pre-treatment first, then crossed over to ABT pre-treatment, and finally hydralazine pretreatment, each with a one week washout period in between inhibitor groups. Deshmukh, et al previously reported ABT had no residual effects on drug disposition in male SD rats following a 7-day washout (Deshmukh et al., 2008). Blood and plasma collection was carried out as described above, with blood collected at 0, 0.033, 0.117, 0.25, 0.5, 1, 2, 4, and 8 hours after VU0409106 administration. Administration was conducted via the mesenteric ileal vein as a substitution for the hepatic portal vein in order to avoid potential problems with maintaining portal vein cannulation throughout this extended study period, as hepatic portal vein cannulation requires an invasive surgical procedure. Prior to conducting studies with inhibitors, a pilot study was conducted to ensure that dosing via the mesenteric ileal vein would produce similar pharmacokinetics to hepatic portal vein administration. For this study, VU0409106 was formulated as described above and administered to a mesenteric ileal vein cannulated rat (n =1) and to hepatic portal vein cannulated rats (n = 2), followed by blood collection at 0.033, 0.117, 0.25, 1, 2, 4, 8, and 24 hours.

***In Vitro* Biotransformation and Clearance of Zaleplon, O⁶-Benzylguanine,
Zoniporide, BIBX1382, and SGX523**

Biotransformation in hepatic S9 incubations

The *in vitro* metabolism of zaleplon, O⁶-benzylguanine, zoniporide, BIBX1382, and SGX523 was investigated in human (mixed gender), and male CD-1 mouse, Sprague-Dawley rat, Hartley guinea pig, cynomolgus monkey, rhesus monkey, and Gottingen minipig S9 fractions. A potassium phosphate-buffered reaction (100 mM, pH 7.4) of substrate (25 μ M), hepatic S9 (5 mg/mL), and MgCl₂ (3 mM), with or without NADPH (2 mM) was incubated at 37°C in borosilicate glass test tubes under ambient oxygenation for 60 minutes. The total incubation volume was 1 mL. Reactions were initiated by the addition of substrate, terminated with the addition of 2 volumes of acetonitrile, and subsequently centrifuged at 3500 rcf for 10 min. The resulting supernatant was dried under a stream of nitrogen and reconstituted in 85:15 (v/v) water:acetonitrile in preparation for LC/MS analysis.

Intrinsic clearance and estimated hepatic clearance from hepatic S9 incubations

Zaleplon, O⁶-benzylguanine, zoniporide, BIBX1382, or SGX523 (1 μ M) was incubated at 37°C in a potassium phosphate-buffered reaction (100 mM, pH 7.4) containing hepatic S9 from human (mixed gender) or male and female CD-1 mouse, Sprague-Dawley rat, Hartley guinea pig, cynomolgus monkey, rhesus monkey, or Gottingen minipig (2.5 mg/mL), MgCl₂ (3 mM), with or without NADPH (1 mM). Reactions were initiated with addition of substrate, and at designated times (t = 0, 7, 15, 30, 45, and 60 min), aliquots were removed and precipitated with ice-cold

acetonitrile containing an internal standard (carbamazepine, 50 nM). The mixture was centrifuged at 3500 rcf for 5 min and resulting supernatants diluted with water in preparation for LC/MS/MS analysis of substrate depletion, by monitoring the analyte/internal standard ratio. Experiments were performed in triplicate. Hepatic intrinsic clearance (CL_{int}) was estimated using the substrate depletion method (see Figure II.1 and Equation II.1). Hepatic clearance (CL_{HEP}) was estimated using the well-stirred model, described by Equation II.2, and the hepatic extraction ratio (E) was estimated using Equation II.3. Subsequently, CL_{int} obtained from incubations in S9 of male preclinical species were used to predict human S9 CL_{int} by multispecies simple allometry (Equation II.13) and single-species scaling (Equation II.14).

Estimation of fraction metabolized by aldehyde oxidase ($F_{m,AO}$) in hepatic S9

Zaleplon, O⁶-benzylguanine, zoniporide, BIBX1382, or SGX523 (1 μ M) was incubated at 37°C in a potassium phosphate-buffered reaction (100 mM, pH 7.4) containing hepatic S9 from human (mixed gender) or male CD-1 mouse, Sprague-Dawley rat, Hartley guinea pig, cynomolgus monkey, rhesus monkey, or Gottingen minipig (2.5 mg/mL), MgCl₂ (3 mM), with or without NADPH (1 mM), and with or without 15 minute pre-incubation with the AO inhibitor hydralazine. Reactions were initiated with addition of substrate, and at designated times (t = 0, 7, 15, 30, 45, and 60 min), aliquots were removed and precipitated with ice-cold acetonitrile containing an internal standard (carbamazepine, 50 nM). The mixture was centrifuged at 3500 rcf for 5 min and resulting supernatants diluted with water in preparation for LC/MS/MS analysis of substrate depletion, by monitoring the analyte/internal standard ratio. Experiments were performed in triplicate. Hepatic

intrinsic clearance (CL_{int}) was estimated using the substrate depletion method (Figure II.1 and Equation II.1). Subsequently, the $F_{m, A0}$ of the five substrates was estimated for each species, using two different methods (A and B), described by Equations II.4 and II.5, respectively

Multispecies Determination of Pharmacokinetic Parameters of Zaleplon, O⁶-Benzylguanaine, Zoniporide, BIBX1382, and SGX523

Intravenous cassette administration of zaleplon, O⁶-benzylguanaine, zoniporide, BIBX1382, and SGX523

In-life studies in minipigs and guinea pigs were conducted at WIL Research (Ashland, OH) and studies in rats and mice were conducted at Frontage Laboratories (Exton, PA). Test articles were formulated (5% DMSO/5% ethanol/40% PEG-400/50% phosphate buffered saline) and administered as a cassette via an IV bolus dose at 0.2 mg/kg per compound. Male Gottingen minipigs (n = 2) age 3-5 months weighing approximately 7.5 kg were purchased from Marshall Bioresources and Hartley guinea pigs (n = 3) age 4-6 weeks weighing 400-430 g were purchased from Charles River Laboratories. Minipigs received the test article formulation (2 mL/kg) via ear vein administration and blood (1 mL) was collected via the jugular vein. Guinea pigs were cannulated in the left jugular vein for administration (2 mL/kg) and the right jugular vein for blood collection (500 μ L). Blood samples were collected from minipigs and guinea pigs at 2, 7, 15, and 30 minutes and 1, 2, 4, 8, 12, and 24 hours post-dosing. Male Sprague-Dawley rats (n=

3) age 7-9 weeks weighing approximately 300-400 g and CD-1 mice (n = 3 per time point, 30 mice in total) age 8-12 weeks weighing 19-25 g were purchased from Charles River Laboratories. Jugular vein cannulated rats received the test article formulation (2 mL/kg) via the femoral vein and blood (200 μ L) was collected via the jugular vein. Mice were administered the test article formulation (4 mL/kg) via the tail vein and blood was collected (100-200 μ L) via terminal cardiac puncture. Blood samples were collected from rats and mice at 2, 5, 15, and 30 minutes and 1, 2, 4, 6, 8, and 24 hours post-dosing. Blood was collected over EDTA and centrifuged for plasma isolation. Plasma was stored at -80°C until shipment on dry ice to Vanderbilt for bioanalysis.

Liquid Chromatography-Mass Spectrometry Methods

Quantitation of analytes (substrate or metabolite) present in extracts of plasma or hepatic S9 incubations was performed using liquid chromatography-tandem mass spectrometry (LC/MS/MS). Qualitative detection/identification of analytes (substrate or metabolite) present in extracts of plasma, hepatic microsomes, S9, or recombinant human P450 incubations was performed using liquid chromatography-ultraviolet detection-tandem mass spectrometry (LC/UV/MS/MS).

Quantitation from hepatic S9 incubations

Substrate depletion or metabolite formation (VU0409106 metabolites M1 and M6) in S9 fraction incubations with VU0409106, zaleplon, O⁶-benzylguanine,

zoniporide, BIBX1382, or SGX523 was determined by quantitation of the analyte:internal standard (carbamazepine, 237→194) peak area ratio using LC/MS/MS via electrospray ionization on a Sciex API-4000 triple quadrupole instrument (Sciex, Foster City, CA) coupled to LC-10AD pumps (Shimadzu, Columbia, MD) and a CTC PAL autosampler (Leap Technologies, Carrboro, NC) or on an AB Sciex API-5500 QTrap instrument (Applied Biosystems, Foster City, CA) coupled to LC-20AD pumps (Shimadzu, Columbia, MD) and a CTC PAL autosampler (Leap Technologies, Carrboro, NC). Analytes were separated by gradient elution (Table II.1) using a Fortis C18 column (3 × 50 mm, 3 μm; Fortis Technologies Ltd., Cheshire, UK) warmed to 40°C. Mobile phase A was 0.1% formic acid in water (pH unadjusted); mobile phase B was 0.1% formic acid in acetonitrile, and the flow rate was 0.5 mL/min. Mass spectral analyses were performed using multiple reaction monitoring (MRM), with transitions (Table II.1) and voltages specific for each analyte using a Turbo Ion Spray source (source temp 500°C) in positive ionization mode (5.0 kV spray voltage). Data were analyzed using Sciex Analyst 1.5.1 software.

Analyte	HPLC Gradient							Ion Transition (MRM)
Zaleplon	Time (min)	0.0	0.2	1.0	1.4	1.5	2.0	306 → 236
	% Mobile Phase B	30	30	90	90	30	30	
O ⁶ benzylguanine	Time (min)	0.0	0.2	1.0	1.4	1.5	2.0	242 → 91
	% Mobile Phase B	10	10	90	90	10	10	
Zoniporide	Time (min)	0.0	0.2	1.0	1.4	1.5	2.0	321 → 262
	% Mobile Phase B	10	10	90	90	10	10	
BIBX1382	Time (min)	0.0	0.2	1.0	1.4	1.5	2.0	388 → 98
	% Mobile Phase B	10	10	90	90	10	10	
SGX523	Time (min)	0.0	0.2	1.0	1.4	1.5	2.0	360 → 160
	% Mobile Phase B	10	10	90	90	10	10	
VU0409106	Time (min)	0.0	0.2	1.0	1.4	1.5	2.0	331 → 217
	% Mobile Phase B	30	30	90	90	30	30	
M1 (VU0409106)	Time (min)	0.0	0.2	1.0	1.4	1.5	2.0	347 → 233
	% Mobile Phase B	30	30	90	90	30	30	
M6 (VU0409106)	Time (min)	0.0	0.2	1.0	1.4	1.5	2.0	347 → 217
	% Mobile Phase B	30	30	90	90	30	30	

Table II.1. HPLC gradients and ion transitions monitored (multiple reaction monitoring) during LC/MS/MS quantitative analysis.

Quantitation from plasma

The quantitation of VU0409106 and its metabolites (M1, M2, M4-M6) from rat plasma or zaleplon, O⁶-benzylguanine, zoniporide, BIBX1382, and SGX523 (cassette dose) from plasma of mouse, rat, guinea pig, or minipig was conducted via electrospray ionization on an AB Sciex API-5500 QTrap (Applied Biosystems, Foster

City, CA) instrument that was coupled with LC-20AD pumps (Shimadzu, Columbia, MD). Analytes were separated by gradient elution using a Fortis C18 column (3 × 50 mm, 3 μm; Fortis Technologies Ltd., Cheshire, UK) warmed to 40°C. Mobile phase A was 0.1% formic acid in water (pH unadjusted); mobile phase B was 0.1% formic acid in acetonitrile. HPLC flow rate was 0.5 mL/min. The source temperature was set at 500°C, and mass spectral analyses were performed using multiple reaction monitoring, with transitions (Table II.1) and voltages specific for each analyte using a Turbo Ion Spray source in positive ionization mode (5.0 kV spray voltage). Data were analyzed using Sciex Analyst 1.5.1 software. Concentrations of analytes were determined using matrix-matched standard curves (8 – 10 points) with a lower limit of quantitation = 0.5 ng/mL for VU0409106, zaleplon, and O⁶-benzylguanine, 5 ng/mL for zoniporide, 5 ng/mL for BIBX523, and 1 ng/mL for SGX523. As no authentic standard was available to determine VU0409106 metabolite concentrations, a semi-quantitative analysis was expressed as the analyte:internal standard (carbamazepine, 237→194) peak area ratio (Morrison et al., 2012).

Metabolite detection in hepatic microsomal, S9, and rhP450 incubations and in rat plasma

Detection of VU0409106 metabolites generated *in vitro* or obtained from pooled rat plasma samples was performed with an Agilent 1100 HPLC system coupled to a LCQ Deca XP^{PLUS} ion trap mass spectrometer (Thermoelectron Corp., San Jose, CA) and an Agilent 1100 diode array detector. Detection of metabolites of zaleplon, O⁶-benzylguanine, zoniporide, BIBX1382, and SGX523 generated in S9 incubations was performed with an Agilent 1290 Infinity HPLC system coupled to a

Thermo LTQ XL ion trap mass spectrometer (Thermoelectron Corp., San Jose, CA) and an Agilent 1290 Infinity diode array detector. Analytes were separated by gradient elution using a Supelco Discovery C18 column (5 μm , 2.1 \times 150 mm; Sigma-Aldrich, St. Louis, MO) over a total run time of 30 minutes (Table II.3). Solvent A was 10 mM (pH 4.1) ammonium formate, and solvent B was acetonitrile. For the deuterium exchange experiment (VU0409106 metabolite M6), solvent A was 10 mM (pH 4.1) ammonium formate prepared in deuterium hydroxide. The flow rate was 0.400 ml/min. The HPLC eluent was first introduced into the diode array detector (254 nm) followed by electrospray ionization-assisted introduction into the ion trap mass spectrometer operated in positive ionization mode. Ionization was assisted with sheath and auxiliary gas (ultra-pure nitrogen), according to Table II.2. Electrospray temperatures and voltages and heated ion transfer capillary temperatures and voltages are also listed in Table II.2. Data were analyzed using Thermo Xcalibur 2.0 (LCQ Deca XP) or Xcalibur 2.2 (LTQ XL) software.

Detector	Sheath Gas Flow (psi):	Auxillary Gas Flow (psi):	Source Voltage (kV):	Capillary Voltage (V):	Capillary Temp ($^{\circ}\text{C}$):
Thermo LTQ XL	50	20	5	31	350
Thermo LCQ Deca XP ^{PLUS}	60	40	5	30	300

Table II.2. Tune settings for ion trap mass spectrometers used in LC/UV/MS/MS analysis of biotransformation.

Compound	HPLC Gradient						
Zaleplon	Time (min)	0	5	20	22	25	30
	% Mobile Phase B	15	15	80	80	15	15
O6 Benzylguanine	Time (min)	0	5	23	25	26.5	30
	% Mobile Phase B	5	5	80	80	5	5
Zoniporide	Time (min)	0	5	21	23	25	30
	% Mobile Phase B	10	10	80	80	10	10
BIBX1382	Time (min)	0	5	21	23	25	30
	% Mobile Phase B	10	10	80	80	10	10
SGX523	Time (min)	0	5	21	23	25	30
	% Mobile Phase B	10	10	80	80	10	10
VU0409106	Time (min)	0	5	20	22	25	30
	% Mobile Phase B	15	15	80	80	15	15

Table II.3. HPLC gradients for LC/UV/MS/MS analysis of biotransformation.

Data Analyses

Plots and graphs were generated using GraphPad Prism version 5.04 (GraphPad Software, San Diego, CA). Area-under-the-curve (AUC) values of VU0409106 metabolites M1 and M6 from S9 experiments were also generated in GraphPad Prism (trapezoid rule). Pharmacokinetic (PK) parameters were obtained using WinNonLin (noncompartmental analysis; Phoenix version 6.2; Pharsight, Mountain View, CA). Allometric coefficients and exponents for multispecies allometry were obtained from plots of body weight versus intrinsic clearance using linear regression analysis in Microsoft Excel 2010 by fitting data points to the power function described by Equation II.13.

In vitro clearance measurements

In vitro hepatic intrinsic clearance (CL_{int}) was estimated from hepatic S9 incubations with substrate, using the substrate depletion method (*in vitro* half-life method). The *in vitro* half-life is calculated from the elimination rate constant, k , which represents the slope determined from linear regression analysis of the natural log of the percent remaining substrate as a function of incubation time (Figure II.1). Equation II.1 is then applied to calculate hepatic CL_{int} (mL/min/kg) from the *in vitro* half-life (Zientek et al., 2010).

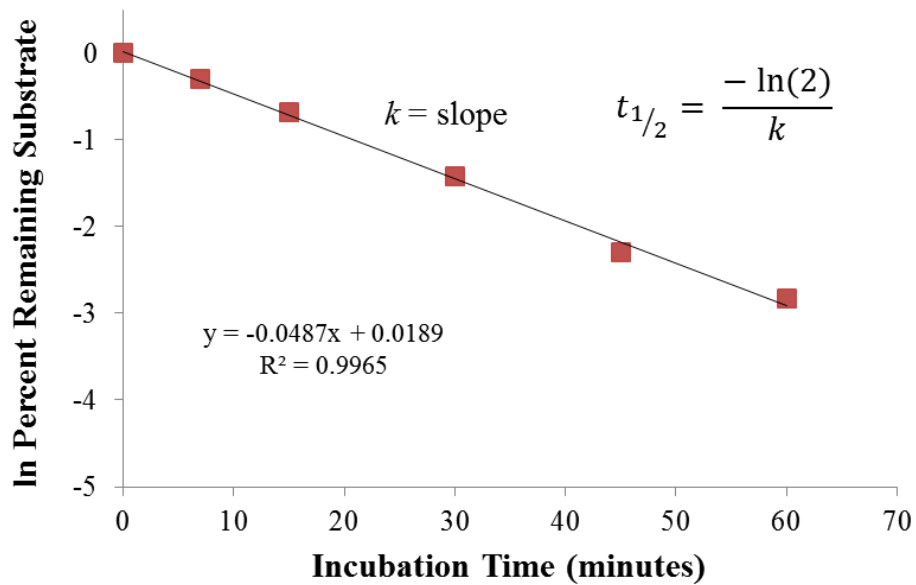


Figure II.1. Representative plot of the natural log of the percent remaining substrate versus incubation time for the determination of *in vitro* half-life.

$$CL_{int} = \frac{\ln 2}{t_{1/2} \text{ (min)}} \times \frac{mL}{2.5 \text{ mg protein}_{S9}} \times \frac{120.7 \text{ mg protein}_{S9}}{g \text{ liver weight}} \times \frac{(A)g \text{ liver weight}}{kg \text{ body weight}}$$

Equation II.1. Determination of hepatic intrinsic clearance (CL_{int}) by the *in vitro* half-life method (substrate depletion method). The species-specific hepatic scaling factor, A , is listed below in Table II.4.

Species	Mouse	Rat	Guinea pig	Cyno	Rhesus	Minipig	Human
Scaling Factor (g liver/kg body weight)	87.5 ^a	45 ^d	45 ^c	30 ^a	30 ^a	17 ^b	20 ^d

Table II.4. Species-specific hepatic scaling factors (A) applied to Equation II.1 for determination of hepatic intrinsic clearance (CL_{int}). Cyno, cynomolgus monkey

^a Davies and Morris,(1993) *Pharm Res.* **10(7)**:1093-95.

^b Suenderhauf and Parrott,(2013) *Pharm Res.* **30(1)**:1-15.

^c Boxenbaum,(1980) *J Pharmicokinet Biopharm.* **8(2)**:165-76.

^d Lin et al,(1994) *Drug Metab Dispos.* **24(10)**:1111-20.

Subsequently, CL_{int} was used to estimate hepatic clearance (CL_{HEP}) according to the well-stirred model, uncorrected for protein binding, described by Equation II.2 (Wilkinson and Shand, 1975; Pang and Rowland, 1977; Obach, 1999). The well-stirred model assumes the liver to be a single, well-stirred, homogenous compartment, where the rate of drug elimination is a function of the rate of drug presentation to the liver (governed by hepatic blood flow) and the intrinsic clearance of the drug (governed by drug metabolizing enzyme capacity).

$$CL_{HEP} (mL/min/kg) = \frac{Q_H \times CL_{int}}{Q_H + CL_{int}}$$

Equation II.2. Determination of CL_{HEP} , where Q_H is the species-specific hepatic blood flow, listed below in Table II.5.

Species	Mouse	Rat	Guinea pig	Cyno	Rhesus	Minipig	Human
Hepatic Blood Flow (mL/min/kg)	90 ^a	70 ^c	61 ^c	44 ^a	44 ^a	28 ^b	21 ^a

Table II.5. Species-specific hepatic blood flow (Q_H) applied to Equation II.2 for estimation of hepatic clearance. Cyno, cynomolgus monkey

^a Davies and Morris,(1993) *Pharm Res.* **10(7)**:1093-95.

^b Suenderhauf and Parrott,(2013) *Pharm Res.* **30(1)**:1-15.

^c Boxenbaum,(1980) *J Pharmicokinet Biopharm.* **8(2)**:165-76.

The hepatic extraction (E), which is a measure of the efficiency of the liver to remove drug, can be estimated from the CL_{HEP} and Q_H , and was calculated according to Equation II.3 (Rane et al., 1977). E represents the fraction of drug removed during one pass through the liver.

$$E = \frac{CL_{HEP}}{Q_H}$$

Equation II.3. Determination of hepatic extraction (E).

In vitro estimation of fraction metabolized by aldehyde oxidase ($F_{m,AO}$)

The $F_{m,AO}$ of zaleplon, O⁶-benzylguanine, zoniporide, BIBX1382, and SGX523 was estimated in hepatic S9 of human (mixed gender) and male minipig, rhesus monkey, cynomolgus monkey, guinea pig, rat, and mouse. Hydralazine has been proposed as a selective AO inhibitor suitable for use in determination of $F_{m,AO}$ in hepatocytes (Strelevitz et al., 2012). Utilizing this method in hepatic S9 fractions, incubations

were fortified with NADPH in the presence or absence of hydralazine, and Equation II.4 (method A) was applied to estimate the $F_{m,AO}$.

$$F_{m,AO(A)} = \frac{CL_{int} - CL_{int(+Hyd)}}{CL_{int}}$$

Equation II.4. Estimation of $F_{m,AO}$ in hepatic S9 by method A, where CL_{int} is the intrinsic clearance in S9 fortified with NADPH, and $CL_{int(+Hyd)}$ is the intrinsic clearance in S9 containing both NADPH and the AO inhibitor hydralazine.

Alternatively, the $F_{m,AO}$ can also be estimated with Equation II.5 (method B), utilizing S9 in the absence of NADPH. This method takes advantage of the NADPH-dependent nature of P450 and the NADPH-independent nature of AO to distinguish AO-mediated clearance from P450 (or other NADPH-dependent enzymes present in S9, such as FMO). Because xanthine oxidase (XO) is also present in S9 and is NADPH-independent, hydralazine serves to distinguish any potential XO activity (or other NADPH-independent enzyme such as esterases) from AO activity.

$$F_{m,AO(B)} = \frac{CL_{int(no\ NADPH)} - CL_{int(no\ NADPH+Hyd)}}{CL_{int}}$$

Equation II.5. Estimation of $F_{m,AO}$ in hepatic S9 by method B, where CL_{int} is the intrinsic clearance in S9 fortified with NADPH, $CL_{int(no\ NADPH)}$ is the intrinsic clearance in S9 without NADPH, and $CL_{int(no\ NADPH+Hyd)}$ is the intrinsic clearance in S9 containing the AO inhibitor hydralazine without NADPH.

In some cases, low turnover prevented an estimation of CL_{int} in S9 incubations containing NADPH and hydralazine ($CL_{int (+Hyd)} = 0$) or in S9 incubations absent NADPH ($CL_{int (no NADPH)} = 0$), which results in an $F_{m,A0}$ estimation equal to 1 by method A or 0 by method B, respectively. Due to this limitation, both methods A and B were used to approximate $F_{m,A0}$ in the event that at least one method would permit a calculation of $F_{m,A0}$. In addition, agreement between the two methods provides more confidence in the estimate. In some cases, low turnover prevented a calculation of $F_{m,A0}$ by both methods A and B.

Pharmacokinetic parameters

Pharmacokinetic parameters described below (AUC , CL_p , $t_{1/2}$, V_{ss} , MRT , and C_{max}) reported for VU0409106 and its metabolites, and for zaleplon, O⁶-benzylguanine, zoniporide, BIBX1382, and SGX523 were obtained by noncompartmental analysis (NCA) of their plasma concentration versus time profiles using WinNonLin (Phoenix version 6.2; Pharsight, Mountain View, CA) pharmacokinetic analysis software.

Area under the plasma concentration-time curve (AUC)

The AUC is the area under the plasma concentration-time curve and is a measure of the total drug exposure, expressed in units of amount x time/volume. AUC was estimated by the linear trapezoidal rule (Equation II.6) or the logarithmic trapezoidal rule (Equation II.7).

$$AUC_{t_1}^{t_2} = \frac{C_1 + C_2}{2} (t_2 - t_1)$$

Equation II.6. Estimation of AUC by the linear trapezoidal rule

$$AUC_{t_1}^{t_2} = \frac{C_2 - C_1}{\ln\left(\frac{C_2}{C_1}\right)} (t_2 - t_1)$$

Equation II.7. Estimation of AUC by the logarithmic trapezoidal rule

Plasma clearance (CL_p)

Plasma clearance (CL_p) is the volume of plasma containing drug that is eliminated per unit time, and is expressed in units of volume/time. CL_p was estimated from the AUC and the dose administered, according to Equation II.8.

$$CL_p = \frac{Dose}{AUC}$$

Equation II.8. Estimation of CL_p by noncompartmental analysis (NCA)

Half-life (t_{1/2})

Half-life (t_{1/2}) is the time it takes for the plasma drug concentration to decrease by 50%. For the purpose of these studies, t_{1/2}, represents the terminal half-life, unless otherwise indicated, and is described by Equation II.9.

$$t_{1/2} = \frac{\ln 2}{k_{el}}$$

Equation II.9. Estimation of the terminal half-life ($t_{1/2}$), where k_{el} is the first order elimination rate constant of the terminal exponential phase, estimated by linear regression of time versus log concentration.

Mean residence time (MRT)

Mean residence time (MRT) represents the average amount of time a drug molecule spends in the body, and is expressed in units of time. MRT was estimated by dividing the area under the first moment curve (AUMC, Equation II.10) by the AUC, as described by Equation II.11.

$$AUMC = AUMC_{last} + \frac{t_{last} \times C_{last}}{k_{el}} + \frac{C_{last}}{k_{el}^2}$$

Equation II.10. Estimation of AUMC by NCA. $AUMC_{last}$ is equal to the area under the moment curve from the time of dosing to the last measurable concentration, t_{last} is the time of the last measurable concentration, C_{last} is the last measurable concentration, and k_{el} is the first order elimination rate constant of the terminal exponential phase.

$$MRT = \frac{AUMC}{AUC}$$

Equation II.11. Estimation of MRT by NCA

Volume of distribution at steady state (V_{ss})

The volume of distribution at steady state (V_{ss}) describes the extent of drug distribution into the blood and tissues and is expressed in units of volume. V_{ss} was estimated from the AUC and CL_p , according to Equation II.12.

$$V_{ss} = MRT \times CL_p$$

Equation II.12. Estimation of V_{ss} by NCA.

Maximum plasma concentration (C_{max})

The maximum plasma concentration (C_{max}) is the peak plasma concentration observed in a given plasma concentration-time curve.

Multispecies allometry (MA)

From a biological perspective, the term allometry, which literally means “a different measure,” refers to the study of changes in biological characteristics as a function of size (Mahmood, 2007). Allometry describes a parameter that is not directly proportional to size (i.e., isometry), but rather changes with size according to a power-law function (e.g., Equation II.13, where the parameter, clearance, changes with body weight) (Mahmood, 2007). Allometry was originally used to demonstrate an empirical relationship between body surface area of a species and its body weight, and has since been widely used to quantitatively relate a range of biological parameters to body weight, including pharmacokinetic parameters (Adolph, 1949; Dedrick, 1973; Boxenbaum, 1982). Liver size and liver blood flow,

which govern hepatic drug clearance, are related to body weight according to an allometric relationship. (Boxenbaum, 1982). Accordingly, an allometric relationship has been demonstrated between drug clearance and body weight, and consequently, allometry has been adopted as a common method to predict human clearance from the clearance of preclinical species (Boxenbaum, 1982; Mahmood and Balian, 1996; Nagilla and Ward, 2004; Hosea et al., 2009). In the present investigation, simple allometry was used for the prediction of human clearance values, where preclinical clearance values were plotted against the species' body weight (Figure II.2) and subsequently fit to the simple allometric equation (power function), described by Equation II.13. Simple allometry was used to predict human plasma clearance (CL_p , total body clearance) from CL_p values of three or four preclinical species (minipig, cynomolgus, guinea pig, rat, mouse), which was obtained by IV administration of a cassette dosing formulation containing zaleplon, O⁶-benzylguanine, zoniporide, BIBX1382, and SGX523, or from CL_p values in the literature, where indicated (e.g., cynomolgus monkey data). Simple allometry was also used to predict human *in vitro* S9 intrinsic clearance (CL_{int}) from *in vitro* CL_{int} values obtained from hepatic S9 incubations of three or four preclinical species (minipig, rhesus, cynomolgus, guinea pig, rat, mouse). When plotting *in vitro* CL_{int} values, a standard body weight was used for each species (Table II.6), whereas actual (mean) body weight was used when plotting CL_p , unless otherwise indicated.

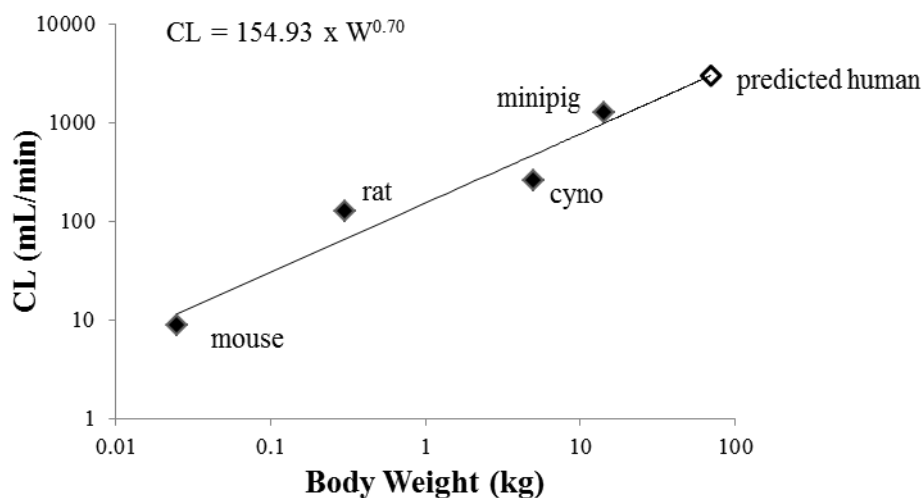


Figure II.2. Representative plot of CL vs Body Weight to obtain the allometric coefficient and exponent (a and b , respectively) used to calculate a predicted human CL with the simple allometric equation (Equation II.13). Solid shapes represent experimental data obtained from preclinical species. The open symbol represents the predicted human CL value. For scaling of *in vitro* data, CL represents CL_{int} obtained from hepatic S9 incubations. For scaling of *in vivo* data, CL represents plasma clearance (CL_p) obtained from *in vivo* administration of drug.

$$CL (mL/min) = a \times W^b$$

Equation II.13. Simple allometric equation for the prediction of human clearance by multispecies allometry (MA), where W is body weight, and a and b are the allometric coefficient and exponent, respectively, obtained from a plot of CL versus W of 3 or 4 species (Figure II.2). The allometric exponent, b , describes the rate of change between CL and W .

Species	Mouse	Rat	Guinea pig	Cyno	Rhesus	Minipig	Human
Standard Body Weight (kg)	0.02	0.25	0.344	4	8	14.2	70

Table II.6. Standard body weights used for multispecies allometry and single-species scaling of *in vitro* S9 intrinsic clearance data (CL_{int}). Cyno, cynomolgus

Single-Species Scaling (SSS)

Following the same principle of multispecies allometry, Equation II.14 was applied in single-species scaling (SSS) analyses, where human clearance is directly extrapolated from the clearance of a single species (Hosea et al., 2009). A fixed exponent of 0.75 has been proposed for prediction of CL by SSS, based on the understanding that many physiological factors including basal metabolic rate and passive renal clearance may be scaled using this exponent (Boxenbaum, 1982; Hosea et al., 2009).

$$CL_{human} (mL/min) = CL_{animal} \times \frac{W_{human}^{0.75}}{W_{animal}}$$

Equation II.14. Prediction of human clearance by single-species scaling (SSS), where CL_{human} is the predicted human clearance value (CL_{int} or CL_p), CL_{animal} is the observed clearance value obtained from the preclinical species *in vivo* (CL_p) or *in vitro* in hepatic S9 (CL_{int}), W_{animal} is the body weight of the preclinical species, and W_{human} is the human body weight.

Success criteria for prediction of human clearance by MA or SSS

The success of each individual human clearance prediction (*in vitro* or *in vivo*) was assessed by calculation of the fold-error, described by Equation II.15. Due to the variability in human pharmacokinetics, it is standard for a fold-error of ≤ 3 to be considered successful in the prediction of human clearance and was therefore used as a benchmark of success in these studies.

$$\text{fold error} = \frac{CL_{pred}}{CL_{obs}}$$

Equation II.15. Determination of fold-error in the prediction of CL_{int} , CL_{HEP} , or CL_p , where CL_{obs} equals either the CL_{int} or CL_{HEP} measured in human hepatic S9 or the human CL_p obtained from the literature, and CL_{pred} equals the predicted human hepatic S9 CL_{int} or CL_{HEP} obtained from either MA or SSS of hepatic S9 CL_{int} from preclinical species, or the predicted human CL_p obtained from either MA or SSS of CL_p from preclinical species.

The success of each prediction method was assessed by calculation of the absolute average fold-error (AAFE) and the average fold error (AFE), described by Equations II.16 and II.17, respectively (Obach et al., 1997; Tang et al., 2007), for the fold-errors in the human clearance predictions obtained for the five compounds, zaleplon, O⁶-benzylguanine, zoniporide, BIBX1382, and SGX523. AFE is equal to the geometric mean of the fold-error and represents a measurement of the overall bias in both directions (above or below the reference value of 1), whereas the AAFE gives both overpredictions and underpredictions equal value. Therefore the overall bias of the prediction method towards under- or overprediction is represented by the AFE, and the AAFE is an unbiased representation of the fold-error. An AAFE of ≤ 3 was considered successful. The percentage of compounds within 2-fold error (fold error = 0.5-2.0) and 3-fold error (fold error = 0.33-3.0) was also considered when assessing each method.

$$AAFE = 10^{\frac{\sum |\log(\text{fold error})|}{N}}$$

Equation II.16. Determination of absolute average fold-error (AAFE), where N equals the total number of compounds, and fold error (Equation II.15) is the ratio of the CL_{pred} to the CL_{obs}.

$$AFE = 10^{\frac{\sum \log(\text{fold error})}{N}}$$

Equation II.17. Determination of average fold-error (AFE), where N equals the total number of compounds, and fold error (Equation II.15) is the ratio of the CL_{pred} to the CL_{obs}.

Statistical Analyses

All statistical analyses were conducted with GraphPad Prism version 5.04 (GraphPad Software, San Diego, CA), including calculations of standard deviations (SD) and standard errors of the mean (SEM). Likewise all plasma concentration-time curves and other data plots were generated in GraphPad Prism, unless otherwise noted.

Pharmacokinetic analysis of VU0409106 and metabolites.

GraphPad Prism was employed in the statistical analyses of *in vivo* pharmacokinetic parameters of VU0409106 and metabolites, using a two-tailed unpaired *t*-test (paired *t*-test for the crossover study) with a significance level of $p < 0.05$.

Calculation of intrinsic clearance from incubations with hepatic S9

CL_{int} was only calculated and reported if the mean $\ln[C]$ versus time slope was significantly different from zero (determined using GraphPad Prism version 5.04 by an F test with a significance level of $p < 0.05$). If the slope was exclusively dependent on the terminal time point in order to be considered different from zero, CL_{int} was not calculated.

SSS Correlation with F_m or E .

The fold-error for *in vitro* SSS predictions (CL_{int} or CL_{HEP}) was plotted against either $F_{m, AO}$ or E , with correlation coefficients (r^2) determined using GraphPad Prism (Figures IV.6-7). For plots involving $F_{m, AO}$, estimates calculated by method B were used, with the exception of zaleplon for mouse and minipig, in which case estimates calculated by method A were instead used since method B assumed an $F_{m, AO} = 0$ (no measurable turnover in the absence of NADPH). Zaleplon and O⁶-benzylguanine data for rat, O⁶-benzylguanine data for mouse and minipig, and BIBX1382 data for mouse were excluded altogether because CL_{int} was only measurable in the presence of NADPH without hydralazine, resulting in an $F_{m, AO}$ estimation of 1 by method A and 0 by method B. $F_{m, AO}$ estimations > 1 , were assumed to be equal to 1 for the purposes of this analysis. In addition, the same correlation analyses were performed using *in vivo* data derived from a report by Deguchi et al of SSS to predict human CL_p of uridine diphosphate-glucuronosyltransferase (UGT) substrates (Figure IV.8) (Deguchi et al., 2011). For twelve UGT substrates, Deguchi et al. reported CL_p in each species (mouse, rat, monkey, and dog), human predictions of CL_p obtained from SSS, and $F_{m, UGT}$ in each

species estimated from *in vivo* production of glucuronide metabolites excreted into the bile and urine. For our correlation analyses using UGT substrate data from Deguchi et al., fold-errors of the SSS predictions were calculated as described above in Equation II.15 from the observed human CL_p values and SSS CL_p predictions reported by Deguchi et al. $F_{m,UGT}$ was not reported by Deguchi et al for imipramine in mouse, nor was it reported for levofloxacin and telmisartan in human, resulting in exclusion of levofloxacin and telmisartan from the $F_{m,UGT}$ analysis. In place of a correlation analysis involving E, a similar analysis was conducted using CL_p as a percentage of Q_H obtained from Deguchi et al's report. Equation II.3 was adapted to calculate CL_p as a percentage of Q_H using CL_p values reported by Deguchi et al. and species-specific hepatic blood flow, resulting in Equation II.18:

$$CL_p \text{ as a percentage of } Q_H = \frac{CL_p}{Q_H}$$

Equation II.18. Determination of plasma clearance (CL_p) as a percentage of liver blood flow(Q_H), where Q_H is the species-specific hepatic blood flow listed in Table II.5.

When CL_p is exclusively mediated by hepatic elimination, this value (CL_p as a percentage of Q_H) will be equal to E. If extra-hepatic elimination is present, this value will be greater than E. Therefore, levofloxacin and furosemide, which are predominantly excreted unchanged in the urine, were excluded from this analysis.

Portions of the following chapter have been reprinted with permission of the American Society for Pharmacology and Experimental Therapeutics. All rights reserved.

Rachel D. Crouch, Ryan D. Morrison, Frank W. Byers, Craig W. Lindsley, Kyle A. Emmitte and J. Scott Daniels, Evaluating the Disposition of a Mixed Aldehyde Oxidase/Cytochrome P450 Substrate in Rats with Attenuated P450 Activity, *Drug Metabolism and Disposition* August 2016, 44(8):1296-1303;
DOI: <http://dx.doi.org/10.1124/dmd.115.068338>

Copyright © 2016 by the American Society for Pharmacology and Experimental Therapeutics

CHAPTER III

EVALUATING THE DISPOSITION OF A MIXED ALDEHYDE OXIDASE/CYTOCHROME P450 SUBSTRATE IN RATS WITH ATTENUATED P450 ACTIVITY

INTRODUCTION

Our initial interest in AO stemmed from the prior discovery in our laboratory that VU0409106, a novel negative allosteric modulator of the metabotropic glutamate receptor subtype 5 (mGlu5 NAM) synthesized at the Vanderbilt Center for Neuroscience Drug Discovery (VCNDD) (Felts et al., 2013), was metabolized in an NADPH-independent manner in rat and human hepatic S9 and cytosolic fractions (Morrison et al., 2012). Further exploration revealed that VU0409106 was oxidized by aldehyde oxidase on the pyrimidine ring to the primary metabolite M1 (Morrison et al., 2012). Our continued interest in VU0409106 has been driven largely by the observation that P450 pathways also contribute to its biotransformation, resulting in formation of metabolites M4, M5 and M6 (Figure III.1). This observation provided us with a unique opportunity to investigate the consequences of inhibiting either the P450 clearance pathway or the AO clearance pathway on the disposition of VU0409106 and the associated P450 and AO metabolites.

The 2012 US Food and Drug Administration (FDA) draft guidance on defining the drug interaction potential of new chemical entities (NCEs) in drug discovery and

development

(<http://www.fda.gov/downloads/Drugs/GuidanceComplianceRegulatoryInformation/Guidances/ucm292362.pdf>) focuses primarily on human *in vitro* and nonclinical *in vivo* approaches to model clinical drug-drug interactions (DDIs) involving cytochrome P450s and drug efflux proteins (Prueksaritanont et al., 2006; Di et al., 2013; Prueksaritanont et al., 2013). However, sparse attention has been paid to the potential for drug interactions involving compounds metabolized by enzymes falling outside these two classes of drug disposition proteins, including AO. Significant strides have been made towards understanding the structure-activity relationships (SAR) of AO binding and metabolism (Beedham et al., 1995; Dalvie et al., 2012; Coelho et al., 2015), species differences (Beedham et al., 1987; Garattini and Terao, 2012; Dalvie et al., 2013), human AO variability (Hartmann et al., 2012; Hutzler et al., 2014b), and inhibition of AO *in vitro* (Obach et al., 2004; Barr and Jones, 2011), while studies defining the importance of this enzyme in an *in vivo* drug interaction scenario are lacking, perhaps owing to a deficiency of well-established specific AO inhibitors considered suitable for *in vivo* pharmacokinetic studies.

To date, limited pharmacokinetic drug interactions involving the few marketed [known] AO substrates have been recognized, despite identification of several clinical drugs demonstrating AO inhibitory activity *in vitro* (Obach et al., 2004). Rather, the few reported clinical interactions for AO-cleared drugs involve inhibition or induction of a secondary non-AO metabolism pathway (Ramanathan et al., 2016). For example, FDA labeling for the nonbenzodiazepine sedative hypnotic zaleplon recommends a dose adjustment when co-administered with cimetidine, which

inhibits not only AO (primary route of zaleplon metabolism in humans), but also P450 3A4 (secondary route of zaleplon metabolism) (http://www.accessdata.fda.gov/drugsatfda_docs/label/2007/020859s011bl.pdf). Additionally, changes in exposure to the phosphatidylinositol 3-kinase- δ inhibitor idelalisib were noted with co-administration of the P450 3A inhibitor ketoconazole, or the inducer rifampin (Ramanathan et al., 2016). A noteworthy report by Li et al. recently indicated an important role for AO in a drug interaction between BILR 355 and the P450 3A inhibitor ritonavir, where co-administration resulted in a metabolic “switch” from P450 3A metabolism of BILR 355 to gut bacterial and subsequent AO metabolism (Li et al., 2012a; Li et al., 2012b). Furthermore, Li’s studies monitoring formation of this AO metabolite in human S9 in the presence and absence of NADPH were consistent with a metabolic shunt towards AO when the P450 pathway was inactive. This report brought attention to the possibility of a drug interaction leading to a metabolic switch and the potential for AO to contribute to such an event.

Drawing on observations from Li’s report demonstrating a drug interaction that elicits a metabolic switch in a unique scenario requiring an intermediate gut bacterial metabolism step, we hypothesized that hepatic P450 inhibition may result in an elevated exposure to the AO metabolite of a drug cleared via both AO and P450 enzymes. Because AO and P450 commonly generate different metabolites due to opposing substrate specificities (AO prefers to oxidize electron-deficient carbons whereas P450 prefers electron-rich sites), this creates a potential scenario for increased exposure to one metabolite when the other metabolic pathway is

inhibited. The observation that VU0409106 was metabolized exclusively by AO to M1 and to M4-M6 by P450 enzymes presented an opportunity to investigate the disposition of a mixed AO:P450 substrate and the corresponding AO and P450 metabolites in a drug interaction scenario of P450 inhibition. Given the similarities in rodent metabolism and clearance of VU0409106 to that observed in human S9 and hepatocytes (Morrison et al., 2012) we designed this drug interaction scenario *in vivo* in Sprague-Dawley (SD) rats, a conventional species historically employed in nonclinical pharmacokinetic investigations (Di et al., 2013), via co-administration of VU0409106 and the *pan*-P450 inactivator 1-aminobenzotriazole (ABT). Observations from these *in vitro* and *in vivo* investigations indicate evidence of metabolic shunting towards AO metabolism in the disposition of VU0409106 in rat when P450 activity is attenuated, resulting in elevated exposure to the AO metabolite M1. In addition, we investigated the impact of inhibiting AO metabolism with the co-administration of the AO inhibitor hydralazine to rats receiving VU0409106. Results from these studies indicate a similar pattern of increased exposure to the P450 metabolite(s); however, as hydralazine possesses characteristics that limit its utility in pharmacokinetic drug interaction studies, identification of a more suitable *in vivo* AO inhibitor will be necessary to gain a better understanding of this potential interaction.

RESULTS

A Mixed AO:P450 Metabolism Phenotype of VU0409106 *in vitro*.

Metabolism of VU0409106 in rat and human hepatic microsomes and recombinant human P450s.

Our laboratory previously reported that the primary biotransformation pathway of VU0409106 was catalyzed by AO to the principal metabolite M1, plus other P450-mediated metabolites (e.g., M4 and M5) detected in nonclinical species and human hepatic S9 fractions (Figure III.1), as well as *in vivo* in Sprague-Dawley (SD) rats receiving intraperitoneal administrations of VU0409106 (Morrison et al., 2012).

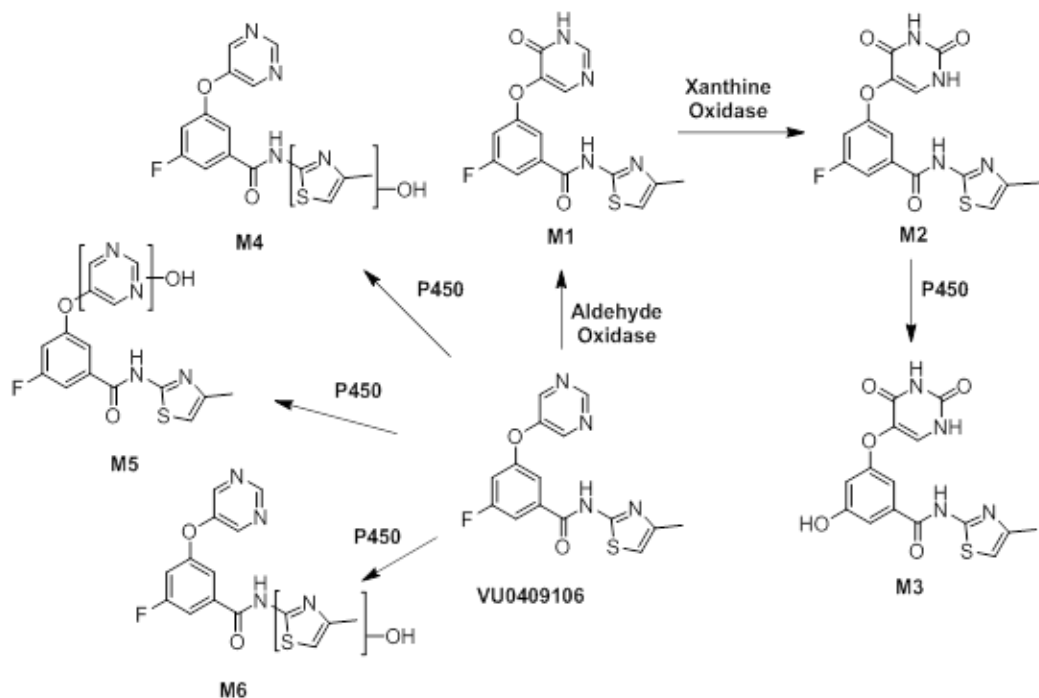


Figure III.1. Metabolism of VU0409106 *in vitro* and *in vivo* in Sprague-Dawley rats and *in vitro* in human.

Furthermore, an *in vitro:in vivo* correlation of the predicted hepatic and plasma clearance of VU0409106 in rats and nonhuman primates was demonstrated, a finding which established the relevancy of a principle AO mechanism of clearance *in vivo*, with a secondary contribution from P450 in the disposition of VU0409106. Presently, we employed liquid chromatographic-mass spectrometry analysis (LC/UV/MS) and hepatic microsomes to define the role of P450 in the metabolism of VU0409106 in rat and human, and to monitor P450 metabolites in the investigation of a metabolic shunt involving AO. Data from hepatic microsomal incubations of VU0409106 indicated the NADPH-dependent formation of the hydroxylated metabolites M5 and M6 (Table III.1); the retention time and respective MS/MS fragmentation data of M5 was consistent with our laboratory's previous report detailing the biotransformation of VU0409106 (Morrison et al., 2012). Structural identification of M6, which was not characterized in Morrison's previous report, is depicted in Figures III.3-6. While the thiazole-hydroxylated metabolite, M4, was observed *in vivo* in rat plasma, as well as in rat and human hepatocytes (attenuated with ABT pretreatment) (Morrison et al., 2012), it was below our detection limits in rat or human hepatic microsomes in the present study. With the rat-to-human translation of the P450 mediated clearance of VU0409106 *in vitro*, we sought to demonstrate the specific P450 enzymes involved in the formation of metabolites observed in human microsomes, specifically, those enzymes commonly associated with drug metabolism and clinical drug interactions. Table III.1 depicts the results of incubations of VU0409106 with recombinant expressed human P450 enzymes (rhP450) 1A2, 2D6, 2C9, 2C19 and 3A4. While the proposed hydroxylated

metabolite M6 was formed in reactions of all five P450 enzymes examined, the hydroxylated-pyrimidine metabolite M5 was observed in all but reactions containing P450 1A2. The AO-mediated metabolite, M1, was not detected in incubations with recombinant expressed P450 enzymes, consistent with prior studies indicating AO exclusively mediates formation of M1 (Morrison et al., 2012).

Matrix	Metabolites Detected					
	M1	M2	M3	M4	M5	M6
Rat Plasma	√	√	√	√	√	√
Rat microsomes	√ ^a				√	√
Human microsomes	√ ^a				√	√
rh1A2						√
rh2C9					√	√
rh2C19					√	√
rh2D6					√	√
rh3A4					√	√

Table III.1. LC/MS detection of metabolites *in vivo* (SD rat) or *in vitro* in SD rat and human microsomes or recombinant human P450 enzymes (rhP450).

^aCytosolic AO contamination of microsomes produced low levels of M1. See Figure III.3.

The appearance of M1 in rat and human microsomal incubations was NADPH-*independent* and indicative of trace contamination of the microsomal fraction with cytosol (containing AO); this finding of background AO activity in contaminated hepatic microsomes is not uncommon (Diamond et al., 2010a), and was confirmed by suppression of M1 formation with the AO-specific inhibitor hydralazine (Figure III.2).

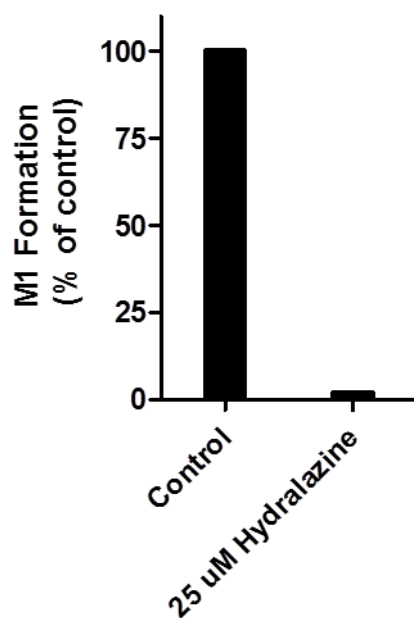


Figure III.2. The AO inhibitor hydralazine inhibited the formation of M1 in incubations of VU0409106 (25 µM) with rat hepatic microsomes.

LC/MS/MS characterization of VU0409106 metabolite M6.

The MS/MS of M6 is depicted in Figure III.3. A protonated molecular ion, $[M + H]^+$, for M6 was observed at m/z 347, a +16 Da mass shift over the parent VU0409106 (indicates oxidation), which produced a $[M + H]^+$ at m/z 331 (Morrison

et al., 2012). A loss of 18 Da (loss of water) represented the major fragment ion at m/z 329. The minor fragment ion at m/z 217, which was also present in the MS/MS spectra of the parent VU0409106, suggested that the oxidation was likely located on the methyl-thiazole moiety. The fragment ion at m/z 320 corresponds to a +16 Da mass shift over the fragment ion at m/z 304 produced by the parent VU0409106.

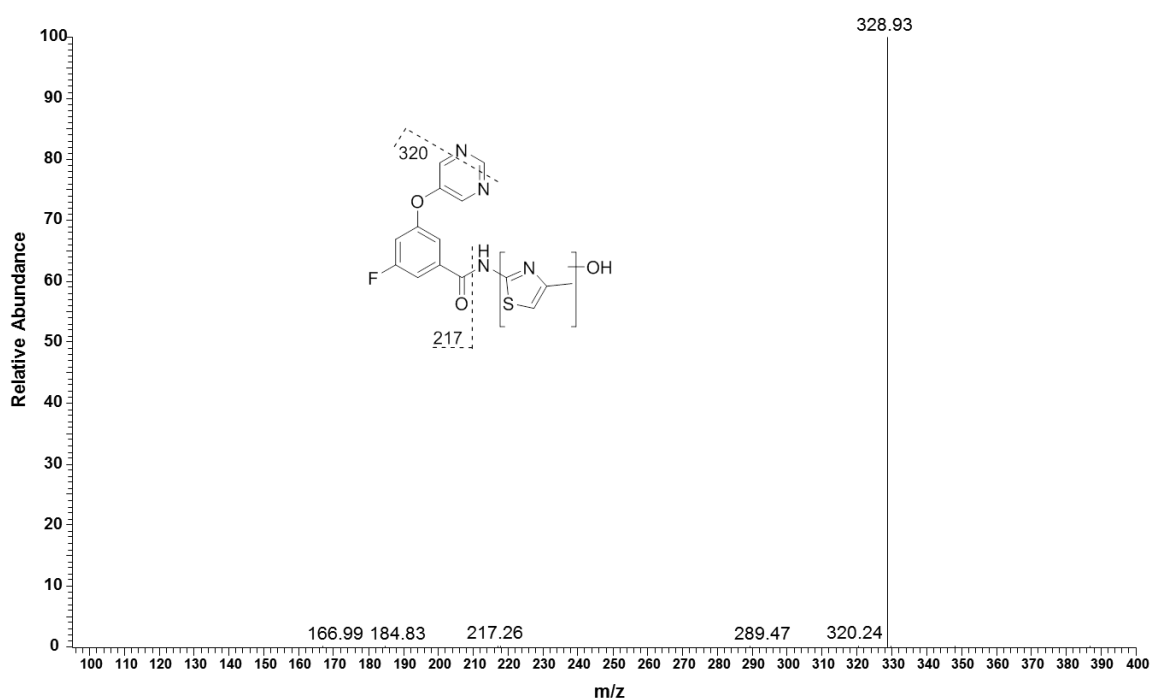


Figure III.3 LC/MS/MS and proposed structure of metabolite, M6, detected in SD rat and human hepatic microsomes and recombinant human P450 incubations.

An MS³ experiment ($347 \rightarrow 329$) produced a fragment ion again at m/z 217 and a fragment ion at m/z 302, which corresponds to loss of water (-18 Da) from the fragment ion at m/z 320 (Figure III.4). These data support the assignment of the oxidation to the methyl-thiazole moiety.

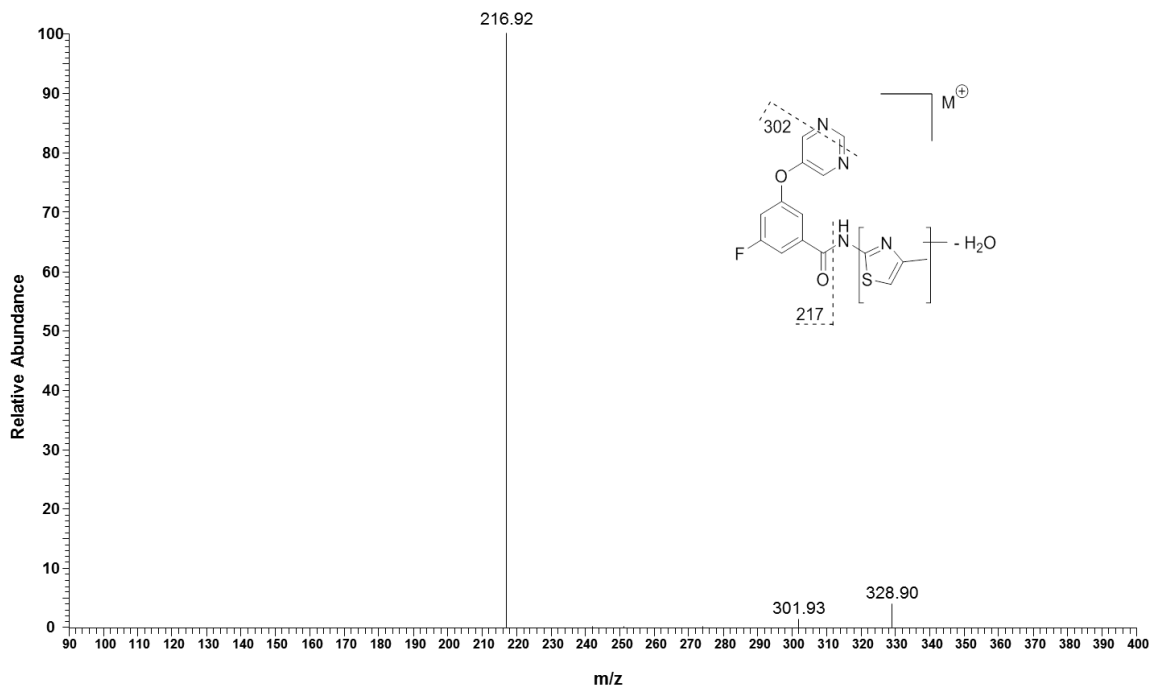


Figure III.4. LC/MS³ and proposed structure of metabolite, M6, detected in SD rat and human hepatic microsomes and recombinant human P450 incubations (MS³: 347→329 (-H₂O; 18 Da)→302, 217 Da).

Available locations for oxidation to occur on the methyl-thiazole moiety include the sulfur or nitrogen atoms, the carbon alpha to the sulfur, or the carbon of the methyl group. In order to determine if the oxidation is located on either of the two heteroatoms versus either of the two carbon atoms, a deuterium exchange experiment was performed, where the mobile phase A buffer (10 mM ammonium formate) used for LC/MS analysis was prepared in D₂O. The protonated molecular ion of VU0409106 contains two exchangeable hydrogen atoms, which upon free exchange with deuterium ions in the mobile phase results in a deuterated molecular ion, [M + D]⁺, at m/z 333 (whereas the [M + H]⁺ = 331). The [M + H]⁺ for M6 occurs at m/z 347; therefore, if the oxidation is located on either of the heteroatoms, the [M + D]⁺ will be one Da lower (m/z 349) than if the oxidation is located on either of the

carbon atoms (m/z 350), as the metabolite would contain one less exchangeable hydrogen in the former case (Figure III.5).

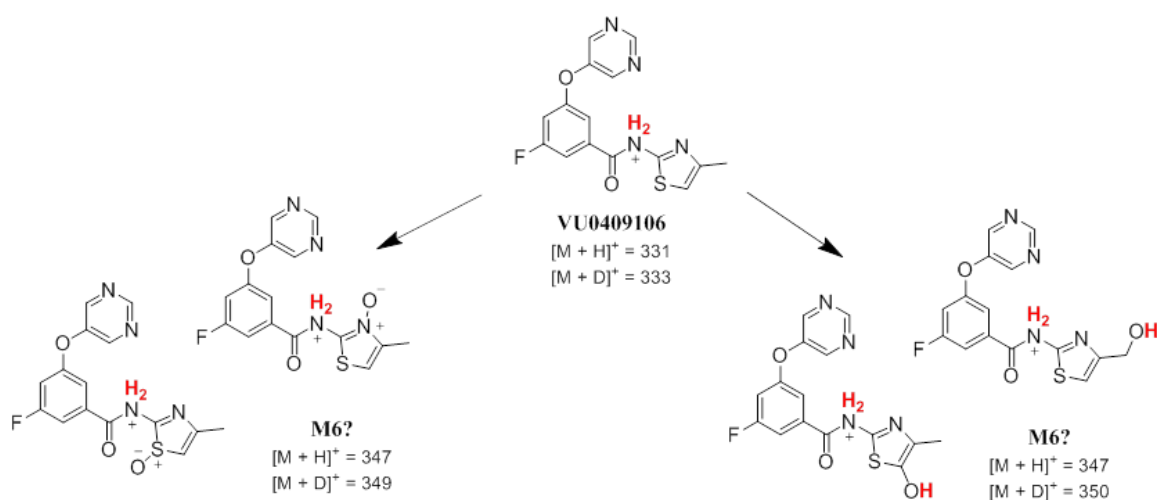


Figure III.5 A full scan LC/MS deuterium exchange experiment, where the mobile phase A buffer (10 mM ammonium formate) is prepared in D₂O, will produce an [M+D]⁺ for M6 at m/z 350 Da if hydroxylation occurs on a carbon atom of the thiazole moiety, versus that of the N or S, in which case calculated [M+D]⁺ = 349 Da. Exchangeable hydrogens are highlighted in red.

The [M + D]⁺ was indeed observed at m/z 350 in the full scan MS experiment (100% relative abundance, Figure III.6), suggesting that the oxidation occurs on a carbon atom. This observation opposes the potential for M6 to also be generated by flavin monooxygenases (FMOs), as these enzymes characteristically oxidize N or S atoms, not carbon atoms.

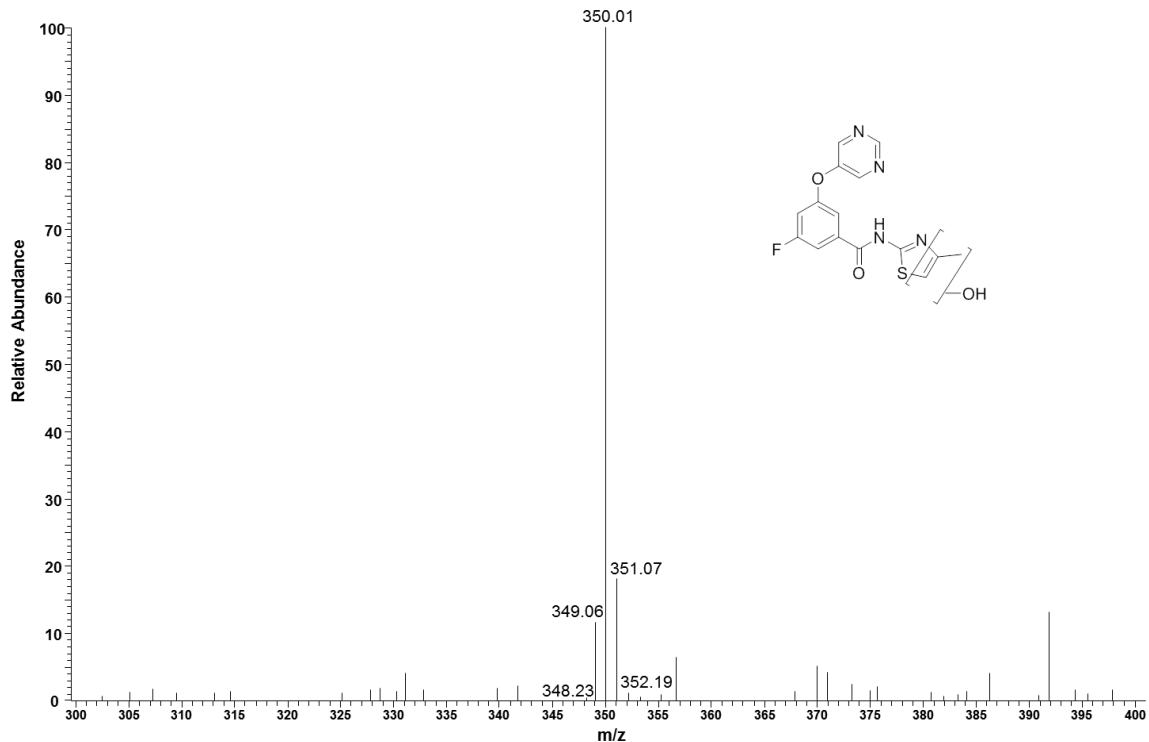


Figure III.6 A full scan LC/MS deuterium exchange experiment, where the mobile phase A buffer (10 mM ammonium formate) was prepared in D₂O, produced an [M+D]⁺ for M6 at *m/z* 350 Da, indicative of a hydroxylation of a carbon atom.

Intrinsic Clearance of VU0409106 and Relative Formation of M1 in Rat and Human S9 Fractions Implicate a Metabolic Shunting Mechanism Mediated by Aldehyde Oxidase

M1 formation in hepatic S9.

When VU0409106 was incubated (1 μM, 60 min incubation) in both rat and human hepatic S9 fractions (+/- NADPH), the observed magnitude of M1 formation in S9 incubations, absent the P450 reducing cofactor NADPH, was greater than that observed when incubations were fortified with NADPH (Figure III.7). An approximate 50% increase in the area under the curve (AUC) of M1 was observed in

S9 incubations absent NADPH relative to those incubations containing NADPH from both human and rat experiments (Table III.2).

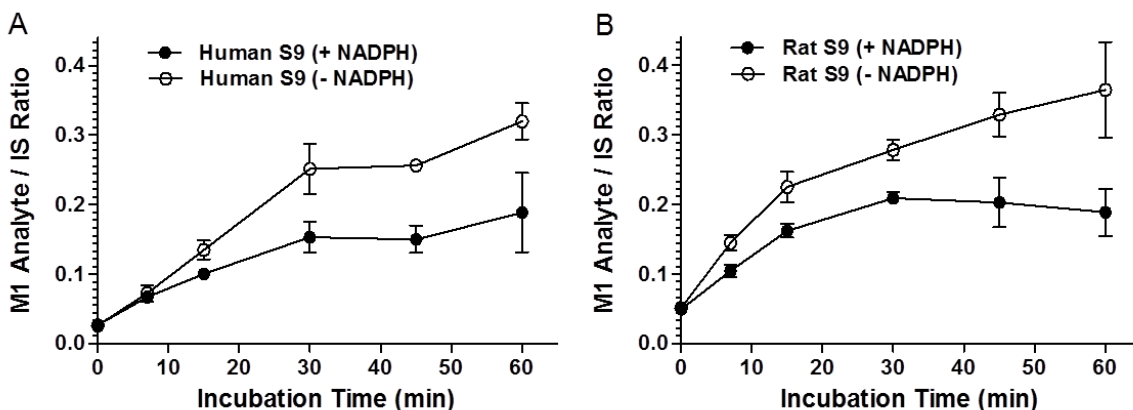


Figure III.7. Formation of M1 in incubations of VU0409106 with (A) human hepatic S9 or (B) SD rat hepatic S9 in the presence (closed circles) or absence (open circles) of NADPH. Data points are expressed as the peak area ratio of analyte/internal standard and represent the mean of a triplicate determination (\pm SD).

<i>In vitro</i> Incubation	+ NADPH	- NADPH
Human S9	7.7 \pm 0.66	12.2 \pm 0.68
Rat S9	10.4 \pm 0.90	15.7 \pm 0.68

Table III.2. Exposure of M1 Formed from human or rat hepatic S9 incubations of VU0409106 in the presence or absence of NADPH. AUC expressed as the peak area ratio (analyte/IS*min) and represent means of triplicate determinations (\pm SD).

Concentration-dependence of total, NADPH-dependent, and NADPH-independent hepatic S9 intrinsic clearance (CL_{int}) of VU0409106.

We previously demonstrated that subsequent metabolism of M1 to M2 is catalyzed by xanthine oxidase (XO) (Figure III.1) (Morrison et al., 2012), an enzyme which does not require the reducing cofactor NADPH for catalytic activity, thus excluding P450-mediated conversion of M1 to M2 as the mechanism responsible for this observation. The observed increase in M1 in S9 incubations absent NADPH may likely be due to an increase in substrate exposure to AO in the absence of NADPH-dependent P450 metabolism. To explore this possibility, we measured the CL_{int} of VU0409106 in rat and human S9 fractions in the presence and absence of NADPH and in the presence of NADPH and the AO inhibitor, hydralazine, to estimate the CL_{int} mediated by both AO and P450, AO only, and P450 only, respectively (Table III.3), and over a concentration range of VU0409106 (0.1 μ M, 1 μ M, and 10 μ M).

Concentration	Rat				Human	
	+NADPH +hydralazine	+NADPH	-NADPH	+NADPH +hydralazine	+NADPH	-NADPH
0.1 μ M	41.5 \pm 4.6	99.6 \pm 8.3	25.3 \pm 2.6	39.3 \pm 1.1	48.8 \pm 7.6	7.2 \pm 1.1
1 μ M	22.4 \pm 1.7	52.1 \pm 6.1	24.5 \pm 2.6	7.7 \pm 1.4	15.3 \pm 2.0	6.4 \pm 1.2
10 μ M	<4.9	24.7 \pm 2.0	24.4 \pm 4.0	<2.2	5.9 \pm 0.4	4.1 \pm 0.7

Table III.3. Total, NADPH-dependent, and NADPH-independent rat and human hepatic S9 intrinsic clearance (mL/min/kg) of VU0409106 at concentrations of 0.1 μ M, 1 μ M, and 10 μ M. Data represent means of triplicate determinations (\pm SD).

While NADPH-dependent CL_{int} in both species decreased with increasing concentration of VU0409106, NADPH-independent CL_{int} remained constant in rat, with some decrease in human S9 incubations. The decrease in NADPH-dependent CL_{int} at higher concentrations was also reflected by a decrease in the total CL_{int} observed when both P450 and AO are active. These data indicate the likelihood that the overall K_m (Michealis constant) for the P450 pathways is lower than that for the AO pathway and are consistent with a mechanism of metabolic shunting towards AO under conditions of attenuated P450 metabolism and greater substrate availability for AO. While the NADPH-independent CL_{int} observed in the present experiments was slightly elevated than previously reported (Morrison et al., 2012), this finding is not surprising, given the potential *in vitro* variability of AO recently described across multiple individual hepatocyte donors, for example (Hutzler et al., 2014b). In addition, various laboratories have reported different AO-mediated CL_{int} values for the same AO substrate (Kitamura et al., 1999; Al-Salmy, 2001; Sahi et al., 2008).

Altogether, the present *in vitro* metabolism and clearance data indicate that SD rat represents an acceptable nonclinical model to study the *in vivo* disposition of VU0409106 and its metabolites under drug interaction duress (e.g., P450 inhibition), particularly the occurrence of metabolic shunting from P450 towards AO.

ABT Pretreatment Results in Increased Exposure to Parent VU0409106 and the AO Metabolite M1 In Vivo in SD Rats.

VU0409106

To evaluate the impact of P450 inhibition on the disposition of VU0409106 and its metabolites, SD rats received an IP administration of VU0409106 (3 mg/kg) with or without oral pretreatment with the pan-P450 inactivator ABT (50 mg/kg). We then generated standard plasma concentration-time profiles (Figure III.8) employing contemporary LC/MS/MS quantitation and reported standard PK parameters (e.g., C_{max} , AUC_{0-inf} , CL_p , V_{ss} , $t_{1/2}$, Table III.4-5). Statistically significant changes were observed in the plasma clearance (CL_p), AUC, and maximal concentration (C_{max}) of VU0409106 in rats pretreated with ABT, versus vehicle pretreatment. In rats pretreated with ABT, a 7.8-fold increase in the plasma AUC of VU0409106 was observed (Figure III.8A, Table III.4). Likewise, the C_{max} was increased 3.1-fold. The PK of VU0409106 was also obtained (Table III.4), following an intravenous (IV) administration of VU0409106 to rats, where an increase in the AUC of VU0409106 was again observed (3.5-fold), along with a corresponding reduction in the average CL_p from 53.5 to 15.3 mL/min/kg in rats pretreated with ABT.

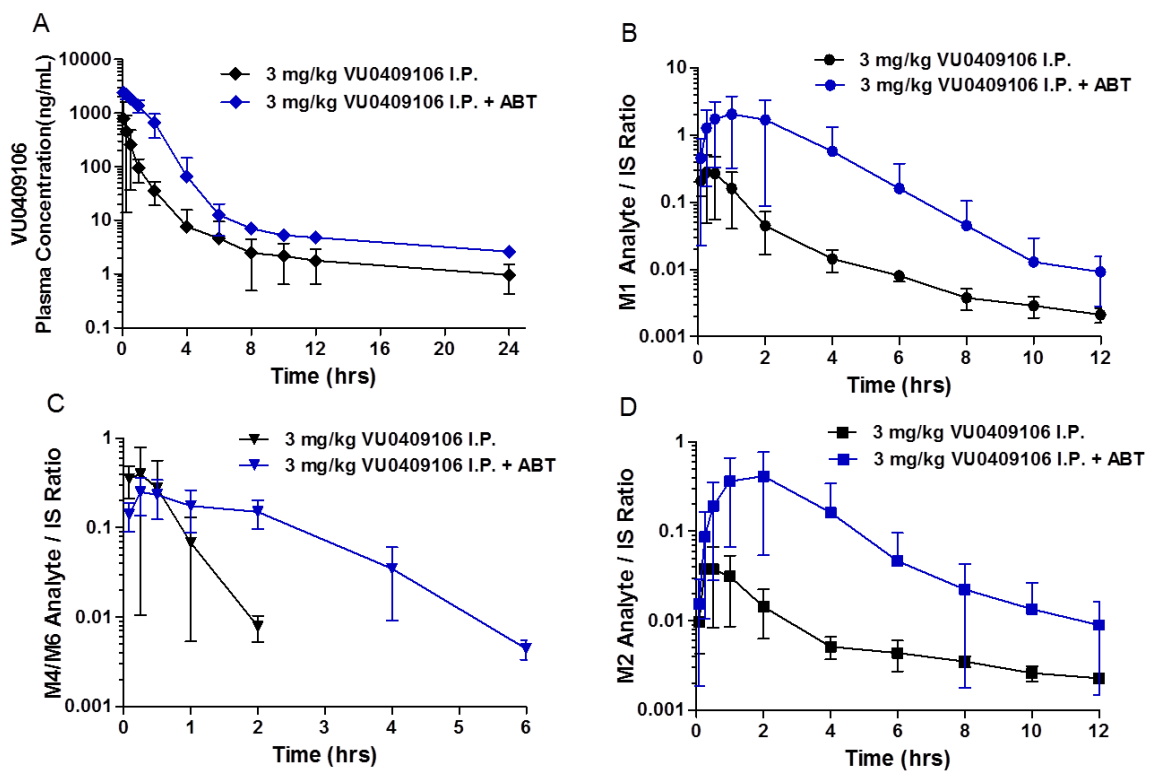


Figure III.8. Mean plasma concentration-time profiles of (A) VU0409106, (B) M1, (C) M4-M6, and (D) M2 following administration of VU0409106 to control (black) or ABT pretreated (blue) SD rats. Each data point represents the mean (\pm SD; $n = 2-3$ (control), $n = 3-4$ ABT pretreated).

Compound Dosed and Quantitated	Dose (route)	PK Parameter	Control	ABT	Mean Fold Over Control
VU0409106	1 mg/kg (IV)	CL (mL/min/kg)	53.5± 1.12	15.3 ± 1.19 **	0.29
		V _{ss} (L/kg)	0.994 ± 0.052	0.946 ± 0.005	0.95
		t _{1/2} (h)	0.215 ± 0.016	0.721 ± 0.061*	3.4
		AUC _{0-inf} (h*ng/mL)	311 ± 6.52	1099 ± 85.7 *	3.5
	3 mg/kg (IP)	C _{max} (ng/mL)	787 ± 782	2453 ± 589 *	3.1
		AUC _{0-inf} (h*ng/mL)	482 ± 247	3742 ± 970 **	7.8

Table III.4. Pharmacokinetic (PK) parameters of VU0409106 following the IV (1 mg/kg) or IP (3 mg/kg) administration of VU0409106 to control rats or rats pretreated with ABT. AUC = area under the plasma concentration-time curve; C_{max} = peak plasma concentration; CL = plasma clearance; t_{1/2} = half-life (t_{1/2} = MRT* ln2); V_{ss} = volume of distribution at steady-state. Data for control and ABT groups represent a mean of n = 2 (± SEM). Data for control (n = 3) and ABT (n = 4) groups represent a mean (± SD). Statistical analysis performed using a two-tailed unpaired t test. *p < 0.05, **p < 0.01.

M1

We also observed an increase in the exposure to the AO metabolite M1 in rats receiving the ABT pretreatment, with a 15-fold and 7.3-fold increases in the average AUC and C_{\max} values, respectively (Figure III.8B, Table III.5). We submit that this finding is consistent with the contributions of a shunting mechanism towards the AO pathway when P450 activity is attenuated by ABT (as was observed in hepatic S9 incubations of VU0409106 that were performed without NADPH). We previously reported that M1 is converted to M2 via XO, followed by an oxidative-defluorination to M3 (Figure III.1) (Morrison et al., 2012). Consequently, a substantial increase in M2 was also observed in rats as a result of ABT pretreatment (11-fold and 14-fold increase in mean C_{\max} and AUC, respectively) (Figure III.8D, Table III.5).

PK Parameter	M1			M2			M4-M6		
	Control (n = 3)	ABT (n = 4)	Mean Fold Over Control	Control (n = 3)	ABT (n = 4)	Mean Fold Over Control	Control (n = 3)	ABT (n = 4)	Mean Fold Over Control
C _{max}	0.282 ± 0.223	2.07 ± 1.74	7.3	0.038 ± 0.028	0.419 ± 0.351	11	0.400 ± 0.389	0.255 ± 0.113	0.64
AUC _{0-inf}	0.432 ± 0.269	6.65 ± 6.41	15	0.109 ± 0.044	1.51 ± 1.36	14	0.280 ± 0.254	0.590 ± 0.160	2.1

Table III.5. Pharmacokinetic (PK) parameters of metabolites M1, M2, and M4-M6 following an IP administration of VU0409106 (3 mg/kg) to control rats or rats pretreated with ABT. AUC and C_{max} of all metabolites reported as peak area ratio analyte/IS*h and analyte/IS, respectively. Data represent a mean (± SD).

While the increase in M2 can be explained by an increase in its precursor metabolite, M1, we considered the possibility that accumulation of M2 in ABT-pretreated rats occurred as a result of *reduced P450-mediated conversion* of M2→M3 (Figure III.1), with the potential to reduce the rate of M1 conversion to M2 (e.g., product inhibition). In order to investigate contributions of secondary P450-mediated metabolism of M2 to the observed plasma levels of M1, rats were orally administered either ABT (50 mg/kg), the XO inhibitor allopurinol (50 mg/kg), or a combination of the two inhibitors prior to the IP injection of compound VU0409106 (10 mg/kg). Similar to rats receiving the 3 mg/kg dose of VU0409106, rats receiving the 10 mg/kg dose displayed a 14-fold increase in the AUC of M2 when pretreated with ABT (Figure III.9A, Table III.6). M2 was below the detection limits in rats pretreated with the XO inhibitor allopurinol and was detectable only at the latter time points collected from rats pretreated with both allopurinol and ABT (these data points, therefore, are not shown in Figure III.9). Pretreatment with allopurinol revealed a relatively small increase of 2.6-fold in the AUC of M1 compared to a 9.1-fold increase following ABT pretreatment (Figure III.9B, Table III.6). Importantly, when rats were pretreated with both allopurinol and ABT, the AUC of M1 increased 15-fold (Figure III.9B, Table III.6). These data indicate that the accumulation of M1 from inhibition of the M2→M3 pathway is likely a minimal contributing factor towards the increase in M1 exposure in rats experiencing the ABT-induced DDI duress.

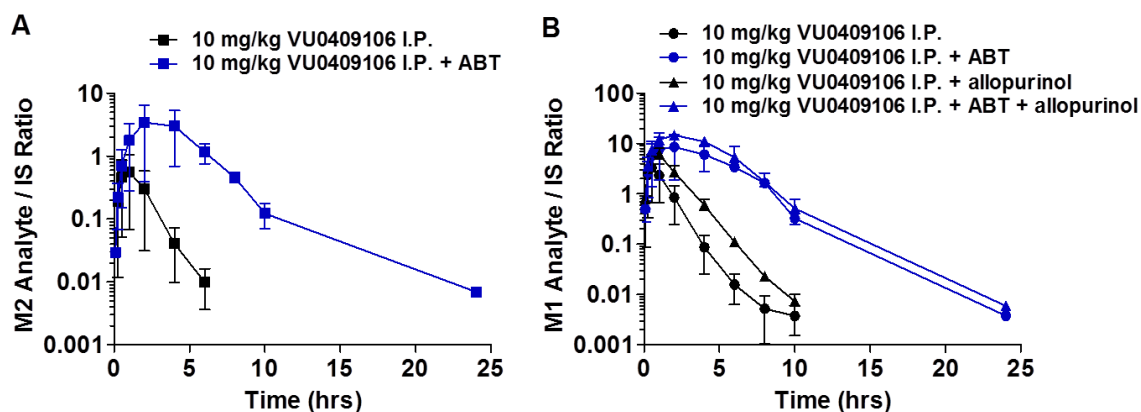


Figure III.9. Mean plasma concentration-time profiles of (A) M2 or (B) M1 after intraperitoneal administration of VU0409106 (10 mg/kg) to rats with or without an inhibitor. (A) Relative levels of M2 in rats pretreated with ABT (blue squares) versus control (black squares). (B) Relative levels of M1 in rats pretreated with ABT (blue circles), allopurinol (black triangles), or ABT + allopurinol (blue triangles) versus control (black circles). Data is expressed as the peak area ratio of analyte/internal standard and represent the mean (\pm SEM, $n = 2$).

Metabolite	Control	ABT	Mean Fold Over Control	Allopurinol	Mean Fold Over Control	Allopurinol + ABT	Mean Fold Over Control
M1	5.10 \pm 3.79	46.3 \pm 24.6	9.1	13.4 \pm 3.98	2.6	74.9 \pm 1.74 **	15
M2	1.20 \pm 1.10	17.1 \pm 11.9	14	n/a	n/a	n/a	n/a

Table III.6. Systemic exposure of metabolites M1 and M2 following an IP administration of VU0409106 (10 mg/kg) to control rats or rats pretreated with ABT, allopurinol, or allopurinol + ABT. AUC reported as peak area ratio (analyte/IS*h), as no authentic metabolite standards were available. Data represent a mean of $n = 2$ (\pm SEM). Statistical analyses performed using a two-tailed unpaired t test. ** $p < 0.01$.

M4-M6

The P450-mediated metabolites M4 and M6 were monitored to ascertain the impact of ABT pretreatment *in vivo* (Figure III.8C). Due to the complexity in the chromatographic resolution of M4 and M6, their isobaric mass, as well as their identical MS/MS transitions, LC/MS/MS peak areas of these metabolites were grouped accordingly, for the purpose of determining a semi-quantitative plasma concentration-time profile and exposure analysis as a measure of the contribution of P450 in the metabolism of VU0409106 *in vivo*. While a decrease was observed in the C_{max} of M4-M6 (0.64-fold), a 2.1-fold increase was observed in the AUC of these metabolites in the ABT pretreated rats (Table III.5). This observation may be due to alterations in the secondary metabolism and clearance mechanisms acting on M4 and/or M6.

Pretreatment of SD Rats with Hydralazine Mildly Increased Exposure to P450 Metabolites M4-M6

To evaluate the impact of AO inhibition on the disposition of VU0409106 and its metabolites, we also pretreated rats with the AO inhibitor hydralazine prior to an IP dose of 10 mg/kg VU0409106. Table III.7 lists the PK parameters for VU0409106, M1, M2, and M4-M6 in control rats or rats receiving hydralazine. Data for rats receiving ABT is included for comparison (Figure III.10, Table III.7). Interestingly, only a 1.3-fold increase in the AUC of VU0409106 was observed in rats pretreated with hydralazine, in comparison to the 4.8-fold increase observed in rats

receiving ABT pretreatment (Figure III.10A, Table III.7). As expected, decreases in the C_{max} and AUC of M1 (0.83-fold and 0.33-fold, respectively) and M2 (0.16-fold and 0.43-fold, respectively) were observed (Figure III.10B and D, Table III.7). As an increase in exposure to the AO metabolite M1 occurred when P450 metabolism was inhibited by ABT, an increase was also observed in the P450 metabolites M4-M6 (1.6-fold increase in AUC) when the AO inhibitor hydralazine was administered, albeit to a much lesser extent (Figure III.10C, Table III.7). In addition, the C_{max} was not increased, but rather decreased 0.77-fold in rats pretreated with hydralazine.

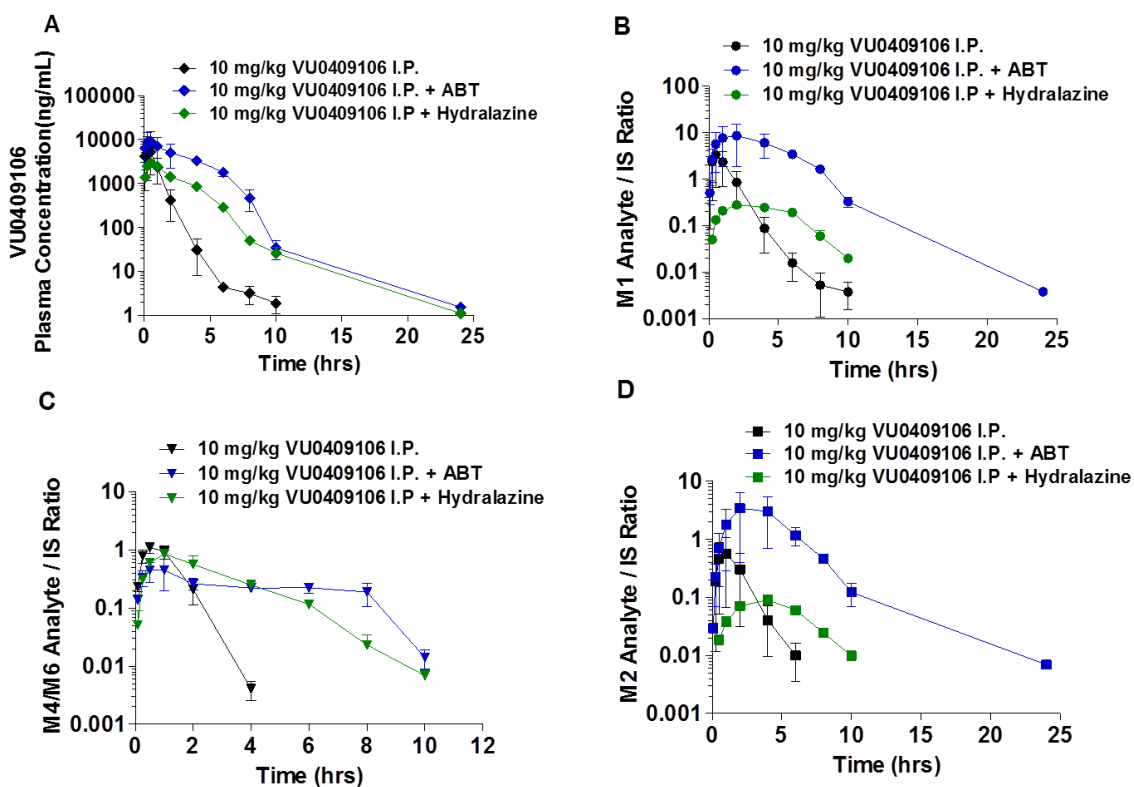


Figure III.10. Mean plasma concentration-time profiles of (A) VU0409106, (B) M1, (C) M4-M6, and (D) M2 following administration of VU0409106 to control (black), ABT pretreated (blue), or hydralazine pretreated (green) SD rats. Each data point represents the mean (\pm SEM, $n = 2$).

Compound	PK Parameter	Control	Hydralazine	Mean Fold Over Control	ABT	Mean Fold Over Control
VU0409106	C _{max} (ng/mL)	6520 ± 4980	2930 ± 90	0.44	9200 ± 5800	1.4
	AUC _{0-inf} (h*ng/mL)	6270 ± 4403	8406 ± 773	1.3	30264 ± 10424	4.8
M1	C _{max}	3.36 ± 2.68	0.280 ± 0.012	0.83	9.18 ± 6.13	2.7
	AUC _{0-inf}	5.10 ± 3.79	1.69 ± 0.088	0.33	46.3 ± 24.6	9.1
M2	C _{max}	0.562 ± 0.494	0.090 ± 0.018	0.16	3.60 ± 2.84	6.4
	AUC _{0-inf}	1.20 ± 1.10	0.527 ± 0.057	0.43	17.1 ± 11.9	14
M4-M6	C _{max}	1.11 ± 0.245	0.853 ± 0.024	0.77	0.490 ± 0.211	0.44
	AUC _{0-inf}	1.63 ± 0.466	2.57 ± 0.512	1.6	2.29 ± 0.071	1.4

Table III.7. Pharmacokinetic (PK) parameters of VU0409106 and metabolites M1, M2, and M4-M6 following an IP administration of VU0409106 (10 mg/kg) to control rats or rats pretreated with ABT or hydralazine. AUC and C_{max} of all metabolites reported as peak area ratio analyte/IS*h and analyte/IS, respectively. Data represent the mean (± SEM, n = 2).

M4, but not M6, was decreased in pooled plasma samples of rats pretreated with ABT.

While the M4-M6 AUC unexpectedly increased in ABT-pretreated rats, the significant increase in AUC and decrease in the total body CL of parent VU0409106 indicates ABT did inhibit P450-metabolism of VU0409106 *in vivo*. A possible explanation for this observation is that ABT also inhibited secondary metabolism of M4-M6. Alternatively, as M4 and M6 were quantified together, it is also possible that the AUC of one metabolite was increased, while that of the other was decreased, potentially resulting from differences in inhibitory activity towards enzymes responsible for formation and/or clearance of M4 and M6. Prior studies of ABT inhibitory activity towards human P450 enzymes found that P450 2C9 is only minimally impacted by ABT (60% remaining activity following 30 min pretreatment

of human liver microsomes with 1 mM ABT) (Linder et al., 2009); the differential inhibitory activity of ABT towards rat P450 isoforms is unknown. Consequently, we analyzed pooled plasma samples (1-6 hours) from rats pretreated with ABT relative to control rats using a 30 minute LC method to chromatographically resolve the two metabolites and found there to be an approximate 65% decrease in M4 compared to a 25% increase in M6 (Figure III.11), indicating ABT may have differentially impacted the disposition of the two metabolites. Conversely, when pre-treated with hydralazine, M4 was increased approximately 2-fold and M6 1.5-fold.

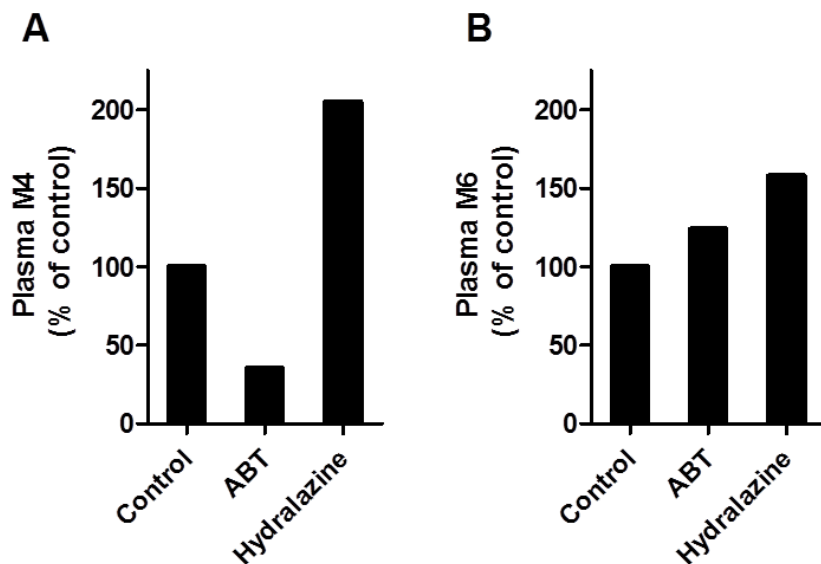


Figure III.11. Relative abundance of (A) M4 and (B) M6 detected in extracts of pooled plasma collected between 1-6 hours from rats ($n = 2$) receiving 10 mg/kg of VU0409106 alone or pretreated with 50 mg/kg ABT or 50 mg/kg hydralazine.

Similar Trends in VU0409106 and Metabolite Disposition in Response to Inhibitors in Crossover Experiment of Rats Receiving 1 mg/kg VU0409106 via Mesenteric Vein Administration

In addition, we conducted a crossover experiment, where rats were administered VU0409106 via the mesenteric vein (as a surrogate for hepatic portal vein administration, as the mesenteric ileal vein drains into the hepatic portal vein) either with vehicle, ABT, or hydralazine pretreatment with a one week washout in between each dosing group. This experiment was designed to reduce potential sources of variability associated with the absorption phase in IP dosing or possible inter-individual variability in AO activity. A pilot study was first conducted to ensure similar exposures were obtained via both hepatic portal vein (n = 2) and mesenteric ileal vein (n = 1) administration (Figure III.12), and a similar VU0409106 AUC was indeed obtained via mesenteric ileal vein administration and hepatic portal vein administration (Table III.8).

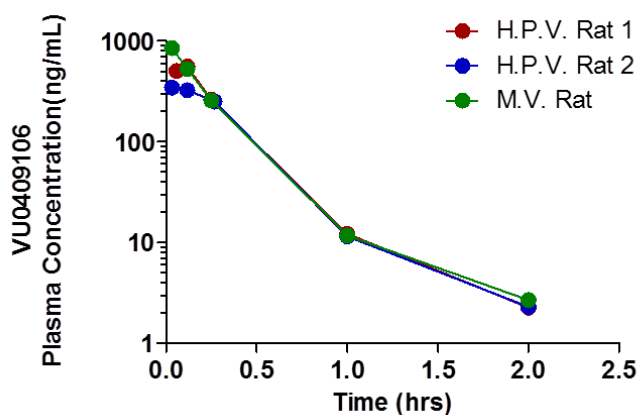


Figure III.12. Individual plasma concentration-time profiles of VU0409106 following administration of VU0409106 via the hepatic portal vein (red and blue) or the mesenteric ileal vein (green) to SD rats.

Animal (Route of Administration)	AUC _{0-inf} (h*ng/mL)
H.P.V. 1	211
H.V.P. 2	180
M.V.	231

Table III.8. Exposure of VU0409106 in SD rats receiving VU0409106 via the hepatic portal vein or the mesenteric ileal vein.

Mean pharmacokinetics of VU0409106 and metabolites

Following inhibitor pretreatment, similar pharmacokinetic trends were again observed, though the average magnitude of change was smaller (Table III.9) versus previous IP dosing studies. The AUC of VU0409106 was increased 2.0-fold and 2.9-fold when rats were pretreated with hydralazine and ABT, respectively, along with 1.5 and 1.9-fold increases in C_{max}, respectively. Relative to vehicle pretreatment, the C_{max} and AUC of M1 was increased (1.3-fold and 2.0-fold, respectively) when rats were pretreated with ABT, and decreased (0.49-fold and 0.51-fold, respectively) when pretreated with hydralazine. The C_{max} of M4-M6, conversely, was increased 1.5-fold and decreased 0.67-fold when rats received hydralazine and ABT pretreatment, respectively. While the AUC was increased 1.9-fold in the hydralazine group, the AUC for the ABT group was again increased 1.4-fold rather than decreased as would be anticipated under conditions of P450 inhibition.

Compound	PK Parameter	Control	Hydralazine	Mean Fold Over Control	ABT	Mean Fold Over Control
VU0409106	C _{max} (ng/mL)	856 ± 485	1253 ± 255	1.5	1640 ± 269	1.9
	AUC _{0-inf} (h*ng/mL)	199 ± 86.6	404 ± 126 *	2.0	570 ± 150 **	2.9
M1	C _{max}	2.54 ± 1.91	1.24 ± 1.63	0.49	3.35 ± 2.49	1.3
	AUC _{0-inf}	1.56 ± 1.16	0.791 ± 0.930	0.51	3.14 ± 1.92	2.0
M2	C _{max}	0.331 ± 0.292	0.131 ± 0.185	0.40	0.762 ± 0.725	2.3
	AUC _{0-inf}	0.205 ± 0.150	0.086 ± 0.104	0.42	0.529 ± 0.318	2.6
M4-M6	C _{max}	0.326 ± 0.096	0.477 ± 0.148	1.5	0.217 ± 0.073	0.67
	AUC _{0-inf}	0.136 ± 0.030	0.259 ± 0.020 *	1.9	0.184 ± 0.041	1.4

Table III.9. Mean pharmacokinetic (PK) parameters of VU0409106 and metabolites M1, M2, and M4-M6 following an administration of VU0409106 (1 mg/kg) via the mesenteric vein to control rats or rats pretreated with ABT or hydralazine. AUC and C_{max} of all metabolites reported as peak area ratio analyte/IS*h and analyte/IS, respectively. Data represent a mean of $n = 3$ (\pm SD). Statistical analysis performed using a two-tailed paired t test. * $p < 0.05$, ** $p < 0.01$.

Individual pharmacokinetics of VU0409106 and metabolites.

Individual plasma concentration-time profiles for VU0409106 and the M1 and M4-M6 metabolites in each rat are displayed in Figure III.13. In each case, when rats were pretreated with ABT, an increase in the exposure of both the parent VU0409106 and the M1 metabolite were observed (Figure III.13A and B, Table III.10). Rat B exhibited approximately 10-fold lower exposure to the M1 metabolite relative to rats A and C. In contrast, concentrations of the M4-M6 metabolites were relatively similar among the three animals (Figure III.13C, Table III.10). Interestingly, though the VU0409106 exposure in rat B was higher than rats A and C, it did not reach 10-fold higher exposure as might be expected considering the 10-fold lower exposure to M1. M2 exposure in rat B was also decreased approximately

10-fold relative to rats A and C, suggesting that the comparatively decreased levels of M1 were not a result of increased conversion to M2.

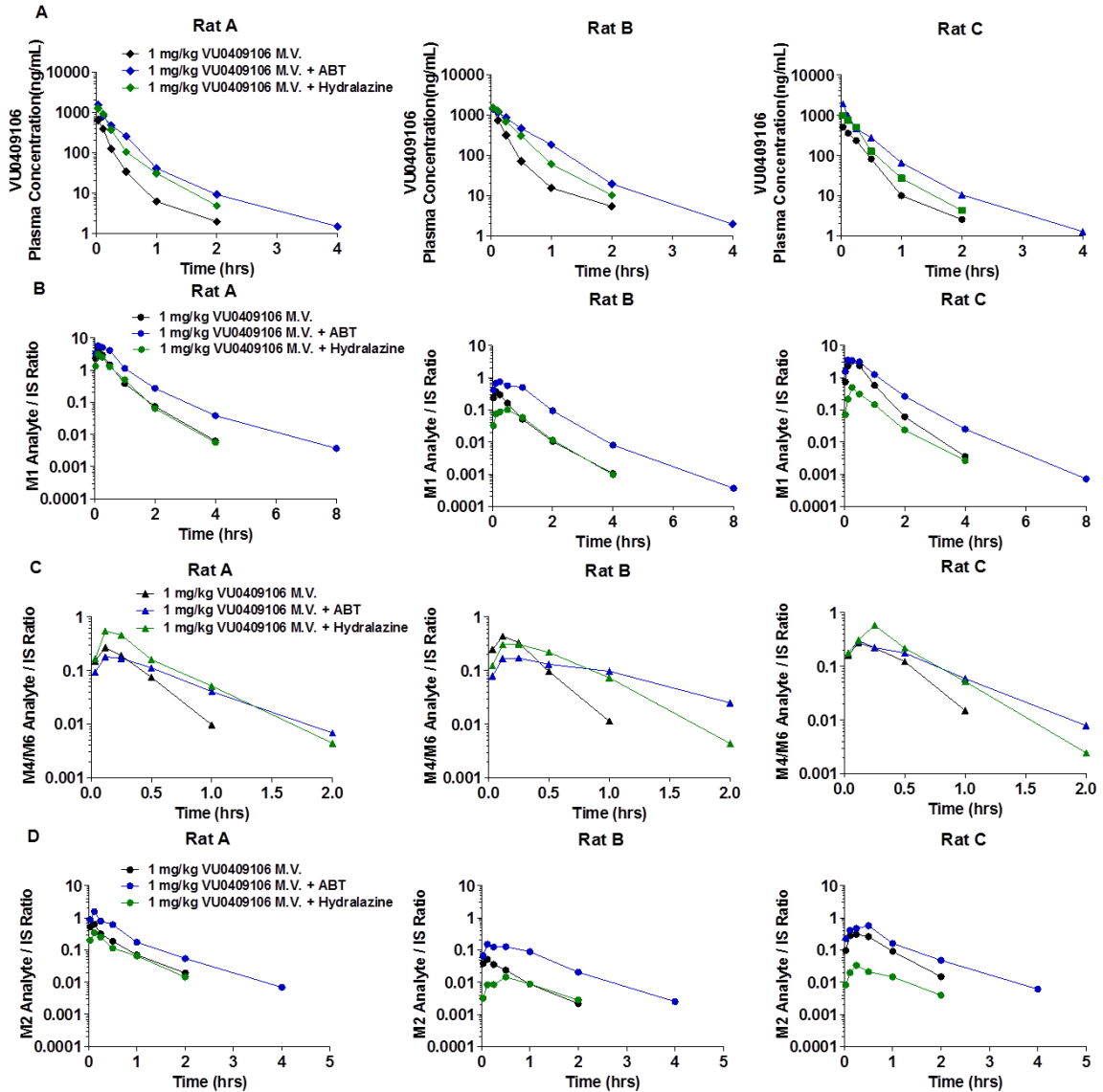


Figure III.13. Individual plasma concentration-time profiles of (A) VU0409106, (B) M1, (C) M4-M6, and (D) M2 following MV administration of VU0409106 to control (black) ABT, (blue) or hydralazine pretreated (green) SD rats. Each of the three rats first received vehicle pretreatment, then after one week washout was crossed over to ABT pretreatment, and then finally hydralazine pretreatment after one week washout.

Compound	Rat	PK Parameter	Control	Hydralazine	Fold Over Control	ABT	Fold Over Control
VU0409106	A	C _{max} (ng/mL)	645	1250	1.9	1560	2.4
		AUC _{0-inf} (h*ng/mL)	136	334	2.5	449	3.3
	B	C _{max} (ng/mL)	1410	1510	1.1	1420	1.0
		AUC _{0-inf} (h*ng/mL)	298	550	1.8	737	2.5
	C	C _{max} (ng/mL)	512	1000	2.0	1940	3.8
		AUC _{0-inf} (h*ng/mL)	164	328	2.0	523	3.2
M1	A	C _{max}	3.97	3.11	0.78	5.71	1.4
		AUC _{0-inf}	2.09	1.85	0.89	4.69	2.2
	B	C _{max}	0.375	0.102	0.27	0.756	2.0
		AUC _{0-inf}	0.229	0.128	0.56	1.00	4.4
	C	C _{max}	3.28	0.500	0.15	3.58	1.1
		AUC _{0-inf}	2.36	0.390	0.17	3.73	1.6
M2	A	C _{max}	0.634	0.344	0.54	1.56	2.5
		AUC _{0-inf}	0.304	0.206	0.68	0.826	2.7
	B	C _{max}	0.051	0.014	0.27	0.151	2.9
		AUC _{0-inf}	0.033	0.019	0.58	0.193	5.8
	C	C _{max}	0.309	0.034	0.11	0.571	1.8
		AUC _{0-inf}	0.277	0.033	0.12	0.566	2.0
M4-M6	A	C _{max}	0.268	0.537	2.0	0.179	0.67
		AUC _{0-inf}	0.107	0.258	2.4	0.136	1.3
	B	C _{max}	0.437	0.308	0.7	0.17	0.39
		AUC _{0-inf}	0.167	0.239	1.4	0.211	1.3
	C	C _{max}	0.272	0.584	2.1	0.301	1.1
		AUC _{0-inf}	0.135	0.279	2.1	0.204	1.5

Table III.10. Individual pharmacokinetic (PK) parameters of VU0409106 and metabolites M1, M2, and M4-M6 following an administration of VU0409106 (1 mg/kg) via the mesenteric vein to rats A, B, and C when pretreated with either vehicle (control), ABT, or hydralazine. AUC and C_{max} of all metabolites reported as peak area ratio analyte/IS*h and analyte/IS, respectively.

DISCUSSION

While successful approaches have been developed to evaluate the impact of enzyme inhibitors and inducers on P450-mediated drug clearance and subsequent changes in drug exposure for prediction of clinical drug interactions (Zhang et al., 2009; Di et al., 2013), approaches towards predicting drug interaction potential of NCEs undergoing *non* P450 metabolism are less established, much less those exhibiting both P450 and AO clearance routes. Recognition of AO and P450 contributions to the clearance of VU0409106 *in vitro* and *in vivo* provided an opportunity to investigate how P450 inhibition may impact the disposition and PK of a mixed AO:P450 substrate and its metabolites. Similarities between rat and human *in vitro* metabolism of VU0409106 permitted the use of rat as a nonclinical P450 inhibition model, which revealed a trend towards increased exposure to the AO metabolite M1 in rats with ABT-attenuated P450 activity (Figure III.14).

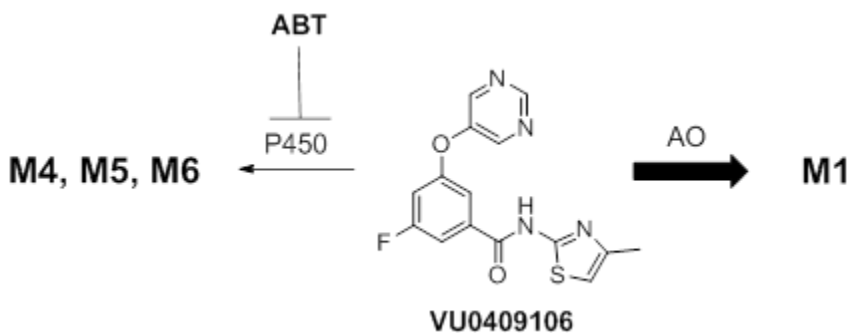


Figure III.14. Increase in M1 formation observed in rats following ABT inhibition of P450.

In principle, co-administration of a perpetrator drug could result in observed elevations in metabolite plasma levels as a consequence of several possible mechanisms: a) decreased metabolite clearance due to inhibition of secondary metabolism, b) metabolic activation (stimulation of enzyme activity), c) enzyme induction, or d) metabolic shunting towards the uninhibited pathway (e.g., AO) when another pathway is inhibited (e.g., P450). It is unlikely that the elevated M1 levels were due to a decrease in M1 clearance in rats pretreated with ABT, as the major M1 clearance pathway *in vitro* was previously determined to be XO-mediated metabolism to M2 (Morrison et al., 2012). While the activation of AO has been previously suggested (Nirogi et al., 2014), the present increased M1 formation observed in hepatic S9 fractions *absent* NADPH relative to NADPH-containing reactions support a mechanism independent of ABT-mediated cooperativity on AO. Furthermore, prior data from our laboratory outlining incubations of VU0409106 with hepatocytes revealed no increase in M1 formation when ABT was present. Finally, while the induction of *AOX1/Aox1* in mice, rats, and rabbits (Garattini and Terao, 2012) has been demonstrated, an induction mechanism accounting for our observations is highly unlikely, given the single dose study design and duration thereof. Our observed increase in M1, therefore, appears to have primarily resulted from a condition of increased substrate availability to AO when the P450 pathway(s) of metabolism was attenuated. In additional support of this mechanism, the decrease in NADPH-dependent S9 CL_{int} (P450 pathway), with a maintenance of NADPH-independent S9 CL_{int} (AO pathway) with increased concentrations of

VU0409106, indicates a lower $K_{m, P450}$ relative to the $K_{m, AO}$, according to the relationship:

$$CL_{int,total} = \left(\frac{V_{max,AO}}{K_{m,AO} + S} \right) + \left(\frac{V_{max,P450}}{K_{m,P450} + S} \right)$$

Equation III.1. Relationship between Michaelis-Menten parameters, V_{max} and K_m , and intrinsic clearance (CL_{int}).

where V_{max} is the maximum reaction velocity of the enzyme, K_m is the substrate concentration that yields half the maximal velocity, and S is the substrate concentration (Pang and Rowland, 1977). Incidentally, our findings associate an increase in metabolite exposure with the co-administration of VU0409106 and an enzyme *inhibitor*, whereas this type of DDI situation would typically be anticipated with co-administration of a victim drug and an enzyme inducer or stimulator. We might have expected this metabolic shunting observation to prevent an extensive increase in the AUC of VU0409106, with AO compensating for loss of P450 activity. However, as ABT is a *pan*-P450 inactivator, we have likely forced the shunt towards a single enzyme (AO), potentially limiting the capacity for compensation (versus inhibiting one enzyme with the possibility of shunting towards multiple enzymes).

Besides significant increases in exposure to the parent compound VU0409106, mean increases observed in the AUC and C_{max} of the AO metabolite M1 highlight the potential for a drug interaction resulting from increased exposure to a *metabolite* of a drug with both AO and P450 clearance routes when co-administered with a P450 inhibitor. Clinically used drugs exhibiting a major clearance pathway

via AO are few, and to date, no clinically relevant DDIs resulting from AO inhibition have been recognized, despite the identification of many clinical drugs demonstrating AO inhibition *in vitro* (Obach et al., 2004). However, our data indicate that inhibition of alternate clearance routes (e.g., P450) for drugs also metabolized by AO may result in elevation of a circulating AO-mediated metabolite, which, importantly, could have clinical implications when metabolites exhibit pharmacological or toxicological activity (Smith and Obach, 2005). For example, cases of dose-dependent renal toxicity associated with AO-mediated formation of a low-solubility metabolite have been reported for methotrexate (Smeland et al., 1996) and the two c-Met inhibitors SGX523 and JNJ-38877605, recently discontinued in clinical trials (Infante et al., 2013; Lolkema et al., 2015). Additionally, the primary circulating metabolite of idealisib, GS-563117, is a mechanism-based inhibitor of P450 3A, which is not the case for the parent drug. In this instance, however, both AO and P450 3A (minor) contribute to the formation of GS-563117 (Ramanathan et al., 2016).

While a small percentage of currently marketed drugs are cleared via AO, a 2010 study indicated the proportion of NCEs in research and development containing potentially AO-susceptible moieties is much higher (Pryde et al., 2010). Drug discovery scientists are more frequently encountering AO metabolism due to incorporation of nitrogen-containing aromatic rings for either target engagement (e.g. kinases) or mitigation of P450 metabolism (reduced lipophilicity). As many AO substrates (e.g., zaleplon and idealisib) are known to also undergo metabolism via enzymes other than AO (Strelevitz et al., 2012; Ramanathan et al., 2016), it is likely

that current and future NCEs exhibiting AO metabolism will also undergo metabolism via alternate enzymes. As such, metabolic shunting may be important to consider during toxicology and DDI assessment of these compounds. Likewise, this consideration may also be important for NCEs not displaying AO metabolism without concomitant administration of an enzyme inhibitor, yet containing an AO-susceptible structural moiety (potential for metabolic switching (Li et al., 2012a; Li et al., 2012b)). The likelihood of substantial elevations in metabolite exposure (via metabolic shunting) may be increased for drugs cleared by both AO and P450 enzymes versus drugs cleared only by multiple P450 pathways, as different P450 enzymes commonly generate the same metabolite, in which case the metabolite would be expected to be generated at decreased or similar levels when one of the P450 pathways is inhibited.

While the P450 inhibition aspect of these studies bears potential clinical significance due to the number of known P450-inhibiting drugs on the market, our studies in rats pretreated with the AO inhibitor hydralazine also indicate a potential for shunting towards P450 metabolism when a mixed AO/P450 substrate is co-administered with an AO inhibitor. Several factors, however, may complicate the interpretation of the *in vivo* data obtained from rats receiving hydralazine pretreatment. First of all, the therapeutic action of hydralazine is vasodilatation. For this reason, it is possible that hydralazine altered hepatic blood flow, in which case any changes in the disposition of VU0409106 and its metabolites may not be the result of changes in AO-mediated intrinsic clearance alone, but also changes in hepatic blood flow, according to the well-stirred model of hepatic drug clearance:

$$CL_{HEP} = \frac{Q_H \times f_u CL_{int}}{Q_H + f_u CL_{int}}$$

Equation III.2. Well stirred model of hepatic clearance.

where CL_{HEP} is hepatic clearance, Q_H is hepatic blood flow, f_u is the unbound drug fraction, and CL_{int} is intrinsic clearance (Wilkinson, 1987). Wolf et al. and Saretok et al. reported that hydralazine increased hepatic blood flow by approximately 30% in healthy human subjects (Wolf et al., 1994) and by 57% in normovolemic dogs (Saretok et al., 1984), respectively. In addition, a report by Svensson et al. found that administration of a 7.5 mg/kg oral hydralazine pretreatment to male SD rats resulted in a small, but significant, decrease in antipyrine plasma clearance, which was proposed to be associated with hypothermia in animals receiving hydralazine (Svensson et al., 1987). Furthermore, while hydralazine is considered to be a selective inhibitor of AO, it has been reported to potentially inhibit P450 2D6 as well (Strelevitz et al., 2012; Zientek and Youdim, 2015). The rat P450 inhibition profile of hydralazine is not known, and we did not conduct reaction phenotyping of VU0409106 to determine which rat isoforms are responsible for M6 formation; however, we did find that M6 was generated in incubations with recombinant human 2D6. Altogether, these factors limit the interpretation of the PK analysis in rats treated with hydralazine. A specific AO inhibitor without these potentially confounding characteristics (which is presently unavailable) would be required to better understand the impact of AO inhibition *in vivo*.

In conclusion, our studies with VU0409106 and ABT using rat as a nonclinical PK model revealed increased exposure to both the parent drug and the AO metabolite. The present investigation highlights the potential drug interactions that may occur with co-administration of a P450 inhibitor and a mixed AO/P450 substrate. The similarities we observed *in vitro* between SD rat and human in the formation of AO and P450 metabolites, trends in the impact of P450 activity on the formation of M1, and in the kinetic behavior of the two enzymatic pathways indicate that our observations *in vivo* in rat may translate to human *in vivo*. We submit that rat may offer a nonclinical model to probe drug interactions (and mechanisms thereof) where a *mixed AO:P450 substrate* experiences a clinical drug interaction duress, while underscoring the potential existence of the *compound-dependent* use of nonclinical models to predict AO-mediated interactions. As investigators are more frequently encountering AO metabolism through the drug discovery and development continuum, understanding the drug interaction potential for drugs exhibiting an AO clearance component will be important in the successful advancement and safe clinical implementation of future drug candidates bearing this nonP450 phenotype.

CHAPTER IV

ALLOMETRIC SCALING OF IN VITRO HEPATIC CLEARANCE OF DRUGS POSSESSING AN ALDEHYDE OXIDASE CLEARANCE PATHWAY IN HUMAN

INTRODUCTION

As noted previously, interest in AO-mediated drug metabolism has increased in recent years as new generations of drug candidates increasingly contain AO-susceptible aromatic azaheterocycles (Pryde et al., 2010). Importantly, the termination of several promising development programs during clinical trial assessment due to unrecognized or underestimated AO metabolism highlights the necessity for innovative approaches to predict human pharmacokinetics (PK) and disposition where AO is the primary clearance mechanism. For example, discontinuation of BIBX1382 (Dittrich et al., 2002), FK3453 (Akabane et al., 2011), and RO1 (Zhang et al., 2011) during clinical trials resulted from unexpectedly poor oral bioavailability attributed to AO-mediated clearance that went unidentified in preclinical and *in vitro* studies. Primary use of microsomes (lacking cytosol, thus lacking AO) and preclinical species with decreased (e.g., rat) or absent (e.g., dog) AO activity towards these candidate drugs relative to humans was deemed responsible for their clinical failures.

A challenge in predicting human drug clearance where AO-mediated metabolism predominates has been attributed to species differences in AO

expression and activity. While humans express only one functional gene, *AOX1*, AO expression in other species commonly used to model human PK range anywhere from 2-4 isoforms (e.g., rat) to none at all (e.g., dog, except for non-liver isoforms) (Garattini and Terao, 2012). Human liver S9, cytosolic fractions, and hepatocytes have proven useful in identifying AO metabolism, although at times these systems have resulted in under-prediction or variable activity, proposed to be associated with possible single nucleotide polymorphisms (SNPs) in the *AOX1* gene, instability of the dimer, or deficiency of the essential molybdenum cofactor (Hartmann et al., 2012; Hutzler et al., 2012; Fu et al., 2013; Hutzler et al., 2014b). Consequently, promising compounds are routinely discarded or structurally modified to eliminate AO metabolism, often at the expense of pharmacological potency and/or selectivity.

The most common methods for estimating human clearance include *in vitro* and *in vivo* approaches (Obach et al., 1997) (Di et al., 2013). *In vitro* systems are commonly employed when metabolism represents the primary mechanism of clearance, where clearance is measured in human hepatocytes or hepatic microsomes and is subsequently scaled up to estimate an *in vivo* (hepatic) clearance (Obach et al., 1997; Di et al., 2013). An alternative approach is to use allometry to predict human *in vivo* clearance via extrapolation from the *in vivo* clearance of preclinical species, where clearance is related to body weight (Obach et al., 1997; Di et al., 2013). While research has been conducted to evaluate human *in vitro* methods to predict AO-mediated clearance (Zientek et al., 2010; Akabane et al., 2012; Hutzler et al., 2012; Hutzler et al., 2014b), studies investigating allometric scaling approaches are limited. Allometric scaling of *in vivo* plasma clearance in

nonclinical species is commonly used to predict human total body clearance of drugs eliminated renally and/or via hepatic metabolism (Mahmood, 2007). However, differences observed in AO expression and activity of species commonly employed in allometric scaling (particularly dog) versus that of human have resulted in decreased confidence in the utility of this method (Garattini and Terao, 2012). Interestingly, despite variability across species in the uridine diphosphate-glucuronosyltransferase (UGT)-mediated clearance of several drugs, success with single- or multi-species allometry in predicting human clearance of these drugs has been demonstrated (Deguchi et al., 2011). Several of these compounds are also metabolized by cytochrome P450s (P450), a factor that may have contributed to the successful scaling, given the established ability to reasonably predict human P450-mediated clearance with allometry (Hosea et al., 2009). Furthermore, while rat underestimated the human plasma clearance of the AO substrate BIBX1382, a report by Hutzler et al. demonstrated comparable BIBX1382 plasma clearance (as a percentage of liver blood flow) between cynomolgus monkey and human, indicating single-species scaling (SSS) may be useful in predicting the clearance of drugs subject to AO metabolism (assuming appropriate species selection) (Hutzler et al., 2014a). Given these findings, we sought to investigate the use of these allometric scaling approaches in predicting the human clearance of AO substrates. However, an additional complication in predicting AO-mediated human clearance is the extra-hepatic expression of AO (Kurosaki et al., 1999; Moriwaki et al., 2001; Nishimura and Naito, 2006; Terao et al., 2016), which is presently understudied, particularly in species other than rodent and human. In particular, the contribution of extra-

hepatic AO metabolism to the total body clearance of AO substrates is poorly understood. Thus, we sought to evaluate the ability to allometrically scale *hepatic* intrinsic clearance of compounds exhibiting an AO metabolic pathway, utilizing hepatic S9 to accomplish this aim. Specifically, the *in vitro* intrinsic clearance (CL_{int}) of five compounds (Figure IV.1) known to be cleared either predominantly or partially by AO in human, was determined in hepatic S9 from multiple preclinical species (mouse, rat, guinea pig, cynomolgus monkey, rhesus monkey, and minipig) and was subsequently subjected to allometric scaling by either multi- or single-species allometry for the prediction of human *in vitro* hepatic CL_{int} . In anticipation that $F_{m,AO}$ (fraction of metabolism mediated by AO) or estimated hepatic extraction (E) between human and preclinical species may influence the accuracy of the human CL_{int} prediction obtained by these scaling methods, we estimated $F_{m,AO}$ and E for the five substrates in each species and evaluated the correlation between these parameters and prediction accuracy by SSS. In addition, we evaluated the biotransformation of each substrate in each of the seven species to understand the metabolic pathways potentially contributing to any species differences observed in the *in vitro* clearance of these substrates. These *in vitro* studies may prove useful in serving as a tool to guide species selection for *in vivo* pharmacokinetic (PK) studies and subsequent allometric scaling of *in vivo* plasma clearance (CL_p) for prediction of human *in vivo* CL_p . In a recent review on nonP450-mediated metabolism, Cerny noted the need to improve *in vitro*-to-*in vivo* extrapolation methods for predicting *in vivo* clearance via these enzymes (Cerny, 2016). The studies presented herein serve

as a step in this direction, towards a better understanding of how to predict human clearance of AO substrates.

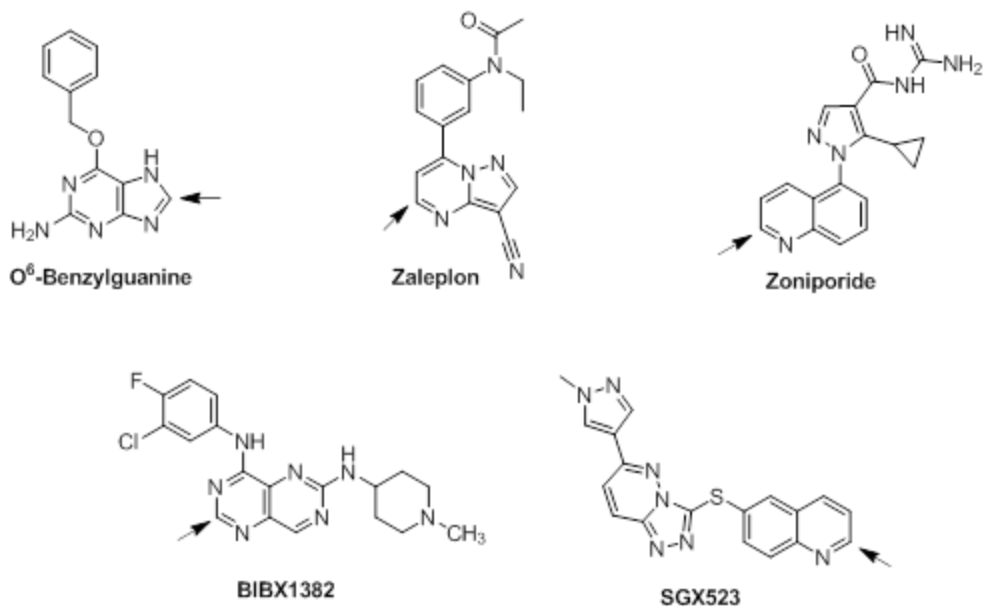


Figure IV.1. Structures of AO substrates subjected to *in vitro* allometric scaling. Arrows indicate site of AO oxidation.

RESULTS

Intrinsic Clearance in Hepatic S9 Fractions

Intrinsic clearance (CL_{int}) estimates measured in hepatic S9 fractions of human and nonclinical species are summarized in Table IV.1. These data represent estimates from incubations in the presence of NADPH, thus encompassing clearance mediated by NADPH-independent (e.g., AO) as well as any NADPH-dependent (e.g. P450) pathways. Hepatic clearance (CL_{HEP}) in each species was also estimated using the well-stirred model, uncorrected for fraction unbound in plasma, and is summarized in Table IV.2. Table IV.2 also lists the estimated hepatic extraction (E). For the purpose of this discussion, the *in vitro* clearance estimates described as low, moderate, or high are characterized as such according to the E value, where $E \leq 0.3$ is considered “low,” and $E \geq 0.7$ is considered “high,” and values falling between 0.3 and 0.7 are considered “moderate.” CL_{int} estimates for zaleplon were generally low, with E estimated to be ≤ 0.32 in each species. O⁶-benzylguanine CL_{int} estimates were moderate in human, monkey, and guinea pig and lower in rat, mouse and minipig, resulting in E estimates that ranged from approximately 0.1 (rat, mouse, minipig) to approximately 0.5 (human, cynomolgus, and guinea pig). Conversely, zoniporide was moderately cleared in human, monkey, guinea pig, and minipig S9 incubations ($E = 0.41 - 0.59$), while it was rapidly cleared in incubations with rat and mouse S9 ($E = 0.87$ and 0.79 , respectively). Estimated CL_{int} of BIBX1382 was high in human, monkey, and minipig ($E = 0.72 - 0.83$), moderate in guinea pig ($E = 0.54$), and low in rat and mouse ($E = 0.30$ and 0.27 , respectively). SGX523 exhibited low-moderate

clearance in all species, with E ranging from 0.25 – 0.50. No single species was fully representative of human when considering E for each compound, but rather, substrate-dependence was observed. However, E estimated in monkey was most similar to human overall, followed by guinea pig and minipig, with rat and mouse generally providing the worst representation of human E.

	Zaleplon	O ⁶ -Benzylguanine	Zoniporide	BIBX1382	SGX523
Human	5.8 ± 1.02	17.8 ± 1.94	17.9 ± 1.77	80.2 ± 9.61	7.1 ± 2.28
Mouse	24.4 ± 5.28	20.7 ± 7.10	332 ± 11.3	33.2 ± 7.10	39.4 ± 7.19
Rat	15.6 ± 3.05	8.3 ± 2.03	466 ± 27.0	30.7 ± 3.56	35.3 ± 6.39
Guinea Pig	14.2 ± 1.89	60.3 ± 4.29	79.9 ± 7.47	72.7 ± 4.05	42.4 ± 4.71
Cynomolgus Monkey	20.3 ± 2.45	42.5 ± 8.40	62.8 ± 8.34	181 ± 11.5	44.4 ± 5.60
Rhesus Monkey	15.0 ± 2.06	22.9 ± 3.98	30.2 ± 3.29	114 ± 7.46	29.6 ± 7.22
Minipig	5.55 ± 1.34	4.43 ± 1.44	23.4 ± 2.07	134 ± 5.69	25.4 ± 1.46

Table IV.1. Multispecies intrinsic clearance (CL_{int}, mL/min/kg) of zaleplon, O⁶-benzylguanine, zoniporide, BIBX1382, and SGX523 in incubations with hepatic S9 of human (mixed gender), and male mouse, rat, guinea pig, cynomolgus monkey, rhesus monkey, and minipig (in the presence of NADPH). Data represent means of triplicate determinations from 2-3 experiments (± SD).

	Zaleplon		O ⁶ -Benzylguanine		Zoniporide		BIBX1382		SGX523	
	CL _{HEP}	E	CL _{HEP}	E	CL _{HEP}	E	CL _{HEP}	E	CL _{HEP}	E
Human	4.55 ± 0.625	0.22	9.62 ± 0.593	0.46	9.64 ± 0.503	0.46	16.6 ± 0.417	0.79	5.22 ± 1.15	0.25
Mouse	19.0 ± 3.35	0.21	16.6 ± 4.51	0.18	70.8 ± 0.517	0.79	24.1 ± 3.85	0.27	27.2 ± 3.66	0.30
Rat	12.7 ± 2.10	0.18	7.40 ± 1.61	0.11	60.8 ± 0.485	0.87	21.3 ± 1.73	0.30	23.3 ± 2.85	0.33
Guinea Pig	11.5 ± 1.25	0.19	30.3 ± 1.11	0.50	34.5 ± 1.40	0.57	33.1 ± 0.838	0.54	24.9 ± 1.64	0.41
Cynomolgus Monkey	13.9 ± 1.16	0.32	21.4 ± 2.28	0.49	25.8 ± 1.43	0.59	35.4 ± 0.434	0.80	22.0 ± 1.39	0.50
Rhesus Monkey	11.2 ± 1.14	0.25	15.0 ± 1.75	0.34	17.9 ± 1.16	0.41	31.7 ± 0.593	0.72	17.5 ± 2.69	0.40
Minipig	4.60 ± 0.934	0.16	3.79 ± 1.04	0.14	12.7 ± 0.620	0.45	23.1 ± 0.170	0.83	13.3 ± 0.401	0.48

Table IV.2. Multispecies hepatic clearance (CL_{HEP}, mL/min/kg) of zaleplon, O⁶-benzylguanine, zoniporide, BIBX1382, and SGX523 in incubations with hepatic S9 (in the presence of NADPH) and the estimated hepatic extraction ratio (E). Data, calculated using CL_{int} values from Table IV.1, represent means of triplicate determinations from 2-3 experiments (± SD).

In addition, comparison of the relative intrinsic clearance for each substrate within any one species (Table IV.1) reveals that the rank order for monkey and guinea pig was the most similar to human, while mouse and rat rank order was the most dissimilar to human. It is important to note, however, that, in some cases, the rank order was determined by a very small difference in CL_{int} between substrates (e.g., zoniporide and O⁶-benzylguanine in human). The substrate rank order of CL_{int} for each species is summarized in Table IV.3.

Species	Rank Order of Intrinsic Clearance
Human	BIBX1382 > zoniporide > O ⁶ -benzylguanine > SGX523 > zaleplon
Cynomolgus Monkey	BIBX1382 > zoniporide > SGX523 > O ⁶ -benzylguanine > zaleplon
Rhesus Monkey	BIBX1382 > zoniporide > SGX523 > O ⁶ -benzylguanine > zaleplon
Rat	zoniporide > SGX523 > BIBX1382 > zaleplon > O ⁶ -benzylguanine
Mouse	zoniporide > SGX523 > BIBX1382 > zaleplon > O ⁶ -benzylguanine
Minipig	BIBX1382 > SGX523 > zoniporide > zaleplon > O ⁶ -benzylguanine
Guinea Pig	zoniporide > BIBX1382 > O ⁶ -benzylguanine > SGX523 > zaleplon

Table IV.3. Substrate rank order of intrinsic clearance obtained from incubations with multiple species' hepatic S9 in the presence of NADPH.

Estimation of $F_{m,A0}$ in Hepatic S9 Fractions

Tables IV.4-8 summarize $F_{m,A0}$ estimated for each compound in each species from incubations with male hepatic S9 (mixed gender for human) using two different methods, A and B (see Equations II.4 and II.5, respectively). $F_{m,A0}$ obtained for O⁶-benzylguanine, zaleplon, zoniporide, and BIBX1382 in human is consistent with those previously reported by others (Hutzler et al., 2012; Strelevitz et al., 2012); a human $F_{m,A0}$ for SGX523 has not been previously reported to our knowledge. In addition, with a few exceptions, the two methods used to estimate human $F_{m,A0}$ generally produced similar values, providing more confidence in these estimates. It is important to note that the lower the rate of depletion, the less accurate the estimation of CL_{int} , (and thus, $F_{m,A0}$) using the substrate depletion

method due to difficulty in distinguishing legitimate metabolism-mediated depletion from biological or bioanalytical noise (Di and Obach, 2015; Hutzler et al., 2015). For example, in some cases, low turnover resulted in an $F_{m,A0}$ estimation of 1 or 0, by method A or B, respectively (e.g., estimation of zaleplon $F_{m,A0}$ in rat), and in these cases, $F_{m,A0}$ was reported as “n/a.”

Zaleplon $F_{m,A0}$

CL_{int} of zaleplon in human S9 incubations with hydralazine could not be measured; however, a $F_{m,A0}$ estimate of 0.71 was determined using method B (Table IV.4), consistent with previous reports (Strelevitz et al., 2012). Cynomolgus monkey, rhesus monkey, and guinea pig demonstrated similar $F_{m,A0}$ to human, with estimates ranging between 0.42-0.70, while mouse and minipig estimates were ≤ 0.22 . Turnover of zaleplon in rat S9 was only measurable in incubations with NADPH absent hydralazine, preventing an $F_{m,A0}$ estimate from being obtained.

Species	Zaleplon CL_{int} (mL/min/kg)				$F_{m,AO}$	
	+NADPH	+NADPH +Hydralazine	-NADPH	-NADPH +Hydralazine	Method A	Method B
Human	5.57 ± 1.01	n/c	3.96 ± 1.35	n/c	1	0.71
Mouse	28.0 ± 2.81	22.0 ± 6.14	n/c	n/c	0.22	0
Rat	18.0 ± 0.698	n/c	n/c	n/c	n/a	n/a
Guinea Pig	13.5 ± 1.90	n/c	6.73 ± 3.63	n/c	1	0.50
Cynomolgus Monkey	18.3 ± 1.41	n/c	12.8 ± 1.34	n/c	1	0.70
Rhesus Monkey	16.7 ± 1.31	9.61 ± 0.964	10.8 ± 0.743	n/c	0.42	0.65
Minipig	6.70 ± 0.621	5.54 ^a	n/c	n/c	0.17	0

Table IV.4. Multispecies CL_{int} of zaleplon estimated from S9 fractions containing NADPH, containing NADPH and hydralazine, without NADPH, or containing hydralazine without NADPH, and the estimated fraction metabolized by AO ($F_{m,AO}$) calculated from the CL_{int} data using methods A and B. CL_{int} data represent means of triplicate determinations (\pm SD). $F_{m,AO}$ was calculated using mean CL_{int} values. n/c = CL_{int} not calculated because mean $\ln[C]$ versus time slope not significantly different from zero; n/a = insufficient CL_{int} data to calculate $F_{m,AO}$; a = mean of duplicate determinations.

*O*⁶-benzylguanine $F_{m,AO}$

A high $F_{m,AO}$ (≥ 0.70) was estimated for *O*⁶-benzylguanine in all species except rat, mouse, and minipig, which could not be determined due to low turnover of the compound (Table IV.5). As was the case for zaleplon in rat S9 incubations, a lack of measurable turnover of *O*⁶-benzylguanine in rat, mouse, and minipig S9 incubations in the presence of both NADPH and hydralazine, as well as in incubations absent NADPH, prevented estimation of $F_{m,AO}$.

Species	O ⁶ -Benzylguanine CL _{int} (mL/min/kg)				F _{m,AO}	
	+NADPH	+NADPH +Hydralazine	-NADPH	-NADPH +Hydralazine	Method A	Method B
Human	17.8 ± 3.05	5.37 ± 1.16	14.8 ± 1.98	n/c	0.70	0.83
Mouse	15.5 ± 2.48	n/c	n/c	n/c	n/a	n/a
Rat	6.59 ± 0.664	n/c	n/c	n/c	n/a	n/a
Guinea Pig	58.7 ± 4.65	15.0 ± 2.14	48.7 ± 5.15	n/c	0.74	0.83
Cynomolgus Monkey	35.6 ± 5.10	n/c	33.5 ± 3.84	n/c	1	0.94
Rhesus Monkey	19.5 ± 2.05	n/c	21.3 ± 1.52	n/c	1	1 ^b
Minipig	4.68 ± 2.20	n/c	n/c	n/c	n/a	n/a

Table IV.5. Multispecies CL_{int} of O⁶-benzylguanine estimated from S9 fractions containing NADPH, containing NADPH and hydralazine, without NADPH, or containing hydralazine without NADPH, and the estimated fraction metabolized by AO (F_{m,AO}) calculated from the CL_{int} data using methods A and B. CL_{int} data represent means of triplicate determinations (± SD). F_{m,AO} was calculated using mean CL_{int} values. n/c = CL_{int} not calculated because mean ln[C] versus time slope not significantly different from zero; n/a = insufficient CL_{int} data to calculate F_{m,AO}; b = calculations resulting in an F_{m,AO} > 1 were assumed to be equal to 1.

Zoniporide F_{m,AO}

A high F_{m,AO} (> 0.70) for zoniporide was estimated in all species (Table IV.6). In human, rat, and guinea pig, NADPH-independent clearance of zoniporide was not completely inhibited by hydralazine. Literature reports indicate hydrolysis as a secondary metabolism pathway of zoniporide (Dalvie et al., 2010; Strelevitz et al., 2012), which may account for this observation. This pathway will be further discussed in the section on biotransformation of zoniporide. Xanthine oxidase (XO) is not expected to contribute to the NADPH-independent clearance observed in the presence of hydralazine, as Dalvie et al. reported that allopurinol did not inhibit

formation of the M1 metabolite (major NADPH-independent metabolite) (Dalvie et al., 2010).

Species	Zoniporide CL_{int} (mL/min/kg)				$F_{m,AO}$	
	+NADPH	+NADPH +Hydralazine	-NADPH	-NADPH +Hydralazine	Method A	Method B
Human	17.0 ± 1.49	4.00 ± 0.442	17.1 ± 1.53	4.80 ± 0.685	0.77	0.72
Mouse	331 ± 17.5	31.7 ± 1.12	297 ± 16.0	n/c	0.90	0.90
Rat	482 ± 13.9	125 ± 11.0	357 ± 25.1	9.70 ± 1.90	0.74	0.72
Guinea Pig	73.6 ± 2.61	11.6 ± 2.06	84.4 ± 2.75	12.9 ± 2.54	0.84	0.97
Cynomolgus Monkey	55.2 ± 1.73	5.74 ± 1.16	55.3 ± 1.63	n/c	0.90	1
Rhesus Monkey	27.8 ± 2.03	6.47 ± 3.97	31.2 ± 2.60	n/c	0.77	1 ^b
Minipig	22.1 ± 1.87	3.67 ± 1.55	21.5 ± 1.01	n/c	0.83	0.97

Table IV.6. Multispecies CL_{int} of zoniporide estimated from S9 fractions containing NADPH, containing NADPH and hydralazine, without NADPH, or containing hydralazine without NADPH, and the estimated fraction metabolized by AO ($F_{m,AO}$) calculated from the CL_{int} data using methods A and B. CL_{int} data represent means of triplicate determinations (\pm SD). $F_{m,AO}$ was calculated using mean CL_{int} values. n/c = CL_{int} not calculated because mean $\ln[C]$ versus time slope not significantly different from zero; n/a = insufficient CL_{int} data to calculate $F_{m,AO}$; b = calculations resulting in an $F_{m,AO} > 1$ were assumed to be equal to 1.

BIBX1382 $F_{m,AO}$

$F_{m,AO}$ for BIBX1382 was estimated to be approximately ≥ 0.70 by both methods in all species except rat and mouse (Table IV.7). BIBX1382 reportedly undergoes some degree of P450 2D6-mediated metabolism (Dittrich et al., 2002), and it has been reported that hydralazine may exert mild human 2D6 inhibition (Strelevitz et al., 2012; Zientek and Youdim, 2015), in which case method A could potentially estimate an inflated $F_{m,AO}$; however, both methods A and B resulted in a very similar $F_{m,AO}$ estimation in human, suggesting that either P450 2D6-mediated

clearance was insignificant, or hydralazine did not inhibit this pathway. This result is in agreement with a previous report phenotyping BIBX1382 clearance in human hepatocytes, where substrate depletion was predominantly mediated by AO (Hutzler et al., 2012). Interestingly, CL_{int} in rat S9 incubations fortified with NADPH was only slightly inhibited by hydralazine (decreased from 29 to 25 mL/min/kg), suggestive of predominantly NADPH-dependent clearance; however, in incubations absent NADPH, a CL_{int} of 19 mL/min/kg still remained. This finding suggests the possibility that the cytosolic enzyme xanthine oxidase (XO) may mediate part of the NADPH-independent clearance in rat S9 since XO is not inhibited by hydralazine; however, no measurable substrate depletion was observed in incubations containing hydralazine without NADPH. Minor depletion of BIBX1382 CL_{int} was observed in human S9 incubations containing hydralazine without NADPH, but no other species exhibited measurable depletion under these conditions. Experiments to confirm XO involvement were not conducted. In addition, while $F_{m,AO}$ was estimated to be 0.69 in rat by method B, similar to other species, the value obtained via method A ($F_{m,AO} = 0.09$) was drastically lower. Given our previous report of metabolic shunting with the mixed AO/P450 substrate VU0409106 (Chapter III), it is possible that a metabolic shunt towards NADPH-dependent pathway(s) in the presence of hydralazine may have compensated for the inhibited AO pathway, resulting in an apparent $F_{m,AO} = 0.09$ via method A, whereas method B yields an estimate of 0.69 because no NADPH-dependent pathways are active to contribute to compensatory metabolism in the presence of hydralazine. It is also possible that the discrepancy may simply be due to low turnover of BIBX1382 by rat S9 and

consequently an inability to accurately measure CL_{int} by the substrate depletion method.

Species	BIBX1382 CL_{int} (mL/min/kg)				$F_{m,AO}$	
	+NADPH	+NADPH +Hydralazine	-NADPH	-NADPH +Hydralazine	Method A	Method B
Human	71.6 ± 1.12	5.83 ± 1.22	69.6 ± 2.10	3.93 ± 1.75	0.92	0.92
Mouse	21.4 ± 10.9	n/c	n/c	n/c	n/a	n/a
Rat	27.6 ± 0.995	25.1 ± 6.29	19.0 ± 3.17	n/c	0.09	0.69
Guinea Pig	69.4 ± 1.66	24.5 ± 2.92	50.4 ± 1.13	n/c	0.65	0.73
Cynomolgus Monkey	172 ± 1.26	n/c	209 ± 19.6	n/c	1	1 ^b
Rhesus Monkey	108 ± 5.43	6.03 ± 3.34	92.7 ± 1.21	n/c	0.94	0.86
Minipig	133 ± 6.98	20.0 ± 2.92	127 ± 7.08	n/c	0.85	0.96

Table IV.7. Multispecies CL_{int} of BIBX1382 estimated from S9 fractions containing NADPH, containing NADPH and hydralazine, without NADPH, or containing hydralazine without NADPH, and the estimated fraction metabolized by AO ($F_{m,AO}$) calculated from the CL_{int} data using methods A and B. CL_{int} data represent means of triplicate determinations (\pm SD). $F_{m,AO}$ was calculated using mean CL_{int} values. n/c = CL_{int} not calculated because mean $\ln[C]$ versus time slope not significantly different from zero; n/a = insufficient CL_{int} data to calculate $F_{m,AO}$; b = calculations resulting in an $F_{m,AO} > 1$ were assumed to be equal to 1.

SGX523 $F_{m,AO}$

Considerable variability between the two methods was observed in the $F_{m,AO}$ of SGX523 in some species (e.g., guinea pig), but overall a low-moderate $F_{m,AO}$ was estimated in all species (range of 0.03 – 0.68, Table IV.8). In some species (mouse, rhesus, and guinea pig), not all NADPH-independent activity was inhibited by hydralazine, suggesting possible XO-mediated clearance; however, experiments to confirm involvement of XO were not conducted.

Species	SGX523 CL _{int} (mL/min/kg)				F _{m,AO}	
	+NADPH	+NADPH +Hydralazine	-NADPH	-NADPH +Hydralazine	Method A	Method B
Human	7.34 ± 3.34	4.70 ± 2.40	4.51 ± 0.310	n/c	0.36	0.61
Mouse	35.9 ± 10.3	24.2 ± 5.04	24.4 ± 9.31	16.5 ± 4.03	0.33	0.22
Rat	36.9 ± 4.23	21.4 ± 0.664	10.4 ± 3.20	n/c	0.42	0.28
Guinea Pig	38.2 ± 1.13	29.4 ± 3.05	15.8 ± 6.15	14.6 ± 6.05	0.23	0.03
Cynomolgus Monkey	39.4 ± 1.25	16.6 ± 3.42	26.9 ± 4.35	n/c	0.58	0.68
Rhesus Monkey	23.6 ± 4.13	15.6 ± 2.43	11.3 ± 0.942	7.97 ± 3.59	0.34	0.14
Minipig	26.0 ± 1.20	21.4 ± 1.98	3.20 ± 0.574	n/c	0.18	0.12

Table IV.8. Multispecies CL_{int} of SGX523 estimated from S9 fractions containing NADPH, containing NADPH and hydralazine, without NADPH, or containing hydralazine without NADPH, and the estimated fraction metabolized by AO (F_{m,AO}) calculated from the CL_{int} data using methods A and B. CL_{int} data represent means of triplicate determinations (± SD). F_{m,AO} was calculated using mean CL_{int} values. n/c = CL_{int} not calculated because mean ln[C] versus time slope not significantly different from zero; n/a = insufficient CL_{int} data to calculate F_{m,AO}.

In general, the F_{m,AO} calculated by the two different methods were in better agreement for compounds/species exhibiting more rapid clearance, and thus, more confidence can be placed in the accuracy of these estimations. Overall, monkey and guinea pig demonstrated F_{m,AO} values most similar to human. However, because low turnover prevented an F_{m,AO} calculation for some compounds in mouse, rat, and minipig, it is unclear how closely these species replicate human F_{m,AO}. Though CL_{int} may also be estimated from Michaelis-Menten kinetic parameters according to the relationship described by Equation IV.1,

$$Cl_{int} = \frac{V_{max}}{K_m + C}$$

Equation IV.1. Determination of intrinsic clearance (CL_{int}) from Michaelis-Menten parameters, where V_{max} is the maximum rate of metabolite formation, K_m is the Michaelis-Menten constant, which is equal to the substrate concentration when the metabolite formation rate is $\frac{1}{2}$ of V_{max} , and C is the substrate concentration.

this method unfortunately is not feasible for the purpose of our studies. In order to estimate the total CL_{int} from the Michaelis-Menten parameters, an authentic standard of each metabolite that contributes to the overall clearance of each substrate would be required. Furthermore, different metabolites are sometimes produced by different species, adding further complication to this method. Therefore, although the substrate depletion method is limited by slow turnover rates, it is the most reasonable method available to obtain the total CL_{int} mediated by all metabolic pathways.

Prediction of Human Hepatic S9 Clearance by Multi- or Single-Species

Allometry

Intrinsic clearance estimates (Table IV.1) from hepatic S9 incubations of male mouse, rat, guinea pig, cynomolgus, rhesus, and minipig were employed in various combinations of 3 or 4 species for allometric scaling (multispecies simple allometry, MA) as well as individually for direct extrapolation from a single-species (single-species scaling, SSS). Human CL_{int} values predicted from MA and SSS were compared to CL_{int} measured in incubations with human hepatic S9. The overall

performance of each method is summarized in Table IV.9 (MA) and Table IV.15 (SSS), measured by the absolute average fold error (AAFE) and the average fold error (AFE), described by Equations II.16 and II.17, respectively, where an AAFE of ≤ 3 was considered successful. An AFE > 1 indicates an overall bias of the method towards over-prediction, while an AFE < 1 indicates bias towards under-prediction. Plots of the observed CL_{int} for each compound versus the human CL_{int} predicted by each method are displayed in Figures IV.2 and IV.3; these data are also tabulated in Tables IV.10-14, along with the allometric exponent and correlation coefficients observed for each MA method (i.e., each species combination).

Multispecies allometry (MA) of CL_{int}

An AAFE of ≤ 2.0 was obtained from all of the 4-species combinations and from the rhesus/rat/mouse combination, with rhesus/rat/mouse yielding the lowest AAFE (1.7) and 80% of the five compounds predicted within 2-fold of the experimentally measured human S9 CL_{int} (Table IV.10). Only two combinations, cynomolgus/rat/mouse and cynomolgus/guinea pig/mouse, resulted in an AAFE of > 3.0 (3.3-fold and 3.5-fold, respectively). SGX523 is the only compound of the five for which a fold-error of < 3 could not be obtained by at least one of the species combinations; however, the minipig/rhesus/guinea pig combination yielded a fold-error of 3.0 (Figure IV.2, Table IV.14). Interestingly, all but one of the species combinations (minipig/rat/mouse) had an AFE of ≥ 1.0 , indicating that the predictions were biased towards over-prediction rather than under-prediction. This clearly was not the case in every instance, however, particularly for O⁶-benzylguanine and zoniporide (Figure IV.2, Table IV.11-12).

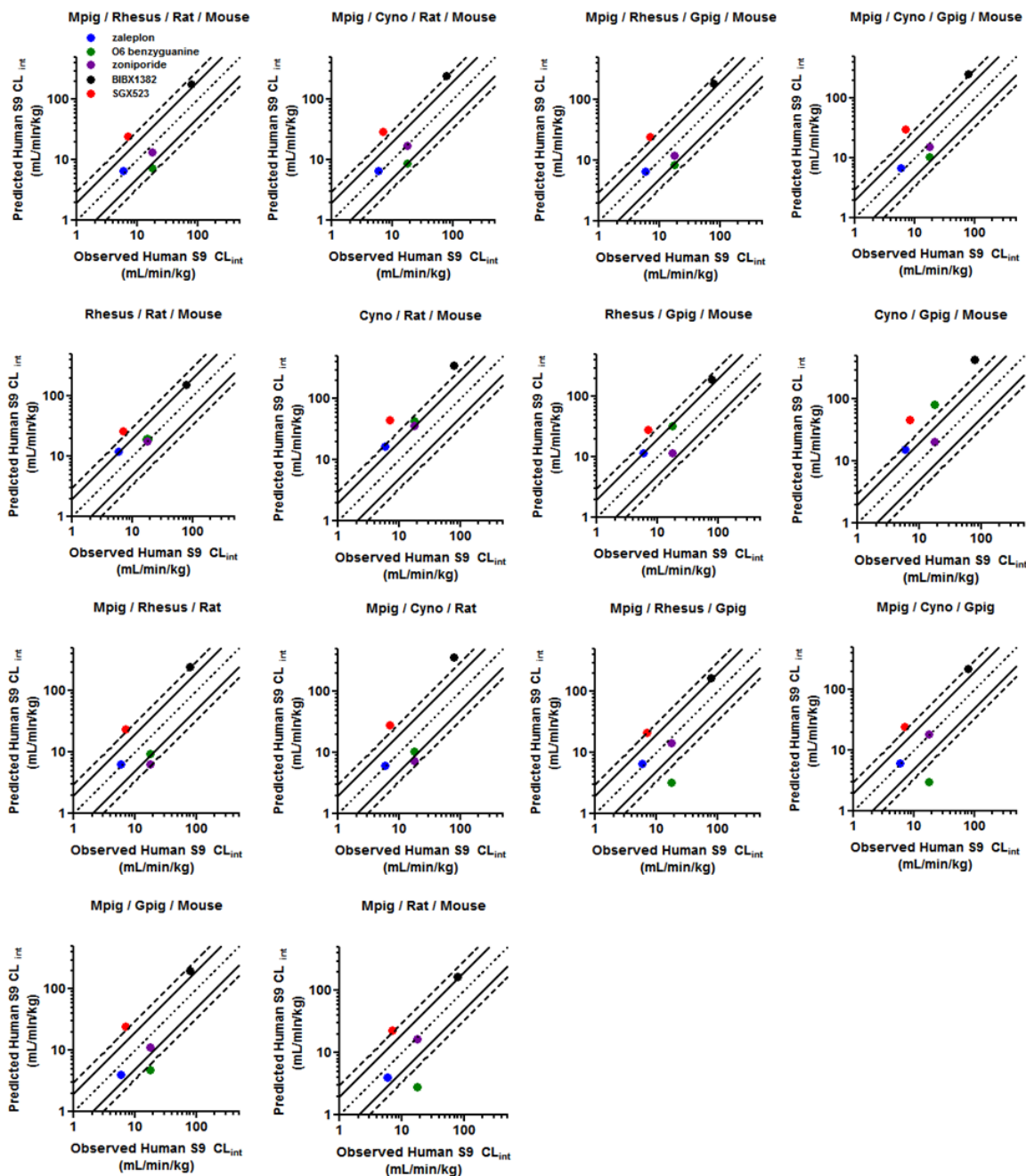


Figure IV.2. Plots of observed human S9 CL_{int} vs that predicted from multispecies allometry. Inner dotted line represents unity, solid line represents 2-fold-error, and outer dashed line represents 3-fold-error. CL_{int} , intrinsic clearance; Cyno, cynomolgus monkey; Gpig, guinea pig; Mpig, minipig

Multispecies simple allometry	AAFE	AFE	% within 2 fold-error	% within 3 fold-error
Minipig/Rhesus/Rat/Mouse	1.9	1.2	40%	80%
Minipig/Cyno/Rat/Mouse	2.0	1.5	40%	60%
Minipig/Rhesus/Gpig/Mouse	1.9	1.2	40%	80%
Minipig/Cyno/Gpig/Mouse	2.0	1.5	60%	60%
Rhesus/Rat/Mouse	1.7	1.7	80%	80%
Cyno/Rat/Mouse	3.3	3.3	20%	60%
Rhesus/Gpig/Mouse	2.2	1.9	60%	80%
Cyno/Gpig/Mouse	3.5	3.5	20%	40%
Minipig/Rhesus/Rat	2.3	1.2	40%	60%
Minipig/Cyno/Rat	2.4	1.4	40%	60%
Minipig/Rhesus/Gpig	2.2	1.0	40%	80%
Minipig/Cyno/Gpig	2.3	1.1	40%	60%
Minipig/Gpig/Mouse	2.4	1.0	40%	60%
Minipig/Rat/Mouse	2.3	0.92	40%	60%

Table IV.9. Absolute average fold-error (AAFE), average fold-error (AFE), and percentage of compounds predicted within 2 or 3 fold-error of observed CL_{int} measured in human S9, as predicted by multispecies allometry (MA). Cyno = cynomolgus monkey; Rhesus = rhesus monkey; Gpig = guinea pig

In addition to the CL_{int} prediction and fold error values, Tables IV.10-14 report the correlation coefficient and the allometric exponent (b) obtained for each MA method. These two values are commonly evaluated when considering the degree of confidence to be placed in predictions generated by MA. Particularly, evaluation of the allometric exponent has been proposed as a tool to guide employment of correction factors, referred to as the “rule of exponents” or ROE (Mahmood and Balian, 1996). Use of these correction factors results in a lower CL prediction, and

therefore serves only to improve an over-prediction (and consequently would worsen an under-prediction). According to the ROE, when $0.55 \leq b < 0.71$, simple allometry with no correction should be employed, when $b \geq 1.0$, a correction for brain weight should be applied, and when $0.71 \leq b \leq 1.0$, a correction for maximum lifespan potential is recommended. In addition, the ROE suggests that a useful prediction will not be obtained for compounds with $b < 0.55$ due to substantial under-prediction. However, a comprehensive analysis evaluating the use of ROE indicated that employment of correction factors was not superior to universal application of simple allometry (Nagilla and Ward, 2004). We did not apply the ROE in our analyses, and a general evaluation of the data reveals that application of ROE would be substrate- and species-dependent in improving the prediction. For example, in several instances, the exponent was > 0.71 , and while the CL_{int} was indeed over-predicted in some cases, in others it was actually under-predicted, and in some the fold-error was near unity. Likewise, while five instances of $b < 0.55$ resulted in some degree of under-prediction, three out of the five cases resulted in < 3 -fold-error (fold error = 0.36 – 0.75).

Zaleplon				
Human Observed CL _{int}	5.8			
	Predicted CL _{int}	Fold Error	R ²	Exponent (b)
Minipig/Rhesus/Rat/Mouse	6.52	1.1	0.980	0.837
Minipig/Cyno/Rat/Mouse	6.82	1.2	0.967	0.837
Minipig/Rhesus/Gpig/Mouse	6.48	1.1	0.979	0.838
Minipig/Cyno/Gpig/Mouse	6.75	1.2	0.966	0.837
Rhesus/Rat/Mouse	11.9	2.0	0.998	0.924
Cyno/Rat/Mouse	16.5	2.8	0.993	0.968
Rhesus/Gpig/Mouse	11.5	2.0	0.996	0.921
Cyno/Gpig/Mouse	15.5	2.7	0.990	0.962
Minipig/Rhesus/Rat	6.42	1.1	0.941	0.831
Minipig/Cyno/Rat	6.20	1.1	0.901	0.802
Minipig/Rhesus/Gpig	6.50	1.1	0.931	0.839
Minipig/Cyno/Gpig	6.13	1.1	0.882	0.802
Minipig/Gpig/Mouse	3.98	0.68	1.00	0.773
Minipig/Rat/Mouse	3.98	0.68	0.999	0.772

Table IV.10. Human CL_{int} (mL/min/kg) of zaleplon predicted by each multispecies allometry (MA) method, fold-error of the prediction by each MA method compared to the reference CL_{int} observed in human S9, correlation coefficient of each MA method, and allometric exponent (b) of each MA method. CL_{int}, intrinsic clearance; Cyno = cynomolgus monkey; Rhesus = rhesus monkey; Gpig = guinea pig

O ⁶ -Benzylguanine				
Human Observed CL _{int}	17.8			
	Predicted CL _{int}	Fold Error	R ²	Exponent (b)
Minipig/Rhesus/Rat/Mouse	7.31	0.41	0.937	0.897
Minipig/Cyno/Rat/Mouse	8.82	0.49	0.885	0.908
Minipig/Rhesus/Gpig/Mouse	8.64	0.48	0.878	0.819
Minipig/Cyno/Gpig/Mouse	10.5	0.59	0.840	0.834
Rhesus/Rat/Mouse	18.9	1.1	0.970	1.03
Cyno/Rat/Mouse	43.0	2.4	0.946	1.14
Rhesus/Gpig/Mouse	32.5	1.8	0.964	1.01
Cyno/Gpig/Mouse	81.5	4.6	0.983	1.14
Minipig/Rhesus/Rat	9.48	0.53	0.874	1.00
Minipig/Cyno/Rat	10.3	0.58	0.746	0.965
Minipig/Rhesus/Gpig	3.27	0.18	0.627	0.431
Minipig/Cyno/Gpig	3.00	0.17	0.452	0.374
Minipig/Gpig/Mouse	4.83	0.27	0.857	0.742
Minipig/Rat/Mouse	2.85	0.16	0.995	0.773

Table IV.11. Human CL_{int} (mL/min/kg) of O⁶-benzylguanine predicted by each multispecies allometry (MA) method, fold-error of the prediction by each MA method compared to the reference CL_{int} observed in human S9, correlation coefficient of each MA method, and allometric exponent (b) of each MA method. CL_{int}, intrinsic clearance; Cyno = cynomolgus monkey; Rhesus = rhesus monkey; Gpig = guinea pig

Zoniporide				
Human Observed CL_{int}	17.9			
	Predicted CL_{int}	Fold Error	R²	Exponent (b)
Minipig/Rhesus/Rat/Mouse	13.5	0.75	0.866	0.539
Minipig/Cyno/Rat/Mouse	17.3	0.97	0.873	0.571
Minipig/Rhesus/Gpig/Mouse	12.1	0.68	0.995	0.608
Minipig/Cyno/Gpig/Mouse	15.4	0.86	0.976	0.636
Rhesus/Rat/Mouse	17.6	1.0	0.833	0.577
Cyno/Rat/Mouse	35.9	2.0	0.883	0.679
Rhesus/Gpig/Mouse	11.6	0.65	0.992	0.602
Cyno/Gpig/Mouse	20.8	1.2	0.972	0.681
Minipig/Rhesus/Rat	6.42	0.36	0.972	0.242
Minipig/Cyno/Rat	7.36	0.41	0.997	0.262
Minipig/Rhesus/Gpig	14.4	0.81	0.999	0.677
Minipig/Cyno/Gpig	18.5	1.0	0.944	0.701
Minipig/Gpig/Mouse	11.4	0.64	0.994	0.600
Minipig/Rat/Mouse	16.4	0.92	0.852	0.565

Table IV.12. Human CL_{int} (mL/min/kg) of zoniporide predicted by each multispecies allometry (MA) method, fold-error of the prediction by each MA method compared to the reference CL_{int} observed in human S9, correlation coefficient of each MA method, and allometric exponent (b) of each MA method. CL_{int}, intrinsic clearance; Cyno = cynomolgus monkey; Rhesus = rhesus monkey; Gpig = guinea pig

BIBX1382				
Human Observed CL_{int}	80.2			
	Predicted CL_{int}	Fold Error	R²	Exponent (b)
Minipig/Rhesus/Rat/Mouse	177	2.2	0.994	1.24
Minipig/Cyno/Rat/Mouse	248	3.1	0.986	1.28
Minipig/Rhesus/Gpig/Mouse	187	2.3	0.999	1.20
Minipig/Cyno/Gpig/Mouse	260	3.2	0.995	1.24
Rhesus/Rat/Mouse	155	1.9	0.991	1.22
Cyno/Rat/Mouse	348	4.3	0.979	1.33
Rhesus/Gpig/Mouse	190	2.4	0.999	1.21
Cyno/Gpig/Mouse	432	5.4	1.00	1.32
Minipig/Rhesus/Rat	247	3.1	1.00	1.37
Minipig/Cyno/Rat	359	4.5	0.978	1.41
Minipig/Rhesus/Gpig	167	2.1	1.00	1.16
Minipig/Cyno/Gpig	226	2.8	0.984	1.19
Minipig/Gpig/Mouse	197	2.5	0.999	1.21
Minipig/Rat/Mouse	165	2.1	0.993	1.23

Table IV.13. Human CL_{int} (mL/min/kg) of BIBX1382 predicted by each multispecies allometry (MA) method, fold-error of the prediction by each MA method compared to the reference CL_{int} observed in human S9, correlation coefficient of each MA method, and allometric exponent (b) of each MA method. CL_{int}, intrinsic clearance; Cyno = cynomolgus monkey; Rhesus = rhesus monkey; Gpig = guinea pig

SGX523				
Human Observed CL _{int}	7.1			
	Predicted CL _{int}	Fold Error	R ²	Exponent (b)
Minipig/Rhesus/Rat/Mouse	24.6	3.5	1.00	0.940
Minipig/Cyno/Rat/Mouse	29.8	4.2	0.994	0.962
Minipig/Rhesus/Gpig/Mouse	25.0	3.5	0.998	0.933
Minipig/Cyno/Gpig/Mouse	30.3	4.3	0.994	0.955
Rhesus/Rat/Mouse	26.8	3.8	1.00	0.952
Cyno/Rat/Mouse	45.0	6.4	0.999	1.02
Rhesus/Gpig/Mouse	28.4	4.0	0.998	0.951
Cyno/Gpig/Mouse	47.4	6.7	1.00	1.02
Minipig/Rhesus/Rat	23.9	3.4	0.999	0.929
Minipig/Cyno/Rat	28.4	4.0	0.983	0.945
Minipig/Rhesus/Gpig	21.5	3.0	1.00	0.871
Minipig/Cyno/Gpig	24.9	3.5	0.983	0.884
Minipig/Gpig/Mouse	24.5	3.5	0.998	0.930
Minipig/Rat/Mouse	23.2	3.3	1.00	0.932

Table IV.14. Human CL_{int} (mL/min/kg) of SGX523 predicted by each multispecies allometry (MA) method, fold-error of the prediction by each MA method compared to the reference CL_{int} observed in human S9, correlation coefficient of each MA method, and allometric exponent (b) of each MA method. CL_{int}, intrinsic clearance; Cyno = cynomolgus monkey; Rhesus = rhesus monkey; Gpig = guinea pig

Single-species scaling (SSS) of CL_{int}

Single-species scaling (SSS) has been demonstrated to be as accurate as or more accurate than MA in predicting human clearance (Hosea et al., 2009). Therefore, we chose to investigate this method in addition to MA for prediction of human S9 CL_{int} (calculated using a fixed exponent of 0.75—see Equation II.14). Plots of the observed CL_{int} for each compound versus the human CL_{int} predicted by each SSS method (each species) are displayed in Figure IV.3; these data are also tabulated in Table IV.16. SSS predictions yielded AAFEs of ≤ 2.0 when scaling from cynomolgus, rhesus, guinea pig, and minipig S9 CL_{int}, with 80% of compounds predicted within 3-fold-error for cynomolgus, guinea pig, and minipig, and 100% for

rhesus (Table IV.15). The compound falling outside of 3-fold-error differed for each species—SGX523 for cynomolgus, BIBX1382 for guinea pig, and O⁶-benzylguanine for minipig (Figure IV.3; Table IV.16). AAFEs for rat and mouse were 4.1 and 3.8, respectively, with only 40% and 60% of compounds predicted within 3-fold-error, respectively. A tendency towards under-prediction was exhibited in all species except monkey, which had AFEs of 1.6 (cynomolgus) and 1.2 (rhesus) (Table IV.15). By comparison of AAFE, MA was not superior to SSS with cynomolgus, rhesus, or guinea pig, but was generally more accurate than SSS with mouse or rat, while SSS with minipig was also more accurate than MA in most cases.

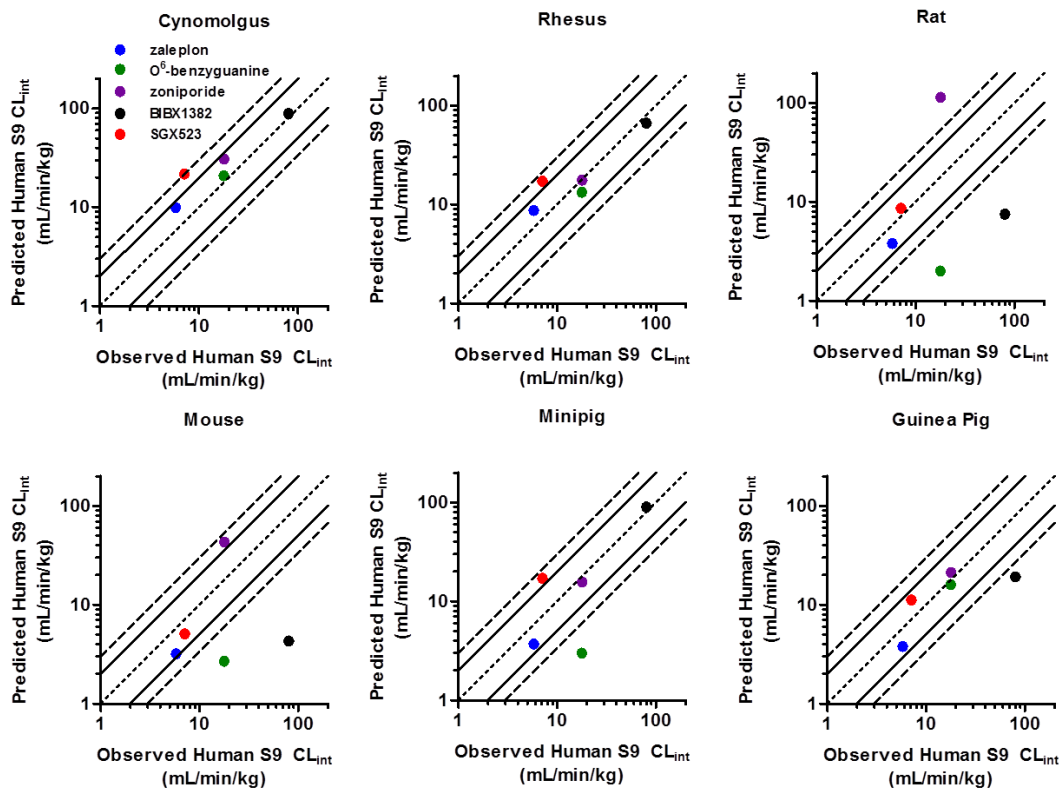


Figure IV.3. Plots of observed human S9 CL_{int} vs that predicted from single-species scaling. Inner dotted line represents unity, solid line represents 2-fold-error, and outer dashed line represents 3-fold-error. CL_{int} , intrinsic clearance

Single species scaling	AAFE	AFE	% within 2 fold-error	% within 3 fold-error
Cynomolgus Monkey	1.6	1.6	80%	80%
Rhesus Monkey	1.4	1.2	80%	100%
Rat	4.1	0.56	40%	40%
Mouse	3.8	0.38	40%	60%
Minipig	2.0	0.76	60%	80%
Guinea Pig	1.7	0.76	80%	80%

Table IV.15. Absolute average fold-error (AAFE), average fold-error (AFE), and percentage of compounds predicted within 2 or 3 fold-error of observed CL_{int} measured in human S9, as predicted by single-species scaling (SSS).

Human Observed CL_{int}	Zaleplon		O ⁶ -Benzylguanine		Zoniporide		BIBX 1382		SGX 523	
	Predicted CL_{int}	Fold Error	Predicted CL_{int}	Fold Error	Predicted CL_{int}	Fold Error	Predicted CL_{int}	Fold Error	Predicted CL_{int}	Fold Error
	5.8		17.8		17.9		80.2		7.1	
Cynomolgus monkey	9.94	1.7	20.8	1.2	30.7	1.7	88.7	1.1	21.7	3.1
Rhesus monkey	8.74	1.5	13.3	0.75	17.6	1.0	66.4	0.83	17.2	2.4
Rat	3.81	0.65	2.04	0.11	114	6.4	7.52	0.09	8.64	1.2
Mouse	3.17	0.54	2.69	0.15	43.1	2.4	4.32	0.05	5.13	0.72
Minipig	3.73	0.64	2.97	0.17	15.7	0.88	89.8	1.1	17.1	2.4
Guinea Pig	3.76	0.64	16.0	0.90	21.2	1.2	19.2	0.24	11.2	1.6

Table IV.16. Human CL_{int} (ml/min/kg) predicted by each SSS method and fold-error of the prediction by each SSS method compared to the reference CL_{int} observed in human S9. CL_{int} , intrinsic clearance; SSS, single-species scaling

Multispecies allometry (MA) of CL_{HEP}

In addition to evaluating the fold-error in CL_{int} predictions, we evaluated the fold-error in these predictions after converting them from CL_{int} estimates to hepatic clearance (CL_{HEP}) estimates according to Equation II.2 (Tables IV.17-20, Figures IV.4-5), in anticipation that substantial over- or under-predictions due to species

differences in metabolic efficiency would be minimized by the hepatic blood flow limitation occurring *in vivo* (particularly when observed or predicted CL_{int} is high). Plots of the observed CL_{HEP} for each compound versus the human CL_{HEP} predicted by each MA method are displayed in Figure IV.4; these data are also tabulated in Table IV.18. The AAFE was improved to < 2.0 for all species combinations and eleven out of the fourteen species combinations predicted 100% of the five compounds within 3-fold and 80% within 2-fold of the experimentally measured human S9 CL_{HEP} (Table IV.17). These improvements were primarily a result of improved BIBX1382 and SGX523 predictions, which exceeded human hepatic blood flow (~ 21 mL/min/kg) prior to conversion to CL_{HEP} .

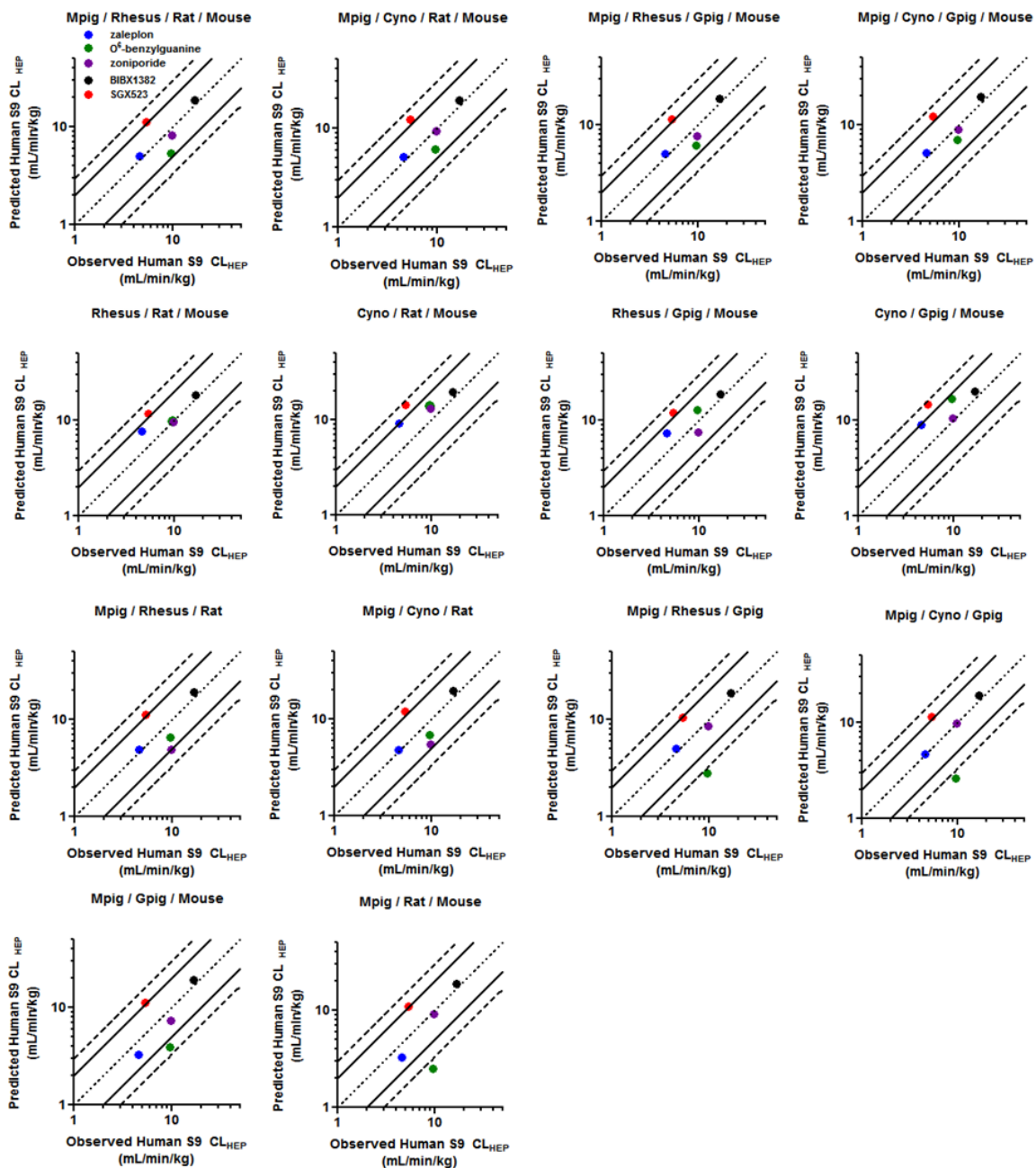


Figure IV.4. Plots of observed human S9 CL_{HEP} vs that predicted from multispecies allometry. Inner dotted line represents unity, solid line represents 2-fold-error, and outer dashed line represents 3-fold-error. CL_{HEP} , predicted hepatic clearance; Cyno, cynomolgus monkey; Gpig, guinea pig; Mpig, minipig.

Multispecies simple allometry	AAFE	AFE	% within 2 fold-error	% within 3 fold-error
Minipig/Rhesus/Rat/Mouse	1.4	1.0	80%	100%
Minipig/Cyno/Rat/Mouse	1.4	1.1	80%	100%
Minipig/Rhesus/Gpig/Mouse	1.4	1.1	80%	100%
Minipig/Cyno/Gpig/Mouse	1.4	1.2	80%	100%
Rhesus/Rat/Mouse	1.3	1.3	80%	100%
Cyno/Rat/Mouse	1.7	1.7	80%	100%
Rhesus/Gpig/Mouse	1.5	1.3	80%	100%
Cyno/Gpig/Mouse	1.6	1.6	80%	100%
Minipig/Rhesus/Rat	1.5	1.0	80%	100%
Minipig/Cyno/Rat	1.5	1.0	80%	100%
Minipig/Rhesus/Gpig	1.6	0.91	80%	80%
Minipig/Cyno/Gpig	1.6	0.93	60%	80%
Minipig/Gpig/Mouse	1.6	0.89	60%	100%
Minipig/Rat/Mouse	1.7	0.84	60%	80%

Table IV.17. Absolute average fold-error (AAFE), average fold-error (AFE), and percentage of compounds predicted within 2 or 3 fold-error of observed CL_{HEP} measured in human S9, as predicted by multispecies allometry (MA). Cyno = cynomolgus monkey; Rhesus = rhesus monkey; Gpig = guinea pig

	Zaleplon		O ⁶ -Benzylguanidine		Zoniporide		BIBX 1382		SGX 523	
Human Observed CL _{HEP}	4.6		9.6		9.7		16.6		5.3	
	Predicted CL _{HEP}	Fold Error	Predicted CL _{HEP}	Fold Error	Predicted CL _{HEP}	Fold Error	Predicted CL _{HEP}	Fold Error	Predicted CL _{HEP}	Fold Error
Minipig/Rhesus/Rat/Mouse	4.98	1.1	5.42	0.56	8.21	0.85	18.8	1.1	11.3	2.1
Minipig/Cyno/Rat/Mouse	5.05	1.1	6.21	0.64	9.49	1.0	19.4	1.2	12.3	2.3
Minipig/Rhesus/Gpig/Mouse	4.95	1.1	6.12	0.63	7.69	0.80	18.9	1.1	11.4	2.2
Minipig/Cyno/Gpig/Mouse	5.11	1.1	6.99	0.72	8.89	0.92	19.4	1.2	12.4	2.3
Rhesus/Rat/Mouse	7.60	1.7	9.95	1.0	9.57	1.0	18.5	1.1	11.8	2.2
Cyno/Rat/Mouse	9.25	2.0	14.1	1.5	13.25	1.4	19.8	1.2	14.3	2.7
Rhesus/Gpig/Mouse	7.42	1.6	12.7	1.3	7.49	0.78	18.9	1.1	12.1	2.3
Cyno/Gpig/Mouse	8.93	2.0	16.7	1.7	10.46	1.1	20.0	1.2	14.6	2.7
Minipig/Rhesus/Rat	4.92	1.1	6.53	0.68	4.92	0.51	19.4	1.2	11.2	2.1
Minipig/Cyno/Rat	4.79	1.0	6.92	0.72	5.45	0.56	19.8	1.2	12.1	2.3
Minipig/Rhesus/Gpig	4.96	1.1	2.83	0.29	8.55	0.88	18.6	1.1	10.6	2.0
Minipig/Cyno/Gpig	4.75	1.0	2.62	0.27	9.82	1.0	19.2	1.2	11.4	2.2
Minipig/Gpig/Mouse	3.35	0.73	3.93	0.41	7.39	0.77	19.0	1.1	11.3	2.1
Minipig/Rat/Mouse	3.35	0.73	2.51	0.26	9.22	1.0	18.6	1.1	11.0	2.1

Table IV.18. Human CL_{HEP} (mL/min/kg) predicted by each MA method and fold-error of the prediction by each MA method compared to the reference CL_{HEP} observed in human S9. CL_{HEP}, hepatic clearance; MA, multispecies allometry

Single-species scaling (SSS) of CL_{HEP}

Plots of the observed CL_{int} for each compound versus the human CL_{HEP} predicted by each SSS method (each species) are displayed in Figure IV.5; these data are also tabulated in Table IV.20. Like the predictions by MA, the predictions by SSS were generally improved when comparing CL_{HEP} in comparison to CL_{int}, with AAFEs of < 3.0 for all species and < 2.0 for all but rat and mouse (Table IV.19). Cynomolgus, rhesus, and guinea pig predicted a human S9 CL_{HEP} for 100% of the five compounds within 2-fold-error and minipig predicted 80% of the compounds within 2-fold (O⁶-benzylguanidine was under-predicted with a fold-error of 0.27; Figure IV.5, Table IV.20).

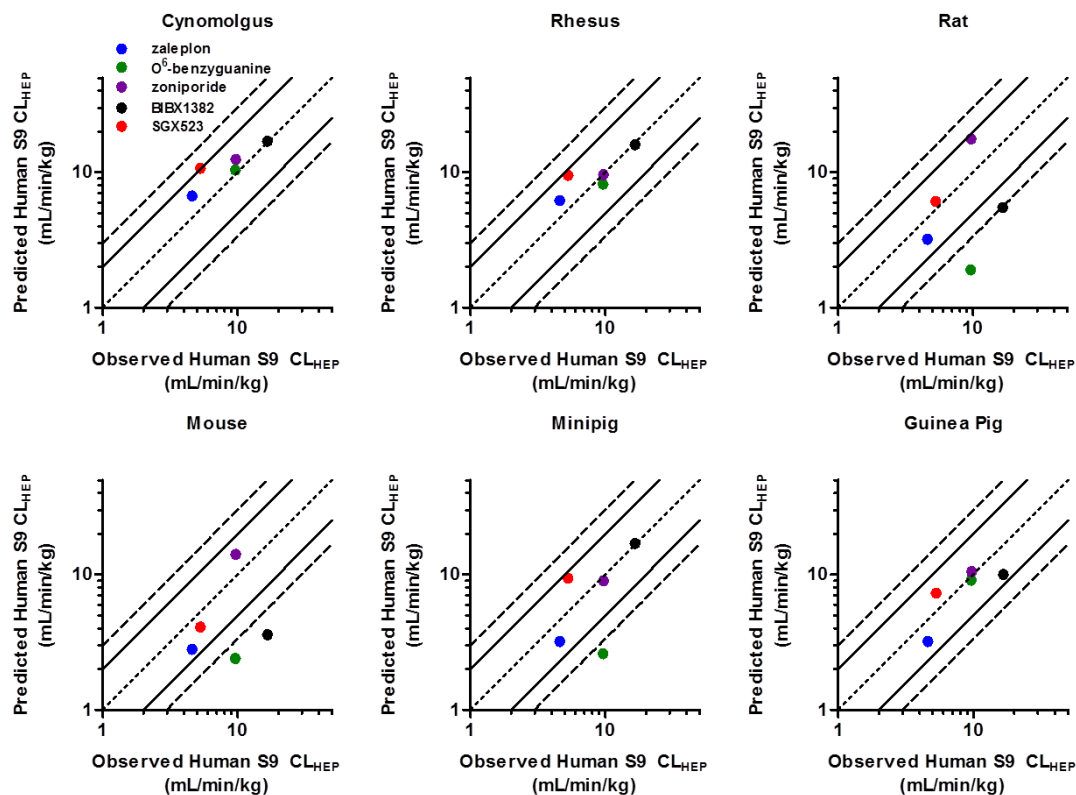


Figure IV.5. Plots of observed human S9 CL_{HEP} vs that predicted from single-species scaling. Inner dotted line represents unity, solid line represents 2-fold-error, and outer dashed line represents 3-fold-error. CL_{HEP} , predicted hepatic clearance

Single species scaling	AAFE	AFE	% within 2 fold-error	% within 3 fold-error
Cynomolgus Monkey	1.3	1.3	100%	100%
Rhesus Monkey	1.2	1.1	100%	100%
Rat	2.2	0.63	80%	80%
Mouse	2.3	0.52	60%	60%
Minipig	1.6	0.79	80%	80%
Guinea Pig	1.3	0.90	100%	100%

Table IV.19. Absolute average fold-error (AAFE), average fold-error (AFE), and percentage of compounds predicted within 2 or 3 fold-error of observed CL_{HEP} measured in human S9, as predicted by single-species scaling (SSS).

	Zaleplon		O ⁶ -Benzylguanine		Zoniporide		BIBX 1382		SGX 523	
Human Observed CL _{HEP}	4.6		9.6		9.7		16.6		5.3	
	Predicted CL _{HEP}	Fold Error	Predicted CL _{HEP}	Fold Error	Predicted CL _{HEP}	Fold Error	Predicted CL _{HEP}	Fold Error	Predicted CL _{HEP}	Fold Error
Cynomolgus monkey	6.74	1.5	10.4	1.1	12.5	1.3	17.0	1.0	10.7	2.0
Rhesus monkey	6.17	1.4	8.15	0.85	9.57	1.0	16.0	1.0	9.5	1.8
Rat	3.22	0.71	1.86	0.19	17.7	1.8	5.54	0.33	6.1	1.2
Mouse	2.75	0.60	2.39	0.25	14.1	1.5	3.58	0.22	4.1	0.78
Minipig	3.16	0.69	2.60	0.27	8.98	0.93	17.0	1.0	9.4	1.8
Guinea Pig	3.19	0.70	9.07	0.94	10.5	1.1	10.0	0.60	7.3	1.4

Table IV.20. Human CL_{HEP} predicted by each SSS method and fold-error of the prediction by each SSS method compared to the reference CL_{HEP} observed in human S9. CL_{HEP}, hepatic clearance; SSS, single-species scaling

SSS Correlation with F_m or E

Based on their studies examining allometric scaling of UGT substrates, Deguchi et al. reported that overall F_{m,UGT} values in monkey were more similar to human than other species evaluated, concluding that this likely contributed to a higher rate of prediction accuracy from monkey SSS relative to the other species investigated (mouse, rat, and dog) (Deguchi et al., 2011). Likewise, we observed similar F_{m,AO} values between monkey and human, as well as better overall success with predictions from monkey SSS. However, a similar F_{m,AO} between animals and human did not always translate to a more accurate CL_{int} prediction. For example, similar F_{m,AO} estimates were observed between cynomolgus (0.58-0.68) and human (0.36-0.61) for SGX523, yet the human CL_{int} prediction by cynomolgus SSS yielded the largest fold-error (3.1) versus all other species, including minipig (2.4-fold-error) which displayed a F_{m,AO} of 0.12-0.18 (Table IV.8, Figure IV.3, Table IV.16). Likewise, rat and human exhibited similar F_{m,AO} estimates for zoniporide (rat = 0.72-

0.74, human = 0.72-0.77) with a rat SSS CL_{int} prediction 6.4-fold higher than the CL_{int} observed in human S9 (Table IV.6, Figure IV.3, Table IV.16). Furthermore, in Deguchi's report it can also be observed when comparing individual $F_{m,UGT}$ of each compound for each species with predicted CL_p by SSS, that a species exhibiting a similar $F_{m,UGT}$ to human did not always yield a more accurate prediction versus another species displaying a $F_{m,UGT}$ substantially different from human (Deguchi et al., 2011). In some cases, however, we observed a similar E between human and a given species (Table IV.2) despite a divergence in $F_{m,AO}$, suggesting that other metabolism pathways are contributing to compensate for the lacking AO pathway, resulting in a reasonable human CL_{int} prediction. For example, the $F_{m,AO}$ of zaleplon in minipig (≤ 0.17) was much lower than the human estimates (≥ 0.71), while the fold-error of human CL_{int} predicted from minipig SSS was less than 2-fold (fold-error = 0.64; Figure IV.3, Table IV.16). Comparison of the E between the species however revealed a similar E, despite the $F_{m,AO}$ discrepancy (minipig E = 0.16, human E = 0.22). This situation was also observed for zaleplon in mouse. To better understand the relationship between $F_{m,AO}$ or E and the accuracy of prediction by SSS, the CL_{int} prediction fold-error by SSS was plotted against the animal:human ratio of either $F_{m,AO}$ or E (Figure IV.6) A very poor correlation was observed between the animal:human ratio of $F_{m,AO}$ and the fold-error in the CL_{int} predicted from SSS ($r^2 = 0.0051$). However, a positive correlation was observed between SSS CL_{int} prediction fold-error and E ($r^2 = 0.6488$).

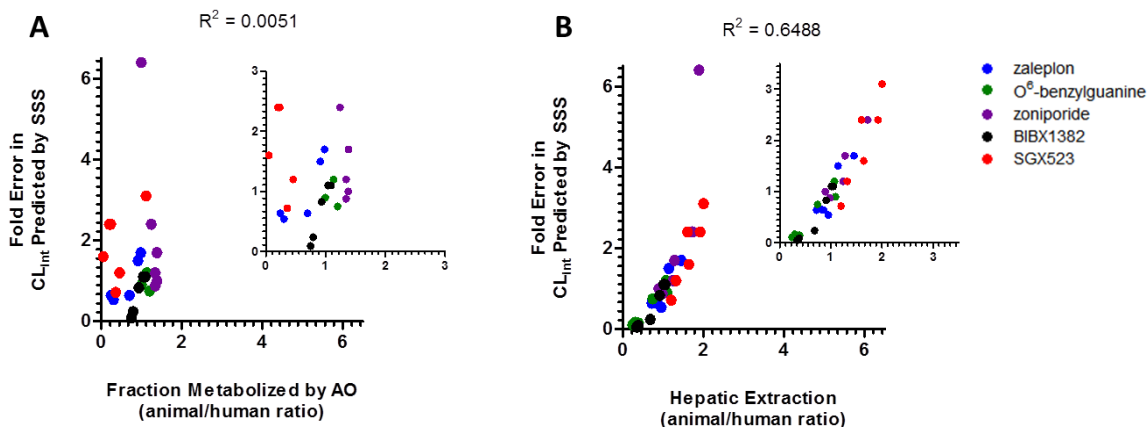


Figure IV.6. Correlation of SSS fold-error and animal/human ratios of $F_{m, AO}$ or E . (A) Fold-error in CL_{int} predicted by SSS vs animal/human ratio of $F_{m, AO}$ (inset, axes magnified). (B) Fold-error in CL_{int} predicted by SSS vs animal/human ratio of E . (inset, axes magnified). Data points represent measurements obtained for each substrate in mouse, rat, guinea pig, cynomolgus monkey, rhesus monkey, or minipig. CL_{int} , intrinsic clearance; E , estimated hepatic extraction; $F_{m, AO}$, fraction metabolized by AO; SSS, single-species scaling.

The same plots were also generated replacing CL_{int} prediction fold-error by SSS with CL_{HEP} prediction fold-error by SSS (Figure IV.7). A poor correlation again was observed between SSS prediction fold-error and $F_{m, AO}$ ($r^2 = 0.00017$), but an even stronger correlation resulted between SSS prediction fold-error and E ($r^2 = 0.9184$).

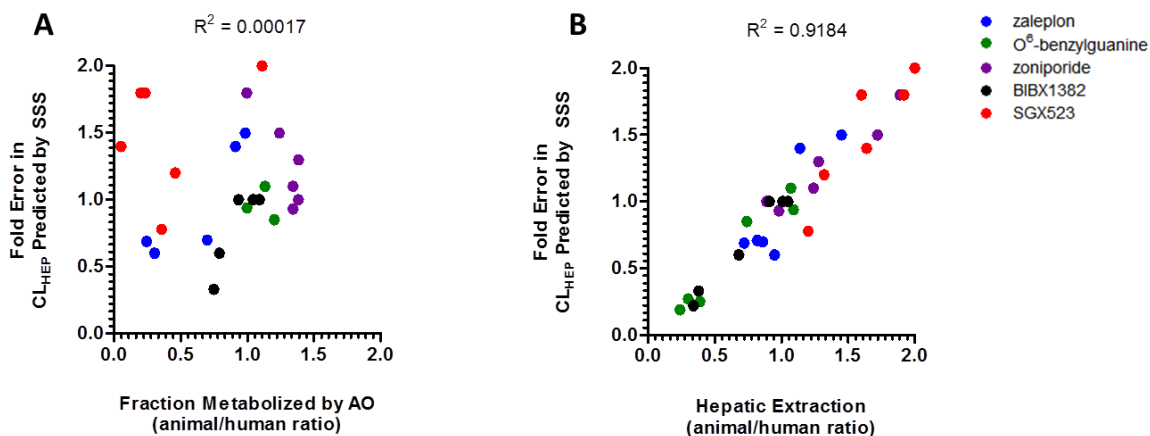


Figure IV.7. Correlation of SSS fold-error and animal/human ratios of $F_{m, AO}$ or E . (A) Fold-error in CL_{HEP} predicted by SSS vs animal/human ratio of $F_{m, AO}$. (B) Fold-error in CL_{HEP} predicted by SSS vs animal/human ratio of E . Data points represent measurements obtained for each substrate in mouse, rat, guinea pig, cynomolgus monkey, rhesus monkey, or minipig. CL_{HEP} , predicted hepatic clearance; E , estimated hepatic extraction; $F_{m, AO}$; fraction metabolized by AO; SSS, single-species scaling.

To determine if similar trends existed among the 12 UGT substrates evaluated by Deguchi et al, data was obtained from this report (Deguchi et al., 2011) to plot the CL_p prediction fold-error by SSS against the animal:human ratio of $F_{m, UGT}$ (Figure IV.8A) or against the animal:human ratio of CL_p as a percentage of Q_H (Figure IV.8B). Because CL_p as a percentage of Q_H will be equal to E when clearance is mediated exclusively by hepatic elimination, but greater than E when extra-hepatic clearance contributes, we excluded UGT substrates that are predominantly cleared renally. Once again, correlation with $F_{m, UGT}$ was very poor ($r^2 = 0.00069$), but was strong with CL_p as a percentage of Q_H ($r^2 = 0.9581$). Overall, these data suggest that the fold-error in clearance prediction by SSS is more closely associated with the overall hepatic extraction efficiency than the F_m between human and a given species.

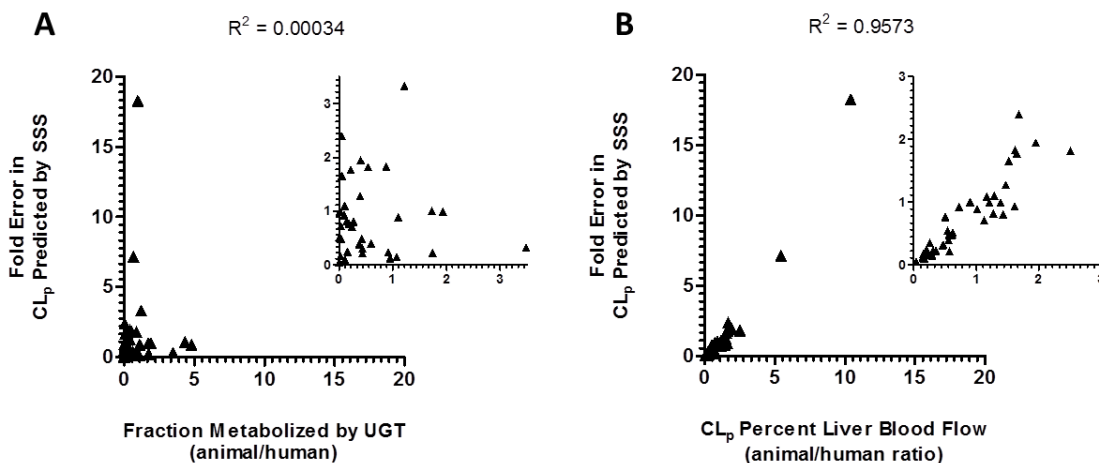


Figure IV.8. Correlation of SSS fold-error and animal/human ratios of $F_{m, UGT}$ or CL_p as a percentage of liver blood flow for *in vivo* data of UGT substrates reported by Deguchi et al. (A) Fold-error in CL_p predicted by SSS vs animal/human ratio of $F_{m,UGT}$ (inset, axes magnified). (B) Fold-error in CL_p predicted by SSS vs animal/human ratio of CL_p as a percentage of liver blood flow (inset, axes magnified). Data points represent measurements obtained for each UGT substrate in rat, mouse, monkey, or dog. CL_p , plasma clearance, E , estimated hepatic extraction; $F_{m,UGT}$, fraction metabolized by UGT; UGT, uridine diphosphate-glucuronosyltransferase; SSS, single-species scaling.

Sex Differences in Intrinsic Clearance

Species-specific sex differences exist in the expression and/or activity of some drug metabolizing enzymes (e.g., certain P450s) (Martignoni et al., 2006) (Mugford and Kedderis, 1998; Bogaards et al., 2000). For example, male rats generally exhibit higher P450 activity than female rats, particularly with regard to P450 3A-mediated metabolism (Bogaards et al., 2000), the predominant metabolic pathway for drugs on the market (Wienkers and Heath, 2005). Consequently, male rats are more representative of human P450 metabolism (Bogaards et al., 2000) and thus are typically employed rather than female rats in preclinical studies used to

predict human clearance of compounds cleared via P450s. Sex differences in AO-mediated metabolism have also been noted in the literature (Beedham, 1985; Klecker et al., 2006; Akabane et al., 2011; Dalvie et al., 2013). This observation, as previously described, has occurred in both a species- and substrate-dependent manner, and has primarily been investigated in mice, rats, and humans. As sex selection could potentially influence human clearance predictions obtained from allometric scaling, we elected to evaluate the intrinsic clearance of the five AO substrates in female pooled hepatic S9. Intrinsic clearance is reported in the presence or absence of NADPH, providing insight as to the enzymatic source (e.g., P450 vs. AO) responsible for any observed male-to-female differences in intrinsic clearance. We did not evaluate CL_{int} in male versus female human S9, although literature reports have consistently demonstrated no sex differences in AO activity in humans (Al-Salmy, 2001; Klecker et al., 2006; Dalvie et al., 2013).

Male and female rat S9 CL_{int}

Total CL_{int} (NADPH-dependent and -independent) in female rat S9 was generally low compared to that obtained from male rat S9 (Figure IV.9). CL_{int} of BIBX1382 was only measurable in female S9 when fortified with NADPH. In some cases (O⁶-benzylguanine and zaleplon), substrate turnover was too slow in female S9 to measure intrinsic clearance even in the presence of NADPH. In the case of SGX523, NADPH-independent CL_{int} was similar between male and female rat S9, while a greater disparity was observed in the presence of NADPH, with higher activity in male S9. This observation indicates higher P450 activity in male S9, which is consistent with the current understanding that male rats exhibit higher

P450 activity than female rats. This may also explain the ability to measure O⁶-benzylguanine and zaleplon CL_{int} in male S9 fortified with NADPH (due to contribution of P450 metabolism), but not in female S9. Unlike the observation with SGX523, NADPH-independent CL_{int} of zoniporide was substantially higher in male rat S9 versus female. While a difference in AO activity may be responsible for this observation, it is also possible that another enzyme may be involved, as hydrolysis has also been demonstrated as a metabolic pathway of zoniporide in rats (though it was reported to be a minor pathway) (Dalvie et al., 2010).

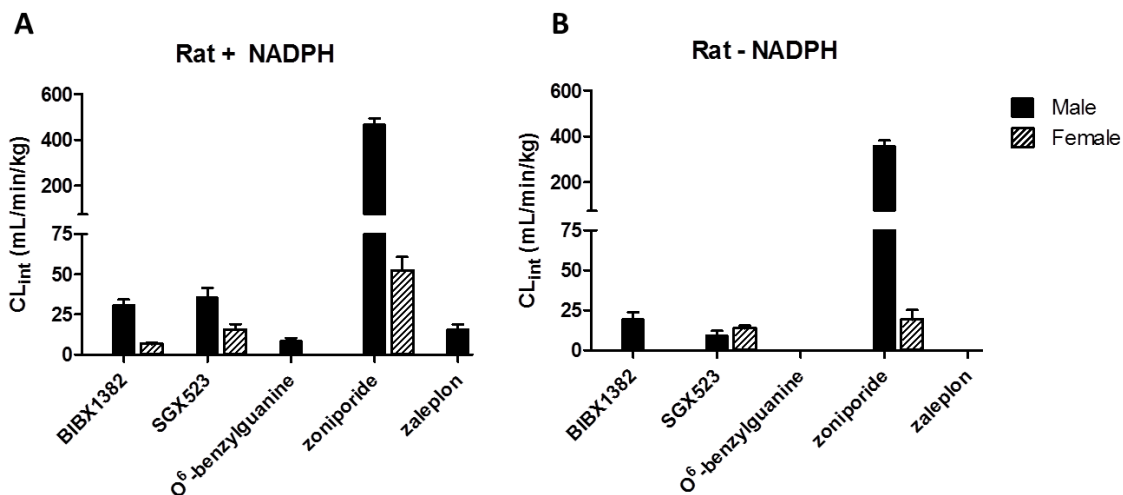


Figure IV.9. Intrinsic clearance in male and female rat hepatic S9 in the presence (A) or absence (B) of NADPH. Data represent the mean (\pm SD) of triplicate determinations from 1-3 experiments.

Male and female mouse S9 CL_{int}

Total CL_{int} in female mouse S9 was low compared to that obtained in male mouse S9, with the exception of O⁶-benzylguanine, which was higher in female

(Figure IV.10). NADPH-independent substrate depletion was only measurable in male mouse S9 for SGX523 and zoniporide and only for zoniporide in female S9, which was lower than that observed in male S9. The inability to measure substrate depletion in the absence of NADPH in most cases in mouse S9 prevents an assignment of any observed sex differences to AO versus NADPH-dependent enzymes.

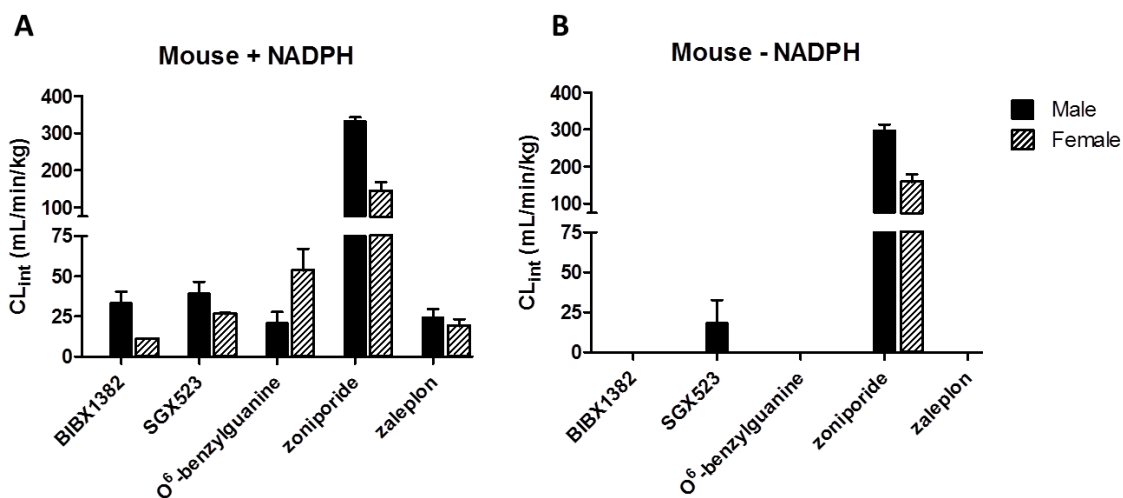


Figure IV.10. Intrinsic clearance in male and female mouse hepatic S9 in the presence (A) or absence (B) of NADPH. Data represent the mean (\pm SD) of triplicate determinations from 1-4 experiments.

Male and female cynomolgus S9 CL_{int}

Female cynomolgus S9 demonstrated low substrate turnover of all compounds in the presence of NADPH compared to that obtained in male cynomolgus S9 (Figure IV.11). In fact, CL_{int} could only be calculated from female cynomolgus S9 incubations for BIBX1382 and SGX523. Low turnover was also

observed in female cynomolgus S9 incubations absent NADPH, permitting an NADPH-independent CL_{int} calculation only for BIBX1382 and SGX523, which were much lower than that observed in male S9. Our observation of decreased NADPH-independent activity in female cynomolgus S9 relative to male is consistent with a previous report by Dalvie et al, who observed 4-fold higher CL_{int} of zonisporide in male S9 versus female (Dalvie et al., 2013). Dalvie's studies did not evaluate NADPH-dependent activity.

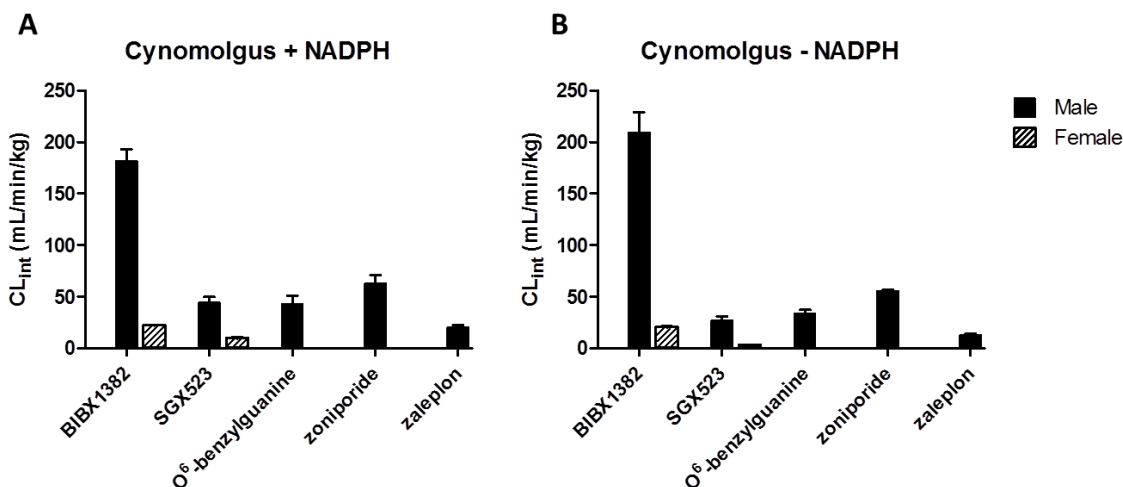


Figure IV.11. Intrinsic clearance in male and female cynomolgus monkey hepatic S9 in the presence (A) or absence (B) of NADPH. Data represent the mean (\pm SD) of triplicate determinations from 1-2 experiments.

Male and female rhesus S9 CL_{int}

Male and female rhesus S9 exhibited similar activity towards all compounds in the presence of NADPH, with slightly higher CL_{int} observed in female S9 in most cases (Figure IV.12). Similar results were obtained from incubations absent NADPH,

where female exhibited slightly higher CL_{int} in most cases. Interestingly, these results contrast the data obtained from cynomolgus S9 incubations, which demonstrated very little activity in female versus male S9. Dalvie reported a much higher CL_{int} of zonisporide in female rhesus S9 versus male, whereas we saw a relatively moderate difference between the sexes (Dalvie et al., 2013). It is unclear as to why we observed much higher activity in our studies with male rhesus S9 (zoniporide CL_{int} = 30.2 mL/min/kg versus 2.5 mL/min/kg in Dalvie's report); however, we observed very similar activity in our female rhesus S9 experiments (zoniporide CL_{int} = 39.8 mL/min/kg versus 31.5 mL/min/kg in Dalvie's report).

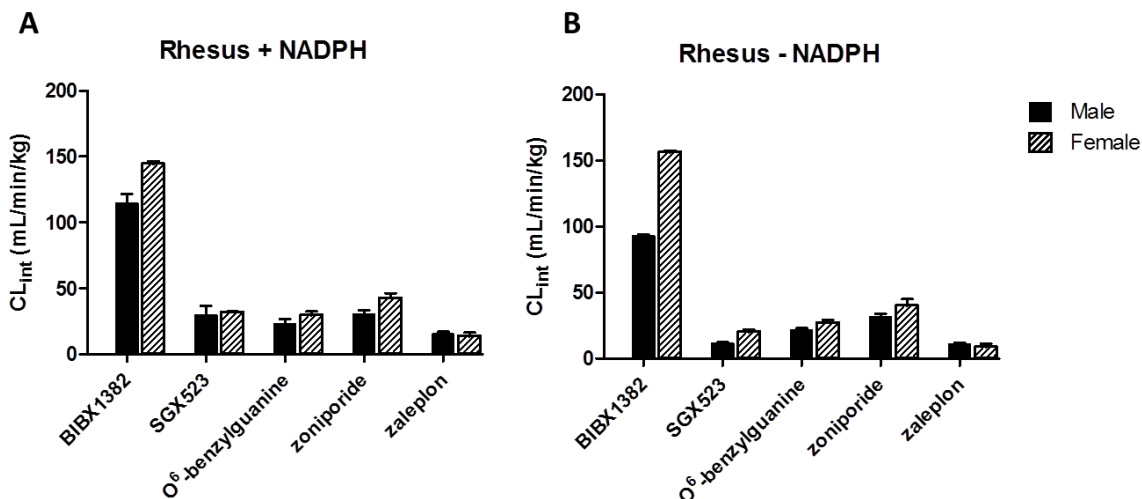


Figure IV.12. Intrinsic clearance in male and female rhesus monkey hepatic S9 in the presence (A) or absence (B) of NADPH. Data represent the mean (\pm SD) of triplicate determinations from 1-4 experiments.

Male and female guinea pig S9 CL_{int}

CL_{int} measured in female guinea pig S9 was similar to or lower than that observed in male guinea pig S9 for all compounds in the presence of NADPH (Figure IV.13). Turnover of zaleplon was too slow to calculate CL_{int} in female guinea pig S9 (with or without NADPH). In the absence of NADPH, female activity again was similar to male or somewhat lower towards all compounds. While male and female guinea pig S9 demonstrated similar activity towards BIBX1382 and O⁶-benzylguanine in the presence of NADPH, NADPH-independent CL_{int} of these two substrates was decreased in female S9 relative to male. Dalvie et al also reported NADPH-independent CL_{int} of zonisporide in male and female guinea pig S9, observing mildly decreased activity in female S9 (Dalvie et al., 2013).

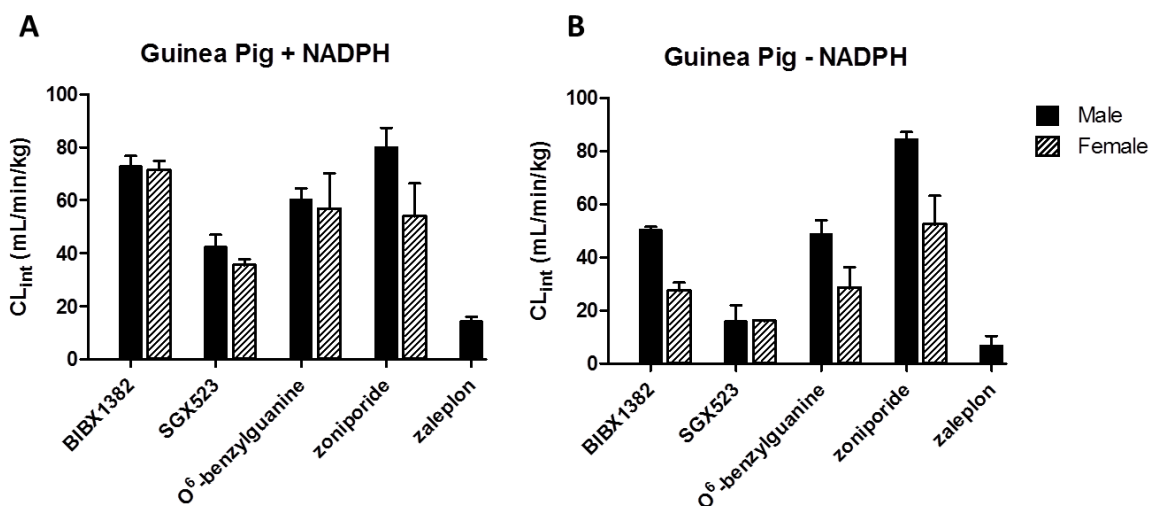


Figure IV.13. Intrinsic clearance in male and female guinea pig hepatic S9 in the presence (A) or absence (B) of NADPH. Data represent the mean (\pm SD) of triplicate determinations from 1-4 experiments.

Male and female minipig S9 CL_{int}

Unlike most cases in the previous species evaluated, CL_{int} measured in female minipig S9 was higher than that observed in male minipig S9 for all compounds in the presence of NADPH (Figure IV.14). Likewise, in the absence of NADPH, female minipig S9 also exhibited higher activity toward all compounds; however, turnover of zaleplon was too slow in both male and female S9 to calculate NADPH-independent CL_{int} for this compound. It should be noted that because the elimination of BIBX1382 from female minipig S9 was so rapid, the CL_{int} value obtained for BIBX1382 in female S9 was estimated using only 2 data points (0 and 7 minutes), as the compound was below the limits of detection beyond these time points. These data again replicate male:female differences in zonisporide CL_{int} observed in Dalvie's report, where female minipig S9 exhibited 4-fold higher NADPH-independent activity (Dalvie et al., 2013).

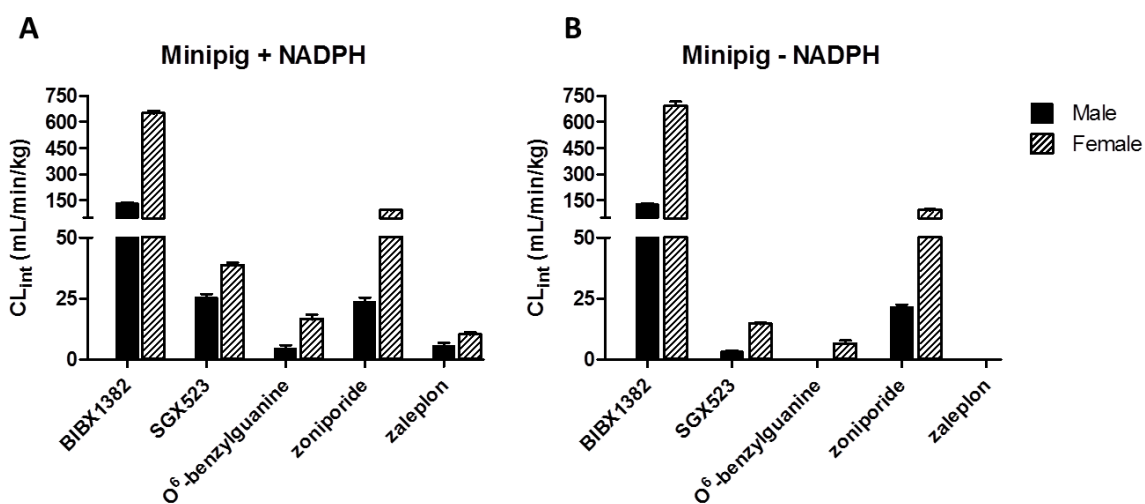


Figure IV.14. Intrinsic clearance in male and female minipig hepatic S9 in the presence (A) or absence (B) of NADPH. Data represent the mean (\pm SD) of triplicate determinations from 1-4 experiments.

In almost all cases, any difference observed in the CL_{int} between male and female S9 in the presence of NADPH was also observed in the absence of NADPH, and was often exaggerated in the absence of NADPH. This observation is consistent with literature reports of sex differences in AO activity (Beedham, 1985; Klecker et al., 2006; Akabane et al., 2011; Dalvie et al., 2013). In particular, our data are similar to that observed by Dalvie et al. with regard to sex differences observed among each species in the NADPH-independent metabolism of zoniporide, with the exception of rhesus monkey, in which case Dalvie observed much lower CL_{int} in male versus female rhesus S9 (Dalvie et al., 2013). In addition, these data indicate that while sex differences may or may not be present in the AO-mediated metabolism of a compound, the sex-dependency of its overall CL_{int} may depend on metabolism via other pathways (e.g. P450) which may exhibit different sex-dependent patterns from AO.

Single species scaling (SSS) of female CL_{int}

Together with prior published reports of sex differences in AO activity, our observations highlight the possibility that sex may influence human clearance predictions obtained from single- or multi-species scaling and may warrant consideration when selecting a preclinical model. Using Equation II.14, we estimated human S9 CL_{int} by SSS of the CL_{int} data obtained from incubations with female S9 (Table IV.21). Because the CL_{int} of BIBX1382 in female minpig S9 was estimated using only 2 data points, these data were therefore excluded from the analysis.

	Zaleplon		O ⁶ -Benzylguanine		Zoniporide		BIBX 1382		SGX 523	
Human Observed CL _{int}	5.8		17.8		17.9		80.2		7.1	
	Predicted CL _{int}	Fold Error	Predicted CL _{int}	Fold Error	Predicted CL _{int}	Fold Error	Predicted CL _{int}	Fold Error	Predicted CL _{int}	Fold Error
F. Cynomolgus monkey	n/a	n/a	n/a	n/a	n/a	n/a	10.8	0.13	4.6	0.66
F. Rhesus monkey	7.9	1.3	17.2	0.97	24.8	1.4	83.9	1.0	18.6	2.6
F. Rat	n/a	n/a	n/a	n/a	12.7	0.71	1.6	0.02	3.8	0.53
F. Mouse	2.5	0.42	7.0	0.39	18.6	1.0	1.4	0.02	3.4	0.49
F. Minipig	6.8	1.2	11.0	0.62	61.2	3.4	n/a	n/a	25.9	3.7
F. Guinea Pig	n/a	n/a	15.0	0.84	14.3	0.8	18.9	0.24	9.4	1.3

Table IV.21. Human CL_{int} (ml/min/kg) predicted by SSS with female S9 and fold-error of the prediction by each SSS method compared to the reference CL_{int} observed in human S9. CL_{int}, intrinsic clearance; SSS, single-species scaling

In accordance with the CL_{int} data obtained from male versus female hepatic S9, human CL_{int} predictions from SSS of female CL_{int} were mostly higher than predictions obtained from SSS of male data in rhesus and minipig, with more pronounced increases in minipig. Alternatively, predictions were mostly lower by SSS with female cynomolgus, rat, mouse, and guinea pig S9 CL_{int} relative to SSS predictions obtained using male CL_{int}. For comparison, Figure IV.15 displays the CL_{int} predictions obtained from SSS with male or female data, with the observed human CL_{int} value indicated by the dotted line.

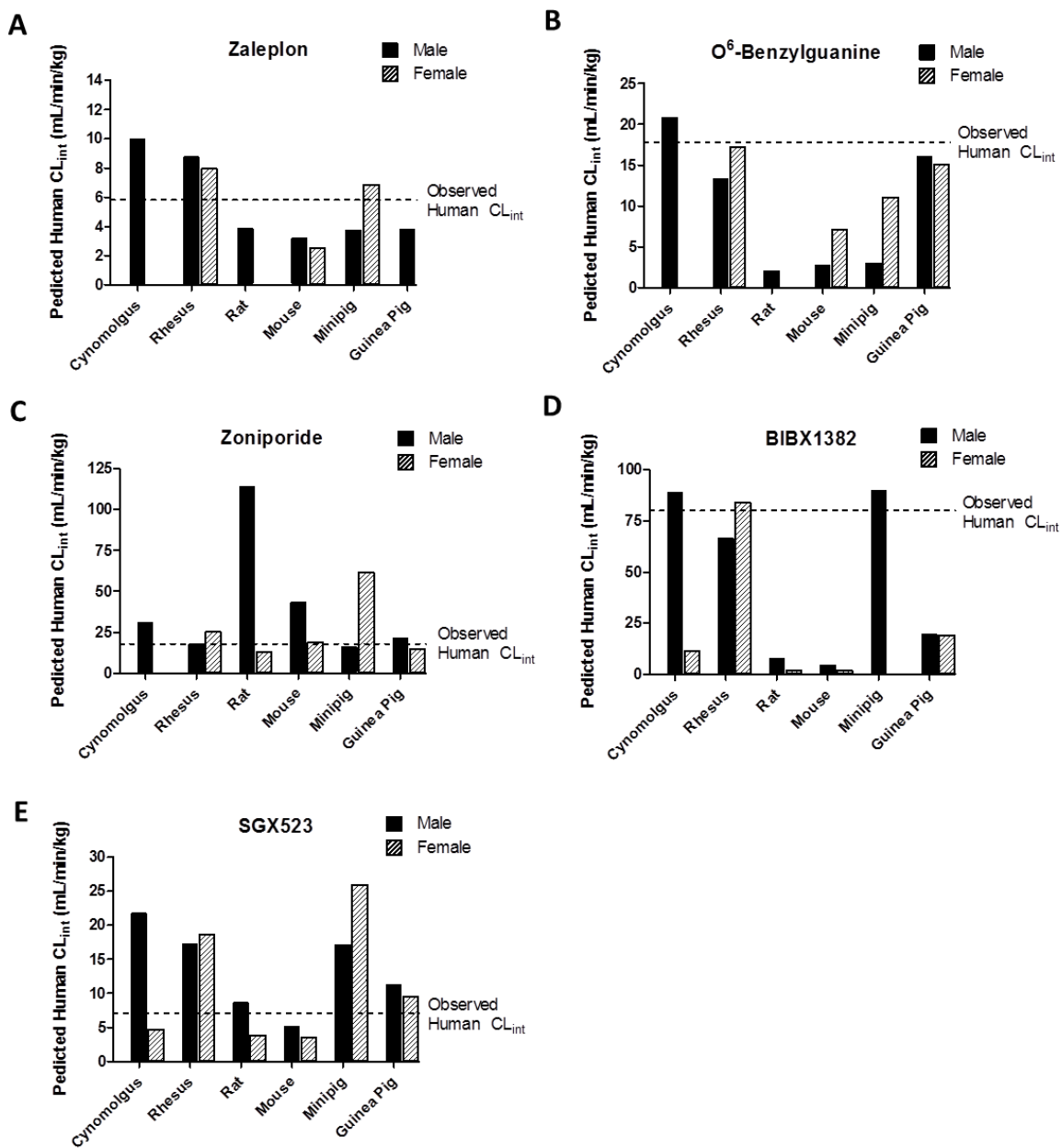


Figure IV.15. Predicted human CL_{int} of zaleplon (A), O⁶-benzylguanine (B), zoniporide (C), BIBX1382, or SGX523 (E) from SSS with male and female hepatic S9. Dotted line indicates the observed human S9 CL_{int} .

Multispecies allometry (MA) with female minipig CL_{int} substitution for male minipig CL_{int}

In addition, when female minipig data is substituted for male data in MA for zaleplon, O⁶-benzylguanine, zoniporide, and SGX523, human CL_{int} predictions are increased in all cases relative to those obtained from MA of only male data (Table IV.22, Figure IV.16). While human CL_{int} of zoniporide and O⁶-benzylguanine was mostly under-predicted by each MA method using all male data, the substitution of male for female minipig data resulted mostly in over-prediction by each MA method. Consequently, over-predictions obtained from MA of all male data for zaleplon and SGX523 were worsened by substitution of female minipig data into the MA analysis. Overall, improvements in prediction fold-error using CL_{int} obtained from female hepatic S9 versus male hepatic S9 were substrate-dependent, and therefore do not indicate that SSS or MA using one sex over the other is always preferable in any of the six species evaluated.

Human Observed CL _{int}	Zaleplon				O ⁶ -benzylguanine				Zoniporide				SGX523			
	5.8				17.8				17.9				7.1			
	Predicted CL _{int}	Fold Error	R ²	Exponent (b)	Predicted CL _{int}	Fold Error	R ²	Exponent (b)	Predicted CL _{int}	Fold Error	R ²	Exponent (b)	Predicted CL _{int}	Fold Error	R ²	Exponent (b)
F. Minipig/Rhesus/Rat/Mouse	9.8	1.7	0.997	0.896	17.8	1.0	0.98	1.03	34	1.9	0.886	0.672	32.6	4.6	0.999	0.980
F. Minipig/Cyno/Rat/Mouse	10.9	1.9	0.990	0.906	24.3	1.4	0.958	1.06	49.7	2.8	0.936	0.728	41.1	5.8	0.999	1.01
F. Minipig/Rhesus/Gpig/Mouse	9.7	1.7	0.996	0.897	20.8	1.2	0.965	0.947	30.2	1.7	0.936	0.741	33.1	4.7	0.998	0.973
F. Minipig/Cyno/Gpig/Mouse	10.7	1.8	0.989	0.906	28.5	1.6	0.957	0.985	43.6	2.4	0.965	0.792	41.6	5.9	1.0	1.0
F. Minipig/Rhesus/Rat	10.7	1.8	0.993	0.928	28.4	1.6	0.993	1.21	20.1	1.1	0.667	0.462	34.9	4.9	0.996	0.996
F. Minipig/Cyno/Rat	11.6	2.0	0.974	0.928	39.9	2.2	0.938	1.24	29.9	1.7	0.835	0.544	43.6	6.2	0.998	1.03
F. Minipig/Rhesus/Gpig	11	1.9	0.991	0.947	10.3	0.58	0.997	0.665	47.3	2.7	0.909	0.92	30.8	4.4	0.994	0.945
F. Minipig/Cyno/Gpig	11.9	2.0	0.967	0.943	12.2	0.69	0.952	0.679	81.5	4.6	0.991	1.02	39.1	5.5	0.999	0.981
F. Minipig/Gpig/Mouse	7.9	1.4	0.999	0.869	21.2	1.2	0.956	0.949	53.0	3.0	0.967	0.815	39.2	5.5	1.0	0.996
F. Minipig/Rat/Mouse	8.0	1.4	1.00	0.870	13.0	0.73	0.98	0.984	79.8	4.5	0.967	0.784	37.5	5.3	1.0	0.999

Table IV.22. Human CL_{int} (mL/min/kg) predicted by multispecies allometry (MA) using CL_{int} data from female minipig and male data from all other species, fold-error of the prediction by each MA method compared to the reference CL_{int} observed in human S9, correlation coefficient of each MA method, and allometric exponent (b) of each MA method. CL_{int}, intrinsic clearance; Cyno = cynomolgus monkey; Rhesus = rhesus monkey; Gpig = guinea pig

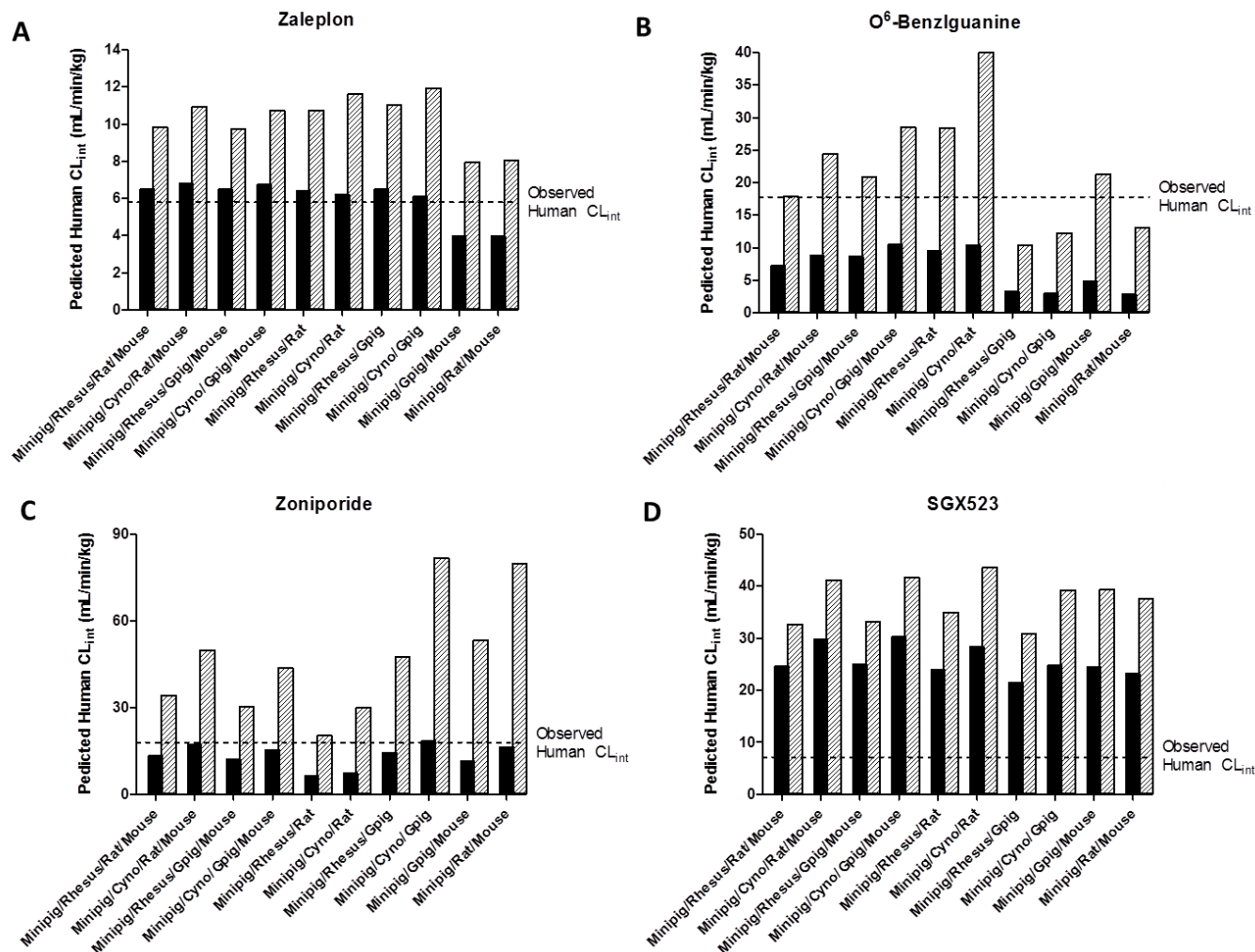


Figure IV.16. Predicted human CL_{int} of zaleplon (A), O⁶-benzylguanidine (B), zoniporide (C), or SGX523 (D) from MA using all male data (black bars) or male data for all species except minipig (patterned bars). Dotted line indicates the observed human S9 CL_{int} .

Multispecies Biotransformation

As described above, species differences were observed in $F_{m,AO}$ and/or E of zaleplon, O⁶-benzylguanine, zoniporide, BIBX1382, and SGX523. To further understand the species differences in metabolism-mediated clearance of the five compounds, biotransformation experiments were conducted in male hepatic S9 of human (mixed gender), mouse, rat, guinea pig, cynomolgus monkey, rhesus monkey, and minipig in the presence or absence of NADPH. Structures of proposed metabolites were elucidated by LC-MS/MS using full scan MS and data dependent full scan MS/MS (selection of most intense ion or fixed mass) techniques, coupled with comparison to any metabolite/fragmentation data available in the literature for the compounds of interest. As the primary goal of these experiments was to understand species differences in NADPH-dependent versus NADPH-independent metabolism rather than structural identification of metabolites, additional experiments or use of authentic metabolite standards were not conducted to confirm proposed metabolite structures. The metabolism of each compound in human and structural identity of the associated AO metabolite have been thoroughly reviewed by others, as noted in the following sections. Throughout this section, metabolites denoted as "M1," refer to the AO-mediated metabolite, which was identified based on the NADPH-independent nature and MS/MS spectra, but was not confirmed in our studies to be solely mediated by AO with hydralazine (it is possible that XO could potentially contribute to M1 formation in some species), nor was its identity confirmed by comparison to an authentic standard.

Zaleplon

The metabolism of zaleplon was previously reported in human, rat, and monkey *in vitro* and/or *in vivo* (Beer et al., 1997; Kawashima et al., 1999; Lake et al., 2002b; Renwick et al., 2002). The principal NADPH-dependent and -independent metabolism of zaleplon observed in hepatic S9 is summarized in Figure IV.17. HPLC-UV chromatograms depicting the principal metabolites formed in the presence or absence of NADPH in each species are shown in Figures IV.18-19, and the MS/MS spectra and proposed fragmentation of each metabolite are shown in Figures IV.21-24. Fragmentation of a metabolite detected at 8.9 min ($[M+H]^+$ at m/z 322) was indicative of zaleplon oxidation to M1 (Figure IV.21) in all species in extracts from S9 incubations both in the absence (Figure IV.18) and presence (Figure IV.19) of NADPH. Consistent with no quantifiable substrate depletion in mouse, rat, and minipig S9 CL_{int} experiments without NADPH, turnover of zaleplon to M1 appeared to be decreased in these species relative to monkey, guinea pig, and human (Figure IV.18). The metabolite eluting at 9.1 min, M2 ($[M+H]^+$ at m/z 278), produced fragments indicative of zaleplon N-deethylation, was detected in all species in S9 containing NADPH, and was the predominant metabolite in minipig (Figure IV.19, Figure IV.22). Trace amounts of M2 were also detected in minipig S9 incubations without NADPH fortification, likely resulting from low levels of endogenous NADPH present in the minipig S9 fractions (Figure IV.18). An N-desethyl-monooxidative metabolite, designated as M3 ($[M+H]^+$ at m/z 294, 5.8 min), was also detected in S9 extracts of all species when NADPH was present (Figure IV.19, Figure IV.23). It is likely that M3 corresponds to the N-desethyl analog of M1,

which has been previously reported (Beer et al., 1997; Kawashima et al., 1999; Lake et al., 2002b; Renwick et al., 2002). Trace amounts of another NADPH-dependent metabolite, M4 ($[M+H]^+$ at m/z 236, 9.0 min), having a mass consistent with the deacetylated analog of M2 (Lake et al., 2002b), were detected in all species except human and guinea pig (Figure IV.19, Figure IV.24).

Overall, with regard to metabolites produced as well as the relative amounts of each metabolite, guinea pig exhibited a metabolism profile most similar to human, though cynomolgus and rhesus were also quite similar with the exception of M4 formation. Minipig exhibited the most dissimilar profile to human with regard to relative amounts of metabolites generated (M1 and M2). Though the low substrate turnover created a challenge in estimating $F_{m,A0}$ of zaleplon in all species, the metabolism data supports the higher $F_{m,A0}$ in human, guinea pig, and monkey, and the low or immeasurable $F_{m,A0}$ in mouse, rat, and minipig. Interestingly, despite the apparently lower NADPH-independent turnover to M1 in mouse, rat, and minipig, the hepatic extraction in these species was similar to human, as described previously (Table IV.2), supporting the notion that the NADPH-dependent metabolism (e.g., to M2) may have compensated for the lesser NADPH-independent metabolism in these species to result in a similar hepatic extraction efficiency (E) to human, but a lower $F_{m,A0}$. Likewise, this observation appears to contribute to the successful SSS of human CL_{int} by all species, including those with a decreased AO-mediated metabolism.

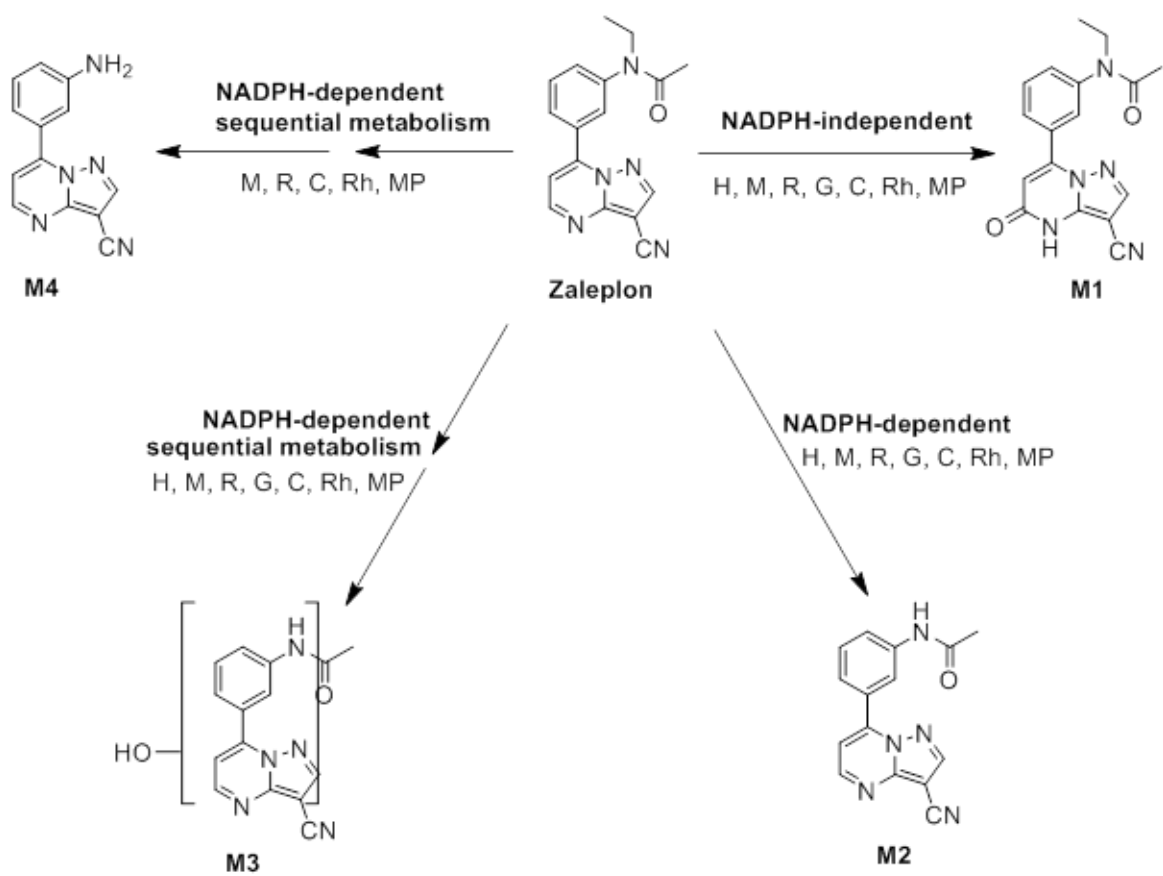


Figure IV.17. Proposed multispecies metabolism of zaleplon in hepatic S9. H, human; M, mouse; R, rat; G, guinea pig; C, cynomolgus monkey; Rh, rhesus monkey; MP, minipig

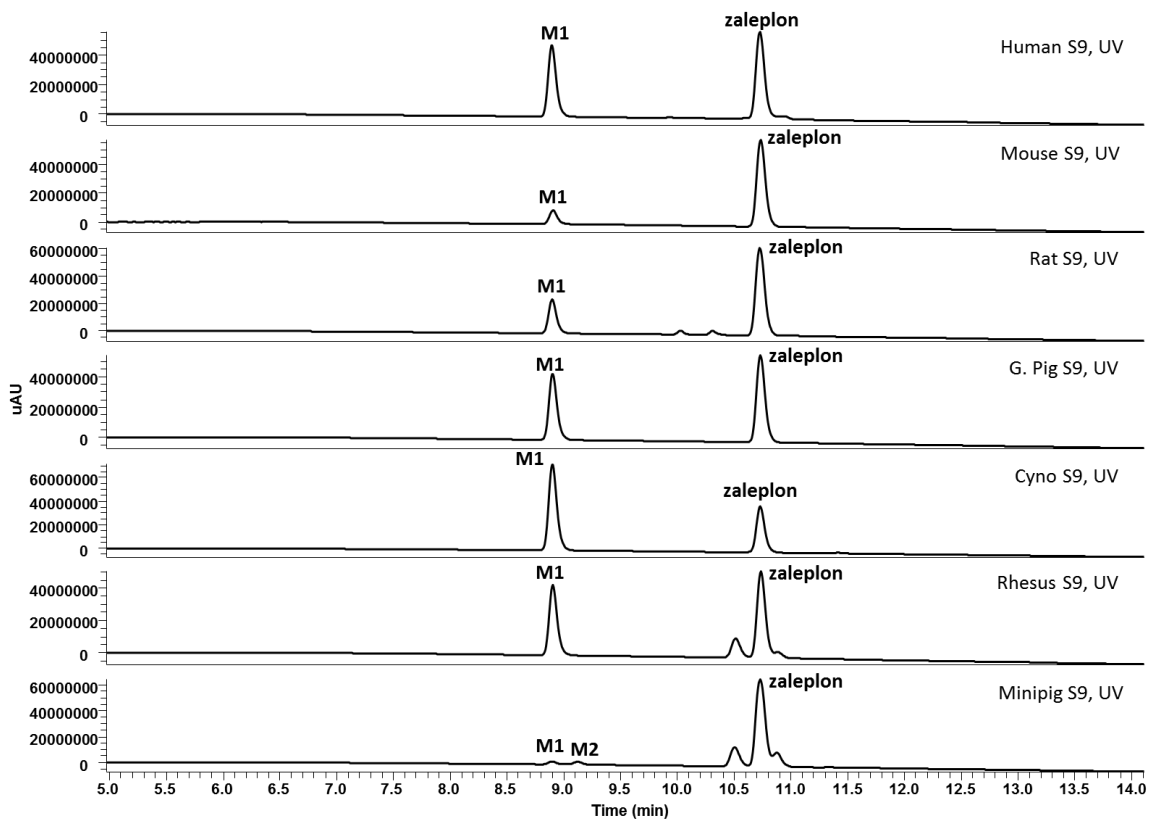


Figure IV.18. Representative LC-UV chromatograms depicting principal metabolite(s) from S9 extracts of human, mouse, rat, guinea pig, cynomolgus monkey, rhesus monkey, and minipig incubated with zaleplon in the absence of NADPH.

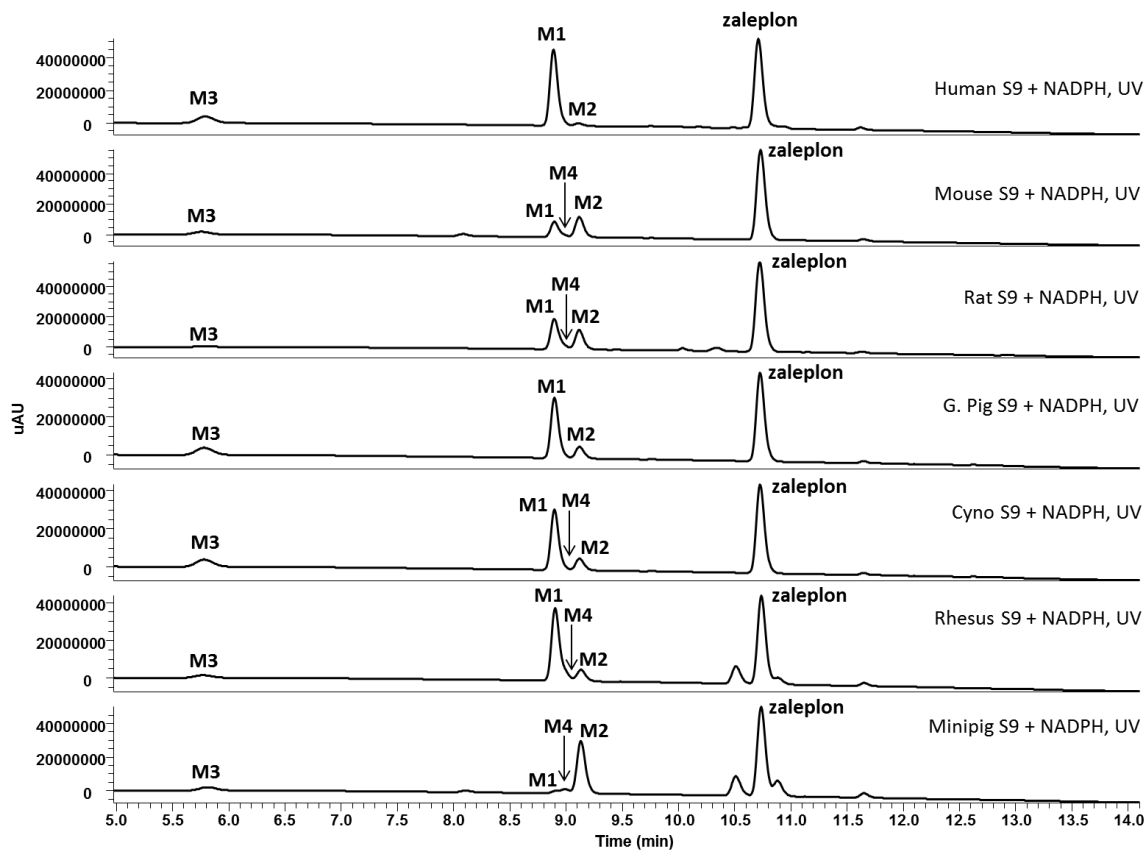


Figure IV.19. Representative LC-UV chromatograms depicting principal metabolites from S9 extracts of human, mouse, rat, guinea pig, cynomolgus monkey, rhesus monkey, and minipig incubated with zaleplon in the presence of NADPH.

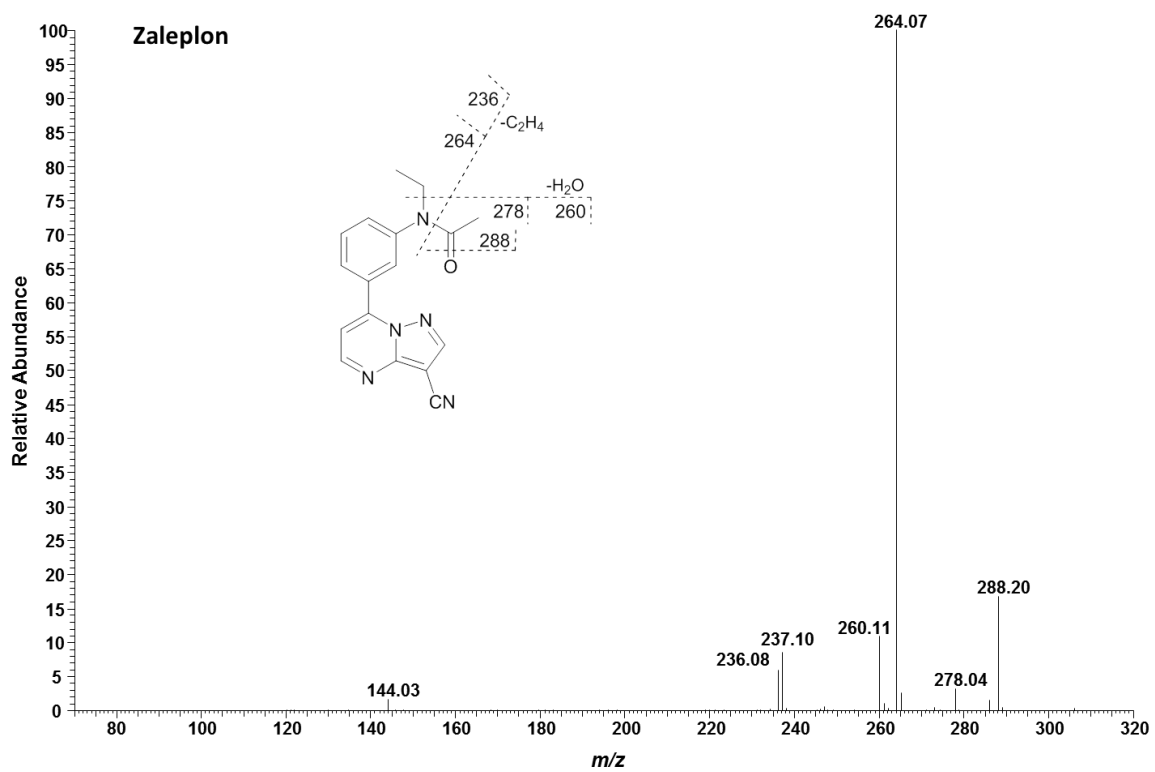


Figure IV.20. LC/MS/MS spectra of zaleplon ($[M+H]^+$ at m/z 306).

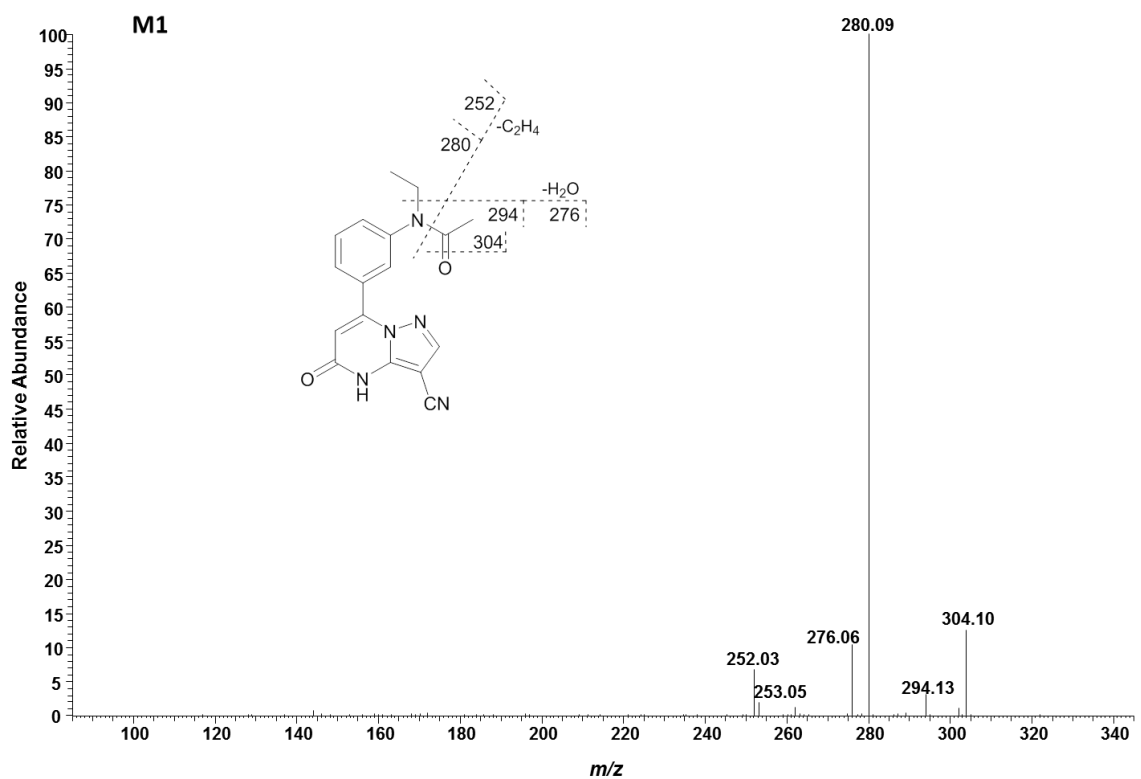


Figure IV.21. LC/MS/MS spectra of zaleplon metabolite M1 ($[M+H]^+$ at m/z 322). Fragment ions occurring at m/z 304, 294, 280, 276, and 252 correspond to a 16-Da increase over zaleplon fragment ions at m/z 288, 278, 264, 260, and 236, respectively.

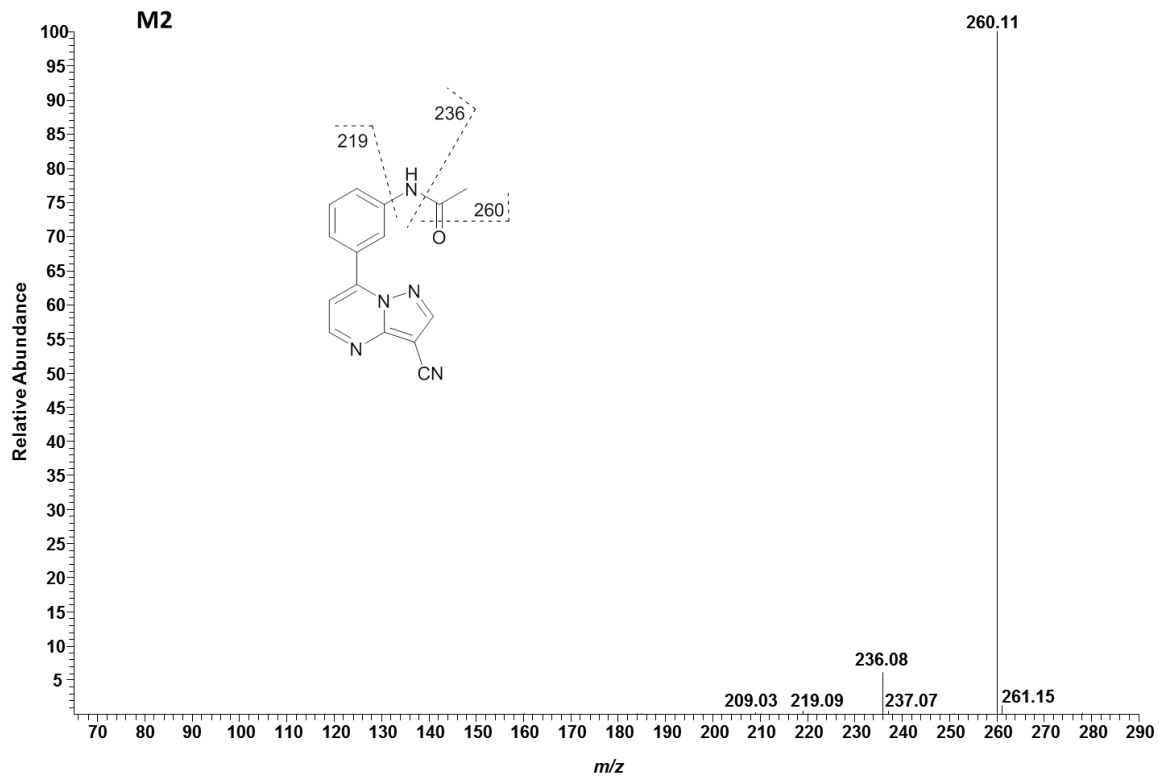


Figure IV.22. LC/MS/MS spectra of zaleplon metabolite M2 ($[M+H]^+$ at m/z 278). Fragment ions occurring at m/z 260 and 236 correspond to a 28-Da decrease relative to zaleplon fragment ions at m/z 288 and 264, respectively.

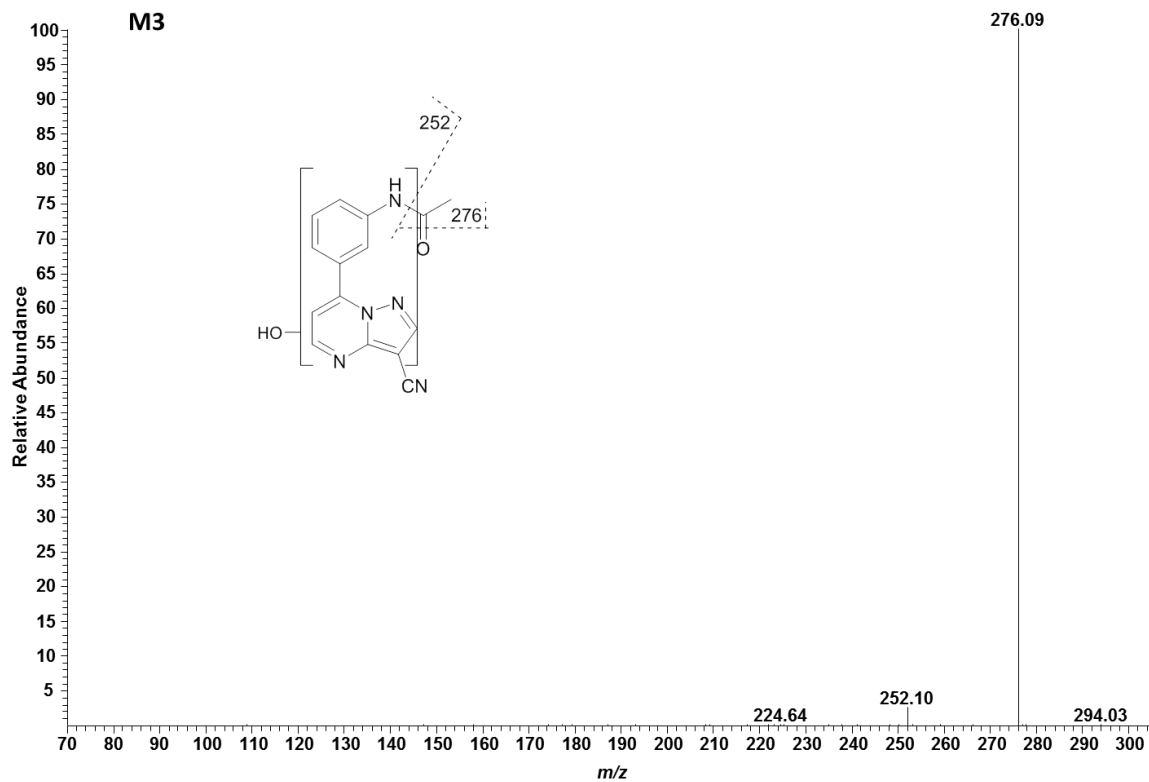


Figure IV.23. LC/MS/MS spectra of zaleplon metabolite M3 ($[M+H]^+$ at m/z 294). Fragment ions occurring at m/z 276 and 252 correspond to a 12-Da decrease (+16 -28) relative to zaleplon fragment ions at m/z 288 and 264, respectively.

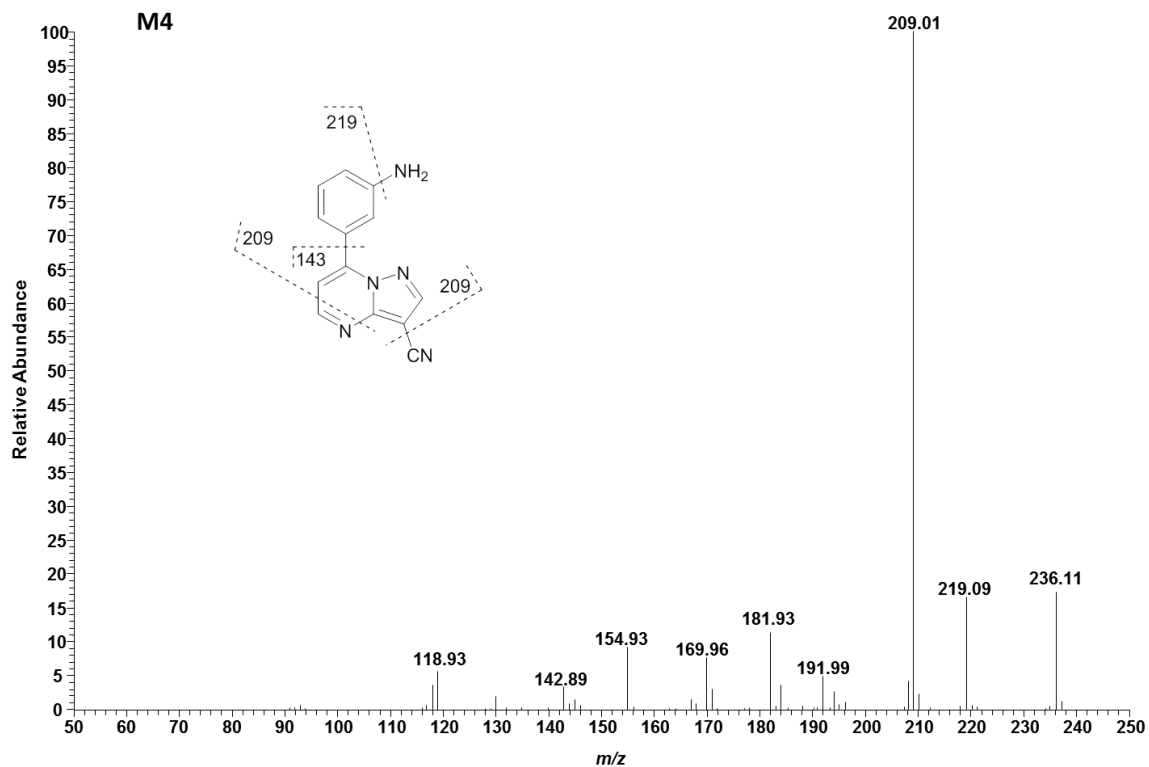


Figure IV.24. LC/MS/MS spectra of zaleplon metabolite M4 ($[M+H]^+$ at m/z 236). The fragment ion occurring at m/z 209 may correspond to fragmentation of the pyrazolopyrimidine or loss of the cyano moiety.

*O*⁶-benzylguanine

In vitro and/or *in vivo* metabolism of *O*⁶-benzylguanine in rat, mouse, and human was previously investigated (Dolan et al., 1994; Roy et al., 1995a; Roy et al., 1995b). Only a single principal metabolite was detected in S9 incubations both in the presence and absence of NADPH, depicted in Figure IV.25. *O*⁶-benzylguanine was metabolized to M1 (Figure IV.32) in S9 fractions absent NADPH in all species. Co-elution of a protonated molecular ion at *m/z* 258 with the parent compound ([M+H]⁺ at *m/z* 242), resulted in a single peak in the UV chromatograms (Figures IV.26-27); however, extracted ion chromatograms (XIC, Figure IV.28) for *m/z* 242 (parent) and *m/z* 258 (M1) reveal slightly different retention times for the two peaks (parent = 11.60 min, metabolite = 11.54 min). Species comparison of MS/MS chromatograms for M1 (total ion current (TIC), *m/z* 258) indicate decreased NADPH-independent turnover to M1 in mouse, rat, and minipig, relative to the other species (Figure IV.29). This observation is consistent with the low turnover observed in rat, mouse, and minipig S9 intrinsic clearance experiments absent NADPH (Table IV.5). However, in mouse, rat, and minipig S9 incubations fortified with NADPH, higher levels of M1 were detected (Figure IV.30), indicating that NADPH-dependent enzyme(s) (e.g., P450) contributed to the generation of M1 in these species. By comparison of the M1 peak area in Figure IV.30 versus Figure IV.29, it appears that NADPH-dependent enzymes were largely responsible for M1 formation in mouse S9 (M1 peak area ratio of 3.64) and rat S9 (M1 peak area ratio of 2.64); these ratios for human, guinea pig, cyno, rhesus, and minipig were 1.06, 1.08, 1.49, 1.11, and 1.65, respectively, indicating a primary NADPH-independent

(e.g., AO) mechanism in these species (Table IV.23). These data are consistent with a prior report of *in vitro* metabolism of O⁶-benzylguanine in male SD rat, which demonstrated M1 formation was greater in microsomes relative to cytosol, was induced by the P450 inducer phenobarbital, and was inhibited by carbon monoxide bubbling (inactivates P450s) into microsomal incubations (Roy et al., 1995a), all of which indicate a role of P450.

Overall, with regard to M1 formation, all species except rat and mouse exhibited similar NADPH-dependency to human, where the majority of M1 was formed in an NADPH-independent manner, indicating AO as the primary pathway. These data support the high $F_{m,AO}$ estimated in all species except rat, mouse, and minipig, which could not be determined due to low substrate turnover. Accordingly, SSS with cynomolgus, rhesus, and guinea pig resulted in predictions within 2-fold of the observed human CL_{int} , while scaling with rat, mouse, and minipig resulted in substantial under-prediction. Unlike the case for zaleplon, an alternate major metabolite was not identified in S9 extracts from mouse, rat, or minipig when O⁶-benzylguanine was incubated with NADPH, which may explain why the estimated hepatic extraction in these species was lower than human, monkey, and guinea pig, and consequently resulted in the under-prediction.

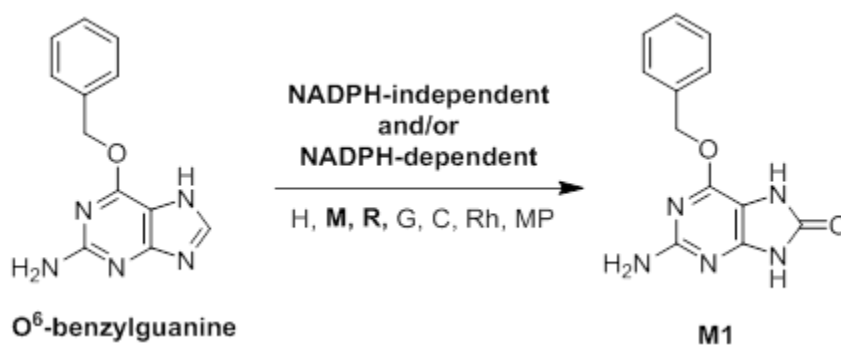


Figure IV.25. Proposed multispecies metabolism of O⁶-benzylguanine in hepatic S9. Species highlighted in bold (rat and mouse) exhibited greater dependence on NADPH for formation of M1 versus other species, which exhibited predominantly NADPH-independent formation of M1. H, human; M, mouse; R, rat; G, guinea pig; C, cynomolgus monkey; Rh, rhesus monkey; MP, minipig

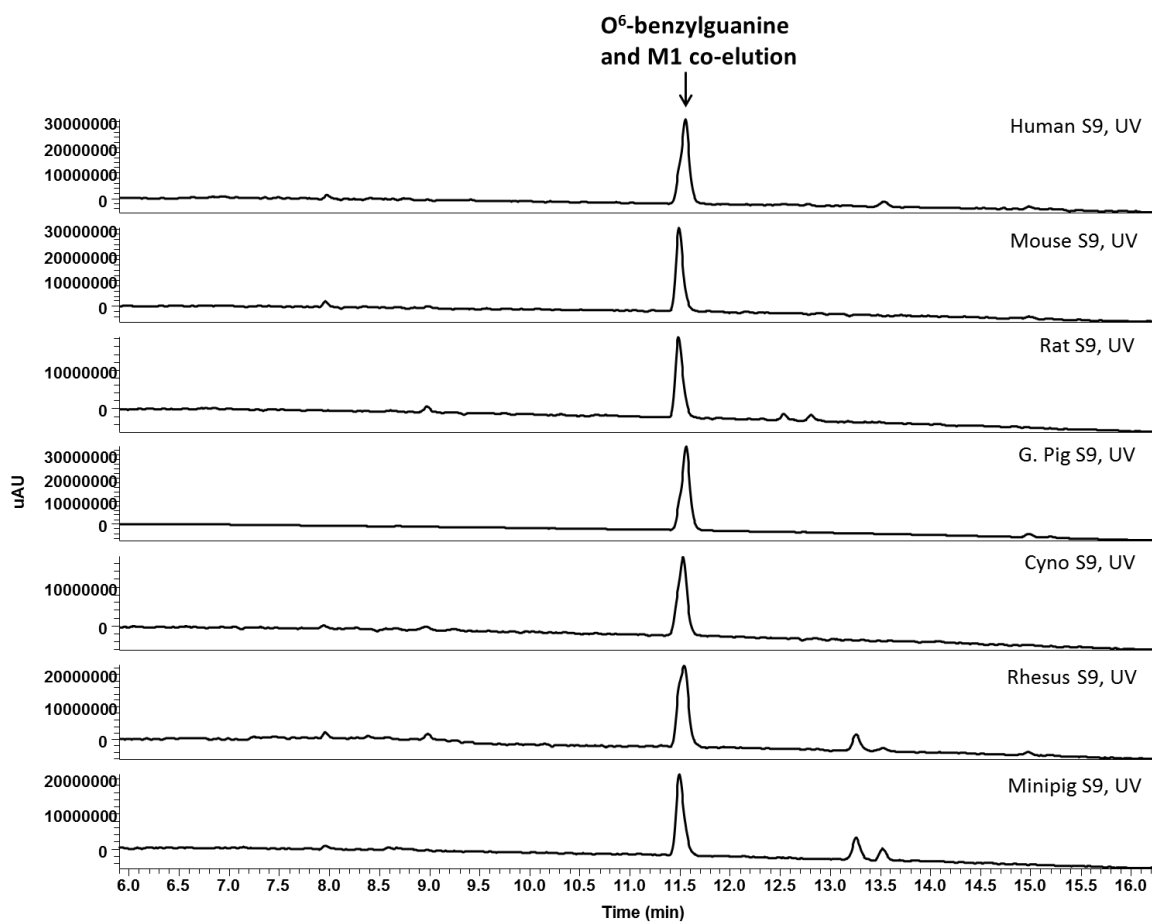


Figure IV.26. Representative LC-UV chromatograms depicting principal metabolite from S9 extracts of human, mouse, rat, guinea pig, cynomolgus monkey, rhesus monkey, and minipig incubated with O⁶-benzylguanine in the absence of NADPH.

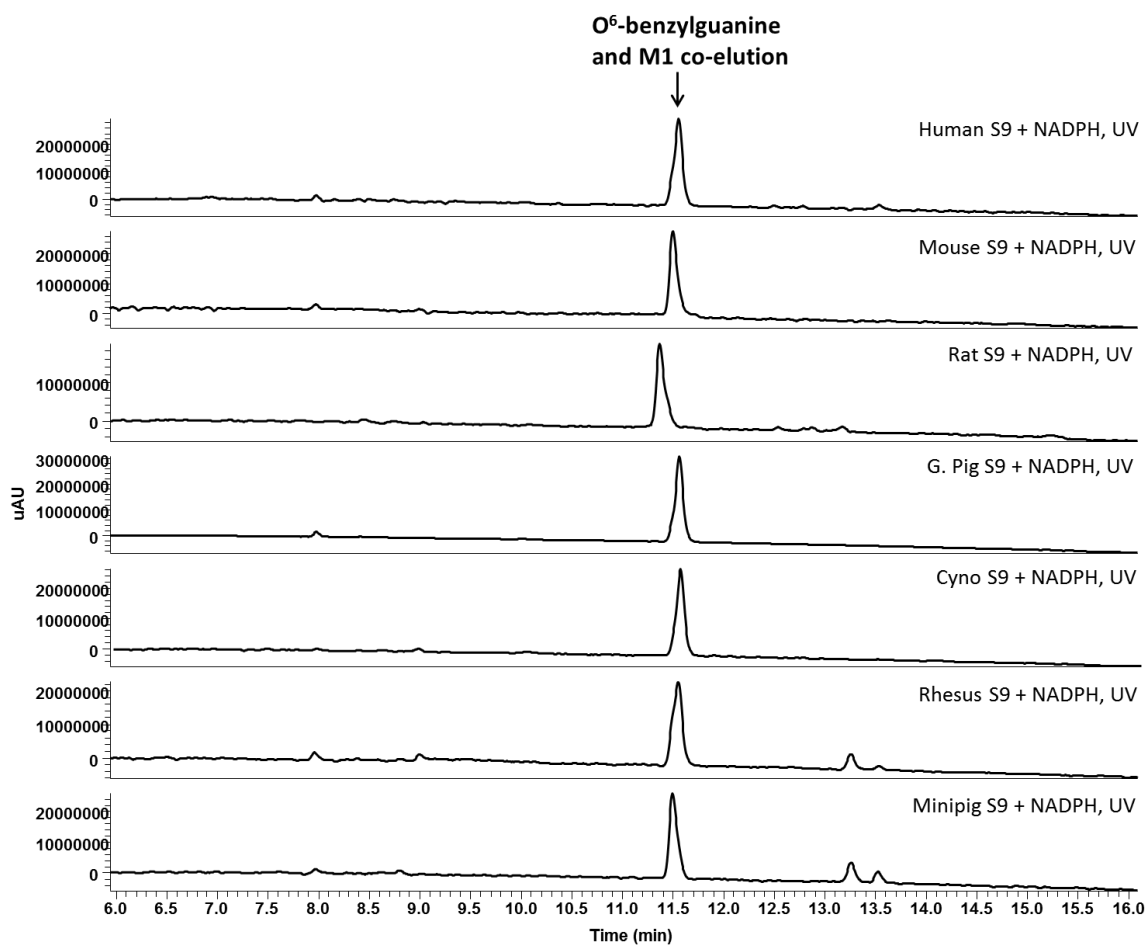


Figure IV.27. Representative LC-UV chromatograms depicting principal metabolite from S9 extracts of human, mouse, rat, guinea pig, cynomolgus monkey, rhesus monkey, and minipig incubated with O^6 -benzylguanine in the presence of NADPH.

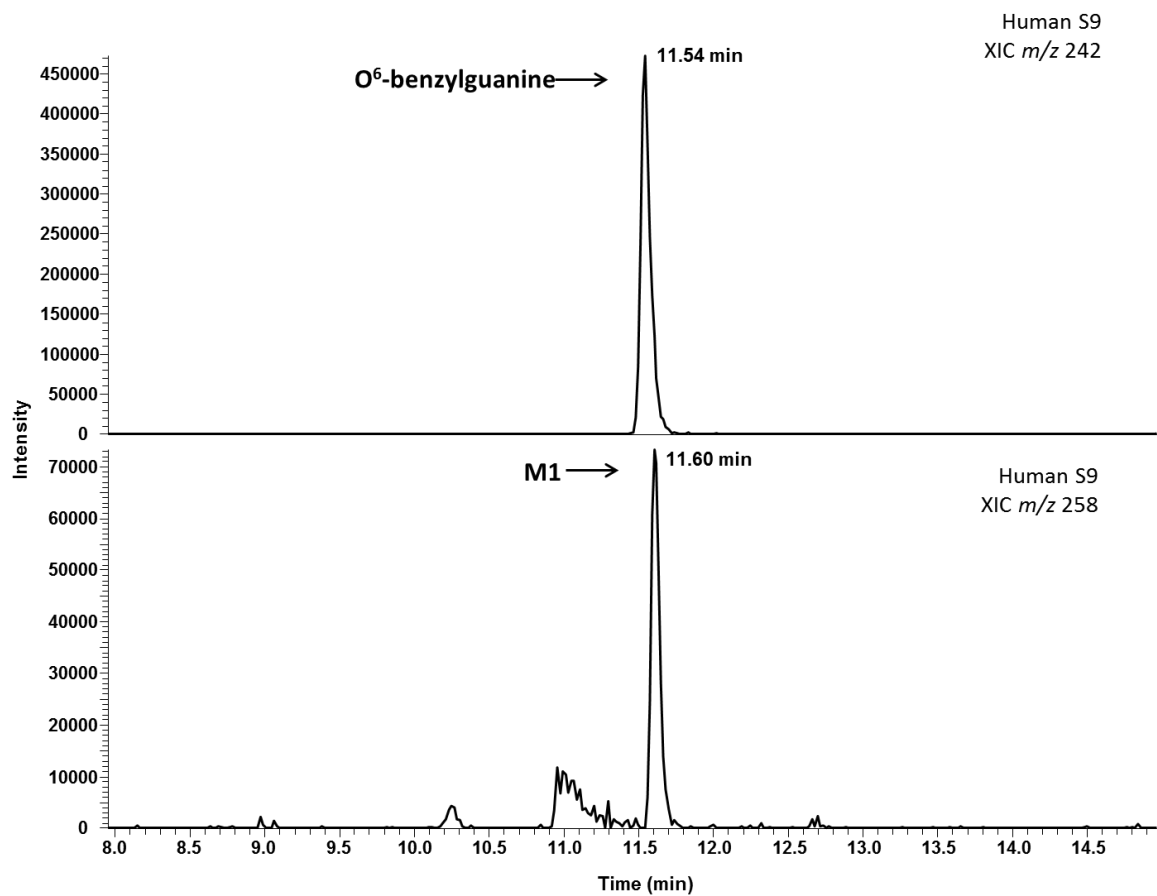


Figure IV.28. Extracted ion chromatograms of m/z 242 (top) and m/z 258 (bottom) revealing elution times of 11.54 min and 11.60 min, respectively, for the parent O⁶-benzylguanine and the AO metabolite M1. The representative chromatogram was obtained from an extract of human S9 incubated with O⁶-benzylguanine in the absence of NADPH. XIC, extracted ion chromatogram

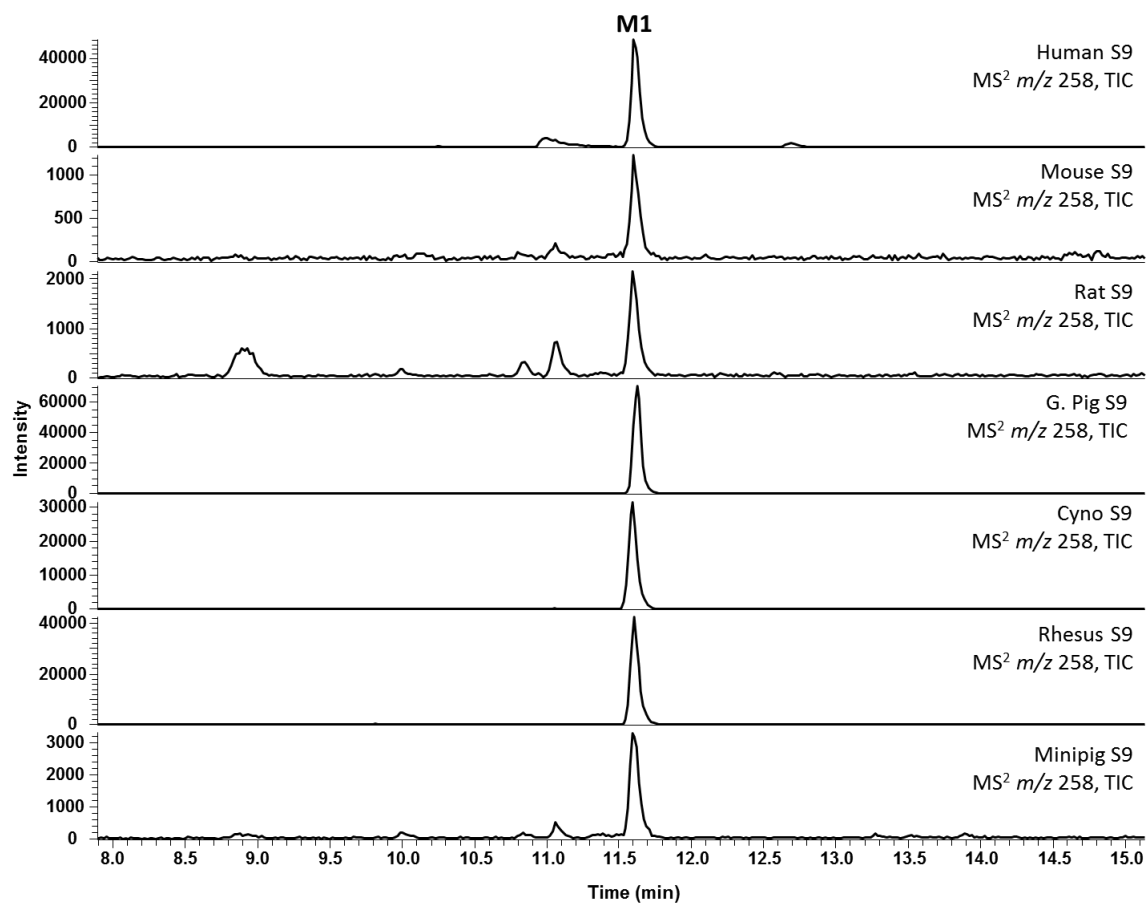


Figure IV.29. Chromatograms representing the total ion current of fragment ions produced by m/z 258 (M1) from S9 extracts of human, mouse, rat, guinea pig, cynomolgus monkey, rhesus monkey, and minipig incubated with O^6 -benzylguanine in the absence of NADPH. TIC, total ion current

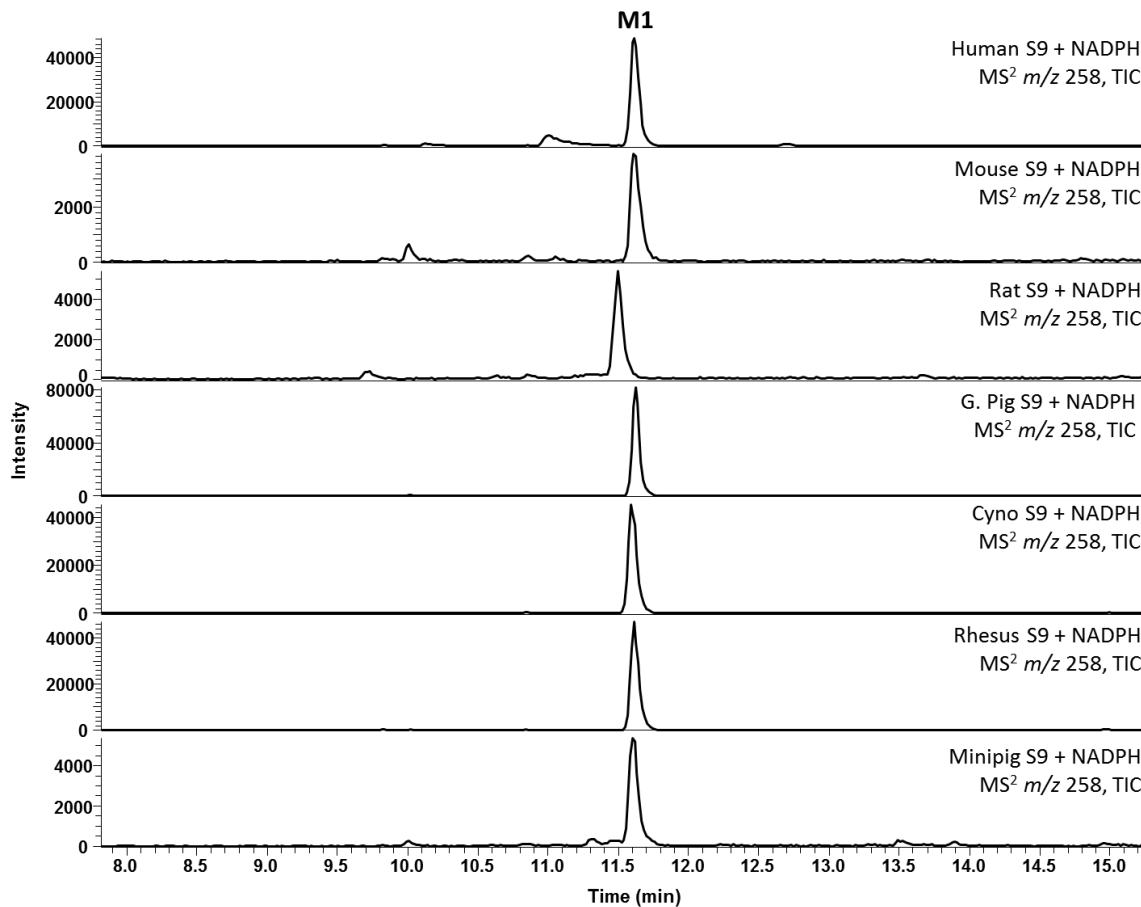


Figure IV.30. Chromatograms representing the total ion current of fragment ions produced by m/z 258 (M1) from S9 extracts of human, mouse, rat, guinea pig, cynomolgus monkey, rhesus monkey, and minipig incubated with O^6 -benzylguanine in the presence of NADPH. TIC, total ion current

Human	Mouse	Rat	G.Pig	Cyno	Rhesus	Minipig
1.06	3.64	2.64	1.08	1.49	1.11	1.65

Table IV.23. Peak area ratio of M1 (presence of NADPH/ absence of NADPH) detected in S9 extracts of human, mouse, rat, guinea pig, cynomolgus monkey, rhesus monkey, and minipig incubated with O^6 -benzylguanine. Ratios determined from peak areas of the XICs in Figure IV.30 versus Figure IV.29.

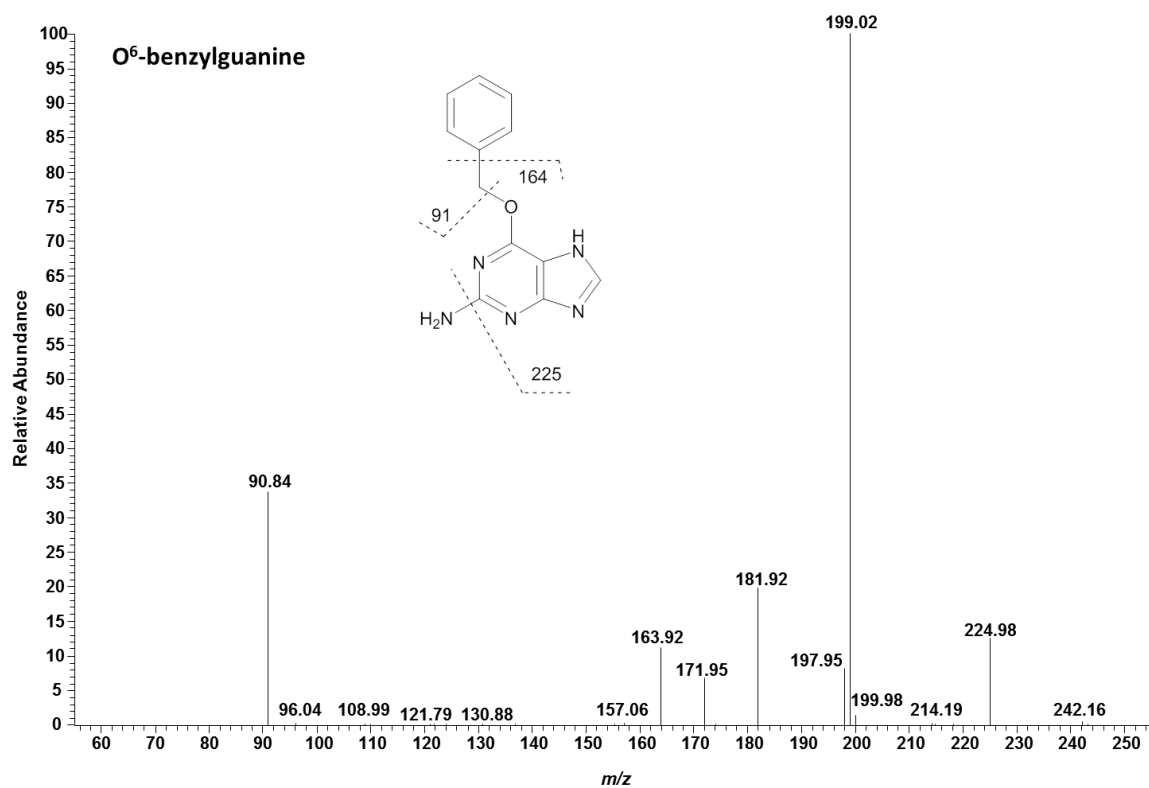


Figure IV.31. LC/MS/MS spectra of O⁶-benzylguanine ([M+H]⁺ at m/z 242).

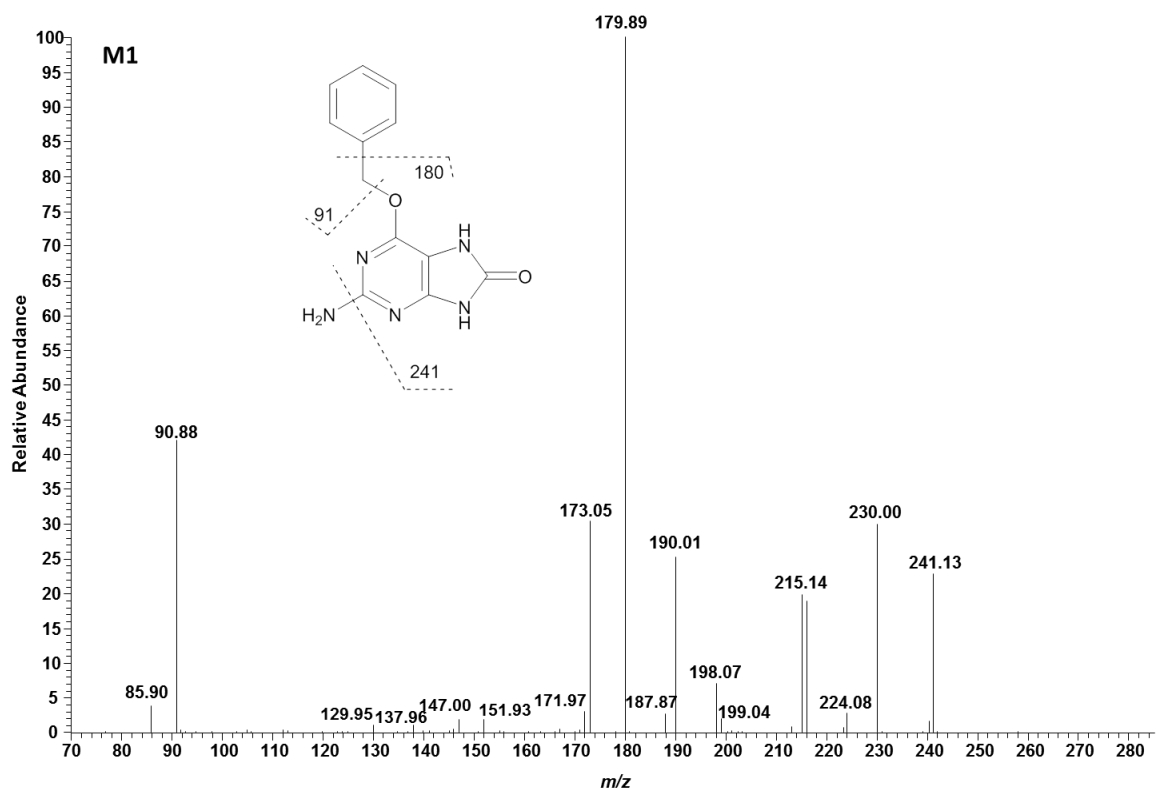


Figure IV.32. LC/MS/MS spectra of O⁶-benzylguanine metabolite M1 ([M+H]⁺ at *m/z* 258). Fragment ions occurring at *m/z* 241 and 180 correspond to a 16-Da increase over O⁶-benzylguanine fragment ions at *m/z* 225 and 164, respectively.

Zoniporide

The *in vivo* metabolism of zoniporide was previously characterized in rat, dog, and human following IV administration of radiolabeled zoniporide (Dalvie et al., 2010). The principal NADPH-dependent and -independent metabolism of zoniporide observed in hepatic S9 is summarized in Figure IV.33. HPLC-UV chromatograms depicting the principal metabolites formed in the presence or absence of NADPH in each species are shown in Figures IV.34-35, and the MS/MS spectra and proposed fragmentation of each metabolite are shown in Figures IV.37-38. Fragmentation of the metabolite detected at 7.9 min ($[M+H]^+$ at m/z 337) was indicative of zoniporide oxidation to M1 (Figure IV.37) in all species in extracts from S9 incubations both in the absence (Figure IV.34) and presence (Figure IV.35) of NADPH. Extensive conversion of zoniporide to M1 in mouse and rat S9 was consistent with the rapid intrinsic clearance observed in mouse and rat S9 in both the presence and absence of NADPH. Unlike the low conversion of zaleplon and O⁶-benzylguanine to their respective M1 metabolites (5-oxozaleplon and 8-oxo-O⁶-benzylguanine) in minipig S9, conversion of zoniporide to M1 (2-oxozoniporide) in minipig S9 was similar to that in human S9 (Figures IV.28-29). A minor oxidative metabolite, M2 (Figure IV.38), was observed at 5.3 min ($[M+H]^+$ at m/z 337) in S9 extracts of all species in incubations containing NADPH (Figure IV.35). Fragmentation of M2, similar to that of M1, indicates likely oxidation of the quinoline or the pyrazole. Particularly, the loss of 17 Da (-OH) from the fragment ion at m/z 278 (resulting in a fragment ion at m/z 261), is indicative of an N-oxide (Figure IV.38). Dalvie noted minor formation of an N-oxide detected in rat urine, but

not in human (Dalvie et al., 2010). Dalvie also identified a carboxylic acid derivative of zoniporide, as well as a carboxylic acid derivative of M1, *in vivo* in human plasma and feces, respectively (the former was also detected in rat plasma and urine) (Dalvie et al., 2010). Though the carboxylic acid derivative of zoniporide represented as much as 6-9% of circulating radioactivity in human and rat, respectively, it was reportedly only detected at trace levels in incubations with human S9 (Dalvie et al., 2010). The carboxylic acid derivative of M1 reportedly was not detected at all in S9 extracts, and because it was only detected in human feces, it was proposed that this metabolite may be formed via gut microflora (Dalvie et al., 2010). In our S9 studies, neither of these two metabolites was detected. It is possible that the ionization efficiency of the carboxylic acid metabolites did not permit detection via positive electrospray ionization (ESI), as ESI negative mode was not explored; however, an unidentified prominent peak was not observed in the UV chromatogram, indicating that if this were the case, the metabolite(s) were present at very low levels. Alternatively, it is also possible that the carboxylic acid metabolite(s) were not retained on the C18 column, as the carboxyl group may have been deprotonated at the pH used (4.1) for the aqueous mobile phase (a pH of 3.0 was utilized in Dalvie's studies) or that the extraction of the metabolite from S9 was inefficient.

Overall, all species exhibited similar metabolite profiles with regard to metabolites produced (M1 and M2), while minipig and rhesus exhibited the most similar profiles to human with regard to the efficiency of zoniporide turnover to M1. Unfortunately, these data are inconclusive as to the source of metabolism

accounting for the minor NADPH-independent clearance observed in human, rat, and guinea pig S9, as only one metabolite (M1) was observed in extracts of incubations absent NADPH. It is possible that XO could play a minor role in M1 formation in these cases; however, Dalvie reported that the XO inhibitor allopurinol had no effect on M1 formation (Dalvie et al., 2010). These data are, however, consistent with the high $F_{m,A0}$ estimated in all species. The substrate turnover to metabolites mirrored the estimated hepatic extraction (E) in each species, with mouse and rat demonstrating higher E relative to other species, and accordingly, SSS with mouse and rat resulted in the greatest degree of over-prediction of human S9 CL_{int} .

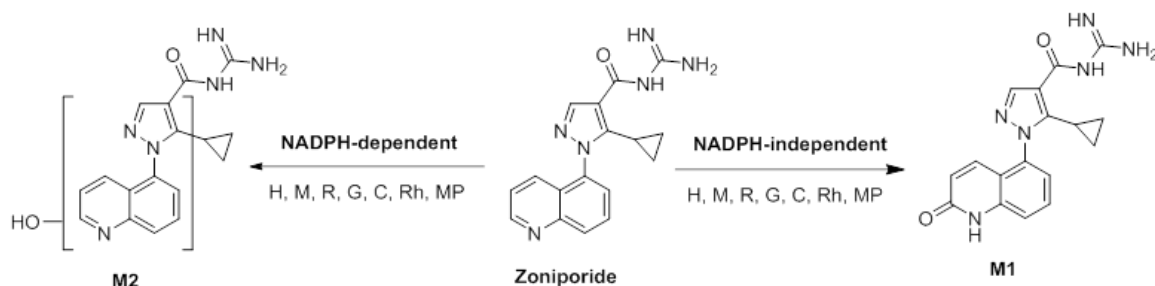


Figure IV.33. Proposed multispecies metabolism of zoniporide in hepatic S9. H, human; M, mouse; R, rat; G, guinea pig; C, cynomolgus monkey; Rh, rhesus monkey; MP, minipig

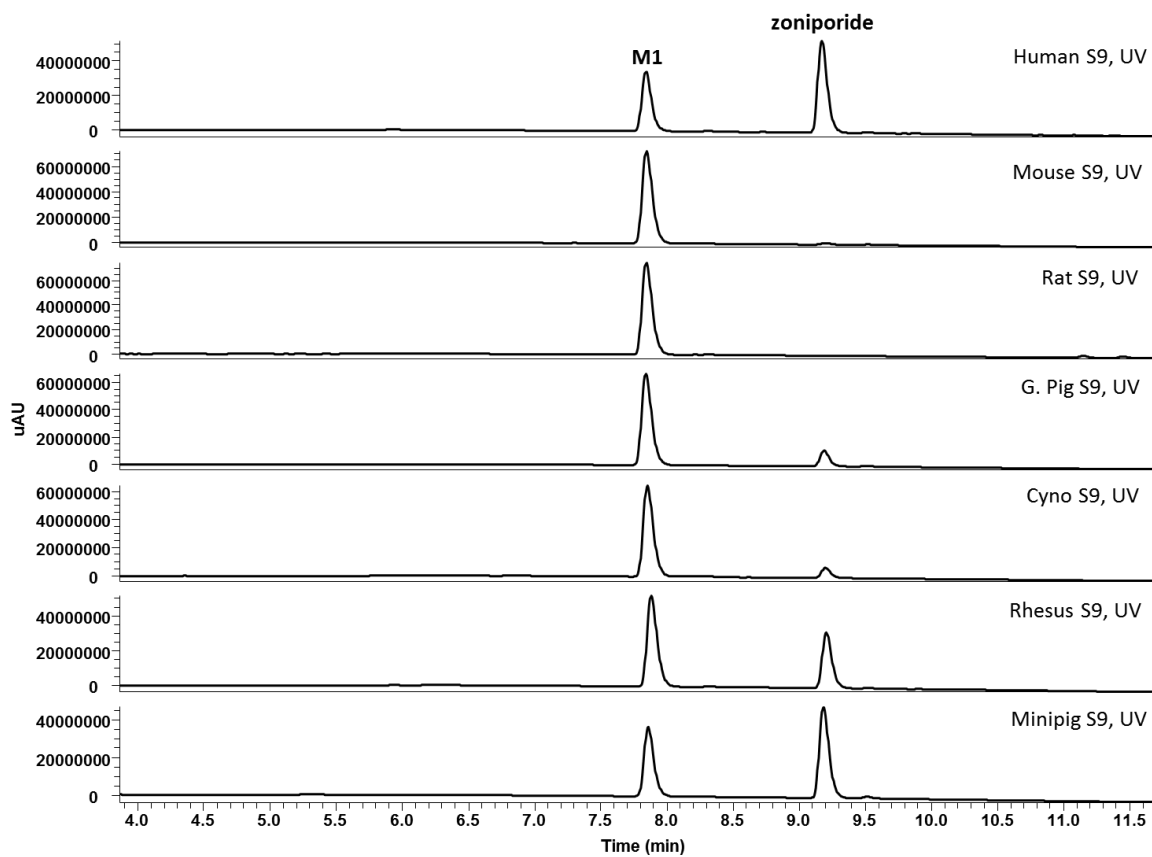


Figure IV.34. Representative LC-UV chromatograms depicting principal metabolite from S9 extracts of human, mouse, rat, guinea pig, cynomolgus monkey, rhesus monkey, and minipig incubated with zoniporide in the absence of NADPH.

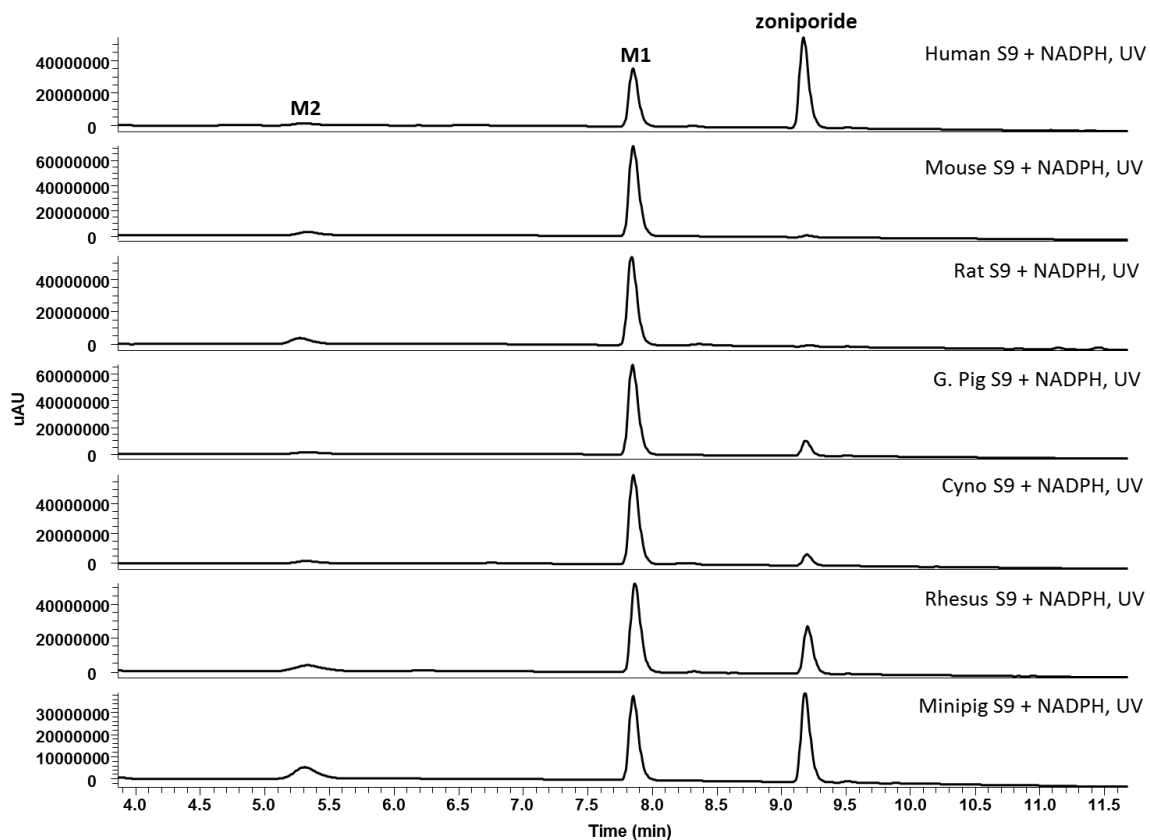


Figure IV.35. Representative LC-UV chromatograms depicting principal metabolites from S9 extracts of human, mouse, rat, guinea pig, cynomolgus monkey, rhesus monkey, and minipig incubated with zoniporide in the presence of NADPH.

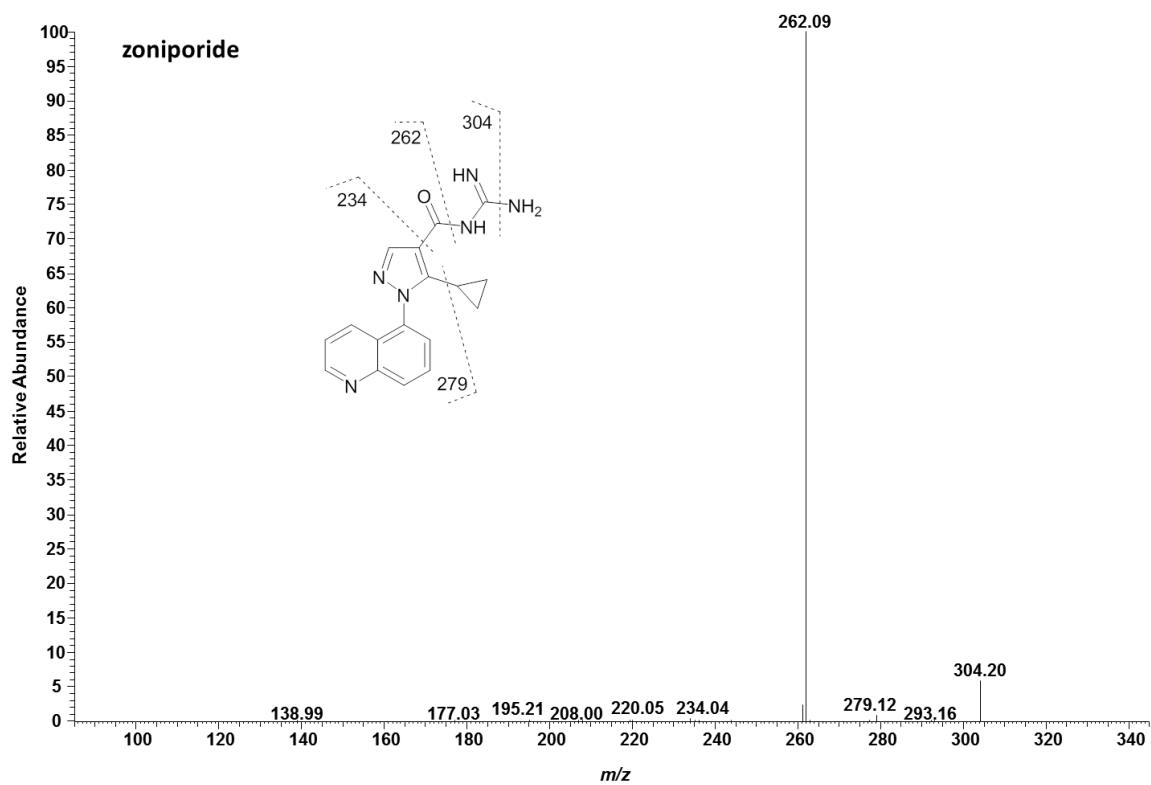


Figure IV.36. LC/MS/MS spectra of zoniporide ($[M+H]^+$ at m/z 321).

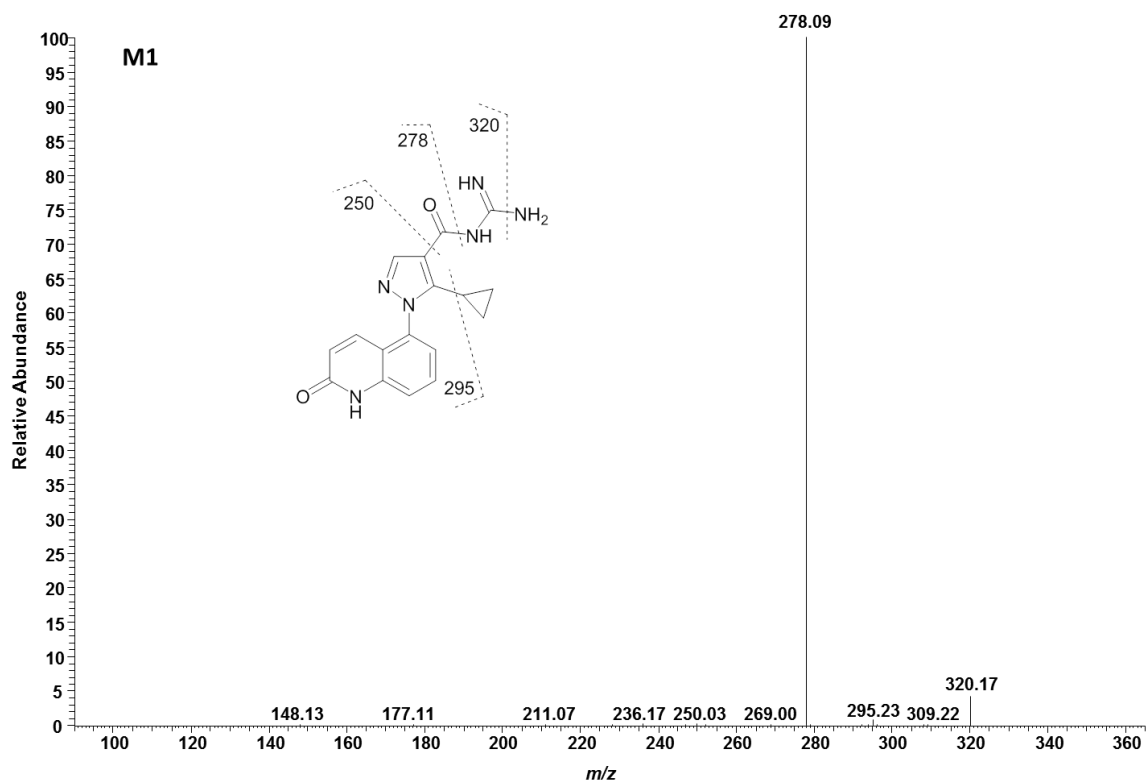


Figure IV.37. LC/MS/MS spectra of zonisporide metabolite M1 ($[M+H]^+$ at m/z 337). Fragment ions occurring at m/z 320, 295, 278, and 250 correspond to a 16-Da increase over zonisporide fragment ions at m/z 304, 279, 262, and 234, respectively.

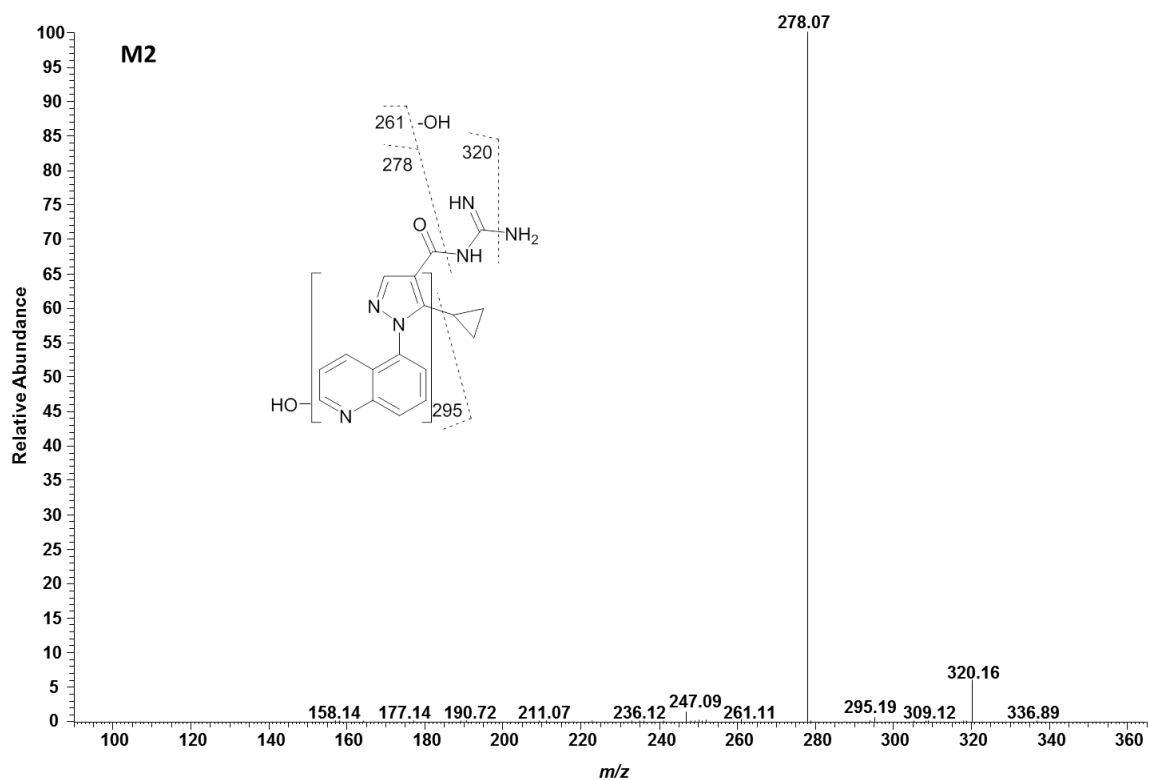


Figure IV.38. LC/MS/MS spectra of zoniporide metabolite M2 ($[M+H]^+$ at m/z 337). Fragment ions occurring at m/z 320, 295, and 278 correspond to a 16-Da increase over zoniporide fragment ions at m/z 304, 279, and 262, respectively. Loss of 17(-OH) from the fragment ion at m/z 278 to form the fragment ion at m/z 261 is indicative of an N-oxide.

BIBX1382

The metabolism of BIBX1382 was previously characterized in human and cynomolgus monkey hepatic cytosol, S9, and hepatocytes (Hutzler et al., 2014a). The principal NADPH-dependent and -independent metabolism of BIBX1382 observed in hepatic S9 is summarized in Figure IV.39. Extracted ion chromatograms (XIC) depicting the principal metabolites formed in the presence or absence of NADPH in each species are shown in Figures IV.40-41, and the MS/MS spectra and proposed fragmentation of each metabolite are shown in Figures IV.43-51. Fragmentation of a metabolite detected at 9.6 min ($[M+H]^+$ at m/z 404) was indicative of BIBX1382 oxidation to M1 (Figure IV.43) in all species in extracts from S9 incubations both in the absence (Figure IV.40) and presence (Figure IV.41) of NADPH. In addition, an NADPH-independent secondary oxidation to M2 ($[M+H]^+$ at m/z 420, 9.3 min) was observed in all species and was a prominent metabolite in most species (Figure IV.40-41). Fragmentation of M1 (Figure IV.43) and M2 (Figure IV.44) is consistent with that reported for metabolites denoted as M1 and M2 by Hutzler et al (Hutzler et al., 2014a). Low levels of an additional monooxidative metabolite, M3 ($[M+H]^+$ at m/z 404, 11.3 min) were detected in rat, mouse, and guinea pig S9 both in the absence (Figure IV.40) and presence (Figure IV.41) of NADPH, producing a major fragment at m/z 373 (Figure IV.45), as well as other minor fragments also produced by M1. Given the NADPH-independent nature of M3, it is likely that M3 results from AO or XO-mediated oxidation of the pyrimido-pyrimidine core and that M2 results from dioxidation of the pyrimido-pyrimidine core (e.g., $M1 \rightarrow M2$ and/or $M3 \rightarrow M2$), as both AO and XO typically oxidize carbon

atoms alpha to a nitrogen of aromatic heterocycles. Overall, NADPH-independent metabolism appeared to be low in mouse and rat compared to other species and moderate in guinea pig, consistent with S9 intrinsic clearance experiments. Prior studies reported that BIBX1382 is N-demethylated in rat and mouse (Dittrich et al., 2002). This metabolite, M4 ($[M+H]^+$ at m/z 374, 12.0 min), was detected in mouse, rat, and guinea pig, but was below detection in the other species (Figure IV.41 and Figure IV.46). Two additional oxidative metabolites, M5 (Figure IV.47) and M6 (Figure IV.48), were also detected in S9 extracts of mouse, rat, and guinea pig at 12.9 min ($[M+H]^+$ at m/z 404) and 13.1 min ($[M+H]^+$ at m/z 404), respectively, in incubations both absent and present NADPH. Fragmentation of these metabolites; however, indicated possible oxidation of the N-methyl piperidine moiety (Figures IV.47-48), and when incubated in the presence of NADPH (Figure IV.41), peak areas of M5 and M6 were approximately 10-fold higher than in the absence of NADPH (Figure IV.40). There are examples in the literature of AO-mediated oxidation of an aliphatic nitrogen-containing ring; however, these examples required P450-mediated generation of an intermediate iminium ion prior to oxidation of the carbon located alpha to the nitrogen (Pryde et al., 2010). It is possible that low levels of NADPH were already present in the S9, resulting in minor NADPH-dependent metabolism even when S9 was not fortified with the cofactor. M5 and M6 were also detected in S9 extracts of minipig in the presence of NADPH, as was M5 in rhesus, though M5 was a very minor metabolite in these species (Figure IV.41). A prominent NADPH-dependent metabolite in minipig and guinea pig with a mass shift of +32 Da, M7 ($[M+H]^+$ at m/z 420, Figure IV.49), was observed at 10.0 min,

followed by a minor +32 Da metabolite, M8 ($[M+H]^+$ at m/z 420, Figure IV.50) at 10.4 min (Figure IV.41). Though less prominent than in minipig or guinea pig extracts, M7 was also detected in extracts of all other species, and M8 was detected in all species except mouse and rat. Based on the fragmentation and retention times, it is possible that these metabolites result from sequential oxidation of M5 and M6 (e.g., $M5 \rightarrow M7$ and $M6 \rightarrow M8$). The presence of a fragment ion at m/z 373 and absence of m/z 389 suggests that one of the oxidations occurs on the nitrogen or the methyl substituent of the N-methyl piperidine moiety (Figure IV.49-50). Finally, a trace NADPH-dependent metabolite, M9 (Figure IV.51), with a mass shift of +16 Da ($[M+H]^+$ at m/z 404) was observed at 10.4 min in mouse and rat extracts, but was not detected in other species (Figure IV.41). Similar fragmentation to M1 and M3, for example, fragments at m/z 373, m/z 361, m/z 307, and m/z 292, indicate the likelihood that the oxidation occurs on the pyrimido-pyrimidine core or possibly the phenyl ring.

Overall, substantial species differences were observed in the metabolism of BIBX1382, particularly when comparing rodent species to human. Rhesus exhibited a profile most similar to human with regard to the relative levels of each metabolite, though trace levels of an additional metabolite, M5, were detected in rhesus, but not human or cynomolgus. Low turnover in S9 of mouse, rat, and guinea pig is consistent with substantial under-prediction of human S9 CL_{int} by SSS with these species. The presence of M2 in human extracts absent NADPH suggests the possibility that the minor NADPH-independent substrate depletion observed in the presence of hydralazine in CL_{int} experiments resulted from XO-mediated formation

of an M2-precursor metabolite (e.g., M3, which may not have been detected in human extracts due to conversion to M2). These data support the $F_{m,AO}$ estimates obtained from CL_{int} experiments, which were high (≥ 0.85) in human, rhesus, cynomolgus, and minipig, and lower or immeasurable in guinea pig, rat, and mouse. Unfortunately, from these experiments, a clear explanation could not be determined as to the discrepancy in $F_{m,AO}$ calculated by methods A and B in rat. However, as previously mentioned, it is possible that the metabolism of BIBX1382 could have been shunted towards NADPH-dependent metabolism (e.g., to M4, M5, M6, and/or M9) when AO was inhibited by hydralazine, resulting in a compensatory effect in the CL_{int} .

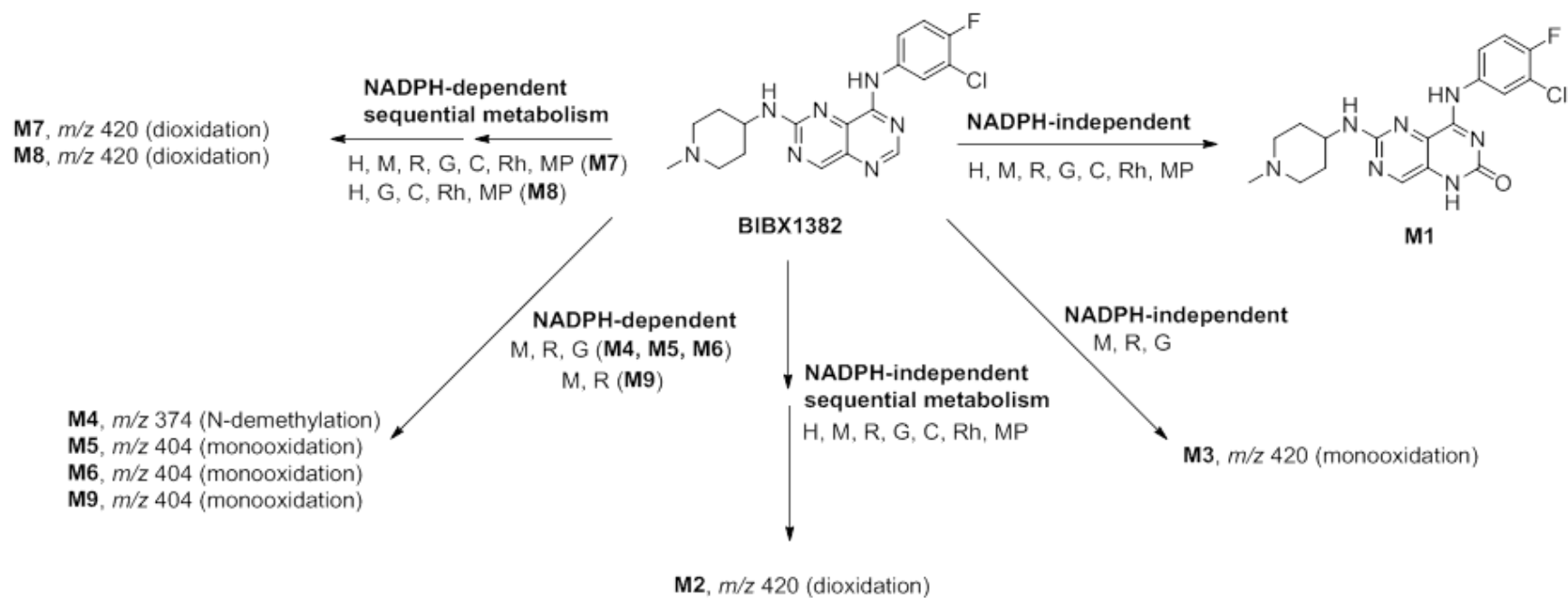


Figure IV.39. Proposed multispecies metabolism of BIBX1382 in hepatic S9. H, human; M, mouse; R, rat; G, guinea pig; C, cynomolgus monkey; Rh, rhesus monkey; MP, minipig

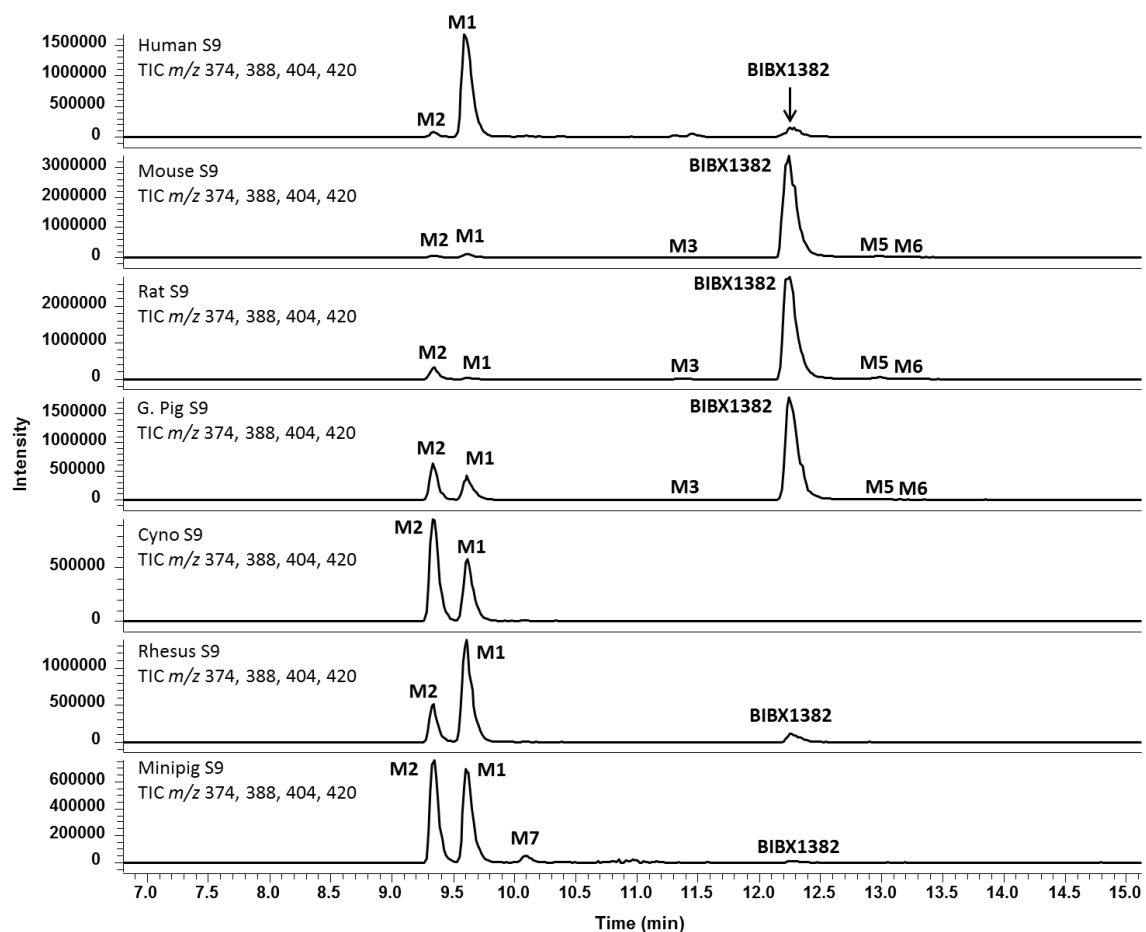


Figure IV.40. Representative extracted ion chromatograms (m/z 388, 374, 404, and 420) depicting principal metabolites from S9 extracts of human, mouse, rat, guinea pig, cynomolgus monkey, rhesus monkey, and minipig incubated with BIBX1382 in the absence of NADPH.

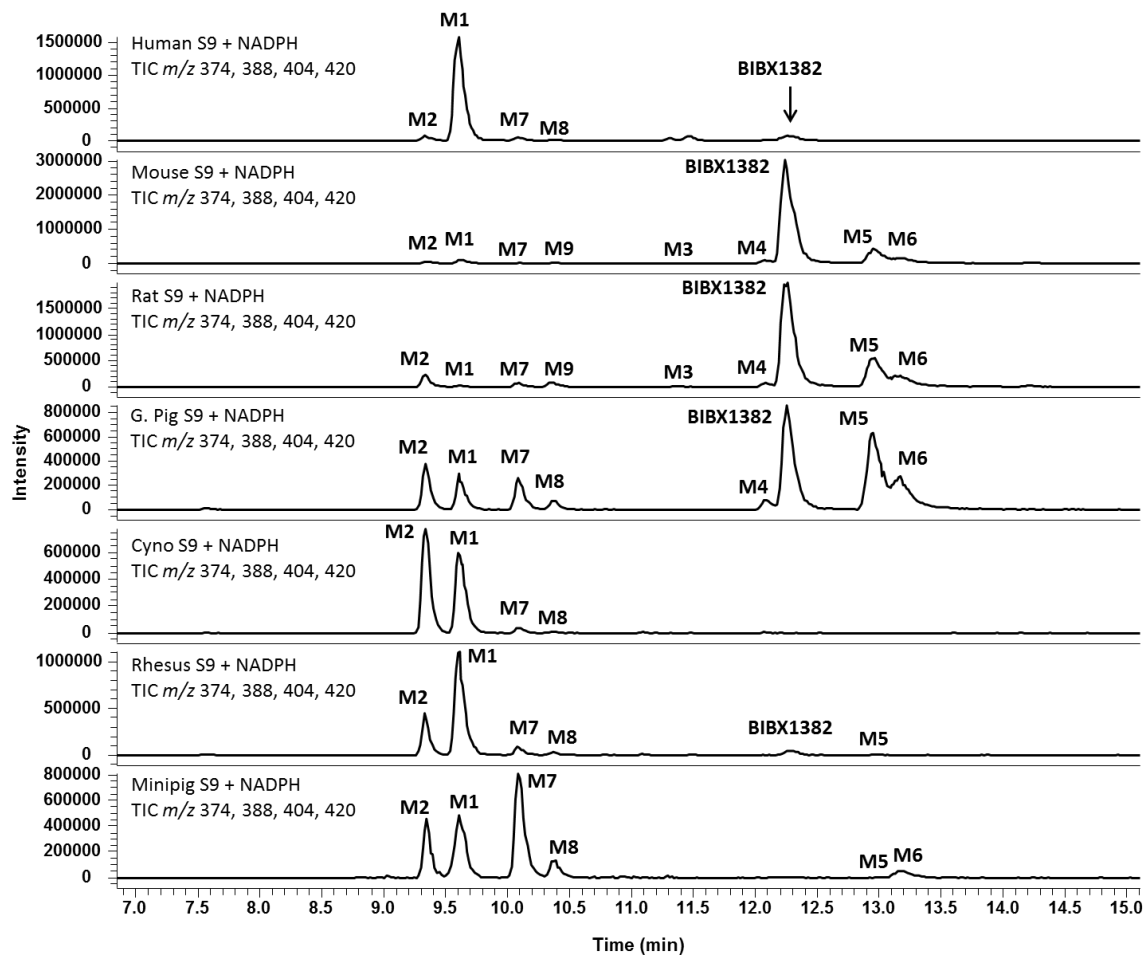


Figure IV.41. Representative extracted ion chromatograms (m/z 388, 374, 404, and 420) depicting principal metabolites from S9 extracts of human, mouse, rat, guinea pig, cynomolgus monkey, rhesus monkey, and minipig incubated with BIBX1382 in the presence of NADPH.

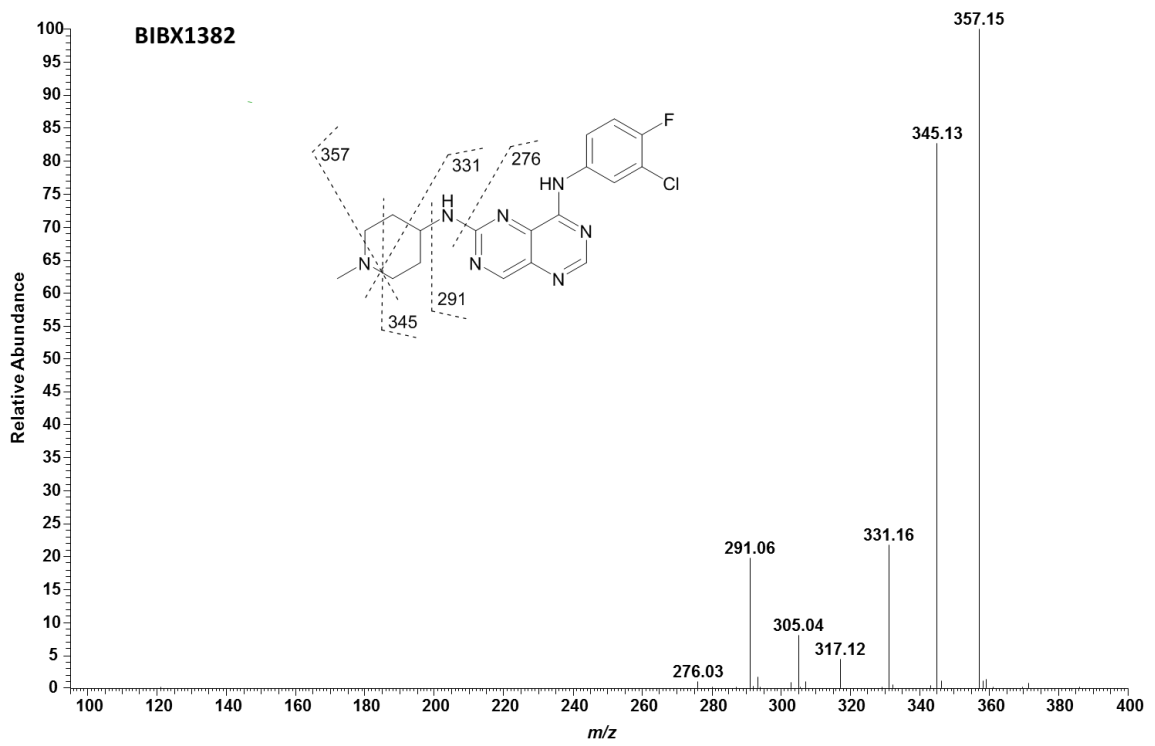


Figure IV.42. LC/MS/MS spectra of BIBX1382 ($[M+H]^+$ at m/z 388).

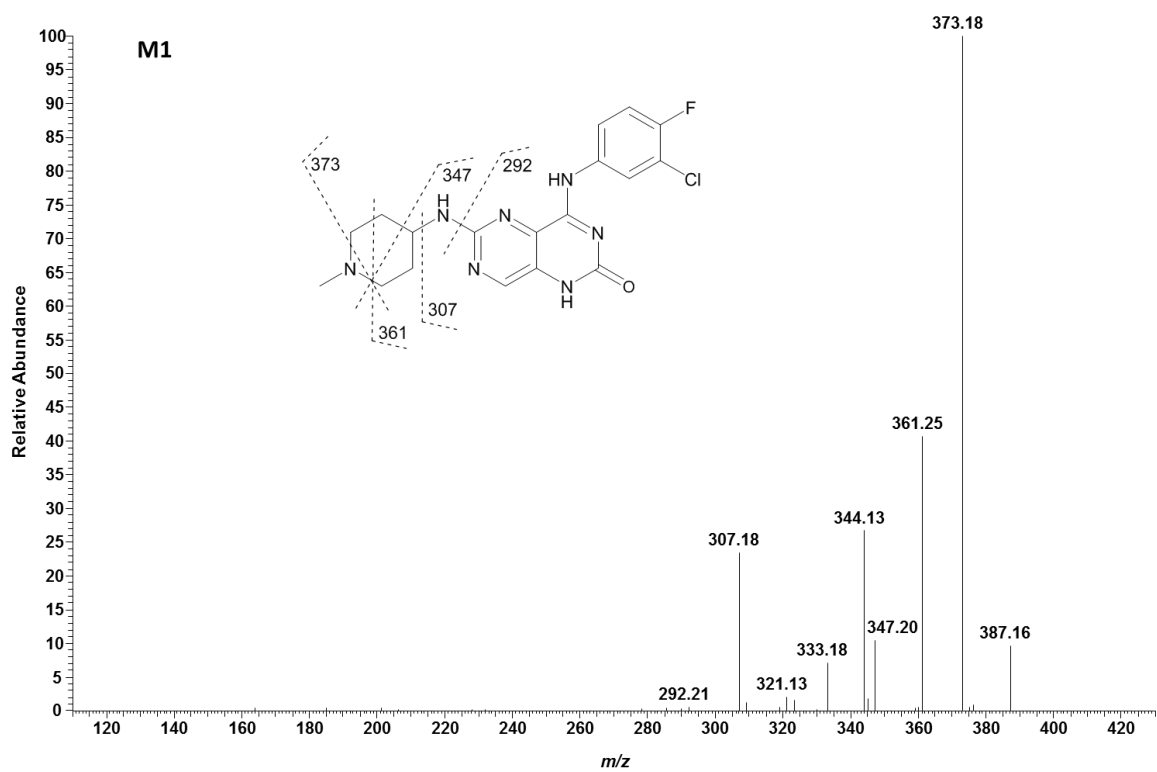


Figure IV.43. LC/MS/MS spectra of BIBX1382 metabolite M1 ($[M+H]^+$ at m/z 404). Fragment ions occurring at m/z 292, 307, 347, 361, and 373 correspond to a 16-Da increase over parent fragment ions at m/z 276, 291, 331, 345, and 357, respectively.

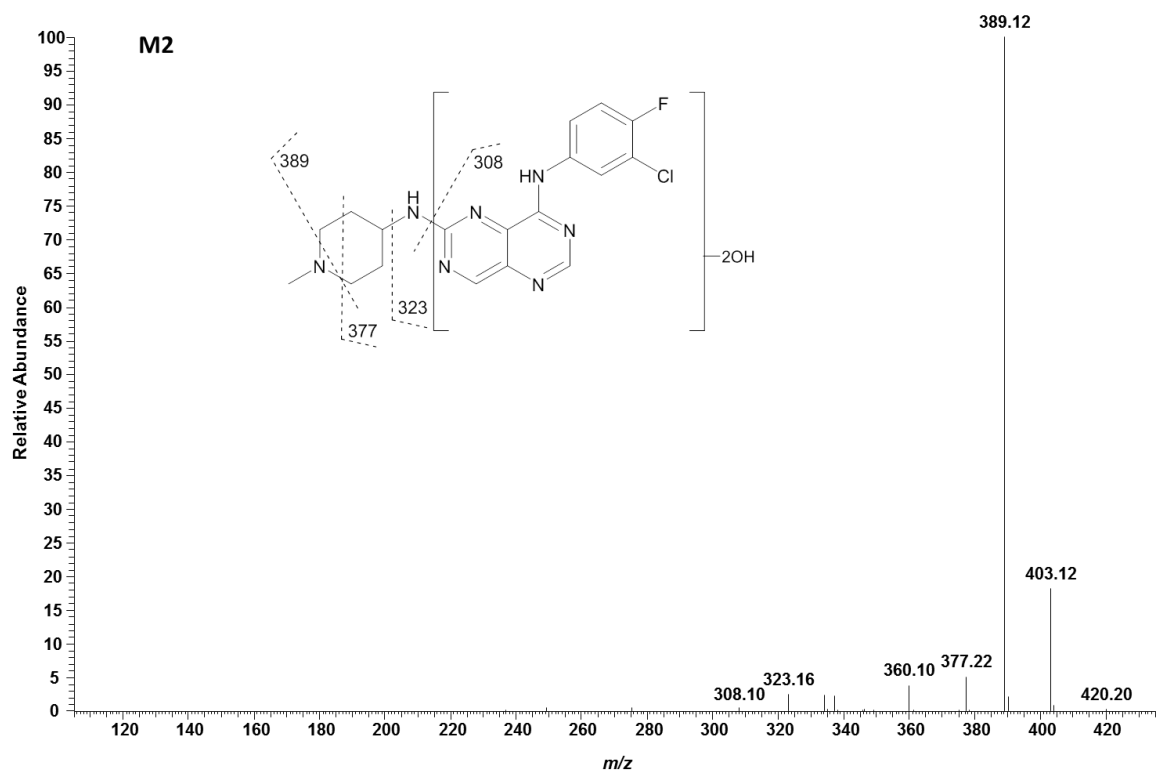


Figure IV.44. LC/MS/MS spectra of BIBX1382 metabolite M2 ($[M+H]^+$ at m/z 420). Fragment ions occurring at m/z 308, 323, 377, and 389 correspond to a 32-Da increase over parent fragment ions at m/z 276, 291, 345, and 357, respectively.

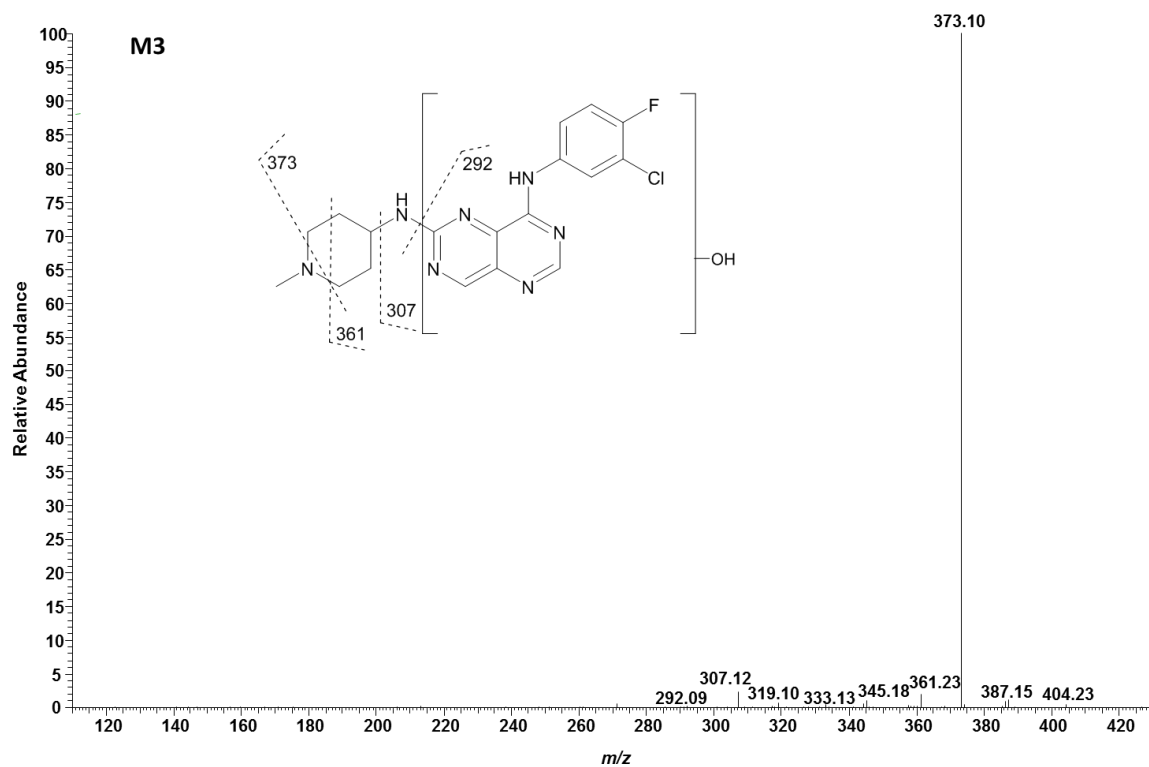


Figure IV.45. LC/MS/MS spectra of BIBX1382 metabolite M3 ($[M+H]^+$ at m/z 404). Fragment ions occurring at m/z 292, 307, 361, and 373 correspond to a 16-Da increase over parent fragment ions at m/z 276, 291, 345, and 357, respectively.

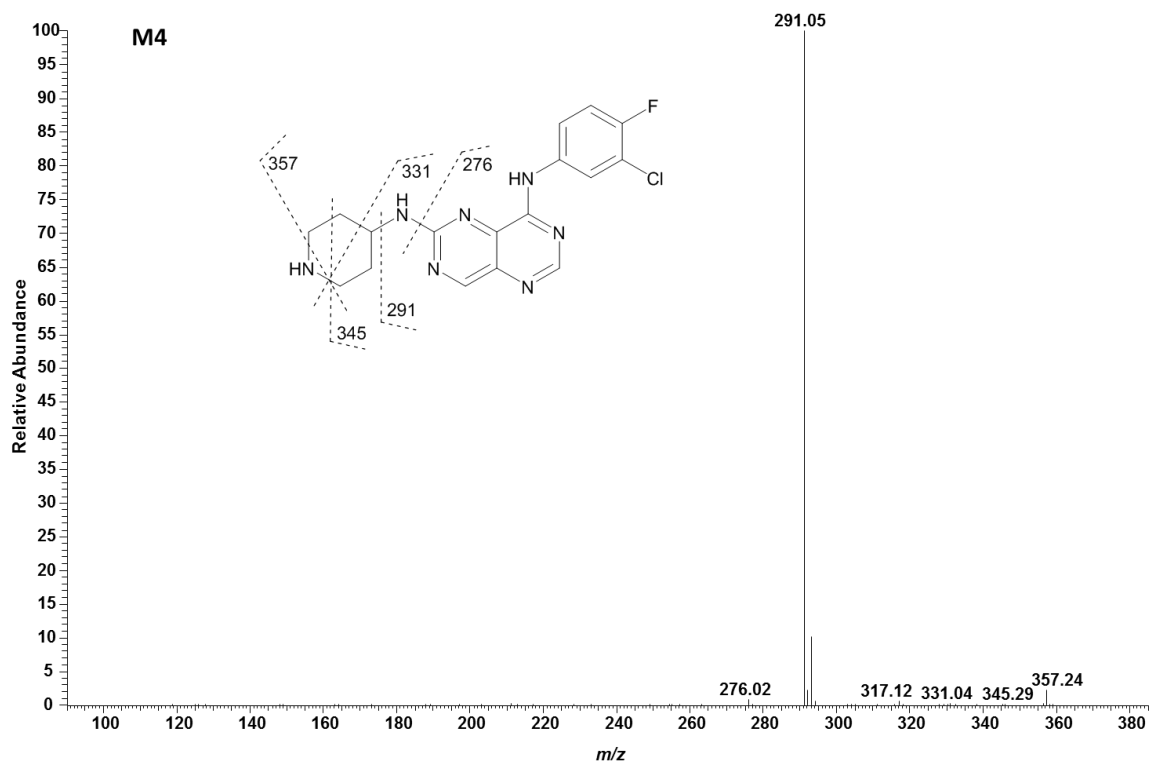


Figure IV.46. LC/MS/MS spectra of BIBX1382 metabolite M4 ($[M+H]^+$ at m/z 374). The major fragment at m/z 291, along with other minor fragments at m/z 276, 345, 331, and particularly the fragment ion at m/z 357, which were also all produced by the parent BIBX1382, indicates that the mass shift of -14 Da from the parent $[M+H]^+$ of m/z 388 is a result of N-demethylation of the N-methyl piperidine moiety.

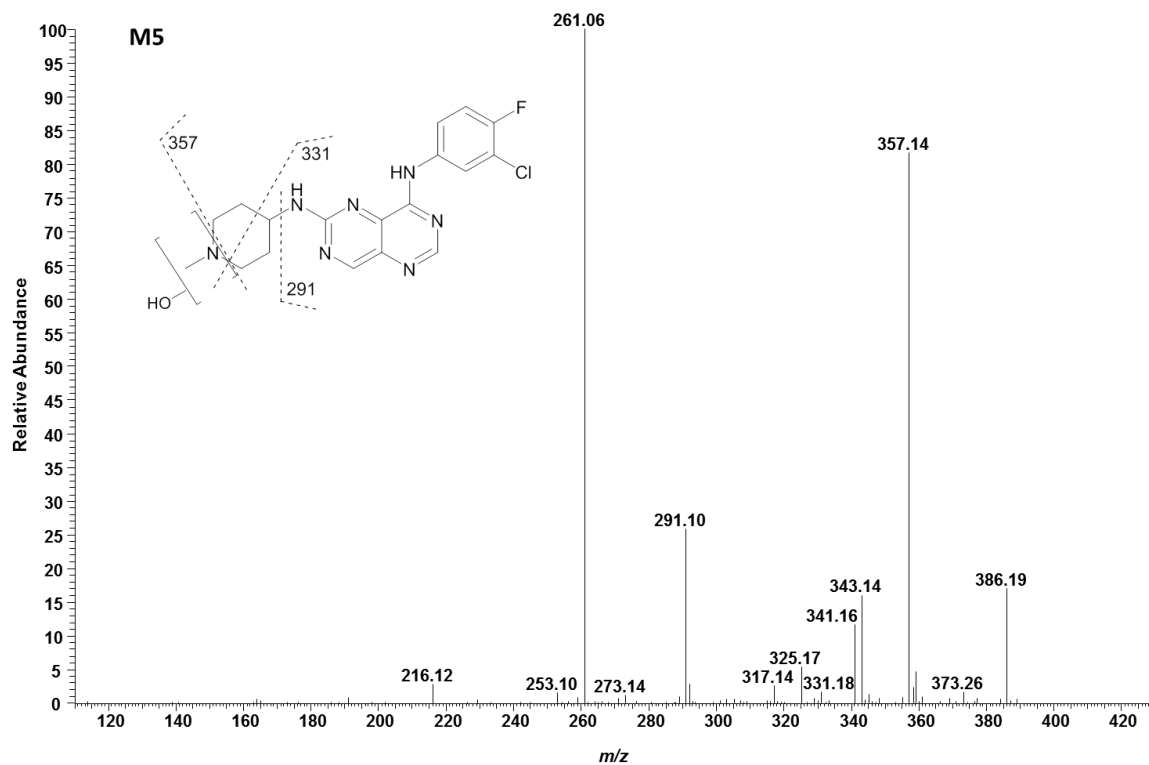


Figure IV.47. LC/MS/MS spectra of BIBX1382 metabolite M5 ($[M+H]^+$ at m/z 404). The fragment ion at m/z 357, along with m/z 291 and 331, which were all produced by the parent, BIBX1382, indicates that the mass shift of +16 Da from the parent $[M+H]^+$ at m/z 388 is a result of oxidation of the nitrogen or methyl substituent of the N-methyl piperidine moiety.

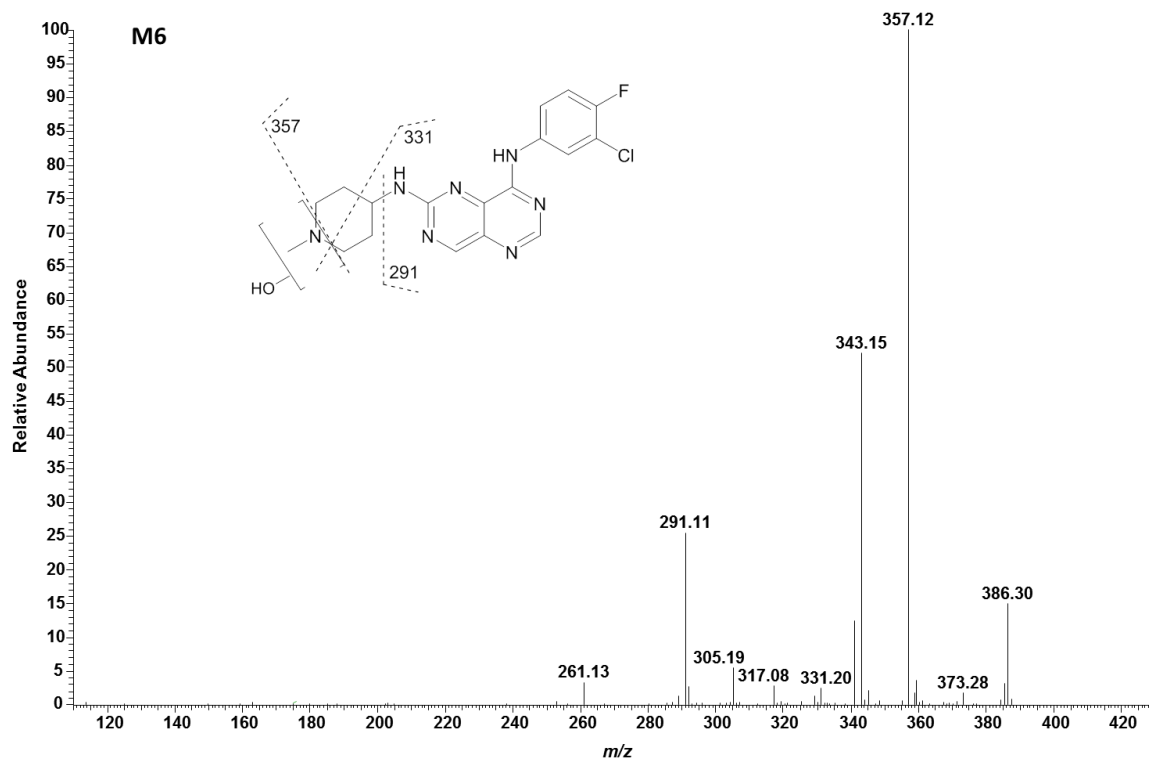


Figure IV.48. LC/MS/MS spectra of BIBX1382 metabolite M6 ($[M+H]^+$ at m/z 404). The fragment ion at m/z 357, along with m/z 291 and 331, which were all produced by the parent, BIBX1382, indicates that the mass shift of +16 Da from the parent $[M+H]^+$ at m/z 388 is a result of oxidation of the nitrogen or methyl substituent of the N-methyl piperidine moiety.

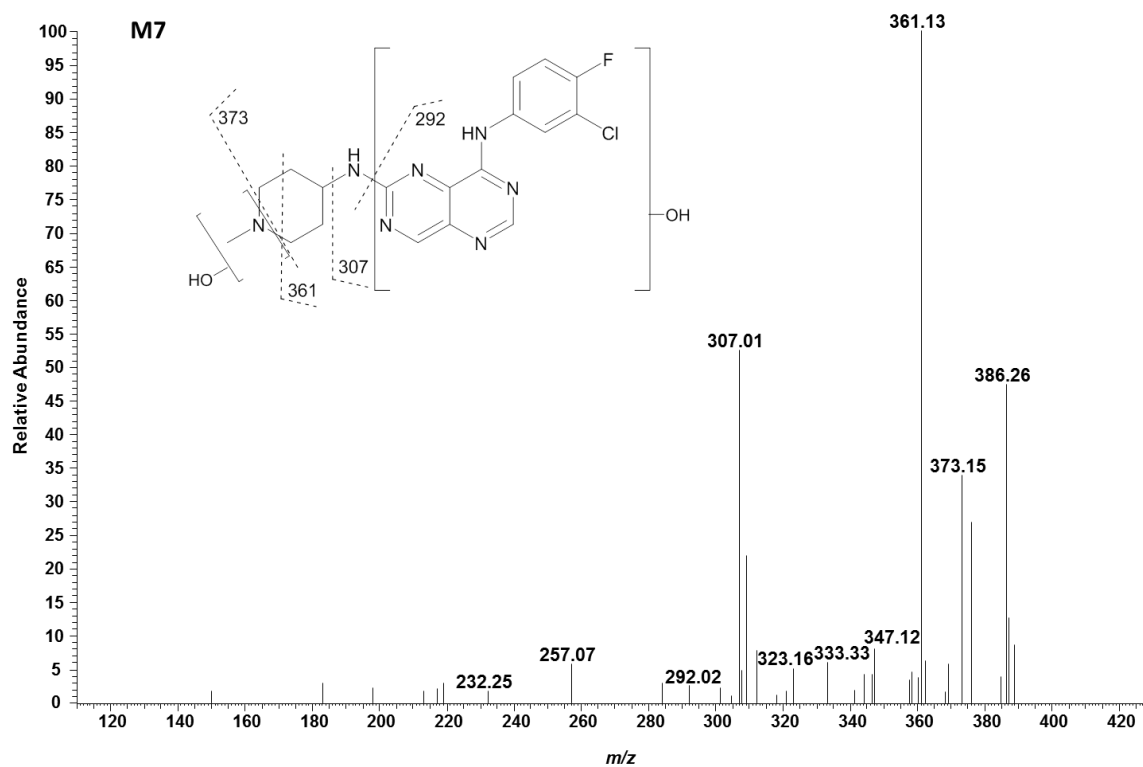


Figure IV.49. LC/MS/MS spectra of BIBX1382 metabolite M7 ($[M+H]^+$ at m/z 420). Fragment ions occurring at m/z 292, 307, 361, and 373 correspond to a 16-Da increase over parent fragment ions at m/z 276, 291, 345, and 357, respectively, indicating that one oxidation occurs to the left of the mass fragmentation producing the fragment ion at m/z 373, while the fragment ion at m/z 292 suggests the other oxidation occurs to the right of this fragmentation.

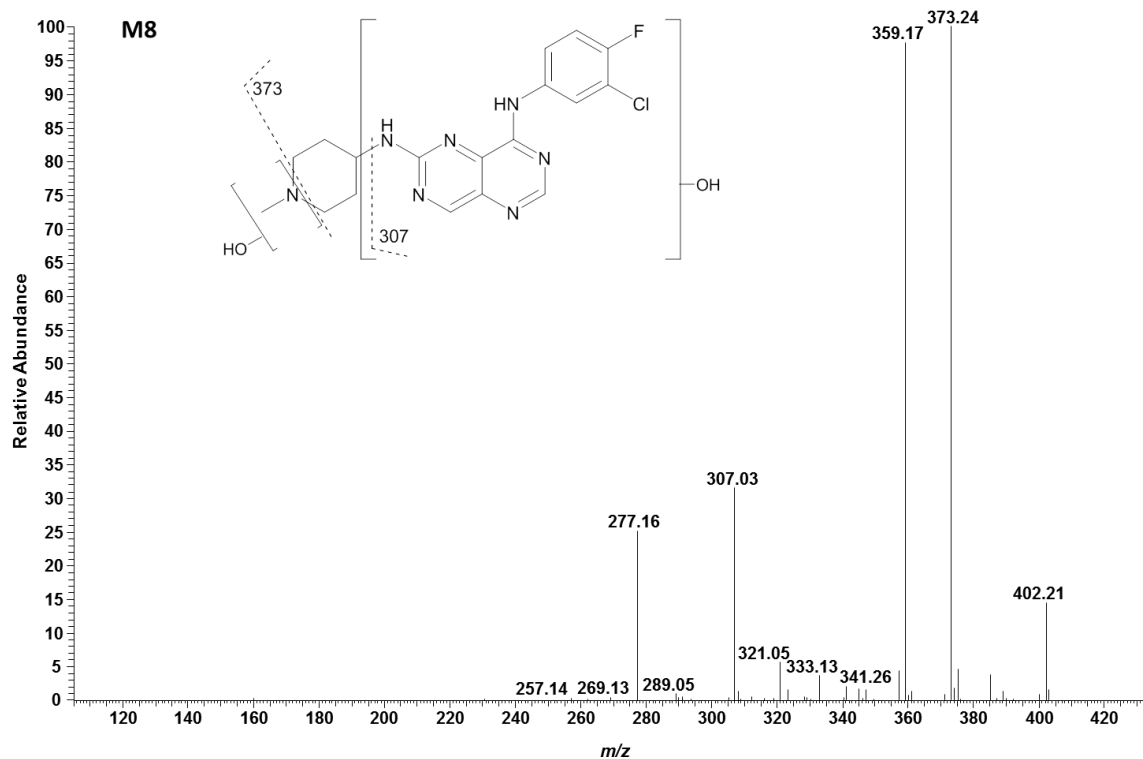


Figure IV.50. LC/MS/MS spectra of BIBX1382 metabolite M8 ($[M+H]^+$ at m/z 420). Fragment ions occurring at m/z 307 and 373 correspond to a 16-Da increase over parent fragment ions at m/z 291 and 357, respectively, indicating that one oxidation occurs to the left of the mass fragmentation producing the ion at m/z 373, while the fragment ion at m/z 307 suggests the other oxidation occurs to the right of this fragmentation.

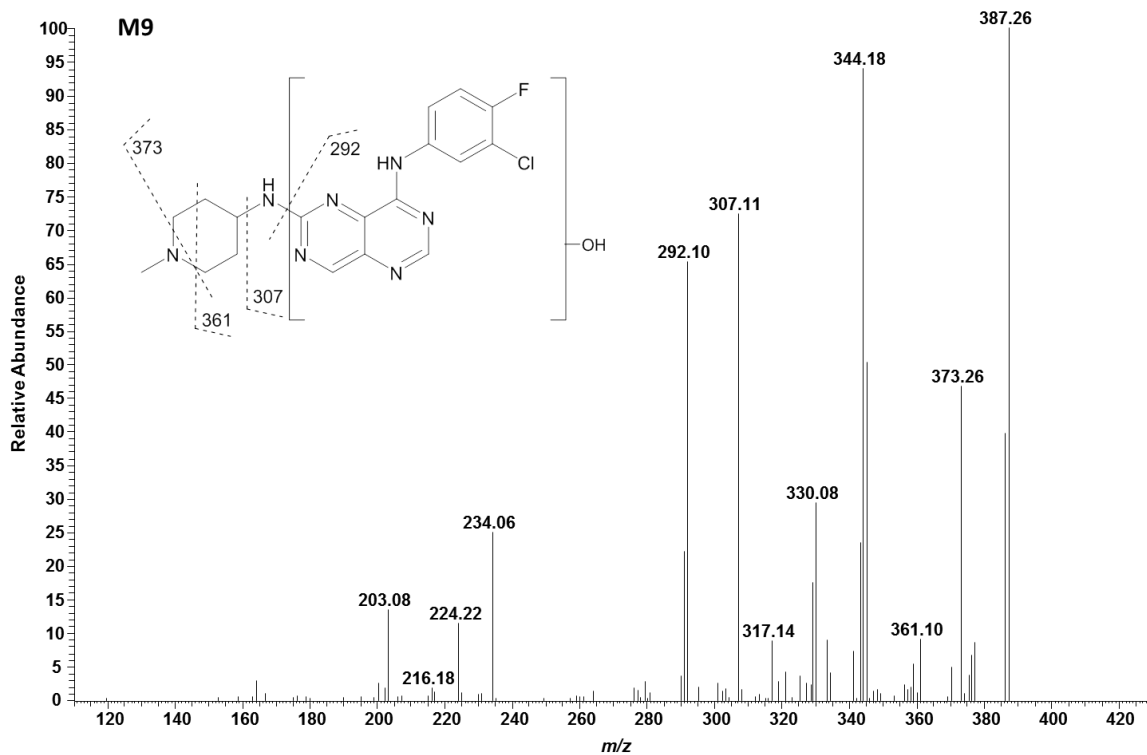


Figure IV.51. LC/MS/MS spectra of BIBX1382 metabolite M9 ($[M+H]^+$ at m/z 404). Fragment ions occurring at m/z 292, 307, 361, and 373 correspond to a 16-Da increase over parent fragment ions at m/z 276, 291, 345, and 357, respectively.

SGX523

The metabolism of SGX523 was previously reported in human, cynomolgus monkey, dog, and rat S9 and *in vivo* in monkey (Diamond et al., 2010a). The principal NADPH-dependent and -independent metabolism of SGX523 observed in hepatic S9 is summarized in Figure IV.52. HPLC-UV chromatograms depicting the principal metabolites formed in the presence or absence of NADPH in each species are shown in Figures IV.53-54, and the MS/MS spectra and proposed fragmentation of each metabolite are shown in Figures IV.67-68. Several of the metabolites either co-elute or elute very closely together, which can be better viewed in Figure IV.55, depicting XICs of each metabolite from extracts of human S9 (+NADPH). Fragmentation of the metabolite detected at 10.3 min ($[M+H]^+$ at m/z 376) was indicative of SGX523 oxidation to M1 (Figure IV.57) in all species in S9 fractions absent (Figure IV.53) and present (Figure IV.54) NADPH. Two additional major NADPH-dependent oxidative metabolites, M2 and M3 (Figures IV.58-59), co-eluted at 9.7 min ($[M+H]^+$ at m/z 376) and were generated by all species (Figure IV.54). The fragment occurring at m/z 176 for both M2 and M3 suggests the oxidation is likely located on the quinoline moiety or the sulfur atom. The major loss of 18 Da (m/z 358, indicates loss of water) from M2 is indicative of S-oxidation, while the loss of 18 Da as well as 17 Da (m/z 359, indicates possible loss of OH radical) from M3 is indicative of N-oxidation. However, a fragment ion produced by SGX523 at m/z 343 corresponds to a loss of 17 Da, in which case, it is unclear without further investigation whether the M3 fragment at m/z 359 resulted from loss of an OH radical. Several other minor NADPH-dependent metabolites were also detected in

all species (Figure IV.54), including an N-desmethyl metabolite, M4 (Figure IV.60), at 10.5 min ($[M+H]^+$ at m/z 346), and two other metabolites, M5 and M6 (Figures IV.61-62), at 10.6 and 10.7 min, respectively, both with a mass shift of +16 Da ($[M+H]^+$ at m/z 376) over the parent. The presence of a fragment at m/z 176 in M5 and M6 again suggests that the oxidation may be located on the quinoline moiety. NADPH-dependent metabolites with a mass shift of +32 over the parent ($[M+H]^+$ at m/z 392), M7, M8, and M9 (Figures IV.63-65), eluting at 10.9, 8.0, and 8.5 min, respectively, were also detected in S9 extracts of all species (Figure IV.54). Fragments at m/z 192 (+32 Da over the parent fragment at m/z 160) and m/z 247 (+16 over the parent fragment at m/z 231) suggested M8 and M9 were S-oxides with a secondary oxidation located on the quinoline moiety. Fragmentation of M7 (Figure IV.63), as well as the late retention time (10.9 min) indicates the likelihood that both oxidations are located on the sulfur atom, producing a sulfone metabolite. Finally, three NADPH-dependent metabolites, M10, M11, and M12, with a mass shift of +2 Da over the parent ($[M+H]^+$ at m/z 362) and fragmentation suggestive of N-demethylation and monooxidation (Figures IV.66-68), were detected in a species-specific manner (Figure IV.54). M10 was detected in extracts of all species except mouse, M11 in all but mouse and rat, and M12 in all but mouse, rat, and minipig. Overlapping retention times of M10 and M11 (9.0 min) as well as similarities in fragmentation, including the major loss of 18 Da from M10 (Figure IV.66) and the major loss of both 17 and 18 Da from M11 (Figure IV.67) suggest the likelihood that these two metabolites are the N-desmethyl analogs of M2 and M3, respectively. M12, which eluted at 9.6 min, also produced fragments indicative of N-

demethylation and oxidation, with fragment ion intensities at m/z 145, 176, and 217 mirroring those of fragment ions produced by M1 at m/z 159, 176, and 231 (each + 14 Da over M12 fragments), indicating the possibility that M12 is the N-desmethyl analog of M1.

Overall, metabolism of SGX523 was relatively similar across all species, with cynomolgus, rhesus, and guinea pig demonstrating the most similar profile with regard to detection of all 12 metabolites. Despite the lack of detection of M10, M11, and/or M12 in rat or mouse, the rodents (including guinea pig) demonstrated the most similarities in overall turnover of the substrate. Accordingly, SSS with mouse, rat, and guinea pig resulted in the most accurate predictions of human S9 CL_{int} . These data also support the low $F_{m,A0}$ observed in minipig and the low-moderate $F_{m,A0}$ in the remaining species. The detection of only a single metabolite (M1) in S9 extracts absent NADPH suggests that the portion of NADPH-independent clearance not inhibited by hydralazine in mouse, guinea pig, and rhesus monkey S9 could be attributed to the contribution of XO to the formation of M1. Diamond et al previously reported little-to-no inhibition of M1 formation in incubations of human and cynomolgus S9 in the presence of allopurinol or oxypurinol (XO inhibitors) (Diamond et al., 2010a).

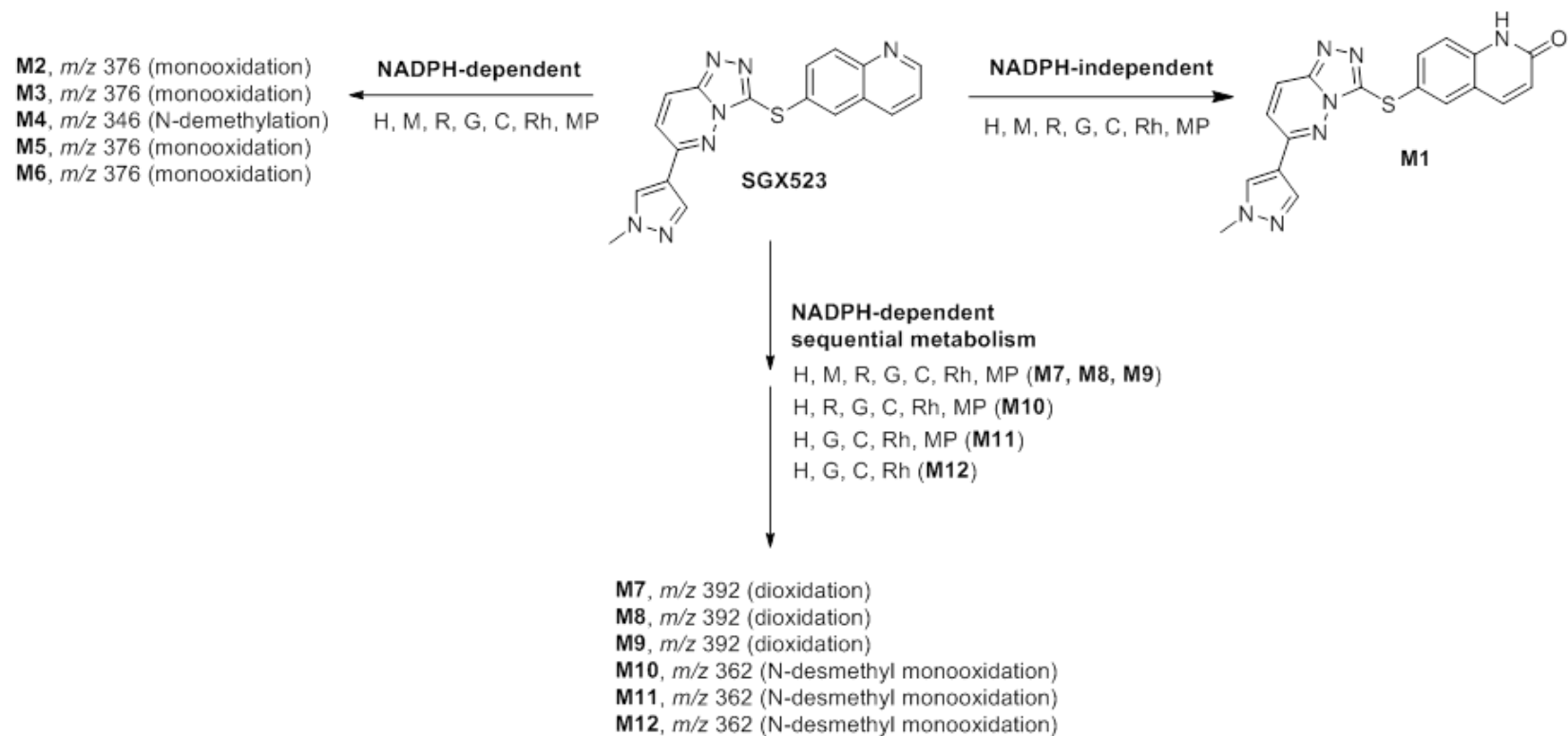


Figure IV.52. Proposed multispecies metabolism of SGX523 in hepatic S9. H, human; M, mouse; R, rat; G, guinea pig; C, cynomolgus monkey; Rh, rhesus monkey; MP, minipig

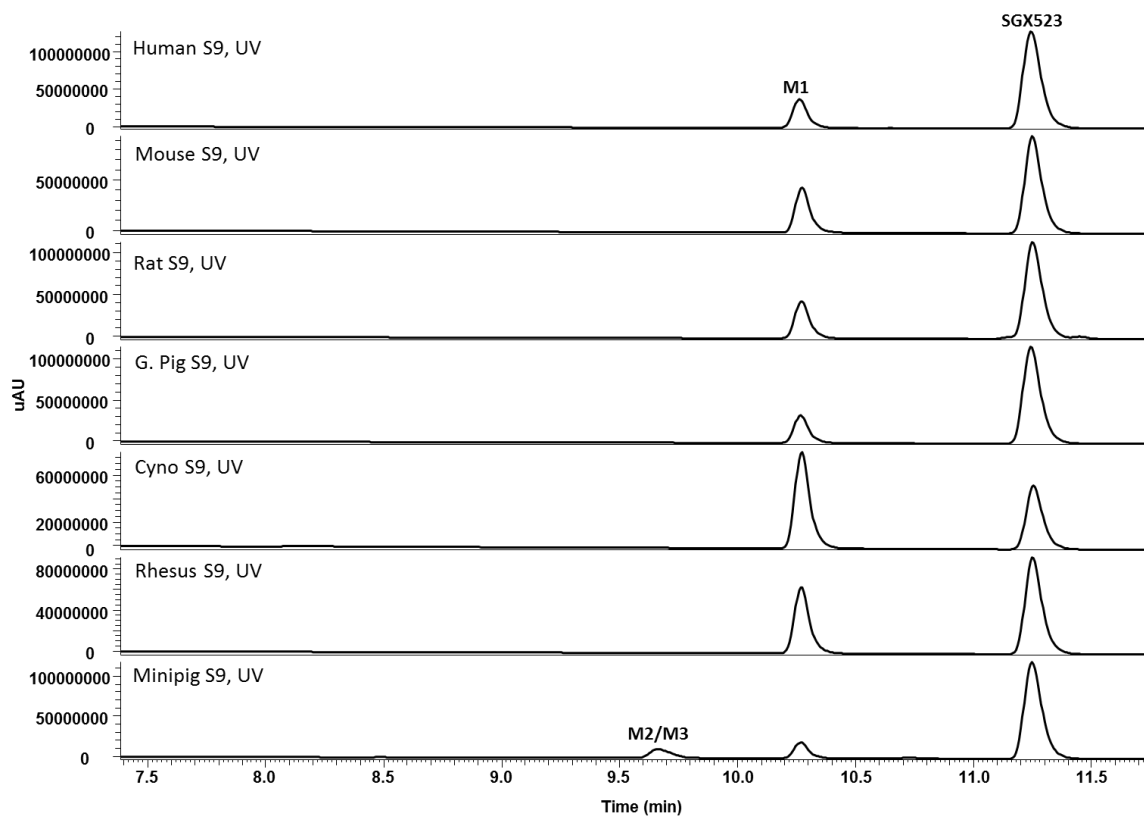


Figure IV.53. Representative LC-UV chromatograms depicting principal metabolite(s) from S9 extracts of human, mouse, rat, guinea pig, cynomolgus monkey, rhesus monkey, and minipig incubated with SGX523 in the absence of NADPH.

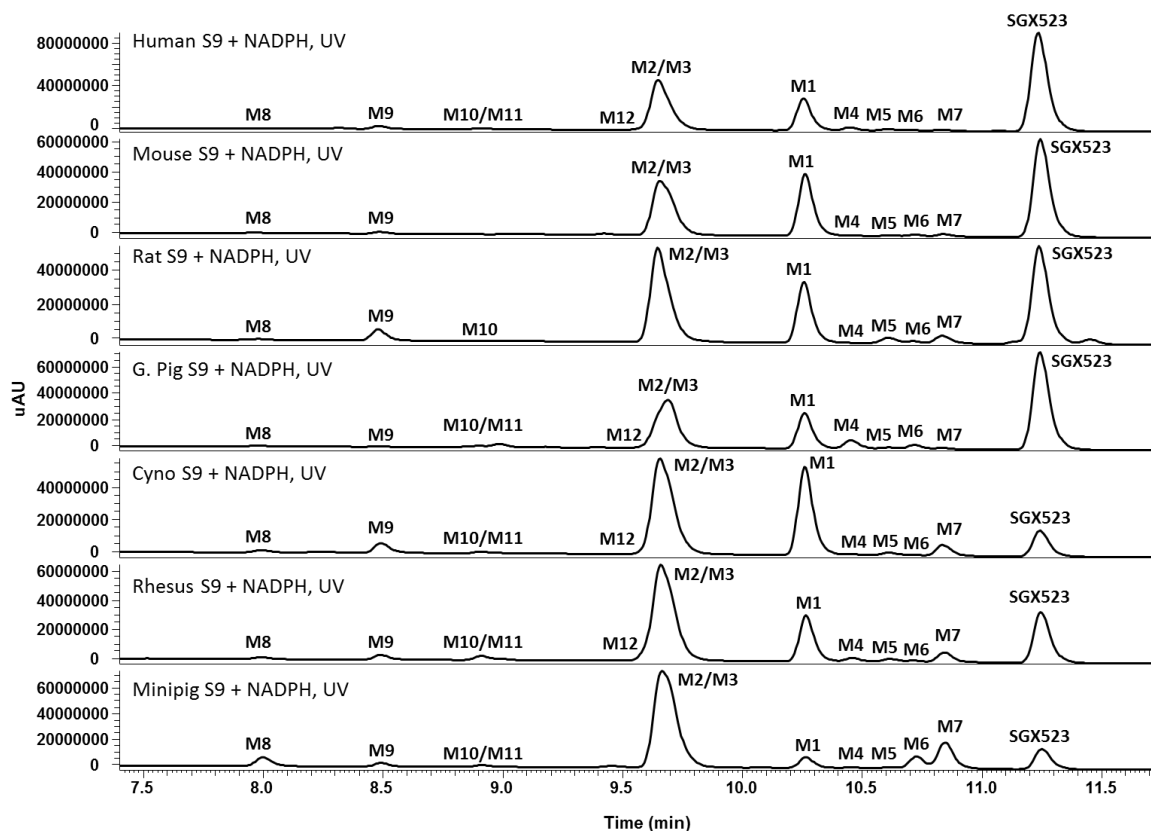


Figure IV.54. Representative LC-UV chromatograms depicting principal metabolites from S9 extracts of human, mouse, rat, guinea pig, cynomolgus monkey, rhesus monkey, and minipig incubated with SGX523 in the presence of NADPH.

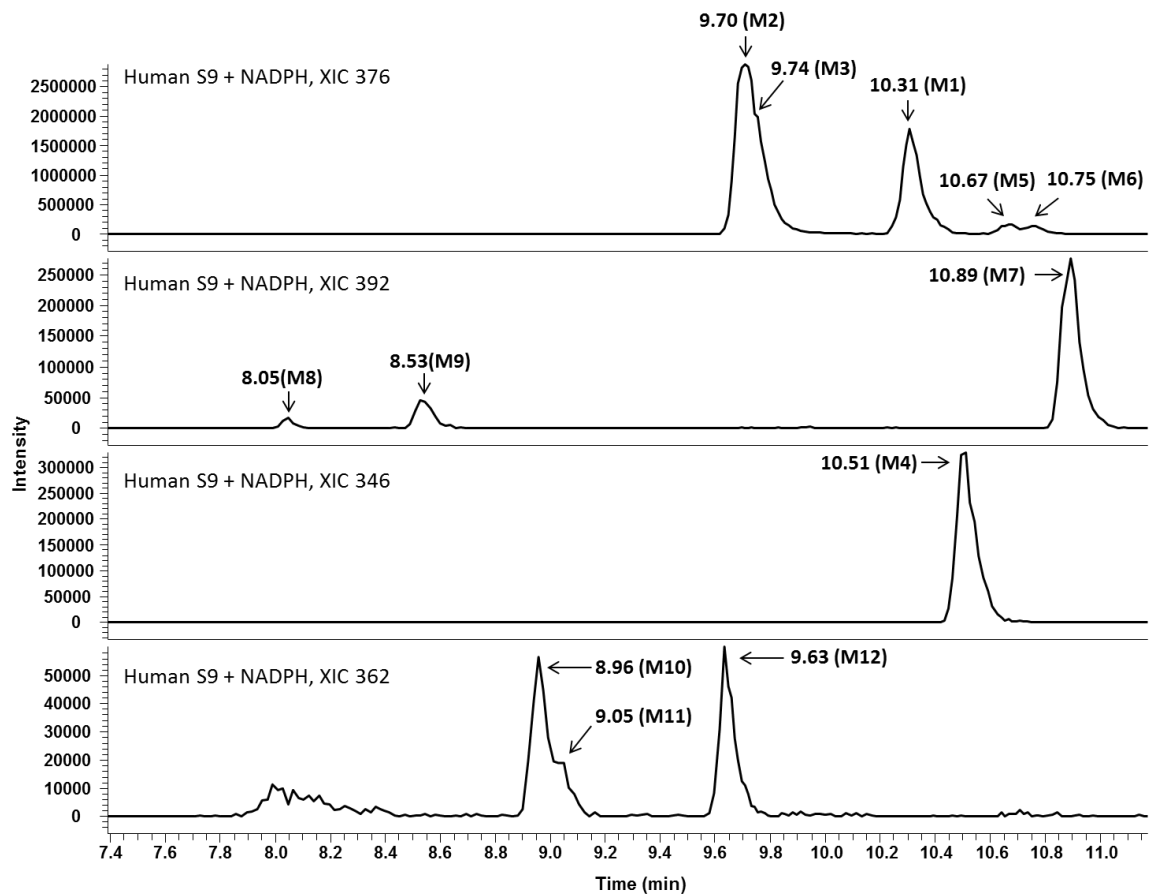


Figure IV.55. Representative extracted ion chromatograms (XIC, m/z 376, 392, 346, and 362) depicting principal metabolites from S9 extracts of human incubated with SGX523 in the presence of NADPH.

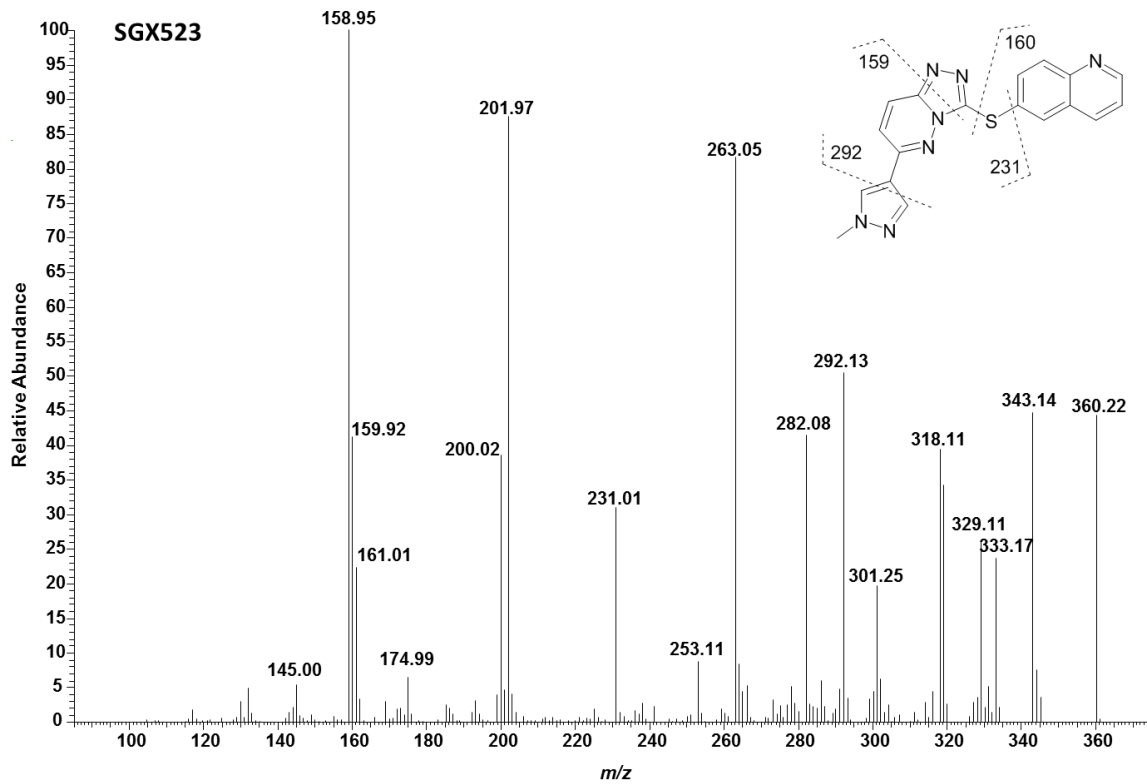


Figure IV.56. LC/MS/MS spectra of SGX523 ($[M+H]^+$ at m/z 360).

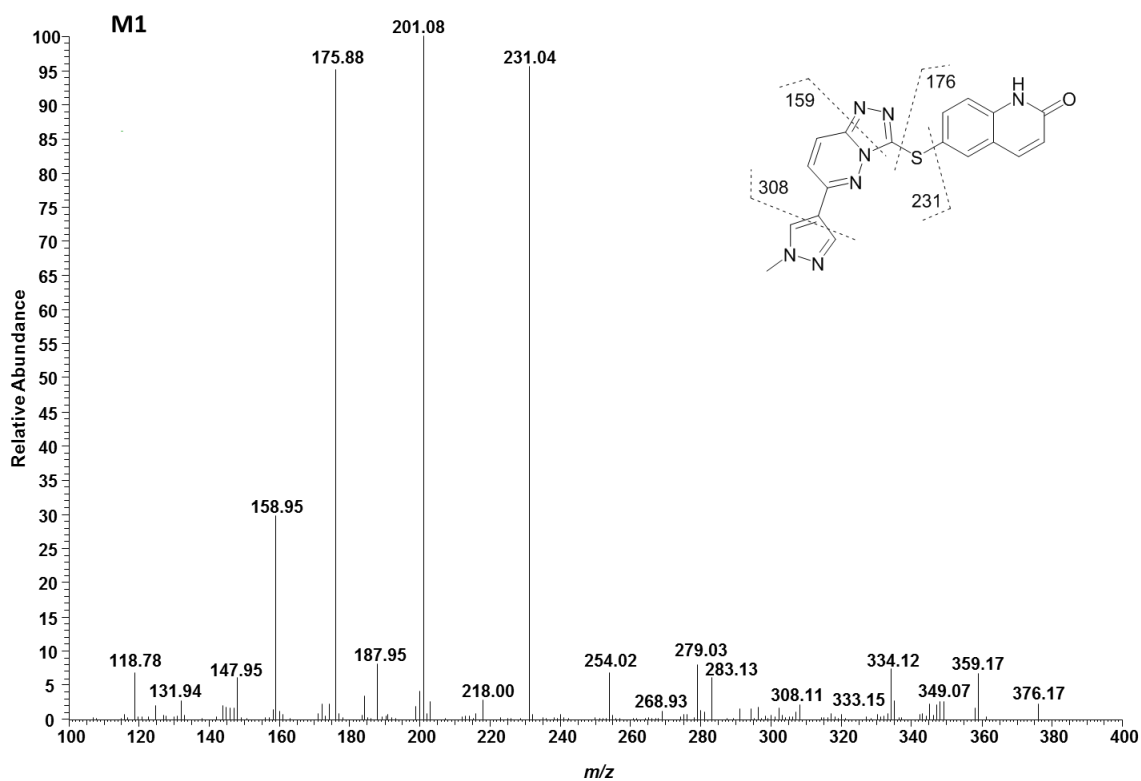


Figure IV.57. LC/MS/MS spectra of SGX523 metabolite M1 ($[M+H]^+$ at m/z 376). Fragment ions occurring at m/z 308 and 176 correspond to a 16-Da increase over parent fragment ions at m/z 292 and 160, respectively, while fragment ions to the left of the quinoline moiety at m/z 231 and 159 remained the same.

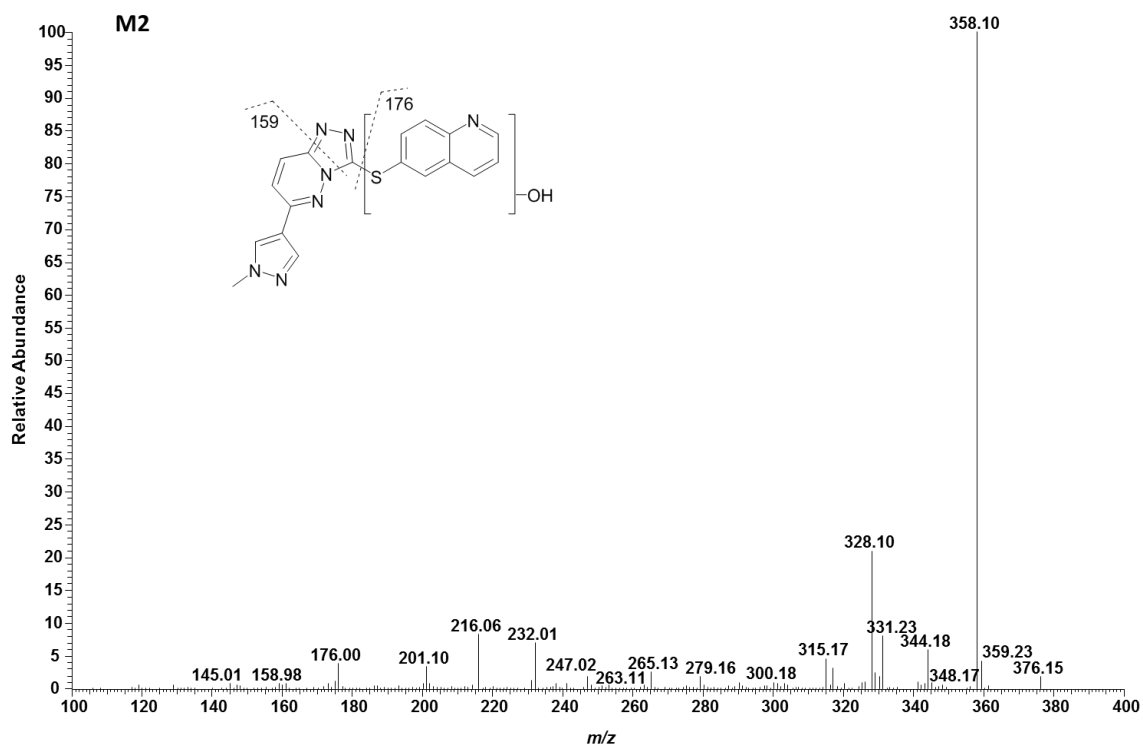


Figure IV.58. LC/MS/MS spectra of SGX523 metabolite M2 ($[M+H]^+$ at m/z 376). The fragment ion occurring at m/z 176 corresponds to a 16-Da increase over parent fragment ion at m/z 160, while the fragment ion at m/z 159 remained the same. The major fragment at m/z 358 represents loss of water, with an intensity of 100% suggesting the likelihood that the oxidation is located on the sulfur atom.

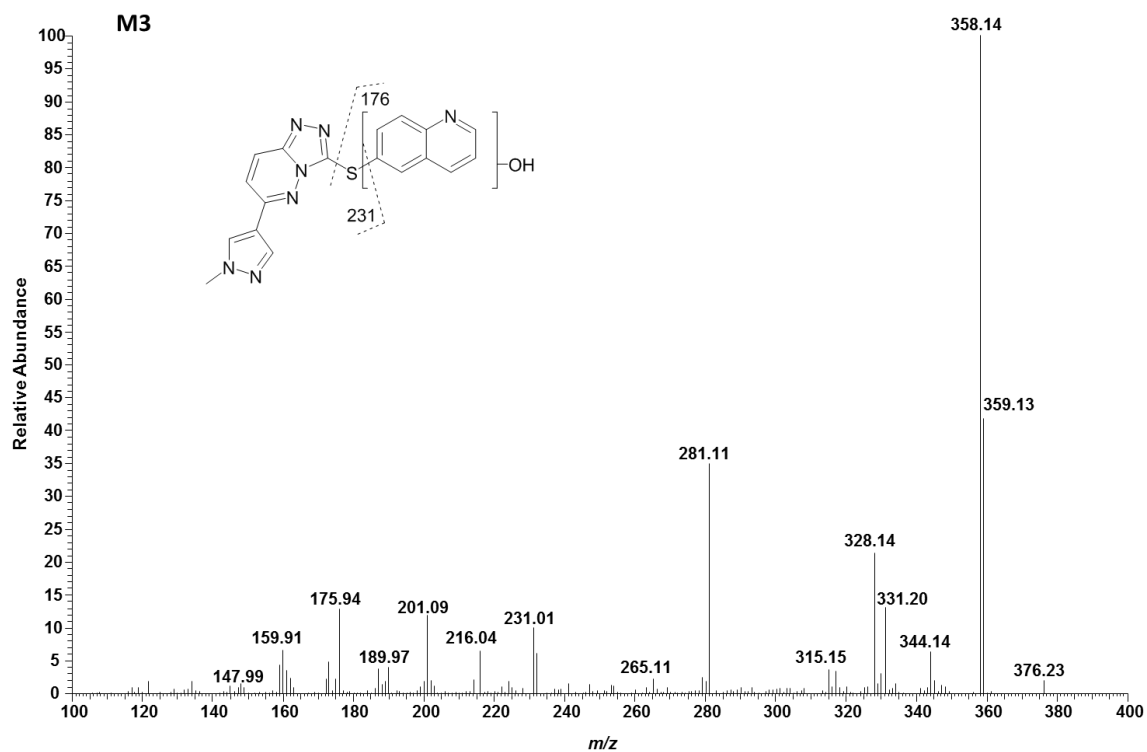


Figure IV.59. LC/MS/MS spectra of SGX523 metabolite M3 ($[M+H]^+$ at m/z 376). The fragment ion occurring at m/z 176 corresponds to a 16-Da increase over parent fragment ion at m/z 160, while the fragment ion at m/z 231 remained the same. The major fragment at m/z 358 representing loss of water, along with the fragment ion at m/z 359 (possible loss of OH radical), suggests the possibility that the oxidation is located on the nitrogen of the quinoline moiety.

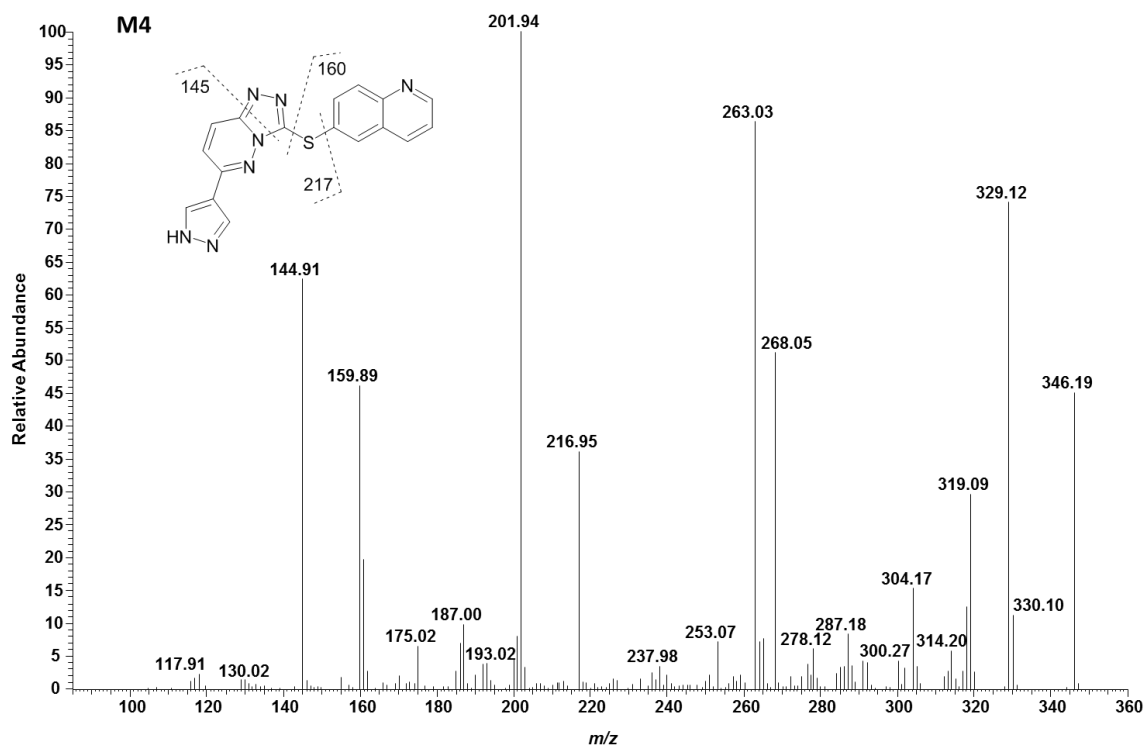


Figure IV.60. LC/MS/MS spectra of SGX523 metabolite M4 ($[M+H]^+$ at m/z 346). Fragment ions occurring at m/z 217 and 145 correspond to a 14-Da decrease from parent fragment ions at m/z 231 and 159, respectively, while the fragment ion at m/z 160 remained the same.

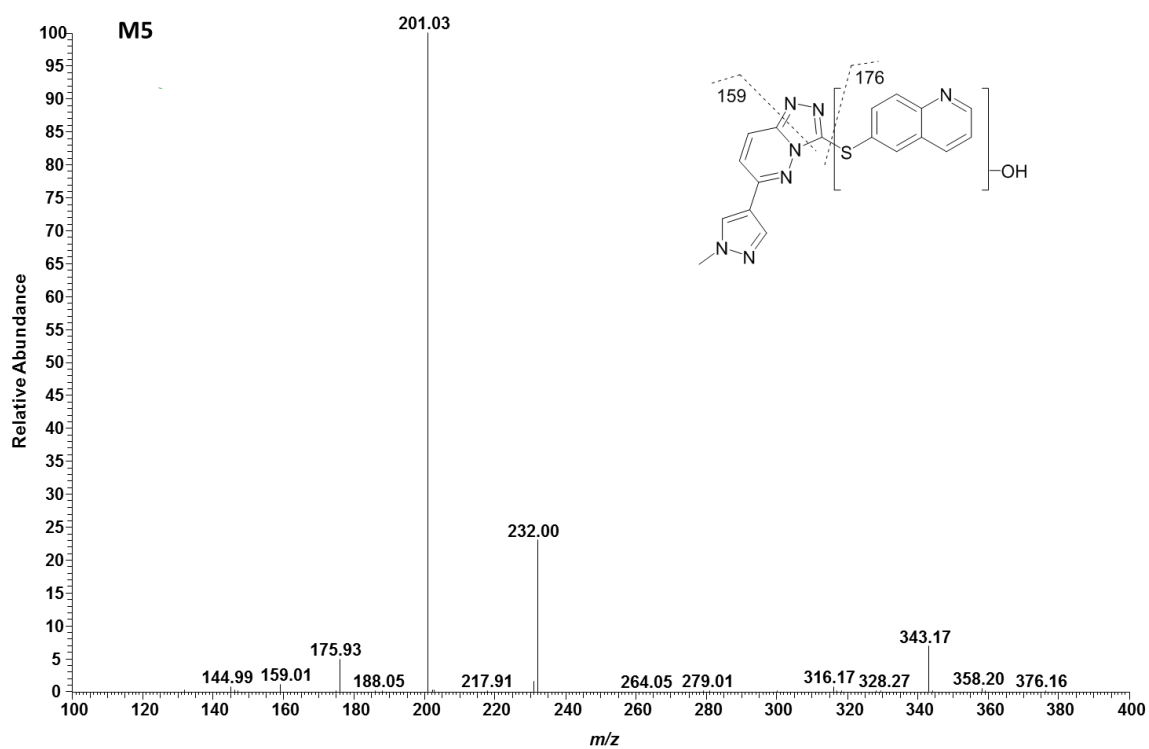


Figure IV.61. LC/MS/MS spectra of SGX523 metabolite M5 ($[M+H]^+$ at m/z 376). The fragment ion occurring at m/z 176 corresponds to a 16-Da increase over parent fragment ion at m/z 160, while the fragment ion at m/z 159 remained the same.

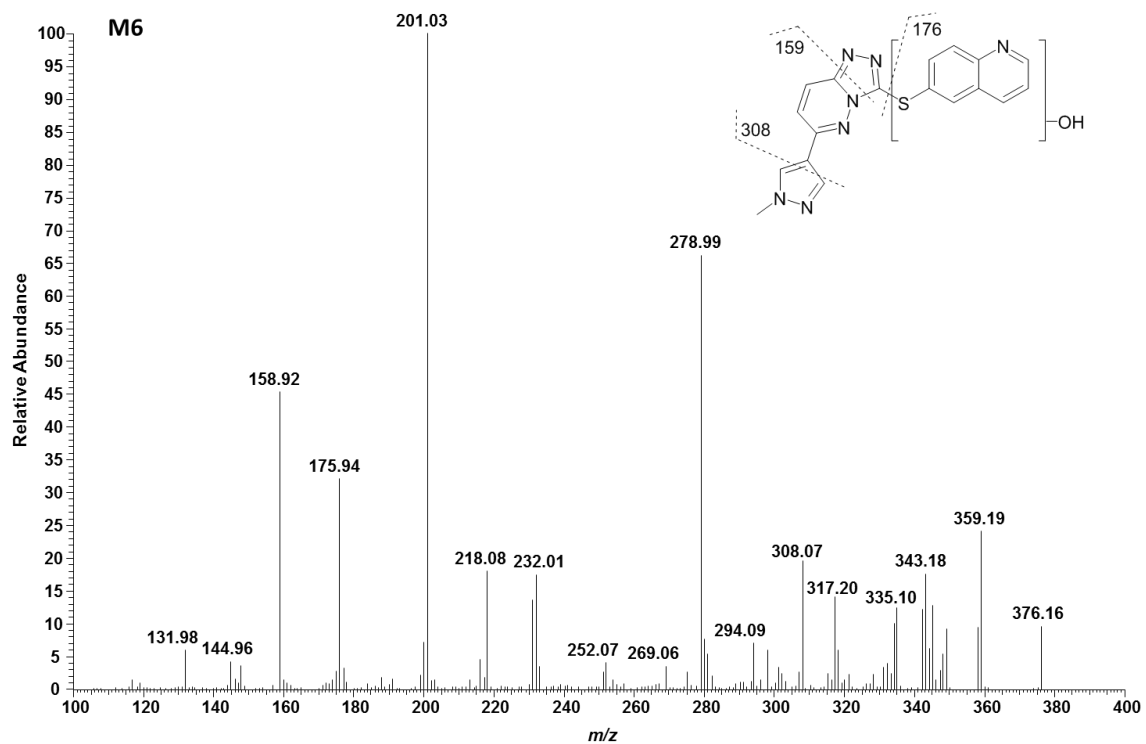


Figure IV.62. LC/MS/MS spectra of SGX523 metabolite M6 ($[M+H]^+$ at m/z 376). The fragment ions occurring at m/z 308 and 176 correspond to a 16-Da increase over parent fragment ions at m/z 292 and 160, respectively, while the fragment ion at m/z 159 remained the same.

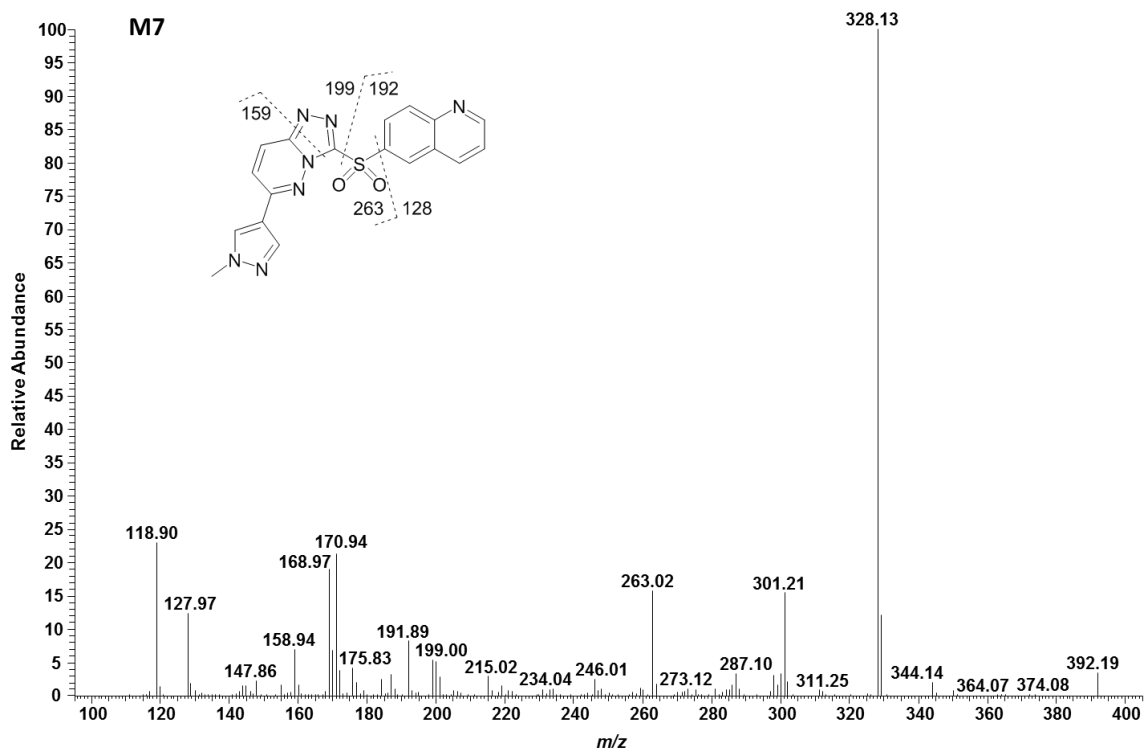


Figure IV.63. LC/MS/MS spectra of SGX523 metabolite M7 ($[M+H]^+$ at m/z 392). The fragment ions occurring at m/z 263 and 192 correspond to a 32-Da increase over parent fragment ions at m/z 231 and 160, respectively, while the fragment ion at m/z 159 remained the same.

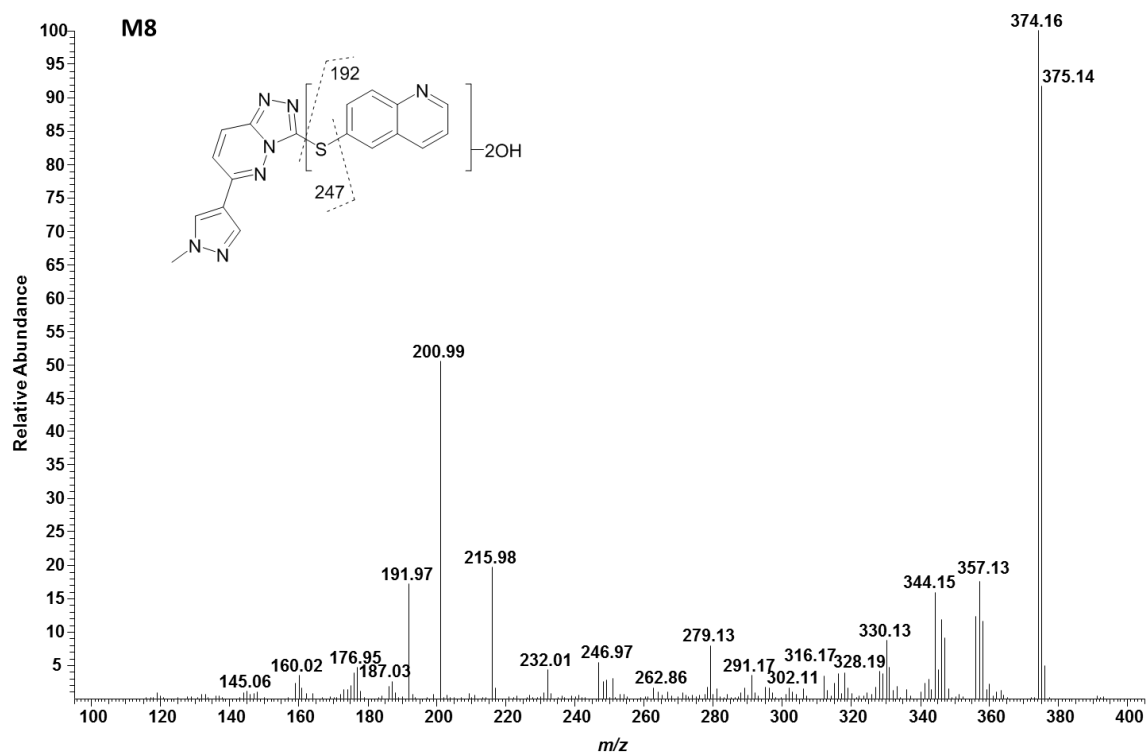


Figure IV.64. LC/MS/MS spectra of SGX523 metabolite M8 ($[M+H]^+$ at m/z 392). The fragment ions occurring at m/z 247 and 192 correspond to a 32-Da and 16-Da increase, respectively, over parent fragment ions at m/z 231 and 160, respectively, likely placing one of the oxidations on the sulfur atom and the other on the quinoline moiety.

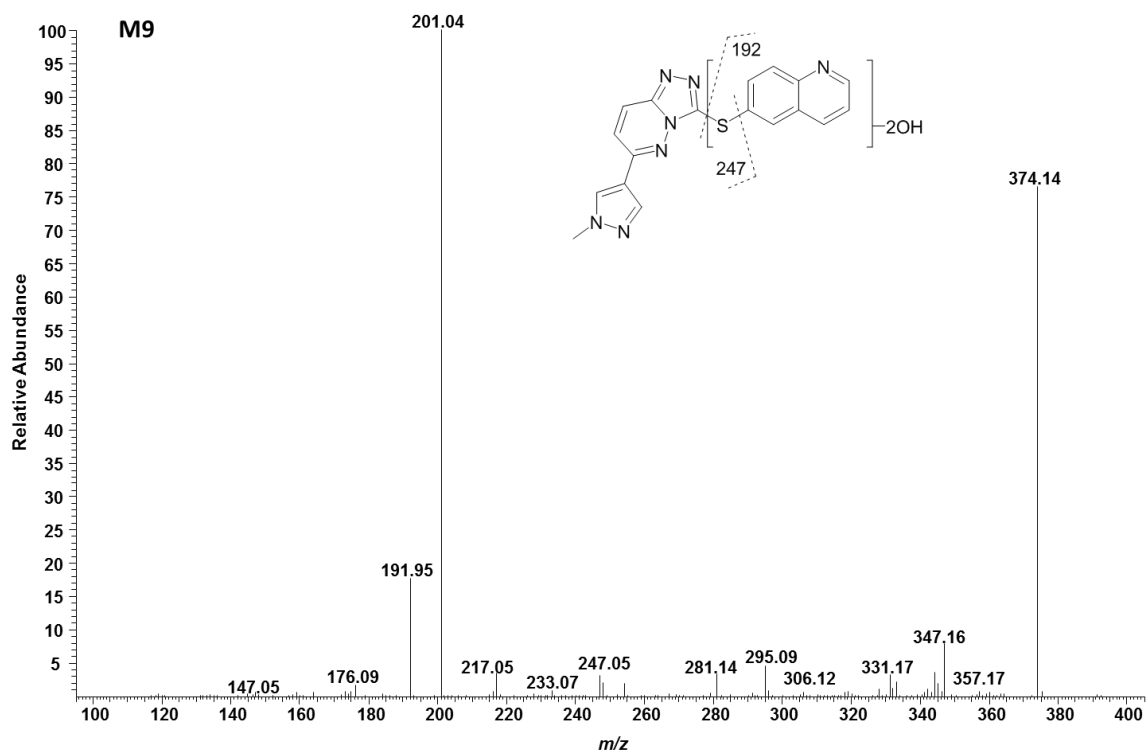


Figure IV.65. LC/MS/MS spectra of SGX523 metabolite M9 ($[M+H]^+$ at m/z 392). The fragment ions occurring at m/z 247 and 192 correspond to a 32-Da and 16-Da increase, respectively, over parent fragment ions at m/z 231 and 160, respectively, likely placing one of the oxidations on the sulfur atom and the other on the quinoline moiety.

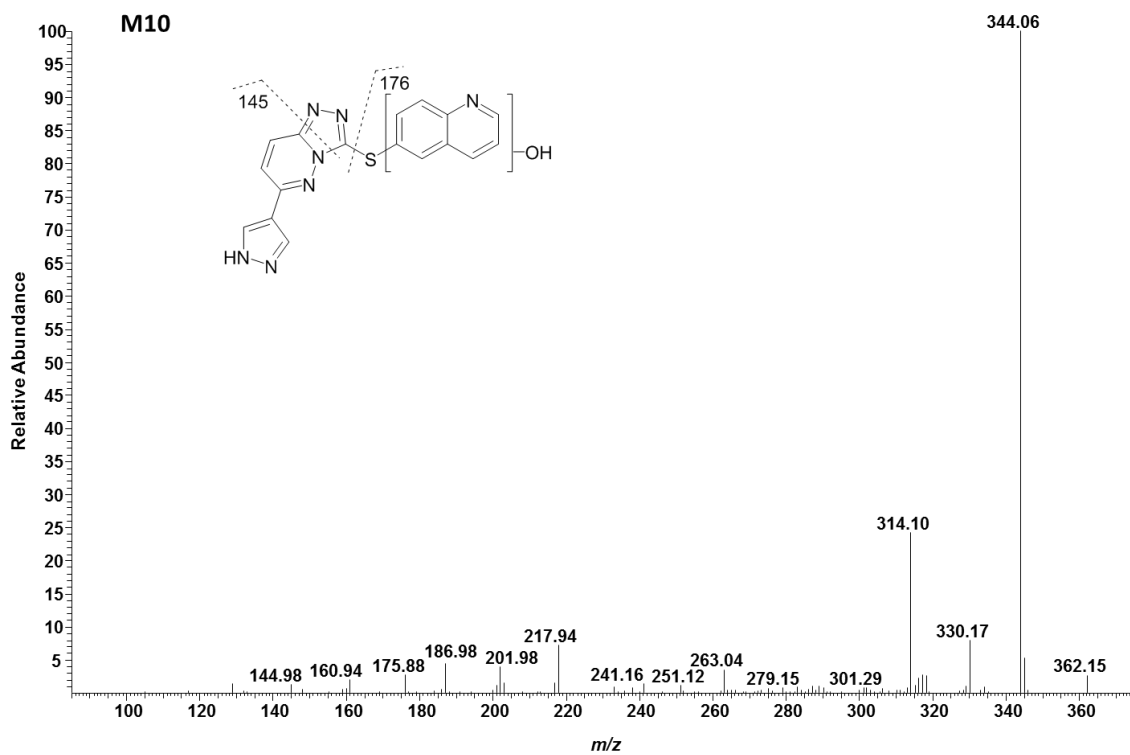


Figure IV.66. LC/MS/MS spectra of SGX523 metabolite M10 ($[M+H]^+$ at m/z 362). The fragment ions occurring at m/z 176 and 145 correspond to a 16-Da increase and 14-Da decrease, respectively, from parent fragment ions at m/z 160 and 159, respectively. The major fragment at m/z 344 represents loss of water, with an intensity of 100% suggesting the likelihood that the oxidation is located on the sulfur atom.

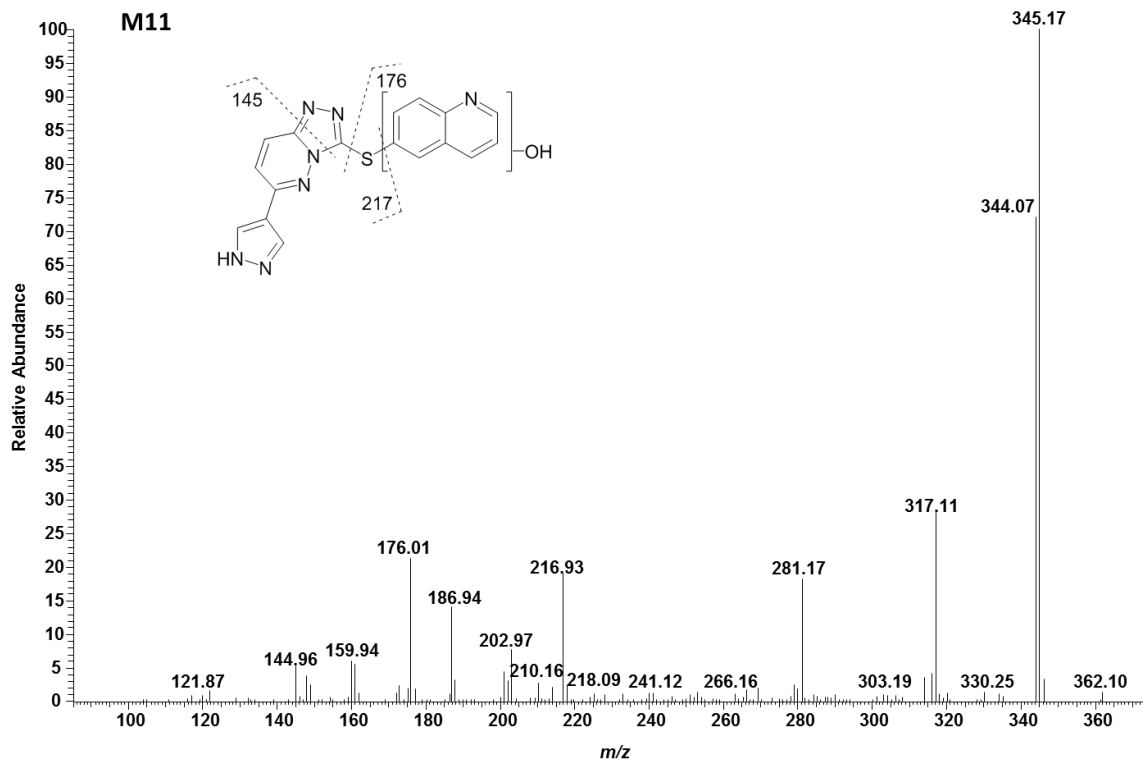


Figure IV.67. LC/MS/MS spectra of SGX523 metabolite M11 ($[M+H]^+$ at m/z 362). The fragment ions occurring at m/z 176 corresponds to a 16-Da increase over the parent fragment ion at m/z 160 and fragment ions at m/z 217 and 145 correspond to a 14-Da decrease from parent fragment ions at 231 and 159, respectively. The major fragment at m/z 344 representing loss of water, along with the fragment ion at m/z 345 (possible loss of OH radical), suggests the possibility that the oxidation is located on the nitrogen of the quinoline moiety.

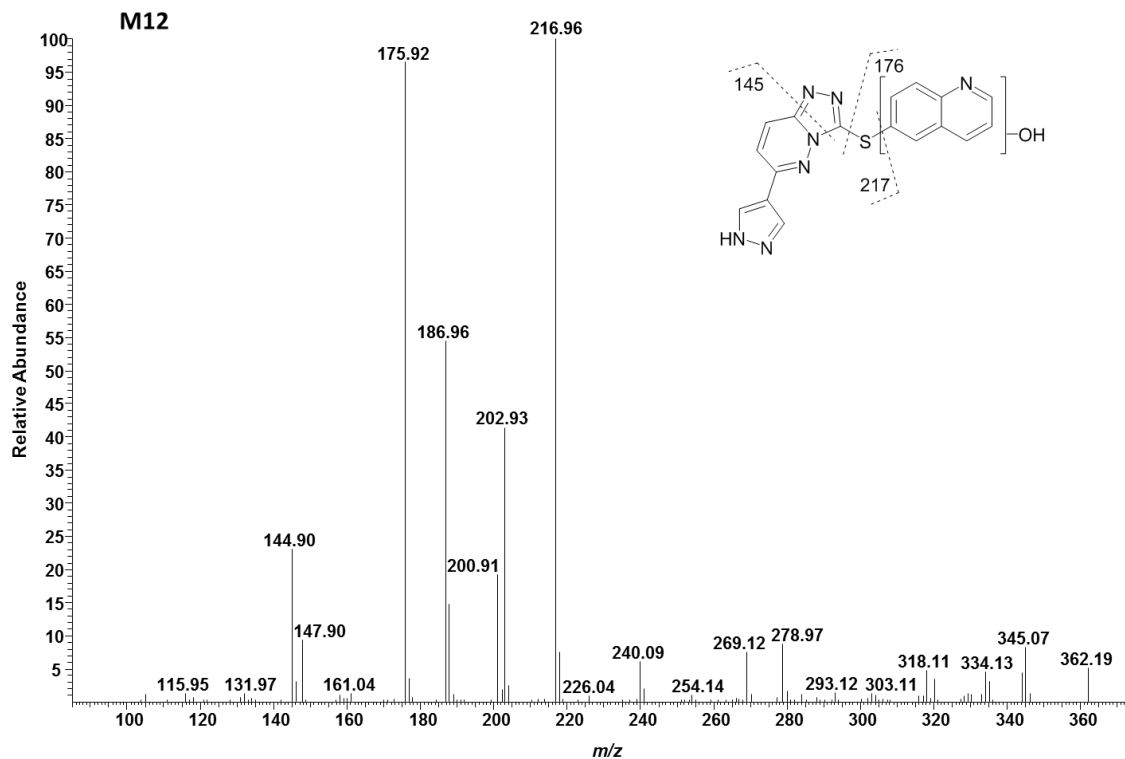


Figure IV.68. LC/MS/MS spectra of SGX523 metabolite M12 ($[M+H]^+$ at m/z 376). The fragment ion occurring at m/z 176 correspond to a 16-Da increase over the parent fragment ion at m/z 160, while fragment ions at 217 and 145 correspond to a 14-Da decrease from parent fragment ions at m/z 231 and 159, respectively. Intensities of fragment ions at m/z 217 (100%), 176 (~100%), and 145 (~25%) are similar to the corresponding fragments of M1 (m/z 231, 176, and 145, respectively), suggesting the possibility that M12 is the N-desmethyl analog of M1.

In general, major differences were not observed in the qualitative assessment of interspecies metabolism of the five compounds. In some cases, metabolites were detected in a species-specific manner, though in general, these metabolites were only present at trace levels. Instead, the primary differences observed between species concerned the relative amounts of each metabolite detected. In agreement with the intrinsic clearance data, similarities in metabolite profile between human and any one species was substrate-dependent. Likewise, mouse and rat generally exhibited metabolite profiles least similar to human, particularly with regard to efficiency of substrate turnover to M1 versus NADPH-dependent metabolites. Interestingly, the difference in turnover efficiency to M1 in mouse and rat was not always decreased relative to human, but in the case of zoniporide was increased. Minipig generally exhibited greater NADPH-dependent metabolism versus human, with similar or decreased NADPH-independent metabolism. Guinea pig metabolite profiles in some instances were very similar to human, while in others (zoniporide and BIBX1382) it better resembled the rat and mouse profiles. Overall, the greatest similarities were observed between human and the two monkey species.

DISCUSSION

The general assumption in the utility of allometric scaling to predict human clearance is that it requires conserved drug elimination mechanisms across species. Accordingly, where AO-mediated clearance exists, confidence in this approach is lacking due to differences in expression and activity between human and preclinical species traditionally employed with this method (e.g., mouse, rat, dog), resulting in limited studies examining allometry to predict human clearance of AO substrates. Given the successful allometric scaling of human clearance of UGT substrates despite species differences in glucuronidation (Deguchi et al., 2011), we sought to evaluate the ability to scale clearance (specifically, *hepatic* clearance) of compounds exhibiting an AO elimination pathway by MA and SSS. This was accomplished by scaling *in vitro* CL_{int} of five structurally and therapeutically diverse AO substrates, determined in hepatic S9 of several species known to express AO in the liver. In the present investigation, human *in vitro* hepatic clearance of the five AO substrates was successfully predicted by either MA or SSS. By comparison of AAFE, MA was not superior to SSS with cynomolgus, rhesus, or guinea pig, but was generally more accurate than SSS with mouse or rat (summarized in Tables IV.24-25). It was anticipated that these species would out-perform mouse and rat since, like human, they express only the *AOX1* isoform in the liver, unlike rat and mouse which express both *AOX1* and *AOX3* (Garattini and Terao, 2012). When comparing AFEs, with the exception of monkey, SSS tended more toward under-prediction versus most MA approaches.

Summary of Intrinsic Clearance Predictions

Multispecies simple allometry	AAFE	AFE	% within 2 fold-error	% within 3 fold-error
Minipig/Rhesus/Rat/Mouse	1.9	1.2	40%	80%
Minipig/Cyno/Rat/Mouse	2.0	1.5	40%	60%
Minipig/Rhesus/Gpig/Mouse	1.9	1.2	40%	80%
Minipig/Cyno/Gpig/Mouse	2.0	1.5	60%	60%
Rhesus/Rat/Mouse	1.7	1.7	80%	80%
Cyno/Rat/Mouse	3.3	3.3	20%	60%
Rhesus/Gpig/Mouse	2.2	1.9	60%	80%
Cyno/Gpig/Mouse	3.5	3.5	20%	40%
Minipig/Rhesus/Rat	2.3	1.2	40%	60%
Minipig/Cyno/Rat	2.4	1.4	40%	60%
Minipig/Rhesus/Gpig	2.2	1.0	40%	80%
Minipig/Cyno/Gpig	2.3	1.1	40%	60%
Minipig/Gpig/Mouse	2.4	1.0	40%	60%
Minipig/Rat/Mouse	2.3	0.92	40%	60%
Single species scaling	AAFE	AFE	% within 2 fold-error	% within 3 fold-error
Cynomolgus Monkey	1.6	1.6	80%	80%
Rhesus Monkey	1.4	1.2	80%	100%
Rat	4.1	0.56	40%	40%
Mouse	3.8	0.38	40%	60%
Minipig	2.0	0.76	60%	80%
Guinea Pig	1.7	0.76	80%	80%

Table IV.24. Summary of absolute average fold-error (AAFE), average fold-error (AFE), and percentage of compounds predicted within 2 or 3 fold-error of observed intrinsic clearance (CL_{int}) measured in human S9, as predicted by multispecies allometry (MA) or single-species scaling (SSS). Cyno = cynomolgus monkey; Rhesus = rhesus monkey; Gpig = guinea pig

Summary of Hepatic Clearance Predictions

Multispecies simple allometry	AAFE	AFE	% within 2 fold-error	% within 3 fold-error
Minipig/Rhesus/Rat/Mouse	1.4	1.0	80%	100%
Minipig/Cyno/Rat/Mouse	1.4	1.1	80%	100%
Minipig/Rhesus/Gpig/Mouse	1.4	1.1	80%	100%
Minipig/Cyno/Gpig/Mouse	1.4	1.2	80%	100%
Rhesus/Rat/Mouse	1.3	1.3	80%	100%
Cyno/Rat/Mouse	1.7	1.7	80%	100%
Rhesus/Gpig/Mouse	1.5	1.3	80%	100%
Cyno/Gpig/Mouse	1.6	1.6	80%	100%
Minipig/Rhesus/Rat	1.5	1.0	80%	100%
Minipig/Cyno/Rat	1.5	1.0	80%	100%
Minipig/Rhesus/Gpig	1.6	0.91	80%	80%
Minipig/Cyno/Gpig	1.6	0.93	60%	80%
Minipig/Gpig/Mouse	1.6	0.89	60%	100%
Minipig/Rat/Mouse	1.7	0.84	60%	80%
Single species scaling	AAFE	AFE	% within 2 fold-error	% within 3 fold-error
Cynomolgus Monkey	1.3	1.3	100%	100%
Rhesus Monkey	1.2	1.1	100%	100%
Rat	2.2	0.63	80%	80%
Mouse	2.3	0.52	60%	60%
Minipig	1.6	0.79	80%	80%
Guinea Pig	1.3	0.90	100%	100%

Table IV.25. Summary of absolute average fold-error (AAFE), average fold-error (AFE), and percentage of compounds predicted within 2 or 3 fold-error of observed hepatic clearance (CL_{HEP}) measured in human S9, as predicted by multispecies allometry (MA) or single-species scaling (SSS). Cyno = cynomolgus monkey; Rhesus = rhesus monkey; Gpig = guinea pig

The use of minipigs in drug discovery and development is gaining popularity due to similarities in anatomy and physiology to humans, as well as advantages related to regulatory acceptability and animal welfare (Bode et al., 2010; van der Laan et al., 2010). With regard to drug metabolism, minipigs hold an advantage over dogs when AO is involved, as dogs are essentially devoid of AO activity in the liver (Dalgaard, 2015; Terao et al., 2016). In addition, a recent report found minipig to be useful in allometric scaling of drugs mostly cleared by P450 or glucuronidation (Yoshimatsu et al., 2016). Consequently, for our studies we chose to replace dog, which is commonly used for allometric scaling, with minipig, a species of similar body weight. We also evaluated the utility of guinea pig in addition to rat and mouse, since, as previously stated, guinea pig expresses only the *AOX1* isoform in the liver, resembling human. Indeed, the use of minipig for MA enabled human CL_{int} predictions within 3-fold of measured values, and SSS with both minipig and guinea pig predicted CL_{int} within 2-fold for four out of the five substrates (all five with guinea pig for CL_{HEP}). Despite successful SSS with minipig, monkey, and guinea pig, three-species allometry with minipig, monkey, and guinea pig was not always superior to the other species combinations. O^6 -benzylguanine, for example, was under-predicted (0.17-0.18 fold error) by MA with minipig, monkey, and guinea pig; however, the prediction resulting from MA is heavily influenced by the smallest and the largest species included in the analysis (see Figure II.2). In the case of O^6 -benzylguanine, minipig demonstrated very low CL_{int} , and thus the curve fit to these data results in a lower CL_{int} value when extrapolated to human versus MA analyses where monkey (which exhibited higher CL_{int} than minipig) is the largest animal

included in the analysis. When minipig, monkey, and guinea pig each produced good predictions by SSS for a particular compound, this species combination also resulted in good predictions by MA (e.g., zaleplon and zoniporide).

While these data support the notion that allometry could be useful to predict human clearance of AO substrates, they only represent clearance mediated by hepatic metabolism. Substrates with minimal renal clearance were selected to avoid this source of inconsistency between *in vitro* and *in vivo* elimination. However, extra-hepatic expression of AO has been demonstrated in human as well as nonclinical species (Kurosaki et al., 1999; Moriwaki et al., 2001; Nishimura and Naito, 2006; Terao et al., 2016). Furthermore, differences in the *AOX1* mRNA levels observed in various tissues between humans and mice (Terao et al., 2016) indicate tissue-specific expression patterns may not parallel across species. Any extra-hepatic metabolism, therefore, could preclude *in vivo* translation of these data. For example, Hutzler et al. demonstrated elimination of BIBX1382 in lung and kidney S9 fractions of human and cynomolgus monkey (Hutzler et al., 2014a). Furthermore, species differences were noted in the relative elimination of BIBX1382 from these two tissues. Indeed, human CL_p for four of the five substrates we evaluated are reported in the literature and were each under-represented by our CL_{HEP} estimates from human S9 incubations, including BIBX1382 (see Table V.2). This is not an uncommon observation, which may be attributed to extra-hepatic metabolism, among other possibilities, such as SNPs or other sources of donor variability, *ex vivo* protein instability, or procedural differences in tissue procurement (Hartmann et al., 2012; Hutzler et al., 2012; Fu et al., 2013; Hutzler et al., 2014b). Therefore, while our

in vitro data indicate allometric scaling could be a potentially useful method to predict human hepatic clearance of AO substrates, its utility in predicting total body clearance will remain a significant challenge until extra-hepatic expression and activity of AO across species is better resolved. However, despite observed differences in elimination from extra-hepatic S9 fractions of cynomolgus and human, cynomolgus plasma clearance of BIBX1382 was still representative of the rapid clearance observed in clinical pharmacokinetic studies in terms of percentage of liver blood flow (Hutzler et al., 2014a), suggesting preclinical species such as monkey may still be useful for predicting total body clearance.

Comparison of prediction fold-errors by SSS (CL_{int} or CL_{HEP}) with the animal:human ratio of either $F_{m,AO}$ or E revealed little correlation with $F_{m,AO}$, but a positive correlation with E (Figures IV. 6-7). Likewise, the same trends were observed for UGT substrates when plotting SSS prediction fold-error of CL_p versus the animal:human ratio in $F_{m,UGT}$ or versus CL_p as a percentage of Q_H (Figure IV.8). We observed some examples where a discrepancy in $F_{m,AO}$ between human and animal did not preclude a similar E , indicating a non-AO metabolism pathway may compensate for the lacking AO pathway to result in an overall similar hepatic extraction efficiency. For example, the $F_{m,AO}$ obtained for zaleplon was substantially higher in human (≥ 0.71) versus minipig (≤ 0.17), while the E between the two species was similar (human = 0.22, minipig = 0.16). Accordingly, biotransformation experiments revealed decreased NADPH-independent oxidation of zaleplon to M1 in minipig S9 relative to human S9, while instead NADPH-dependent N-deethylation to M2 appeared to be the major metabolite in minipig S9. Consequently, these data

may indicate that compounds containing a mixed AO/P450 metabolism phenotype, or possessing P450 favorable sites in addition to the AO metabolism site, could help to enable allometric scaling approaches since alternate metabolism pathway(s) in certain species may compensate for reduced AO-mediated clearance. Nonetheless, these observations suggest that there is not a strong relationship between F_m and the prediction fold-error by SSS or that methods to obtain F_m are not sufficiently accurate to observe this relationship. With regard to the present study, it should be noted that our $F_{m,AO}$ calculations assume that 50 μ M hydralazine is adequate to selectively and completely inhibit AO metabolism, whereas the potency and selectivity of hydralazine is not known for all species studied. In addition, our $F_{m,AO}$ calculations are dependent on the ability to measure substrate depletion when turnover may be low, which presents an additional challenge in obtaining an accurate $F_{m,AO}$ estimate. Finally, four of the five compounds exhibited an $F_{m,AO}$ in human of ≥ 0.70 . A larger data set consisting of compounds exhibiting a broader range of $F_{m,AO}$ would help to better understand the importance of this value to obtaining an accurate human hepatic clearance prediction by SSS.

Because we cannot assume that human clearance predictions derived from allometrically scaled *in vitro* data are representative of total body clearance, we do not propose that this method should be used for predicting human total body clearance. Instead, it may be useful in selecting the best species for conducting *in vivo* pharmacokinetic (PK) studies and subsequent allometric scaling of *in vivo* data to predict human total body clearance. Recently, Choughule et al., reported that relative hepatic CL_{int} mediated by AO in human, rhesus and guinea pig cytosol was

substrate-dependent, suggesting that no single species could be reliably employed to consistently predict human clearance (Choughule et al., 2013b). We too observed substrate-dependent variability in all species evaluated, with a particular species (or species combination) resulting in over-prediction for some substrates and under-prediction for others. These studies may therefore serve as a useful tool to guide species selection for *in vivo* assessments. Particularly, evaluation of $F_{m,A0}$ and E in combination with the *in vitro* SSS and biotransformation analyses may be useful to support decisions in selecting the most appropriate species, with the suggestion that confidence not be placed in $F_{m,A0}$ alone to indicate which species is expected to provide a more accurate human hepatic clearance prediction by SSS, but rather $F_{m,A0}$ should be considered secondary to E in guiding this decision. For example, based on our SSS analysis, cynomolgus might be selected for *in vivo* studies of BIBX1382, when all *in vitro* data is taken into consideration. Cynomolgus monkey exhibited a similar E to human (cynomolgus = 0.80, human = 0.79) as well as $F_{m,A0}$ (cynomolgus = 1.0, human = 0.92), and the fold-error in prediction of CL_{int} by SSS was 1.1, while the fold-error in CL_{HEP} prediction by SSS was 1.0. Furthermore, biotransformation of BIBX1382 by human and monkey was similar, with the exception of secondary metabolism of $M1 \rightarrow M2$ (appears greater in cynomolgus), which does not directly contribute to elimination of the parent drug. Based on Hutzler's report of *in vivo* clearance in cynomolgus, this species would indeed be an appropriate selection for *in vivo* studies and subsequent human *in vivo* clearance prediction. Rat and mouse, on the other hand, would not be expected to accurately scale human clearance based on our analysis. Both mouse and rat exhibited low E relative to human (mouse =

0.27, rat = 0.30), while $F_{m,AO}$ estimates were unclear. In addition, fold-errors in SSS CL_{int} prediction by mouse and rat were 0.05 and 0.09, respectively, with some improvement when predicting CL_{HEP} at 0.22 and 0.33-fold under-prediction, respectively. Likewise, metabolite profiles of mouse and rat were dissimilar to human, particularly with regard to NADPH-dependent versus -independent metabolism and the major metabolite(s) produced. Accordingly, preclinical studies in rat and mouse PK did not predict the rapid clearance of BIBX1382 observed in clinical trials (Dittrich et al., 2002), and thus were an ineffective species selection. In addition to evaluating *in vitro* data for selection of species, it may also be important to evaluate sex differences for selection of male versus female animals. Sex evaluation may be particularly important for compounds exhibiting other metabolism pathways in addition to AO, as in some cases, the sex differences may oppose one another depending on which enzymes are involved (e.g., females may exhibit higher AO activity, while males may exhibit higher P450 3A4 activity, etc.).

It is also important to note that while we did observe substrate-dependence in the accuracy of the prediction with regard to which species were included in the analysis, this result is not contrary to findings in other evaluations of allometry approaches for compounds cleared by non-AO mechanisms such as cytochrome P450 metabolism. In a report by Hosea et al., for example, half-life of only ~60-80% of 50 proprietary compounds exhibiting P450, nonP450, and renal clearance mechanisms were predicted within 3-fold of clinically observed measurements using multiple different allometric scaling approaches, and of those cleared by P450, the oral clearance of only ~30-50% were predicted within 2-fold by SSS with rat,

dog, or monkey (Hosea et al., 2009). Therefore, according to our *in vitro* results, it may be possible to predict human hepatic clearance of AO substrates with allometry at a rate similar to that obtained for compounds cleared via other mechanisms. The larger issue may rather lie in the potential differences in extra-hepatic expression of AO, and thus, total body clearance prediction.

In conclusion, we have demonstrated that human *in vitro* hepatic CL_{int} may be successfully scaled by MA and SSS using the species presented, albeit in a substrate-dependent manner with regard to species. We have offered a potentially useful approach, not to predict human *in vivo* clearance of AO substrates, but to aid in selection of preclinical species that, when evaluated *in vivo*, may provide the best estimates of human *in vivo* clearance, particularly when *in vivo* clearance is predominantly mediated by hepatic metabolism. *In vivo* studies will be required to fully understand the utility of this approach (Chapter V) as will further work to understand species differences in extra-hepatic metabolism with regard to total body clearance.

CHAPTER V

ALLOMETRIC SCALING OF IN VIVO HEPATIC CLEARANCE OF DRUGS

POSSESSING AN ALDEHYDE OXIDASE PATHWAY IN HUMAN

INTRODUCTION

In vitro clearance measurements in hepatocytes or subcellular liver fractions (e.g., microsomes) are considered to be a reliable tool for estimating *in vivo* human clearance of compounds metabolized by cytochrome P450s (Obach et al., 1997; Hosea et al., 2009; Di et al., 2013). In order to build confidence in *in vivo* human clearance predictions extrapolated from *in vitro* human clearance measurements, cross-species *in vitro: in vivo* correlation (IVIVC) of clearance is commonly evaluated (Di et al., 2013). However, while *in vitro*-based clearance prediction methods are well-established for P450-mediated metabolism, those for metabolism mediated by non-P450 enzymes such as aldehyde oxidase (AO) remain to be improved. Poor IVIVC in the clearance of several AO substrates has been reported for *in vitro* clearance estimates derived from incubations with S9, cytosol, or hepatocytes, with under-prediction of *in vivo* clearance observed in each case (Zientek et al., 2010) (Akabane et al., 2012; Hutzler et al., 2012). These observations were proposed to be potentially attributable to extra-hepatic metabolism or possibly *ex vivo* enzyme instability. Others have studied the donor composition of *in vitro* systems (e.g., hepatocytes) and observed interindividual variability (Hutzler et al., 2014b), which may also play a role in the *in vitro* under-prediction of *in vivo* clearance of AO

substrates. Altogether, these drawbacks have resulted in skepticism toward traditional *in vitro* methods for prediction of *in vivo* clearance mediated by AO. In the absence of reliable *in vitro* techniques, the identification of dependable animal model(s) to estimate human AO clearance would be a highly valuable contribution to the drug discovery community.

Our *in vitro* studies described in Chapter IV indicated reasonable prediction of human hepatic clearance by multispecies simple allometry (MA) or single-species scaling (SSS) may be achievable, despite the observation of species differences in AO-mediated metabolism. However, the potential issues with *in vitro* systems described above could prevent the translation of these results *in vivo*. Thus, our next step in seeking to understand the utility of allometric scaling approaches in predicting the human clearance of AO substrates was to investigate the ability to predict human total body clearance *in vivo*. To conduct this investigation, we administered the five AO substrates previously studied *in vitro* (zaleplon, O⁶-benzlguanine, zoniporide, BIBX1382, and SGX523) to mice, rats, guinea pigs, and minipigs as a single IV bolus cassette dose and collected blood samples to determine their plasma concentration-time profiles for pharmacokinetic (PK) analysis. Plasma clearances (CL_p) obtained from noncompartmental PK analysis were compared to hepatic clearances (CL_{HEP}) estimated *in vitro* (Chapter IV) to determine the IVIVC for each compound in each species. Subsequently, the CL_p obtained from mouse, rat, guinea pig, and minipig were subjected to MA and SSS for the prediction of human CL_p. When available, CL_p values in cynomolgus monkey (as well as mouse and rat in some instances) were obtained from the literature and included in these studies.

Finally, *in vitro* data described in Chapter IV were compared to the *in vivo* data reported here for the purpose of evaluating the use of MA and SSS of *in vitro* CL_{int} as a tool to guide selection of a suitable species for *in vivo* PK analysis and subsequent allometric scaling to predict human CL_p.

RESULTS

Pharmacokinetic Parameters in Preclinical Species

Pharmacokinetic (PK) parameters of SGX523, zonisamide, O⁶-benzylguanine, and zaleplon obtained from an IV cassette dose in minipig, guinea pig, rat, and mouse are summarized in Table V.1, and plasma concentration-time curves are displayed in Figures V.1-4. Low plasma concentrations of BIBX1382 did not permit quantitation in any species evaluated, and thus, PK parameters could not be obtained for this compound. Likewise, quantitation limits prevented PK analysis of zonisamide in all species except minipig. Plasma clearance (CL_p) of zaleplon was highest in mouse (83.9 mL/min/kg) and guinea pig (49.2 mL/min/kg) and moderate in rat and minipig (33.7 and 15.4 mL/min/kg, respectively), with moderate volumes of distribution (V_{ss}) ranging from 1.24 – 1.77 L/kg. O⁶-benzylguanine CL_p exceeded hepatic blood flow in all species (454, 203, and 206 mL/min/kg in mouse, rat, and guinea pig, respectively) except minipig (24.1 mL/min/kg), which was near hepatic blood flow. V_{ss} of O⁶-benzylguanine was moderately high in all species, ranging from 2.32 and 3.01 L/kg, respectively, in guinea pig and minipig to 4.0 and 4.55 L/kg, respectively, in rat and mouse. Clearance of zonisamide from minipig plasma was rapid, exceeding hepatic blood flow (193 mL/min/kg), and V_{ss} was also very high at 42.7 L/kg. Though a PK analysis of zonisamide could not be conducted due to low plasma concentrations in mouse, rat, and guinea pig, zonisamide CL_p has been reported in the literature for rat and mouse, which also exceeded hepatic blood flow (237 and 298 mL/min/kg,

respectively); however, the V_{ss} was reported to be much lower at 7.2 and 2.2 L/kg, respectively (Tracey et al., 2003). SGX523 CL_p varied across species, with rapid clearance in mouse (82.9 mL/min/kg), moderate clearance in minipig and guinea pig (19.1 and 34.5 mL/min/kg, respectively), and low clearance in rat (8.4 mL/min/kg). V_{ss} was also lowest in rat (0.761 L/kg), while higher in mouse (2.34 L/kg), guinea pig (1.75 L/kg), and minipig (4.79 L/kg). The reported CL_p of SGX523 was low in cynomolgus monkey at 3.7 mL/min/kg (Diamond et al., 2010b). Area under the plasma concentration-time curve (AUC), which represents the total drug exposure, as well as mean residence time (MRT) and terminal half-life ($t_{1/2}$), which reflect the amount of time the drug is present in the body, are also listed in Table V.1.

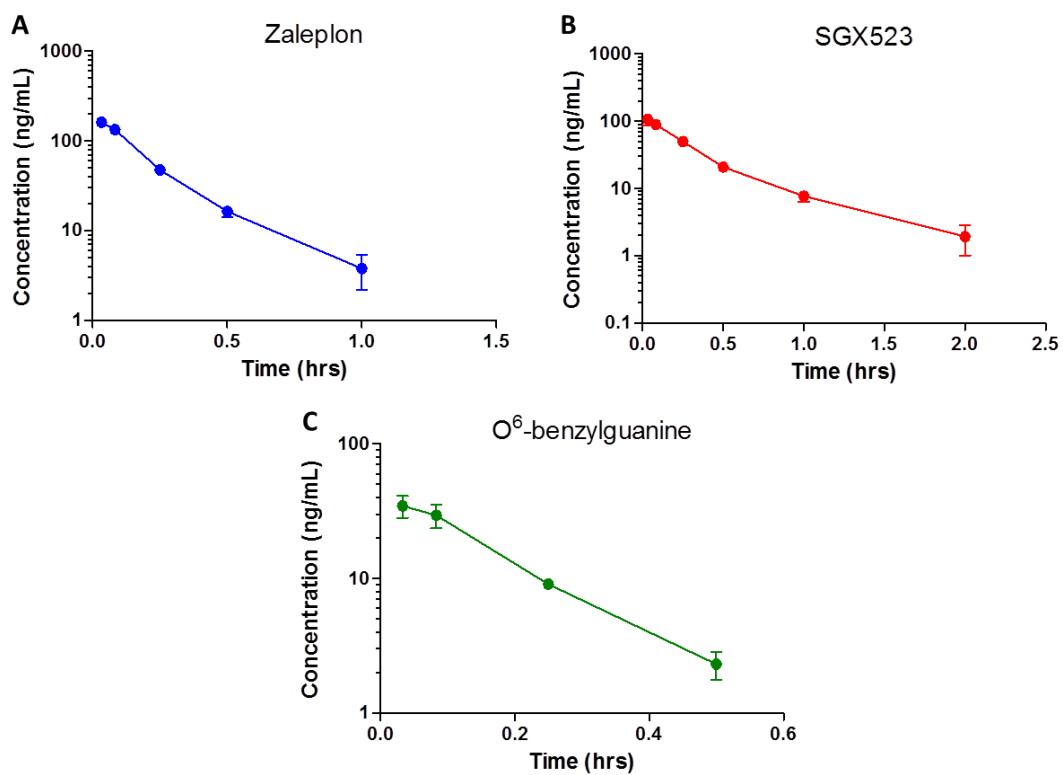


Figure V.1. Plasma concentration-time curves obtained from mouse plasma following an IV cassette dose (0.2 mg/kg) of (A) zaleplon, (B) SGX523, (C) O⁶-benzylguanine, zoniporide (not shown), and BIBX1382 (not shown). Plasma concentrations of zoniporide and BIBX1382 were below the quantitation limit (5 ng/mL). Data represent mean of n = 3 (\pm SD).

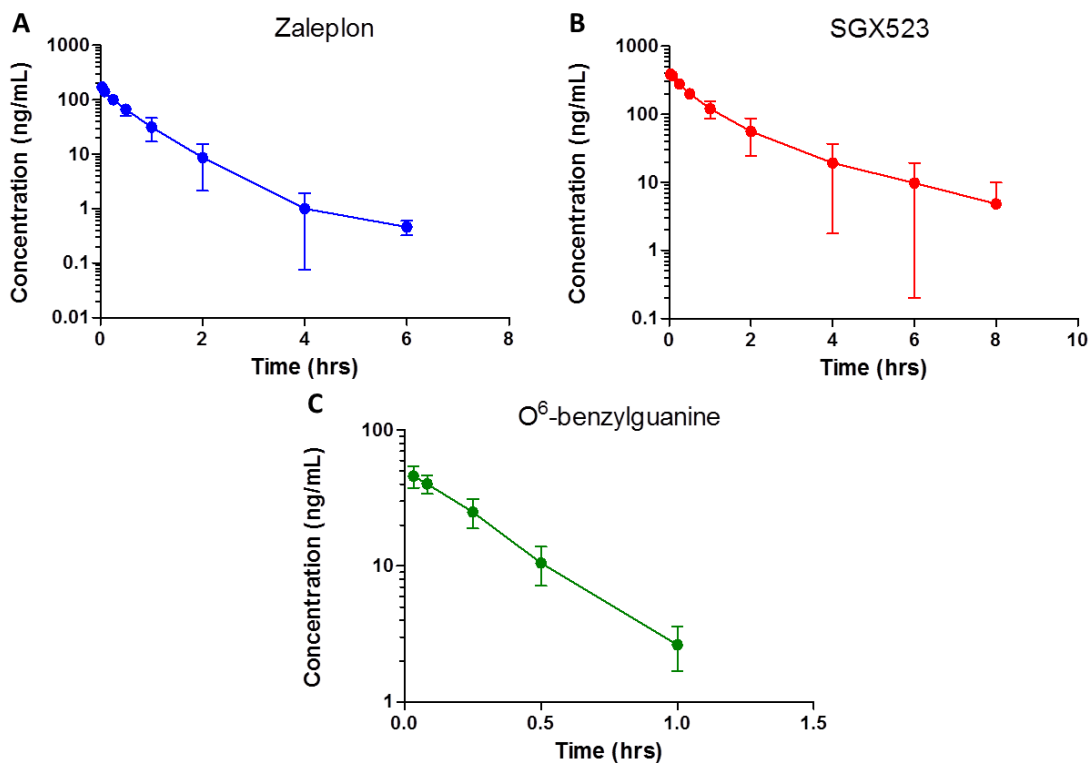


Figure V.2. Plasma concentration-time curves obtained from rat plasma following an IV cassette dose (0.2 mg/kg) of (A) zaleplon, (B) SGX523, (C) O⁶-benzylguanine, zoniporide (not shown), and BIBX1382 (not shown). Plasma concentrations of zoniporide and BIBX1382 were below the quantitation limit (5 ng/mL). Data represent mean of n = 3 (\pm SD)

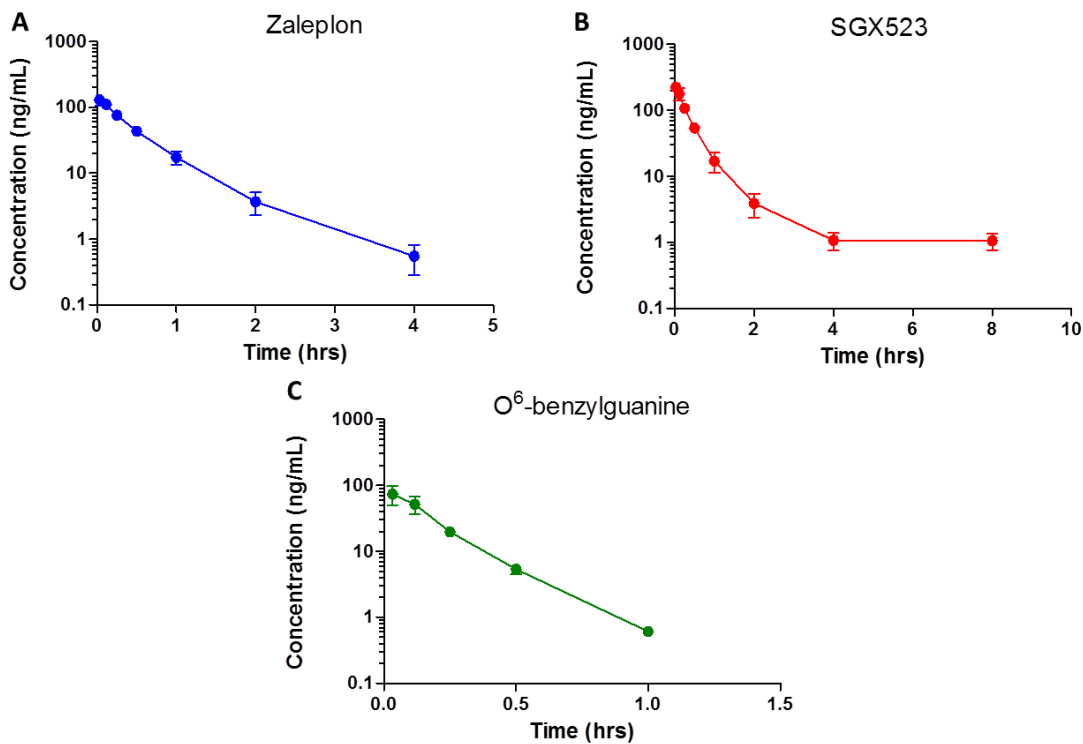


Figure V.3. Plasma concentration-time curves obtained from guinea pig plasma following an IV cassette dose (0.2 mg/kg) of (A) zaleplon, (B) SGX523, (C) O⁶-benzylguanine, zonisporide (not shown), and BIBX1382 (not shown). Plasma concentrations of zonisporide and BIBX1382 were below the quantitation limit (5 ng/mL). Data represent mean of n = 3 (\pm SD).

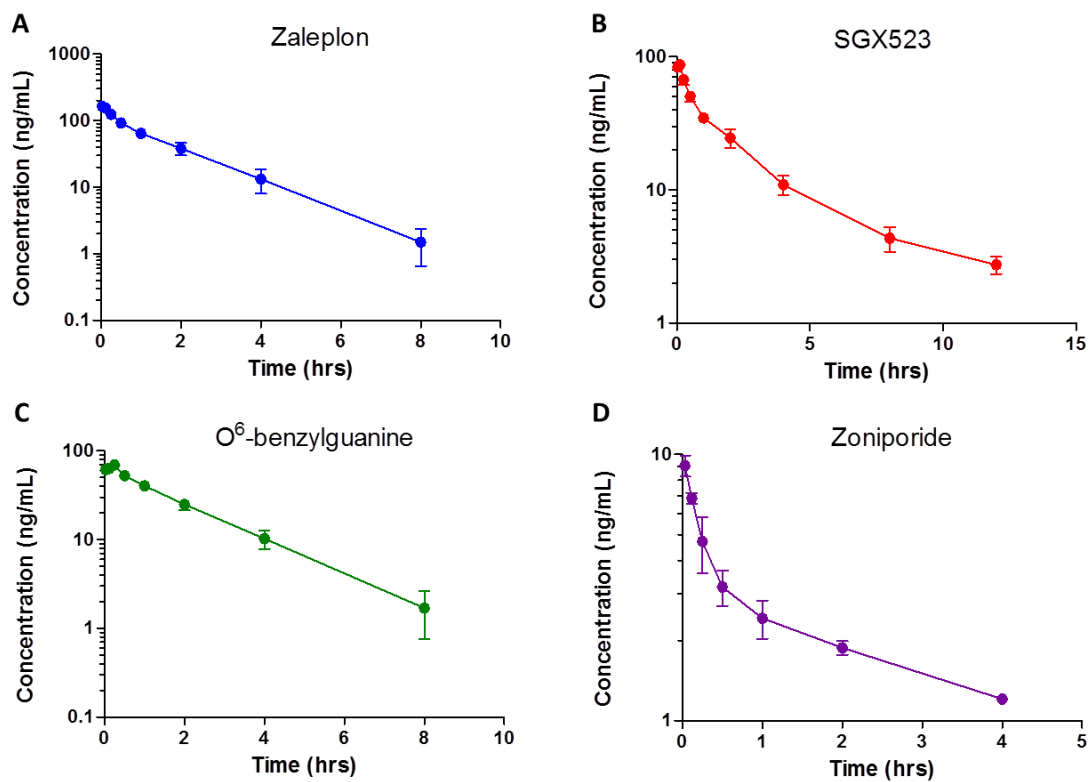


Figure V.4. Plasma concentration-time curves obtained from minipig plasma following an IV cassette dose (0.2 mg/kg) of (A) zaleplon, (B) SGX523, (C) O⁶-benzylguanine, (D) zoniporide, and BIBX1382 (not shown). Plasma concentrations of BIBX1382 were below the quantitation limit (5 ng/mL). Data represent mean of n = 2 (\pm SEM).

	Zaleplon				O ⁶ -benzylguanine				Zoniporide				SGX523			
	MP	GP	R	M	MP	GP	R	M	MP	GP	R	M	MP	GP	R	M
CL _p (mL/min/kg)	15.4	49.2	33.7	83.9	24.1	206	203	454	193	n/a	n/a	n/a	19.1	34.5	8.37	82.9
V _{ss} (L/kg)	1.52	1.77	1.49	1.24	3.01	2.32	4.00	4.55	42.7	n/a	n/a	n/a	4.79	1.75	0.761	2.34
AUC _{0-∞} (h*ng/mL)	225	68.3	105	39.7	142	16.2	17.0	7.36	14.0	n/a	n/a	n/a	177	97.5	432	40.3
MRT _{0-∞} (h)	1.70	0.606	0.765	0.246	2.13	0.187	0.330	0.168	3.68	n/a	n/a	n/a	4.18	0.852	1.66	0.472
Terminal t _{1/2} (h)	1.25	0.560	1.02	0.211	1.51	0.151	0.232	0.116	2.73	n/a	n/a	n/a	4.01	0.791	1.84	0.445

Table V.I. Pharmacokinetic parameters of zaleplon, O⁶-benzylguanine, zoniporide, and SGX523 obtained from a cassette IV bolus dose (0.2 mg/kg per compound) to mouse, rat, guinea pig and minipig. Data represents mean of n = 3 (rat, mouse, and guinea pig) or n = 2 (minipig). MP, minipig; GP, guinea pig; R, rat; M, mouse

In Vitro-in Vivo Correlation (IVIVC)

In vitro hepatic clearance (CL_{HEP}) for zaleplon, O⁶-benzylguanine, zonisamide, SGX523, and BIBX1382 was previously estimated in S9 of human, mouse, rat, guinea pig, cynomolgus, rhesus, and minipig (Chapter IV). Comparisons of these CL_{HEP} values with CL_p obtained for each species are displayed in Table V.2. In instances where CL_p data were available in the literature on species or compounds for which we did not obtain PK parameters, these data were included in the analysis where indicated. In all species evaluated, *in vitro* estimates of zaleplon CL_{HEP} underestimated *in vivo* CL_p . However, the fold-difference between *in vitro* and *in vivo* CL of zaleplon was fairly consistent across all species (range 0.23 - 0.38). O⁶-benzylguanine CL_p was under-estimated by *in vitro* assessments as well in each species. The fold-difference was similar between guinea pig and minipig (0.15 and 0.16, respectively) and between rat and mouse (0.04 in rat and mouse). The under-estimation was less severe in human (fold-difference = 0.66). Zonisamide under-estimations were worst in minipig (fold-difference = 0.07), similar between mouse and rat (0.24 and 0.26, respectively), and were more reasonable in cynomolgus and human (0.83 and 0.46, respectively). Human CL_p of BIBX1382 reported in the literature ranged from 25 - 55 mL/min/kg (Dittrich et al., 2002), resulting in an *in vitro* underestimation of 0.66 - 0.30 fold (Hutzler et al., 2014a). Cynomolgus monkey CL_p BIBX1382 likewise was under-estimated by *in vitro* CL_{HEP} , with a reported CL_p of 118 mL/min/kg and a fold-difference of 0.30 (Hutzler et al., 2014a). BIBX1382 CL_p of 55 mL/min/kg was reported in rat and mouse, with an *in vitro* underestimation of 0.39 and 0.44, respectively (Dittrich et al., 2002). Fold-

differences in estimation of SGX523 were again similar between guinea pig and minipig (0.72 and 0.70, respectively), but were very different between mouse, which under-estimated CL_p (fold-difference = 0.33) and rat, which over-estimated CL_p (fold-difference = 2.65). Cynomolgus monkey overestimated the SGX523 CL_p reported in the literature by 6-fold (Diamond et al., 2010b). Human CL_p was not available in the literature for SGX523 and therefore could not be evaluated.

Overall variability was observed in the IVIVC both across species and across compounds, with most cases resulting in underestimation of *in vivo* CL_p by the CL_{HEP} measured *in vitro*. However, for both zaleplon and BIBX1382, the *in vitro* – *in vivo* fold-difference was fairly consistent across all species examined (~ 0.3 on average), which was also observed in mouse, rat, and human for zoniporide and in mouse for SGX523.

	Zaleplon			O ⁶ -benzylguanine			Zoniporide			BIBX1382			SGX523		
	S9 (in vitro)	CL _p (in vivo)	Fold-diff	S9 (in vitro)	CL _p (in vivo)	Fold-diff	S9 (in vitro)	CL _p (in vivo)	Fold-diff	S9 (in vitro)	CL _p (in vivo)	Fold-diff	S9 (in vitro)	CL _p (in vivo)	Fold-diff
Human	4.55	16.0 ^c	0.28	9.62	14.5 ^c	0.66	9.64	21.0 ^c	0.46	16.6	25 – 55 ^a	0.66 - 0.30	5.22	n/a	n/a
Cynomolgus	13.9	n/a	n/a	21.6	n/a	n/a	25.9	31.0 ^c	0.84	35.4	118 ^a	0.30	22.1	3.70 ^b	6.0
Rhesus	11.2	n/a	n/a	15.1	n/a	n/a	18.1	n/a	n/a	31.7	n/a	n/a	18.0	n/a	n/a
Minipig	4.60	15.4	0.30	3.79	24.1	0.16	12.7	193	0.07	23.1	n/a	n/a	13.3	19.1	0.70
Guinea Pig	11.5	49.2	0.23	30.3	206	0.15	34.6	n/a	n/a	33.1	n/a	n/a	25.0	34.5	0.72
Rat	12.7	33.7	0.38	7.40	203	0.04	60.9	237 ^c	0.26	21.3	55.0 ^d	0.39	22.1	8.37	2.6
Mouse	19.2	83.9	0.23	16.8	454	0.04	70.8	298 ^c	0.24	24.1	55.0 ^d	0.44	27.4	82.9	0.33

Table V.2. *In vitro-in vivo* correlation (IVIVC) of S9 hepatic clearance (CL_{HEP}, mL/min/kg) and plasma clearance (CL_p, mL/min/kg) in preclinical species for zaleplon, O⁶-benzylguanine, zoniporide, BIBX1382, and SGX523. CL_p, plasma clearance

^a Hutzler, et al. (2014a). *Drug Metab Dispos* **42**:1751-1760.

^b Diamond, et al. (2010). *Drug Metab Dispos* **38**:1277-1285.

^c Zientek, et al. (2010). *Drug Metab Dispos* **38**:1322-1327.

^d Dittrich, et al. (2002). *Euro J Canc.* **38**:1072-1080.

Single-Species Scaling (SSS) of Plasma Clearance

Human clearance predicted by SSS is displayed in Table V.3. All species evaluated produced reasonable and similar human CL_p predictions for zaleplon ranging from 8.8 – 13.6 mL/min/kg, with fold-errors ranging from 0.55 – 0.85. O⁶-benzylguanine CL_p was over-predicted by mouse, rat, and guinea pig 4.1, 3.7, and 3.9-fold, respectively (predicted human CL_p = 59.8, 53.8, and 57.2 mL/min/kg, respectively), while minipig predicted a human CL_p of 13.8 mL/min/kg (0.95-fold-error). For zonisamide, however, minipig over-predicted 5.3 fold (predicted human CL_p = 110.6 mL/min/kg). Mouse and rat data taken from the literature scaled to over-predict human zonisamide CL_p to a lesser extent than minipig, with predictions of 39.2 and 62.7 mL/min/kg, respectively, resulting in fold-errors of 1.9 and 3.0, respectively. Cynomolgus monkey CL_p (from literature) more closely predicted human CL_p of zonisamide at 15.3 mL/min/kg, with a fold error of 0.72. Using cynomolgus monkey data reported in the literature, BIBX1382 was predicted within 2.2-fold error at 56.0 mL/min/kg. Literature data for rat and mouse resulted in a human CL_p under-predictions of 14.6 and 7.2 mL/min/kg, respectively, for a fold-error of 0.58 – 0.26 for rat and 0.29 – 0.13 for mouse.

	Zaleplon		O ⁶ -benzylguanine		Zoniporide		BIBX1382	
Observed Human CL _p	16		14.5		21		25 - 55	
	Predict CL _p	Fold Error	Predict CL _p	Fold Error	Predict CL _p	Fold Error	Predict CL _p	Fold Error
Cynomolgus	n/a	n/a	n/a	n/a	15.2	0.72	56	2.2 - 1.0
Rat	8.9	0.56	53.8	3.7	62.7	2.8	14.6	0.58 - 0.26
Mouse	11.0	0.69	59.8	4.1	39.2	1.8	7.2	0.29 - 0.13
Minipig	8.8	0.55	13.8	0.95	111	5.3	n/a	n/a
Guinea Pig	13.6	0.85	57.2	3.9	n/a	n/a	n/a	n/a

Table V.3. Human CL_p (mL/min/kg) predicted by single-species scaling (SSS) of CL_p obtained from IV administration (Table V.1 or from literature data) and fold-error of the prediction for zaleplon, O⁶-benzylguanine, zoniporide, and BIBX1382.

As previously mentioned, human CL_p data are not available in the literature for SGX523, so a fold-error in the prediction could not be calculated. Minipig, guinea pig, and mouse all predicted similar SGX523 CL_p values (11.0, 9.6, and 10.9 mL/min/kg, respectively), while rat and cynomolgus monkey (from literature CL_p) predicted lower, yet similar values of 2.2 and 1.9 mL/min/kg, respectively.

	SGX523	
Observed Human CL _p	n/a	
	Predict CL _p	Fold Error
Cynomolgus	1.9	n/a
Rat	2.2	n/a
Mouse	10.9	n/a
Minipig	11	n/a
Guinea Pig	9.6	n/a

Table V.4. Human SGX523 CL_p (mL/min/kg) predicted by single-species scaling (SSS) of CL_p obtained from IV administration (Table V.1 or from literature data). No human CL_p data are available for SGX523 to perform a fold error analysis.

Prediction accuracy by SSS was substrate-dependent, with each species evaluated demonstrating under-prediction of some substrates and over-prediction of others. With the exception of cynomolgus monkey, no species accurately predicted human CL_p (i.e., ≤ 3-fold error) for all compounds evaluated. However, while cynomolgus monkey SSS provided reasonable predictions for both zoniporide and BIBX1382, data were not available to assess the other three compounds.

Multispecies Simple Allometry (MA) of Plasma Clearance

Human clearance predicted by MA with three or four species is displayed in Table V.5 for zaleplon, O⁶-benzylguanine, zoniporide, and BIBX1382. Three-species MA with minipig/guinea pig/mouse or minipig/rat/mouse produced reasonable predictions for zaleplon with fold-errors of 0.56 and 0.49, respectively. Likewise, predictions with the same three-species combinations resulted in fold-errors of 0.69 and 0.65, respectively, for O⁶-benzylguanine. The minipig/rat/mouse combination, however, resulted in a 7.7-fold over-prediction for zoniporide. Inclusion of cynomolgus monkey data produced predictions of < 3-fold error by three- or four-species MA for zoniporide, with a 0.56 and 2.0-fold error by cynomolgus/rat/mouse and minipig/cynomolgus/rat, respectively and a 2.3-fold error by minipig/cynomolgus/rat/mouse. Three species MA with cyno/rat/mouse predicted BIBX1382 CL_p with a fold error of 2.9 – 6.4.

	Zaleplon				O ⁶ -benzylguanine				Zoniporide				BIBX 1382			
Observed Human CL _p	16				14.5				21				25 - 55			
	Predict CL _p	Fold Error	R ²	Exponent	Predict CL _p	Fold Error	R ²	Exponent	Predict CL _p	Fold Error	R ²	Exponent	Predict CL _p	Fold Error	R ²	Exponent
Mpig/Cyno/Rat/Mouse	n/a	n/a	n/a	n/a	n/a	n/a	n/a	n/a	49	2.3	0.866	0.77	n/a	n/a	n/a	n/a
Cyno/Rat/Mouse	n/a	n/a	n/a	n/a	n/a	n/a	n/a	n/a	11.8	0.56	0.904	0.57	160	2.9 - 6.4	0.995	1.15
Mpig/Cyno/Rat	n/a	n/a	n/a	n/a	n/a	n/a	n/a	n/a	43.9	2.1	0.635	0.74	n/a	n/a	n/a	n/a
Mpig/Gpig/Mouse	9.03	0.56	0.992	0.71	10.1	0.69	0.930	0.50	n/a	n/a	n/a	n/a	n/a	n/a	n/a	n/a
Mpig/Rat/Mouse	7.82	0.49	0.999	0.71	9.48	0.65	0.948	0.50	162	7.7	0.999	0.93	n/a	n/a	n/a	n/a

Table V.5. Human CL_p (mL/min/kg) predicted by multispecies simple allometry (MA) of CL_p obtained from IV administration (Table V.1 or from literature data), fold-error of the prediction, correlation coefficient of each method, and allometric exponent (*b*) for each method for zoniporide, O⁶-benzylguanine, zaleplon and BIBX1382. Cyno, cynomolgus monkey; Gpig, guinea pig

SGX523 human CL_p predictions obtained from MA are listed in Table V.6. Predictions were mostly low, with minipig/cyno/rat and minipig/rat/mouse generating moderately higher predictions.

Observed Human CL_p	SGX523		
	n/a		
	Predict CL_p	R ²	Exponent
Minipig/Cyno/Rat/Mouse	3.04	0.786	0.653
Minipig/Cyno/Gpig/Mouse	3.55	0.825	0.605
Cyno/Rat/Mouse	0.65	0.893	0.430
Cyno/Gpig/Mouse	1.14	0.867	0.441
Minipig/Cyno/Rat	10.3	0.827	1.06
Minipig/Cyno/Gpig	3.04	0.471	0.553
Minipig/Gpig/Mouse	10.5	0.999	0.750
Minipig/Rat/Mouse	6.75	0.855	0.760

Table V.6. Human CL_p (mL/min/kg) predicted by multispecies simple allometry (MA) of CL_p obtained from IV administration (Table V.1 or from literature data), correlation coefficient of each method, and allometric exponent (b) for each method for SGX523. No human CL_p data are available for SGX523 to perform a fold error analysis. Cyno, cynomolgus monkey; Gpig, guinea pig

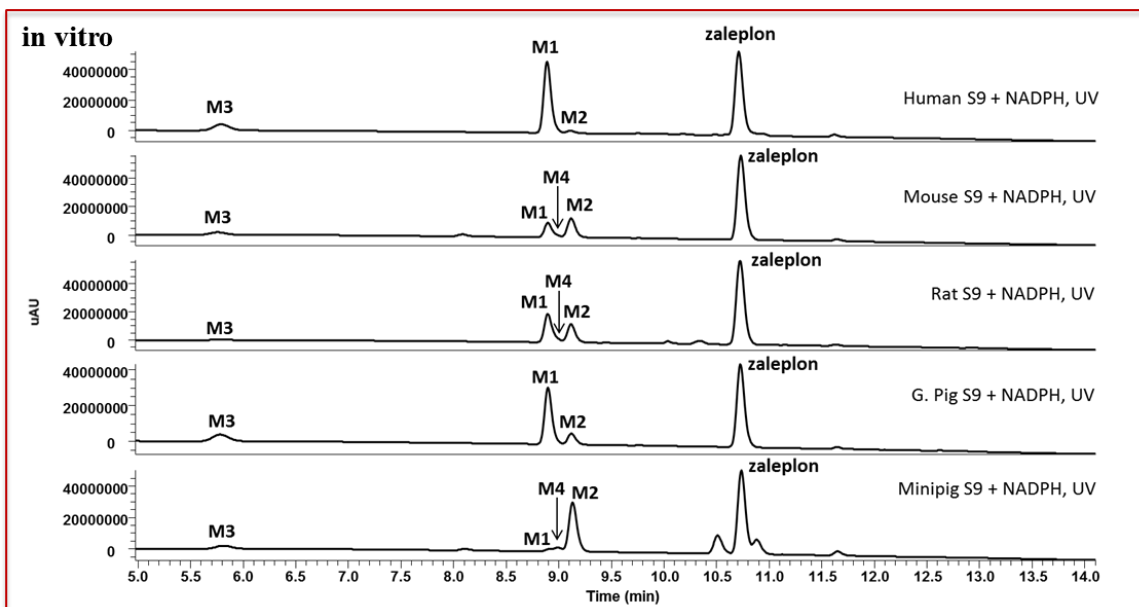
In Vitro Allometry to Guide Species Selection for In Vivo PK Analysis

Due to substrate-dependent species differences in AO-mediated metabolism, no single species is considered to be a reliable resource for estimating human clearance of all AO substrates. However, in Chapter IV we proposed that, taken together, the *in vitro* data (allometry, $F_{m,AO}$, E , and biotransformation) may be a useful guide for selecting an appropriate species for *in vivo* PK studies and

subsequent allometric scaling to predict human CL_p . Comparing our *in vitro* data to the available *in vivo* CL_p data, we evaluated the potential utility of this “*in vitro* guide” toward selecting a species for *in vivo* allometry.

Zaleplon

Evaluation of *in vitro* zaleplon data reveals that SSS of zaleplon CL_{int} in all species (excluding monkey since no *in vivo* CL_p is available), resulted in similar fold errors of around 0.60, as well as similar E of around 0.20 (Figure V.5). While this may indicate that any of the four species might be suitable for predicting zaleplon PK, guinea pig may be the most reasonable selection when also taking $F_{m,AO}$ and biotransformation data into account, as guinea pig exhibited a more similar $F_{m,AO}$ to human versus other species (also reflected in biotransformation experiments, where the AO metabolite was more prominent in guinea pig and human S9 extracts versus other species). Indeed, while SSS with mouse, rat, and minipig resulted in reasonable predictions (8.8-11.0 mL/min/kg, fold error = 0.55- 0.69) of the observed human CL_p (16 mL/min/kg), guinea pig provided the most accurate prediction (13.6 mL/min/kg), with a fold-error of 0.85.



in vitro				
Species	S9 CL_{int} (mL/min/kg)	E	$F_{m,AO}$	SSS Human Predicted S9 CL_{int} (mL/min/kg)
Human	5.8	0.22	≥ 0.71	---
Mouse	24.4	0.21	≤ 0.22	3.17
Rat	15.6	0.18	n/a	3.81
Guinea Pig	14.2	0.19	≥ 0.50	3.76
Minipig	5.6	0.16	≤ 0.17	3.73

in vivo			
Species	CL_p (mL/min/kg)	CL_p as % Liver Blood Flow	SSS Human Predicted S9 CL_p (mL/min/kg)
Human	16.0	76%	---
Mouse	83.9	93%	11.0
Rat	33.7	48%	8.91
Guinea Pig	49.2	81%	13.6
Minipig	15.4	55%	8.80

Figure V.5. Evaluation of *in vitro* data to select a preclinical species for *in vivo* PK of zaleplon and subsequent SSS to predict human CL_p . **Top:** *In vitro* zaleplon biotransformation experiments reveal similar metabolism between human and guinea pig, while greater differences were observed between human and mouse, rat, or minipig. **Middle:** *In vitro* zaleplon CL_{int} experiments reveal similar E across all species, as well as a reasonable prediction of human CL_{int} by SSS; however, guinea pig exhibited a higher $F_{m,AO}$ versus other species, which was more similar to human. **Bottom:** *In vivo* zaleplon PK studies reveal CL_p as a % of liver blood flow most similar between human and guinea pig, which yielded the most accurate human CL_p prediction by SSS. Although guinea pig provided the most accurate CL_p prediction, SSS with all species generated similar predictions.

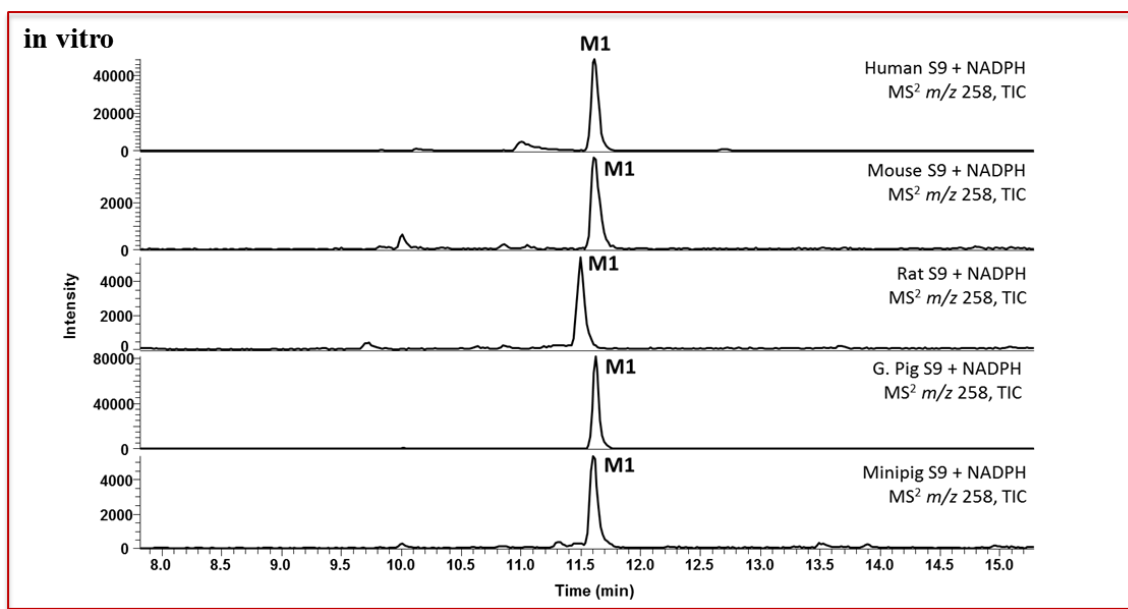
In addition, according to our *in vitro* MA studies, either species combination of minipig/guinea pig/mouse or minipig/rat/mouse may be selected based on the favorable fold error of 0.68 by both methods (Table V.7). However, as guinea pig was selected for SSS based on biotransformation and $F_{m,A0}$ data, guinea pig may also be a more appropriate selection than rat to include in 3-species allometry along with minipig and mouse. Indeed, *in vitro* and *in vivo* MA with minipig/guinea pig/mouse and with minipig/rat/mouse both resulted in human predictions within 2-fold of observed CL values, with the inclusion of guinea pig resulting in a slightly improved *in vivo* prediction (9.03 mL/min/kg) versus inclusion of rat (7.82 mL/min/kg).

MA of CL (Minipig/Gpig/Mouse)	Predicted Human CL_{int} or CL_p	Observed Human CL_{int} or CL_p	Fold Error
<i>in vitro</i> S9 CL _{int}	3.98	5.80	0.68
<i>in vivo</i> CL _p	9.03	16.0	0.56
MA of CL (Minipig/Rat/Mouse)	Predicted Human CL_{int} or CL_p	Observed Human CL_{int} or CL_p	Fold Error
<i>in vitro</i> S9 CL _{int}	3.98	5.80	0.68
<i>in vivo</i> CL _p	7.82	16.0	0.49

Table V.7. *In vitro*-to-*in vivo* comparison of zaleplon human CL (CL_{int} or CL_p) predictions by multispecies allometry (MA) using minipig, guinea pig, and mouse or using minipig, rat, and mouse.

*O*⁶-benzylguanine

All *in vitro* data obtained for *O*⁶-benzylguanine indicates guinea pig may be the most appropriate species selection to predict human CL_p (Figure V.6). Biotransformation experiments (Figure V.6 shows relative formation of M1, which was the only metabolite observed in S9 extracts) revealed low turnover of *O*⁶-benzylguanine to M1 in mouse, rat, and minipig, while guinea pig demonstrated similar M1 formation to human. Likewise, guinea pig demonstrated a similar E and $F_{m,A0}$ to human while the other three species exhibited lower E , and their $F_{m,A0}$ could not be estimated. *In vivo*, however, the rodent species all exhibited very high *O*⁶-benzylguanine CL_p , which exceeded hepatic blood flow (i.e., CL_p as % Liver Blood Flow > 100%), while minipig CL_p was high, but below hepatic blood flow. As a result, SSS with the rodent species generated 3-4 fold over-predictions (53.8-59.8 mL/min/kg) of the observed human CL_p (14.5 mL/min/kg), whereas minipig SSS predicted a human CL_p of 13.8 mL/min/kg, with a fold error of 0.95.



in vitro				
Species	S9 CL _{int} (mL/min/kg)	E	F _{m,AO}	SSS Human Predicted S9 CL _{int} (mL/min/kg)
Human	17.8	0.46	0.70-0.83	---
Mouse	20.7	0.18	n/a	2.69
Rat	8.3	0.11	n/a	2.04
Guinea Pig	60.3	0.50	0.74-0.83	16.0
Minipig	4.4	0.14	n/a	2.97

in vivo			
Species	CL _p (mL/min/kg)	CL _p as % Liver Blood Flow	SSS Human Predicted S9 CL _p (mL/min/kg)
Human	14.5	69%	---
Mouse	454	504%	59.8
Rat	203	290%	53.8
Guinea Pig	206	338%	57.2
Minipig	24.1	86%	13.8

Figure V.6. Evaluation of *in vitro* data to select a preclinical species for *in vivo* PK of O⁶-benzylguanidine and subsequent SSS to predict human CL_p. **Top:** *In vitro* O⁶-benzylguanidine biotransformation experiments reveal low formation of M1 in mouse, rat, and minipig, while guinea pig demonstrated similar M1 formation to human. **Middle:** *In vitro* O⁶-benzylguanidine CL_{int} experiments reveal similar F_{m,AO} and E between human and guinea pig, with low E in mouse, rat, and minipig and low CL_{int} preventing estimation of F_{m,AO} in these species. Likewise, guinea pig SSS accurately predicted human CL_{int}, while predictions from the other three species were low. **Bottom:** *In vivo* O⁶-benzylguanidine PK studies reveal CL_p as a % of liver blood flow most similar between human and minipig, which also yielded the most accurate human CL_p prediction by SSS, while mouse, rat and guinea pig over-predicted human CL_p ~3-4 fold.

MA with minipig/guinea pig/mouse or minipig/rat/mouse yielded reasonable human O⁶-benzylguanine CL_p predictions (10.1 and 9.48 mL/min/kg, respectively) with fold errors of 0.69 and 0.65, respectively (Table V.8). Due to low *in vitro* CL_{int} in mouse, rat, and especially minipig, human *in vitro* CL_{int} predictions by these MA methods were low, as was the case with *in vitro* SSS predictions using these species.

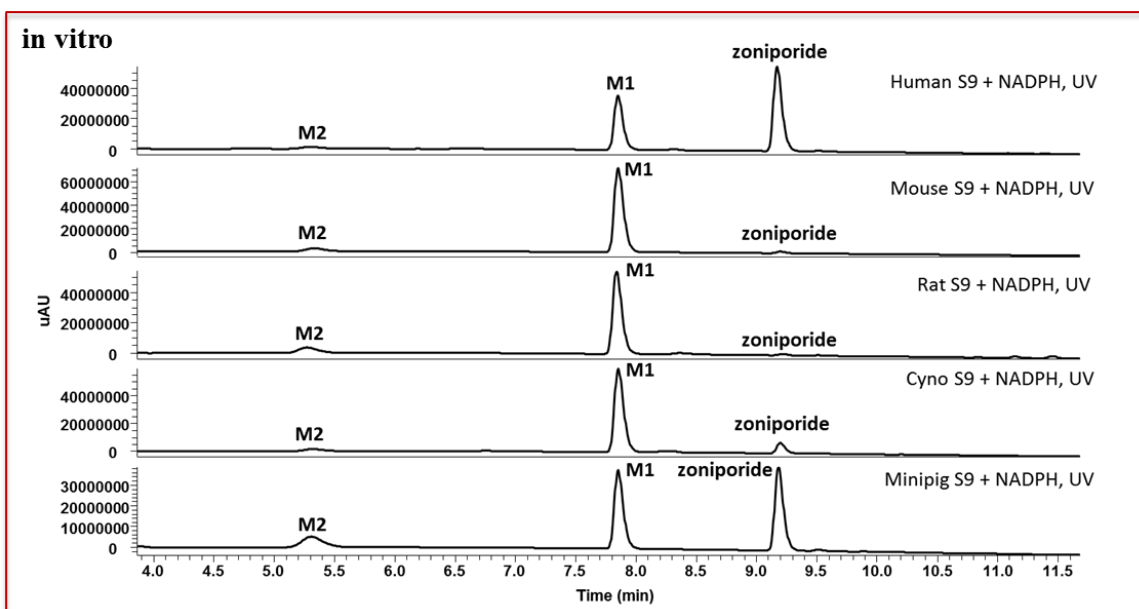
MA of CL (Minipig/Gpig/Mouse)	Predicted Human CL _{int} or CL _p	Observed Human CL _{int} or CL _p	Fold Error
<i>in vitro</i> S9 CL _{int}	4.83	17.8	0.27
<i>in vivo</i> CL _p	10.1	14.5	0.69
MA of CL (Minipig/Rat/Mouse)	Predicted Human CL _{int} or CL _p	Observed Human CL _{int} or CL _p	Fold Error
<i>in vitro</i> S9 CL _{int}	2.85	17.8	0.16
<i>in vivo</i> CL _p	9.48	14.5	0.65

Table V.8. *In vitro*-to-*in vivo* comparison of O⁶-benzylguanine human CL (CL_{int} or CL_p) predictions by multispecies allometry (MA) using minipig, guinea pig, and mouse, or minipig, rat, and mouse.

Zoniporide

When comparing zoniporide *in vitro* data of mouse, rat, cynomolgus monkey, and minipig, the species exhibiting the most similarity to human across all data (with the exception of F_{m,A0}) is minipig, though cynomolgus monkey also produced similar *in vitro* data to human with a SSS CL_{int} prediction fold error of 1.7 (Figure V.7). Rat and mouse *in vitro* data indicated that these species may be likely to over-predict human CL_p, and, as anticipated, rat and mouse did over-predict human CL_p

(21 mL/min/kg), though both over-predictions were within 3-fold (62.7 and 39.2 mL/min/kg, respectively). In addition, cynomolgus monkey did generate a more accurate prediction (15.2 mL/min/kg) than mouse and rat, with a fold error of 0.72. SSS with minipig, however, produced a 5-fold over prediction (111 mL/min/kg) of human CL_p . The CL_p data employed in the SSS analysis for mouse, rat, and cynomolgus were obtained from the literature, as plasma concentrations obtained from our cassette dosing studies in rat and mouse were below our quantitation limits, therefore preventing PK analysis. Observed concentrations in minipig plasma were also very low (peak concentrations < 10 ng/mL), which may have limited the ability to obtain an accurate PK assessment.



in vitro				
Species	S9 CL_{int} (mL/min/kg)	E	$F_{m,AO}$	SSS Human Predicted S9 CL_{int} (mL/min/kg)
Human	17.9	0.46	0.72 – 0.77	---
Mouse	332	0.79	0.90	43.1
Rat	466	0.87	0.72 – 0.74	114
Cynomolgus Monkey	62.8	0.59	≥ 0.90	30.7
Minipig	23.4	0.45	0.83-0.97	15.7

in vivo			
Species	CL_p (mL/min/kg)	CL_p as % Liver Blood Flow	SSS Human Predicted S9 CL_p (mL/min/kg)
Human	21	100%	---
Mouse	298	331%	39.2
Rat	237	339%	62.7
Cynomolgus Monkey	31	70%	15.2
Minipig	193	689%	111

Figure V.7. Evaluation of *in vitro* data to select a preclinical species for *in vivo* PK of zoniporide and subsequent SSS to predict human CL_p . **Top:** *In vitro* zoniporide biotransformation experiments reveal similar metabolism between all species, with rat and mouse exhibiting much higher turnover of zoniporide relative to human and minipig and somewhat higher relative to cynomolgus monkey. **Middle:** *In vitro* zoniporide CL_{int} experiments reveal similar $F_{m,AO}$ across all species, with rat exhibiting a $F_{m,AO}$ most similar to human. However, minipig and cynomolgus monkey exhibit an E most similar to human, as well as more accurate predictions of human CL_{int} by SSS. **Bottom:** *In vivo* zoniporide PK studies reveal CL_p as a % of liver blood flow most similar between human and cynomolgus monkey, which also yielded the most accurate human CL_p prediction by SSS.

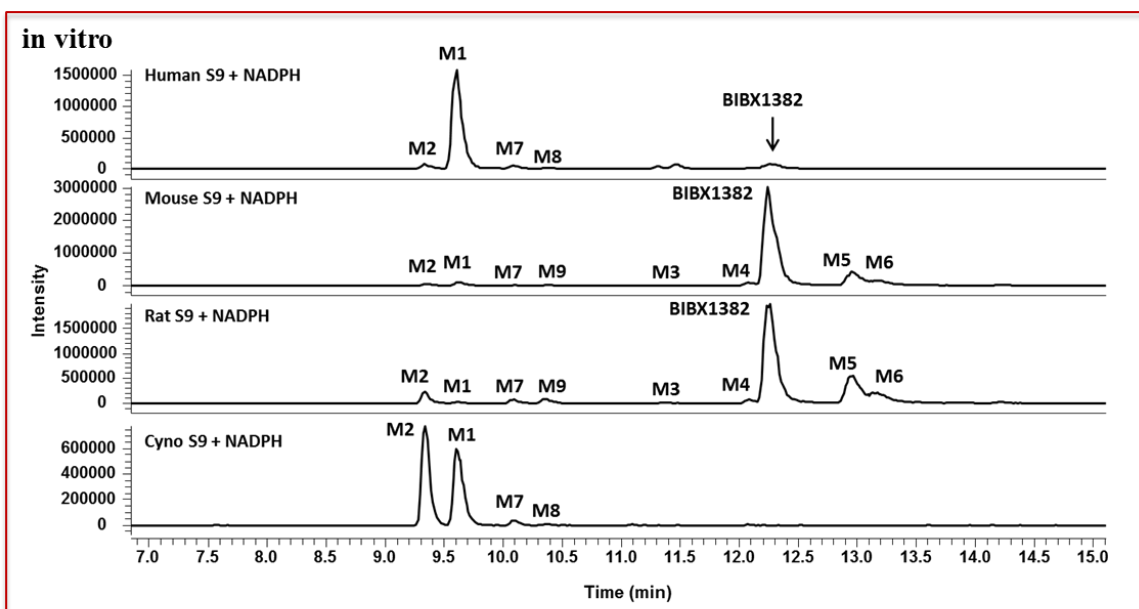
In addition, both *in vitro* and *in vivo* 3- or 4-species MA with minipig, cynomolgus, rat, and/or mouse resulted in zoniporide human CL_{int} or CL_p predictions within 2-fold of observed human values, with the exception of the minipig/rat/mouse combination, which resulted in a > 7-fold over-prediction of human CL_p (Table V.9).

MA of CL (Minipig/Cyno/Rat/Mouse)	Predicted Human CL _{int} or CL _p	Observed Human CL _{int} or CL _p	Fold Error
<i>in vitro</i> S9 CL _{int}	17.3	17.9	0.97
<i>in vivo</i> CL _p	49.0	21.0	2.3
MA of CL (Cyno/Rat/Mouse)	Predicted Human CL _{int} or CL _p	Observed Human CL _{int} or CL _p	Fold Error
<i>in vitro</i> S9 CL _{int}	35.9	17.9	2.0
<i>in vivo</i> CL _p	11.8	21.0	0.56
MA of CL (Minipig/Cyno/Rat)	Predicted Human CL _{int} or CL _p	Observed Human CL _{int} or CL _p	Fold Error
<i>in vitro</i> S9 CL _{int}	7.36	17.9	0.41
<i>in vivo</i> CL _p	43.9	21.0	2.1
MA of CL (Minipig/Rat/Mouse)	Predicted Human CL _{int} or CL _p	Observed Human CL _{int} or CL _p	Fold Error
<i>in vitro</i> S9 CL _{int}	16.4	17.9	0.92
<i>in vivo</i> CL _p	162	21.0	7.7

Table V.9. *In vitro*-to-*in vivo* comparison of zoniporide human CL (CL_{int} or CL_p) predictions by multispecies allometry (MA) using 3- or 4-species combinations of minipig, cynomolgus monkey, rat, and/or mouse.

BIBX1382

Based on our *in vitro* analyses of BIBX1382, cynomolgus monkey appears to be a more appropriate species selection than mouse and rat (Figure V.8). In this case, all *in vitro* data pointed toward cynomolgus monkey over the rodent species, as cynomolgus exhibited similar biotransformation, E, $F_{m,A0}$, and most accurately predicted human CL_{int} by SSS, whereas mouse and rat exhibited dissimilar biotransformation of BIBX1382, lower E values, lower or unobtainable $F_{m,A0}$ estimates, and substantially under-predicted human CL_{int} by SSS. *In vivo* SSS resulted in human CL_p predictions of 56 mL/min/kg with cynomolgus monkey, 7.2 mL/min/kg with mouse, and 13.4 mL/min/kg with rat, revealing that cynomolgus monkey indeed was the more appropriate species to predict the observed human CL_p of BIBX1382 (25-55 mL/min/kg). In addition, literature reports note that oral bioavailability of BIBX1382 in monkey (6%) mirrored that of human (5%) (Hutzler et al., 2014a), unlike rat and mouse which exhibited 50-100% oral bioavailability (Dittrich et al., 2002). Hutzler et al. likewise concluded in their report that cynomolgus monkey accurately represented the rapid clearance of BIBX1382 in human and that cynomolgus may therefore serve as a suitable animal model for estimating human AO metabolism and clearance (Hutzler et al., 2014a).



in vitro				
Species	S9 CL _{int} (mL/min/kg)	E	F _{m,AO}	SSS Human Predicted S9 CL _{int} (mL/min/kg)
Human	80.2	0.79	0.92	---
Mouse	33.2	0.27	n/a	4.32
Rat	30.7	0.30	≤ 0.69	7.52
Cynomolgus Monkey	181	0.80	1.0	88.7

in vivo			
Species	CL _p (mL/min/kg)	CL _p as % Liver Blood Flow	SSS Human Predicted S9 CL _p (mL/min/kg)
Human	25 – 55	104% - 261%	---
Mouse	55	61%	7.2
Rat	55	76%	13.4
Cynomolgus Monkey	118	268%	56

Figure V.8. Evaluation of *in vitro* data to select a preclinical species for *in vivo* PK of BIBX1382 and subsequent SSS to predict human CL_p. **Top:** *In vitro* BIBX1382 biotransformation experiments reveal similar metabolism between human and cynomolgus, while greater differences were observed between human and rodents. **Middle:** *In vitro* BIBX1382 CL_{int} experiments reveal similar E and F_{m,AO} between human and cynomolgus, as well as a reasonable prediction of human CL_{int} by SSS with cynomolgus, while rodents exhibited lower E, F_{m,AO}, and predicted human CL_{int} by SSS. **Bottom:** *In vivo* BIBX1382 PK studies reveal similar CL_p as a % of liver blood flow and oral bioavailability between human and cynomolgus, as well as a reasonable human CL_p prediction by SSS with cynomolgus, while rodents under-represented clearance.

In addition, allometric scaling of *in vitro* CL_{int} with cynomolgus/rat/mouse resulted in a similar fold-error to that obtained from allometric scaling of *in vivo* CL_p using these species (Table V.10). As was the case *in vitro*, SSS from cynomolgus monkey CL_p provides the best prediction of human CL_p over SSS with mouse and rat or over MA with the three species.

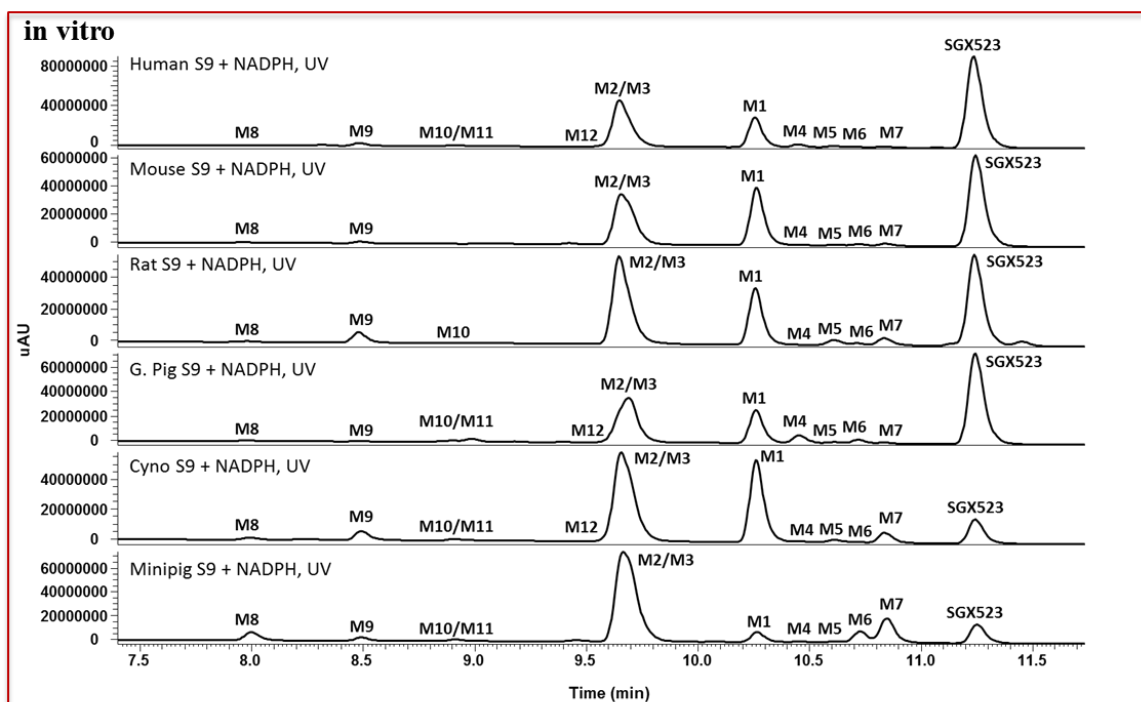
MA of CL (Cyno/Rat/Mouse)	Predicted Human CL _{int} or CL _p	Observed Human CL _{int} or CL _p	Fold Error
<i>in vitro</i> S9 CL _{int}	348	80.2	4.3
<i>in vivo</i> CL _p	160	25 – 55	2.9 – 6.4

Table V.10. *In vitro*-to-*in vivo* comparison of BIBX1382 human CL (CL_{int} or CL_p) predictions by multispecies allometry (MA) using cynomolgus monkey, rat, and mouse.

SGX523

In vivo allometry could not be evaluated for accuracy of prediction of human SGX523 CL_p, as human CL_p data for this compound is not available in the literature. Evaluation of the *in vitro* data indicates that mouse, rat, and perhaps guinea pig may each serve as more suitable species for *in vivo* SSS to predict human CL_p than cynomolgus monkey or minipig when considering E and SSS CL_{int} predictions (Figure V.9). F_{m,A0} estimations were somewhat variable by the two calculation methods (see Chapter IV), and, therefore, may not serve as a useful parameter for species selection in this case. *In vitro* biotransformation of SGX523 was relatively similar across all species, with some trace metabolites detected in human that were not detected in mouse and rat, while minipig produced lower levels of M1 relative to

other species. SSS of *in vivo* CL_p with mouse, guinea pig, and minipig resulted in similar human CL_p predictions ranging from 9.6-11.0, whereas SSS with rat and cynomolgus monkey produced lower predictions of 2.2 and 1.9, respectively. CL_p as a percentage of liver blood flow in guinea pig and minipig (57% and 68%, respectively) were a bit higher (but fairly similar) to the E estimated *in vitro* (0.41 and 0.48, respectively), while rat CL_p as a percentage of liver blood flow was lower (12%) than E estimated *in vitro* (0.33). CL_p as a percentage of liver blood flow was substantially higher than E in mouse (92% and 0.30, respectively); the opposite was true for cynomolgus monkey, where E was much higher *in vitro* (0.50) than CL_p as a percentage of liver blood flow *in vivo* (8%).



Species	S9 CL_{int} (mL/min/kg)	E	$F_{m,AO}$	SSS Human Predicted S9 CL_{int} (mL/min/kg)
Human	7.1	0.25	0.36-0.61	---
Mouse	39.4	0.30	0.22-0.33	5.13
Rat	35.3	0.33	0.28-0.42	8.64
Guinea Pig	42.4	0.41	0.03-0.23	11.2
Cynomolgus Monkey	44.4	0.50	0.58-0.68	21.7
Minipig	25.4	0.48	0.12-0.18	17.1

Species	CL_p (mL/min/kg)	CL_p as % Liver Blood Flow	SSS Human Predicted S9 CL_p (mL/min/kg)
Human	---	---	---
Mouse	82.9	92%	10.9
Rat	8.37	12%	2.2
Guinea Pig	34.5	57%	9.6
Cynomolgus Monkey	3.70	8%	1.8
Minipig	19.1	68%	11.0

Figure V.9. Evaluation of *in vitro* data to select a preclinical species for *in vivo* PK of SGX523 and subsequent SSS to predict human CL_p . **Top:** *In vitro* SGX523 biotransformation experiments reveal similar metabolism across all species, with greater turnover of SGX523 by guinea pig and minipig, and some trace metabolites detected in human which were not detected in mouse and rat. **Middle:** *In vitro* SGX523 CL_{int} experiments reveal mouse and rat E most similar to human and ambiguous $F_{m,AO}$ values in the low-moderate range for all species. Prediction of human CL_{int} by SSS were lower using rat and mouse, higher using cynomolgus and minipig, and in the middle using guinea pig. **Bottom:** *In vivo* SGX523 PK studies reveal similar low human CL_p prediction by SSS with cynomolgus and mouse, and higher predictions by SSS with the other three species.

MA of SGX CL_p resulted in similar human predictions as those obtained from SSS, ranging from 0.6-10.5 mL/min/kg (Table V.11). As was observed with SSS, the rank order (according to predicted CL_{int}) of MA methods *in vitro* did not mirror the *in vivo* rank order—for example, the cyno/rat/mouse combination predicted the highest human CL_{int} *in vitro*, but this method predicted the lowest human CL_p *in vivo*.

MA of CL (Minipig/Cyno/Rat/Mouse)	Predicted Human CL_{int} or CL_p
<i>in vitro</i> S9 CL _{int}	17.3
<i>in vivo</i> CL _p	3.0
MA of CL (Minipig/Cyno/Gpig/Mouse)	Predicted Human CL_{int} or CL_p
<i>in vitro</i> S9 CL _{int}	15.4
<i>in vivo</i> CL _p	3.5
MA of CL (Cyno/Rat/Mouse)	Predicted Human CL_{int} or CL_p
<i>in vitro</i> S9 CL _{int}	35.9
<i>in vivo</i> CL _p	0.65
MA of CL (Cyno/Gpig/Mouse)	Predicted Human CL_{int} or CL_p
<i>in vitro</i> S9 CL _{int}	20.8
<i>in vivo</i> CL _p	1.1
MA of CL (Minipig/Cyno/Rat)	Predicted Human CL_{int} or CL_p
<i>in vitro</i> S9 CL _{int}	7.36
<i>in vivo</i> CL _p	10.3
MA of CL (Minipig/Cyno/Gpig)	Predicted Human CL_{int} or CL_p
<i>in vitro</i> S9 CL _{int}	18.5
<i>in vivo</i> CL _p	3.0
MA of CL (Minipig/Gpig/Mouse)	Predicted Human CL_{int} or CL_p
<i>in vitro</i> S9 CL _{int}	11.4
<i>in vivo</i> CL _p	10.5
MA of CL (Minipig/Rat/Mouse)	Predicted Human CL_{int} or CL_p
<i>in vitro</i> S9 CL _{int}	16.4
<i>in vivo</i> CL _p	6.7

Table V.11. *In vitro*-to-*in vivo* comparison of SGX523 human CL (CL_{int} or CL_p) predictions by multispecies allometry (MA) using minipig, cynomolgus monkey, guinea pig, rat, and/or mouse.

As previously noted, the *in vivo-in vitro* ratios for zaleplon were relatively consistent across all species, and the same was true of the *in vivo-in vitro* ratios for BIBX1382. The *in vivo-in vitro* ratios for zonisporide, O⁶-benzylguanine, and SGX523, alternatively, were more varied across species. This is important to note with regard to MA, as substantial species differences in IVIVC would be expected to impact the translation of *in vitro* MA to *in vivo* MA with regard to maintaining a similar fold-error of prediction between *in vitro* MA and *in vivo* MA. For example, MA of zaleplon clearance resulted in similar prediction fold errors both *in vitro* and *in vivo* (average fold error *in vitro* = 0.68, average fold error *in vivo* = 0.53, Table V.7). MA of BIBX1382 clearance likewise resulted in similar fold errors both *in vitro* and *in vivo* (Table V.10). *In vivo* fold errors obtained for O⁶-benzylguanine and zonisporide, however, deviated (sometimes substantially) from *in vitro* fold errors (Tables V.8-9). In addition, in cases where the fold errors by MA were similar *in vitro* and *in vivo* (i.e., zaleplon and BIBX1382), the allometric exponent (*b*) was also similar *in vitro* and *in vivo* (Table V.12). This observation may suggest that a MA prediction fold error observed *in vitro* may be expected to translate to a similar fold error *in vivo*, when the allometric exponent obtained from *in vitro* MA is similar to the allometric exponent obtained from *in vivo* MA. As noted previously, however, this will likely be dependent on human exhibiting a similar IVIVC (i.e., *in vivo-in vitro* CL ratio) to the species used for MA predictions, which was the case for zaleplon and BIBX1382.

MA Method	Zaleplon		O ⁶ -benzylguanine		Zoniporide		BIBX1382	
	in vitro	in vivo	in vitro	in vivo	in vitro	in vivo	in vitro	in vivo
Minipig/Cyno/Rat/Mouse	n/a	n/a	n/a	n/a	0.57	0.77	n/a	n/a
Cyno/Rat/Mouse	n/a	n/a	n/a	n/a	0.68	0.57	1.3	1.2
Minipig/Cyno/Rat	n/a	n/a	n/a	n/a	0.26	0.74	n/a	n/a
Minipig/GPig/Mouse	0.77	0.71	0.74	0.50	n/a	n/a	n/a	n/a
Minipig/Rat/Mouse	0.77	0.71	0.77	0.50	0.57	0.93	n/a	n/a

Table V.12 *In vitro*-to-*in vivo* comparison of allometric exponents (*b*) obtained from multispecies allometry (MA) using minipig, cynomolgus monkey, guinea pig, rat, and/or mouse. Cyno, cynomolgus monkey; Gpig, guinea pig

DISCUSSION

In Chapter IV, we evaluated species differences in the metabolism and clearance of five AO substrates *in vitro*, as well as the ability to scale *in vitro* hepatic CL_{int} of these substrates by MA and SSS to predict human *in vitro* hepatic CL_{int} . Successful prediction of human *in vitro* hepatic CL_{int} was achieved by one or more of these methods, albeit in a substrate-dependent manner with regard to the species employed in the scaling analysis. As traditional *in vitro* techniques have repeatedly resulted in under-prediction of *in vivo* CL_p for compounds metabolized by AO (proposed to potentially be associated with extra-hepatic AO metabolism, instability of AO *in vitro*, or interindividual AO variability) (Zientek et al., 2010; Akabane et al., 2012; Hutzler et al., 2012), we presently sought to evaluate the multispecies IVIVC (*in vitro-in vivo* correlation) of clearance for these five AO substrates. Furthermore, we evaluated the ability to predict human *in vivo* CL_p of these compounds by MA and SSS, employing CL_p obtained from multiple species. Finally, we assessed the utility of comparing *in vitro* metabolism and clearance data from multiple species for the purpose of selecting suitable species for *in vivo* PK analysis and subsequent human CL_p prediction by MA or SSS.

Of the compounds/species for which *in vivo* data was available to evaluate, a prediction within 3-fold of observed human CL_p was successfully obtained by at least one MA or SSS method for all compounds. In instances where IVIVC was similar across species (i.e., demonstrated a similar *in vivo-in vitro* clearance ratio) employed in MA or SSS analyses, human prediction fold errors obtained from both

in vitro and *in vivo* allometric scaling with these species were also similar. Consequently, for compounds exhibiting similar IVIVC across all species (e.g., zaleplon and BIBX1382) *in vitro* data successfully indicated which species would be suitable for employing *in vivo* CL_p in MA or SSS analyses to predict human CL_p. Furthermore, these two cases resulted in similar *in vitro* and *in vivo* allometric exponents obtained from MA, indicating that the interspecies relationship between *in vitro* CL_{int} and body weight reflected the interspecies relationship between *in vivo* CL_p and body weight (i.e., the rate of change in CL with change in body weight was similar *in vitro* and *in vivo*). However, in cases where IVIVC was inconsistent across species, *in vitro* data was not always predictive of the most appropriate species for *in vivo* allometry. This may indicate that species-specific extra-hepatic mechanisms may contribute to the clearance of these compounds *in vivo*, since the *in vitro* clearance estimated in our studies is limited to hepatic mechanisms (CL_{int} obtained using hepatic S9 fractions).

In addition, the IVIVC analyses may offer some possible insight into which of the previously proposed mechanisms (e.g., extra-hepatic elimination, AO instability *in vitro*, interindividual variability, etc.) may be contributing the observed IVIVC disconnects frequently encountered with AO substrates. For example, for any one species in our cassette dosing studies, the fold difference between *in vitro* and *in vivo* CL was not always consistent across each compound (e.g., rat demonstrated an *in vivo-in vitro* fold-difference of 0.38, 0.04, and 2.6 for zaleplon, O⁶-benzylguanine, and SGX523, respectively). Because the same lot of hepatic S9 was used to obtain *in*

in vitro CL_{int} estimates for each of the three compounds, the substrate-dependent variability in IVIVC for a single species cannot be attributed to variable AO activity in the S9 used to measure the CL_{int} for each compound (e.g., manufacturer differences in preparation of S9 fractions or lot-to-lot donor variability). Likewise, because the same animals were used to obtain *in vivo* CL_p of zaleplon, O⁶-benzylguanine, and SGX523 (all three compounds dosed together as a cassette to the same animals), the variability in IVIVC across the three compounds cannot be attributed to variable AO activity (i.e., interindividual variability) in the animals receiving each compound. Rather, the differences may likely be ascribed to substrate-dependent parameters such as red blood cell distribution and/or extra-hepatic metabolism (tissue or plasma), since the S9 CL_{HEP} data only represents hepatic clearance. This proposal is also supported by CL_p values, either observed in our studies or reported by others, which exceeded hepatic blood flow (e.g. O⁶-benzylguanine, zoniporide, and BIBX1382). Interestingly, the fold-difference was very similar across all species in the *in vitro-in vivo* comparison of zaleplon. This might indicate that the under-estimation is a result of an extra-hepatic mechanism that is conserved across species. Previous studies in rats receiving a 5 mg/kg oral dose of [¹⁴C]-zaleplon found that highest concentrations of the drug were distributed into the liver, kidney, gastrointestinal tract, and adrenal glands (Beer et al., 1997). Human AOX1 mRNA is present in each of these tissues, with the adrenal glands reported as one of the richest sources of the protein in addition to the liver (Terao et al., 2016). However, reported tissue expression patterns of AOX1 and other AO

isoforms between mouse and human are divergent, and the adrenal gland, for example, has not been shown to represent a rich source of mRNA for any AO isoform in mouse (Terao et al., 2016). Unfortunately, until multispecies expression and activity of extra-hepatic AO are better understood, the mechanism(s) responsible for IVIVC disconnects will remain unclear.

While the variability in IVIVC for SGX523, O⁶-benzylguanine, and zaleplon for any given species could not have resulted from differences in preparation of S9 fractions used to measure CL_{int} for each compound or interindividual AO variability in the animals used to measure CL_p for each compound, this does not preclude *in vitro* instability/decreased activity or interindividual variability between the S9 donors and the subjects receiving the test article *in vivo* from speculation as a potential contributor to *in vitro* under-estimation of CL_p. Interestingly, however, SGX523 CL_p was over-estimated by rat S9, while zaleplon and O⁶-benzylguanine were under-estimated. If *in vitro* AO instability or interindividual AO variability between the S9 donor rats and the rats administered substrate *in vivo* were responsible for the IVIVC disconnect, the disconnect would be expected to be in the same direction for all compounds (i.e., all under-estimated or all over-estimated). Notably, however, we previously reported an F_{m,AO} (fraction of metabolism mediated by AO) for SGX523 of 0.28-0.42 in rat S9. This presence of non-AO metabolism pathways in the clearance of these substrates adds an additional complication to the interpretation of IVIVC disconnects for AO substrates. For example, in our *in vitro* CL_{int} studies, we did not observe measurable substrate turnover of O⁶-benzylguanine

in rat, mouse, and minipig S9 in the absence of NADPH, whereas substrate depletion was observed in the presence of NADPH, indicating the contribution of a non-AO pathway. A prior report of O⁶-benzylguanine metabolism in rat and mouse *in vivo* revealed an N-acetyl metabolite in rats and a debenzylated metabolite in both rats and mice (Dolan et al., 1994). It was proposed that the acetylation may occur in the kidney since it was only detected in urine and not in the plasma (Dolan et al., 1994). Neither of these metabolites was detected in our biotransformation experiments in S9 incubations (Chapter IV), suggesting the possibility that these clearance pathways were present *in vivo*, but not *in vitro*, and contributed to the apparent extra-hepatic metabolism and IVIVC disconnect observed with O⁶-benzylguanine. However, even in the absence of extra-hepatic metabolism, differences in $F_{m,AO}$ for each compound could result in variable IVIVC across substrates. Likewise, other non-AO substrate dependent parameters, such as red blood cell distribution, could also contribute to inconsistencies between *in vitro* estimated hepatic clearance (CL_{HEP}) and CL_p , as CL_p reflects substrate clearance from plasma as opposed to whole blood. As additional research is needed to better understand extra-hepatic AO metabolism, additional research to clarify mechanisms of *in vitro* AO instability and interindividual variability (single nucleotide polymorphisms, influence of disease state, etc.) will be necessary to fully elucidate contributing factors to IVIVC discrepancies.

Unfortunately, our studies of BIBX1382 were limited due to plasma concentrations below the limit of quantitation preventing pharmacokinetic

parameters from being obtained for this compound. This perhaps is not altogether surprising, given the exposure in cynomolgus monkeys receiving an IV dose of 1 mg/kg BIBX1382, where peak plasma concentrations only reached approximately 70 nM (~180 ng/mL) (Hutzler et al., 2014a), and animals in our studies only received one fifth of this dose (0.2 mg/kg). It was determined that BIBX1382 partitioned into red blood cells in cynomolgus monkey with a blood-to-plasma ratio of 2.1 (Hutzler et al., 2014a). Thus, it is possible that red blood cell partitioning could account for the low plasma concentrations we observed. In addition, evaluation of human and cynomolgus plasma stability indicated BIBX1382 was stable in plasma (for at least 2 hours); however, it is still possible that plasma instability could contribute to low concentrations in mouse, rat, guinea pig and/or minipig. In particular, plasma instability of BIBX1382 could result from plasma xanthine oxidase (XO) mediated oxidation, as Sharma et al. previously demonstrated that a pyrazine-containing compound was oxidized by XO in plasma of mouse, rat, and guinea pig plasma but was stable in human, monkey, and dog plasma (Sharma et al., 2011). In addition, Hutzler et al. noted high AO activity towards BIBX1382 in cynomolgus monkey lung S9 fractions, suggesting the possibility that pulmonary first pass metabolism could contribute to the low peak plasma concentrations observed in our studies (Hutzler et al., 2014a). These mechanisms could have potentially contributed to low zoniporide plasma concentrations observed in our studies as well. Zoniporide was reported to partition 1:1 into plasma and red blood

cells in rat and human (Tracey et al., 2003), but has not been reported for the other species in our studies.

In conclusion, we have demonstrated that allometric scaling may be useful to predict human CL_p of AO substrates when the appropriate species are employed, as predictions within 2-3 fold of observed human CL_p values were obtained for zaleplon, O⁶-benzylguanine, zoniporide, and BIBX1382 by one or more MA and/or SSS methods. In addition, MA and SSS resulted in similar prediction fold errors *in vitro* and *in vivo* when IVIVC was consistent across species, suggesting that *in vitro* allometry may be useful to guide species selection to conduct *in vivo* allometric scaling for human CL_p prediction. While additional studies to elucidate mechanisms behind discrepancies in IVIVC, as well as allometry studies with a larger sample of AO substrates, would help to better understand the potential to broadly utilize this approach toward species selection and prediction of human CL_p for drug candidates metabolized by AO, these studies offer direction towards a novel approach to estimate human clearance of AO substrates, which is of great necessity for the successful discovery and development of future therapeutics.

CHAPTER VI

CONCLUSIONS AND FUTURE DIRECTIONS

Unacceptable pharmacokinetics (PK) once represented a leading cause of attrition of drug candidates during clinical trials (Kola and Landis, 2004). Today, with major advances in the understanding of cytochrome P450 function, expression, and regulation in human and nonclinical species, standardized methods to predict human PK of drugs metabolized by P450 enzymes are now available, resulting in a reduction in drug attrition rates associated with unexpectedly poor PK (Kola and Landis, 2004; Di et al., 2013). Unfortunately, application of these methodologies to human PK prediction of compounds exhibiting AO-mediated clearance has proven insufficient and consequently resulted in clinical failures of several promising drug candidates over the past several years (Kaye et al., 1985; Dittrich et al., 2002; Diamond et al., 2010a; Akabane et al., 2011; Zhang et al., 2011; Lolkema et al., 2015). Even so, reliable and standardized methodology to predict the human pharmacokinetics and drug interaction liability of compounds metabolized by AO has yet to be firmly established. The research described herein provides a foundation towards a solution to this challenging problem, offering several contributions to advance the field surrounding AO drug metabolism and human PK prediction, which are summarized below along with suggested future directions to continue improving and developing these methodologies.

Drug Interaction Liability Associated with AO-Mediated Drug Clearance

Summary and conclusions

Studies relating to the drug interaction potential associated with inhibition of AO have been conducted, and several drugs have been identified which exhibit inhibitory activity towards AO *in vitro* (Obach, 2004; Barr and Jones, 2011). However, given the numerous drugs which inhibit P450 enzymes currently on the market, studies to evaluate the impact of P450 inhibition on compounds metabolized by both P450 and AO may be of equal importance from a perspective of clinical significance. Interestingly, we found that administration of the mixed AO/P450 substrate VU0409106 along with the P450 inhibitor ABT to rats resulted in a drug interaction, where exposure to not only VU0409106 was elevated, but *exposure to the AO metabolite M1 was also elevated*. Notably, while a drug interaction-mediated elevation in metabolite exposure is typically associated with *induction* of a drug metabolizing enzyme (DME), our studies demonstrated an elevation in metabolite exposure facilitated by DME *inhibition*. Reports of AO metabolite-related toxicity associated with methotrexate and the failed clinical drug candidates SGX523 and JNJ-38877605 highlight an additional concern regarding the potential clinical significance of this type of drug interaction (Diamond et al., 2010a; Lolkema et al., 2015). *Taken together, these data reveal that mixed AO/P450-metabolized drugs are susceptible to potentially clinically relevant interactions with P450-inhibiting drugs, and attention to this liability by the pharmaceutical industry is warranted.*

Future directions

The clinical relevance of a pharmacokinetic drug interaction is typically dependent on the magnitude of change in exposure to the pharmacologically (or toxicologically) active compound in question, in this case, the AO metabolite. Therefore, investigations into understanding how to predict the change in AO metabolite exposure and anticipate the conditions under which this exposure change is likely to occur will be an important next step in characterizing this type of drug interaction. Our studies involved the administration of a pan-P450 inhibitor (ABT), a non-clinical tool which non-selectively inactivates P450 enzymes, resulting in the likelihood that metabolism of VU0409106 was primarily shunted toward a single enzyme (AO), thus maximizing the potential for increased exposure to the AO metabolite. In a clinical setting, the co-administration of a P450-inhibiting drug (or even multiple drugs) would be unlikely to result in inhibition of all P450 enzymes, and consequently, shunting may occur toward other uninhibited P450s in addition to AO, potentially limiting an increase in AO metabolite exposure. For this reason, future investigations with mixed AO/P450 substrates should focus on modeling interactions which are likely to occur in a clinical setting. In addition, determination of the influence of $F_{m,P450}$ vs $F_{m,AO}$ on the magnitude of change in AO metabolite exposure resulting from P450 inhibition will be an important next step toward establishing methods to predict drug interactions involving mixed AO/P450-metabolized drugs. The influence of fraction metabolized via a single P450 isoenzyme (e.g., $F_{m,3A4}$) on drug interaction liability has been established, such that

the increase in *parent drug* exposure under conditions of P450 inhibition can be predicted when the F_m of that P450 isoenzyme is known (Di et al., 2013). In this case, a larger $F_{m, P450}$ is associated with a greater increase in *parent drug* exposure when that P450 isoenzyme is inhibited (Di et al., 2013). Accordingly, a greater increase in *AO metabolite* exposure might be expected under conditions of P450 inhibition when the $F_{m, P450}$ is large; however, studies to demonstrate this relationship have yet to be conducted. Furthermore, as the extra-hepatic expression and activity of AO is poorly understood (Terao et al., 2016), studies examining the potential influence of intestinal AO-mediated metabolism will be important to determine the impact of route of administration (e.g., oral versus intravenous) on the likelihood of a clinically relevant interaction. Many questions remain to be answered concerning the role of intestinal (as well as other extra-hepatic) AO expression to drug metabolism and total body clearance of AO-metabolized drugs, such as endogenous and exogenous factors regulating expression in various tissues (e.g., influence of the gut microbiome on intestinal expression). Likewise, investigations into identifying sources of the interindividual variability (hepatic or extra-hepatic) that has been observed in AO-mediated metabolism (Fu et al., 2013; Hutzler et al., 2014b) will be of great importance to understand the likelihood of experiencing a drug interaction. Many possible factors may contribute to variability, such as disease state, diet, and single-nucleotide polymorphisms (SNPs), and while efforts have been made to identify these associations, none have been firmly established (Hartmann et al., 2012; Hutzler et al., 2012; Fu et al., 2013; Hutzler et al.,

2014b). In addition, though SNPs of AO are currently poorly understood, SNPs of P450 enzymes are well-established (Zhou et al., 2009) and also have the potential to influence the drug interaction liability of a mixed AO/P450 substrate, thus warranting additional evaluation. These future works will all be essential in establishing guidelines on metabolite safety testing and drug interaction studies involving mixed AO/P450 drug substrates, which are likely to increase in number given the emergence of AO-metabolized drug candidates reaching clinical trials.

Multispecies Allometry to Predict Human Clearance of Drugs Metabolized by Aldehyde Oxidase

Summary and conclusions

In addition to gaps in our understanding of how to predict drug interactions associated with AO metabolism, perhaps a more significant challenge remains in identifying reliable methods to predict the human clearance associated with AO metabolism. Likely due to the assumption that species differences in clearance mechanisms precludes the ability to scale clearance by allometry, studies evaluating allometric scaling in the prediction of human clearance of AO-metabolized drugs are sparse. While methotrexate, an AO substrate, ironically represents one of the oldest examples of allometric scaling of clearance, AO-mediated metabolism is a minor contributor to the clearance of this drug, with renal elimination serving as the major clearance mechanism (Boxenbaum, 1982). The work described herein not only provides an evaluation of allometric scaling to predict human plasma clearance

(CL_p) of AO substrates, but also includes assessments using minipig (as opposed to dog, which is typically used in allometric scaling), which has been sparsely studied with regard to AO metabolism and human clearance prediction. Importantly, our evaluations indicate that multispecies allometry (MA) may be useful in predicting human CL_p of AO substrates, as most human CL_p predictions were within 3-fold of observed values (Table V.5). It is also encouraging to note that in the two instances where MA did not predict human CL_p within 3-fold, these were over-predictions rather than under-predictions (over-prediction was also more prevalent than under-prediction in our MA studies using *in vitro* CL_{int}). While a substantial over-prediction of human CL_p may result in the oversight of a compound that actually possesses acceptable human PK, a substantial under-prediction could result in the costly failure of a drug candidate that was inappropriately advanced to clinical trials. Traditional *in vitro* methods used to predict human *in vivo* clearance typically result in under-prediction for AO substrates (Zientek et al., 2010; Akabane et al., 2012), and likewise, *in vivo* PK assessments in traditional preclinical species (mouse, rat, and dog) also commonly under-represent clearance in human (Kaye et al., 1985; Dittrich et al., 2002; Akabane et al., 2011; Zhang et al., 2011). *Multispecies allometry utilizing the species evaluated herein may therefore represent a method which can reduce the risk of encountering unexpectedly rapid human CL_p when advancing an AO-metabolized compound to clinical trials.*

Future directions

While our data indicate potential utility of MA for human CL_p prediction of AO substrates, understanding the full value of this method will benefit from additional investigations extended to a larger collection of substrates with reported clinical PK data (CL_p). In general, the ability to study human clearance prediction of AO substrates is limited by the small number of available compounds for which human (*in vivo*) PK have been reported. In addition, most known AO substrates with reported human PK data are rapidly cleared (Zientek et al., 2010; Akabane et al., 2011; Zhang et al., 2011), limiting the evaluation of prediction methodologies primarily to “high clearance” compounds. Importantly, clearance of “high clearance” compounds are more likely to scale according to an allometric relationship, as the plasma clearance of these compounds is limited by hepatic blood flow (Wilkinson and Shand, 1975; Pang and Rowland, 1977), which scales according to an allometric relationship (Boxenbaum, 1980). Therefore, extension of studies evaluating *in vivo* allometric scaling to predict human *in vivo* CL_p to a larger set of compounds, particularly those exhibiting a wider sampling of low, moderate, and high clearance AO substrates, would provide a better understanding of the broad applicability of these methods.

Application of In Vitro Intrinsic Clearance to Allometric Scaling

Summary and conclusions

In addition to providing a traditional examination of allometric scaling to predict human *in vivo* CL_p of AO-metabolized compounds, we also evaluated a novel approach to allometric scaling with the application of *in vitro* CL_{int} to these analyses. Others have proposed that species expressing only the AOX1 isoenzyme in the liver (e.g., guinea pig, monkey, and pig) may serve as better species to estimate human AO-mediated metabolism versus species expressing both the AOX1 and AOX3 isoenzymes (e.g., rat and mouse) (Garattini and Terao, 2012). Consistent with this proposal, our *in vitro* data indicate that the hepatic CL_{int} of AO substrates may be scaled from preclinical species to human by SSS with monkey, guinea pig, and minipig with reasonable accuracy and precision, while this relationship does not appear to be consistent (highly substrate-dependent) when directly scaling from rat or mouse. However, similar to our observations *in vivo*, use of rat and mouse in combination with guinea pig, monkey, and/or minipig generally enabled allometric scaling to a reasonable human hepatic CL_{int} prediction. In particular, these *in vitro* allometry assessments indicate that 4-species allometry utilizing the species evaluated herein may provide the greatest utility with regard to minimizing substrate-dependence in the ability to reasonably predict human clearance. In addition, comparison of *in vitro* allometry data to *in vivo* allometry data suggest that a fold-error analysis of *in vitro* allometry predictions could be useful to help determine which species would be more likely to permit allometric scaling of *in vivo*

CL_p (MA or SSS) to predict human CL_p. While this approach proved useful for demonstrating appropriate species to predict human CL_p of zaleplon and BIBX1382, overall the translation of *in vitro*-to-*in vivo* allometry (regarding prediction fold-error) was substrate-dependent, with only those compounds which exhibited a consistent IVIVC across species (zaleplon and BIBX1382) resulting in successful species selection. *Overall, these data indicate a potential utility of in vitro allometry in the determination of appropriate species to predict human clearance of AO-metabolized drugs, while elucidation of discrepancies in interspecies IVIVC will be important to better understand the full potential of this approach.*

Future directions

A factor limiting the interpretation of our current approach to *in vitro* allometry is the inconsistent *in vitro*: *in vivo* correlation (IVIVC), illustrating the substrate-dependency of AO mediated metabolism. The assumption that *in vitro* hepatic CL_{int} represents *in vivo* hepatic CL_{int} is hindered by speculation of *ex vivo* AO instability, single-nucleotide polymorphisms, and other sources of possible interindividual variability (e.g., disease state, etc.) (Hartmann et al., 2012; Hutzler et al., 2012; Fu et al., 2013; Hutzler et al., 2014b). Furthermore, pharmacokinetic properties such as plasma stability and red blood cell distribution were not determined in each species, and because these properties could influence *in vivo* CL_p (and consequently the IVIVC since these components are not present *in vitro*) the IVIVC across species could vary if these properties are species-specific. Finally, an additional unknown factor complicating IVIVC interpretation, is the extra-hepatic expression and activity

of AO (Kurosaki et al., 1999; Moriwaki et al., 2001; Nishimura and Naito, 2006; Terao et al., 2016), which is poorly understood at present, particularly concerning its contribution to total body clearance of AO substrates. Prior studies indicate that extra-hepatic AO expression is species-specific (Terao et al., 2016), which could also influence consistency of IVIVC across species if extra-hepatic metabolism contributes to CL_p . Consequently, each of these factors could have impacted the interspecies IVIVC obtained in our studies. As mentioned previously, while others have already initiated research aimed at addressing these questions, a thorough investigation to build upon their findings will be necessary to elucidate the mechanisms behind variable AO activity and will be essential to improve current *in vitro* techniques to estimate AO-mediated clearance. Likewise, future research to establish species-specific tissue expression patterns, mechanisms regulating AO expression, and importantly, to develop standardized *in vitro* scaling factors that can be used to estimate total organ clearance from *in vitro* CL_{int} in extra-hepatic tissues will all be critical steps towards understanding the potential contribution of extra-hepatic metabolism and establishing confidence in *in vitro*-to-*in vivo* extrapolation where AO metabolism is concerned. In addition, as 4-species allometric scaling of *in vitro* CL_{int} appears to exhibit minimal substrate-dependence with regard to obtaining a reasonable human CL_{int} prediction, evaluation of these species combinations *in vivo* will help to validate the proposed use of this method.

Influence of Fraction Metabolized by AO ($F_{m,AO}$) and Hepatic Extraction (E) on SSS Prediction Accuracy

Summary and conclusions

Along with our *in vitro* allometry studies, we estimated interspecies fraction metabolized by AO ($F_{m,AO}$) and hepatic extraction (E) for each of our probe AO substrates in order to evaluate how these parameters might influence the ability to predict human hepatic CL_{int} by SSS. Our findings revealed a poor relationship between the animal:human ratio of $F_{m,AO}$ and prediction accuracy by SSS, while further investigation instead revealed a relationship between animal:human ratio of E and prediction accuracy by SSS. Importantly, these relationships were recapitulated when the analyses were conducted using *in vivo* CL_p and $F_{m,UGT}$ data reported by Deguchi et al. for several UGT substrates (Deguchi et al., 2011), indicating this is not an isolated observation. In addition, biotransformation experiments revealed that human and preclinical species may exhibit a similar E despite divergent $F_{m,AO}$ values due to compensation via greater NADPH-dependent metabolism in the preclinical species (e.g., minipig vs. human metabolism of zaleplon). *Consequently, these findings suggest that $F_{m,AO}$ may be more important to consider from a metabolite exposure (i.e., toxicology) perspective than a clearance perspective concerning extrapolation of animal PK to human, whereas consideration of E should be given priority to $F_{m,AO}$ when selecting species for human clearance estimation.*

Future directions

As four of the five compounds studied herein exhibited human $F_{m,AO}$ values ≥ 0.70 , evaluation of additional compounds exhibiting a wider distribution of $F_{m,AO}$ values in human would improve our understanding of how important this parameter may be to accurately predicting human clearance with allometry. In addition, our understanding of how to appropriately utilize preclinical species for toxicology studies/metabolite safety testing with regard to AO substrates will benefit from future investigations focusing on the influence of interspecies $F_{m,AO}$. In addition, while our findings implicated interspecies E as an important factor associated with SSS prediction accuracy, extension of these analyses to prediction of oral bioavailability would be a valuable next step to understand the utility of preclinical species in predicting human PK of AO-metabolized compounds (again emphasizing the importance of evaluating the role of interspecies expression/regulation of intestinal AO to oral bioavailability).

Interspecies Evaluation of Metabolism, Clearance, and SSS to Predict Human Clearance of AO Substrates

Summary and conclusions

Within our *in vivo* SSS analyses, an apparent substrate-dependency was observed with regard to successful SSS using a particular species (Table V.3). In addition, our data (along with prior clinical failures where rat and/or mouse were

used for preclinical PK assessments) appear to indicate that MA may be more useful than SSS with rat or mouse to predict human CL_p (even when rat and/or mouse are included in the MA assessment), which, as previously discussed, was reiterated by our *in vitro* SSS assessments. SSS with cynomolgus monkey, on the other hand, successfully predicted both zonisamide and BIBX1382 CL_p in human, and though CL_p data in cynomolgus for zaleplon and O⁶-benzylguanine was not available for evaluation, AO-mediated zaleplon metabolite formation *in vivo* in cynomolgus has been reported to be similar to human (Kawashima et al., 1999). In addition, while human CL_p of SGX523 was not available for analysis of prediction fold-error by cynomolgus SSS, Diamond et al. reported that cynomolgus monkey would have served as a more relevant species for nonclinical toxicological evaluation of SGX523 than rat, which produced low levels of the offending AO metabolite *in vivo* (Diamond et al., 2010b). Likewise, comparison of monkey and human *in vitro* data obtained from our studies (SSS of CL_{int} , estimated E and $F_{m,AO}$, and biotransformation) for each of the five AO substrates also supports monkey as a suitable species to estimate human clearance and extent of AO-metabolite formation. Furthermore, a recent report where unexpectedly rapid AO metabolism resulted in clinical failure of Lu AF09535 indicated that monkey would have been a suitable species to predict the poor oral exposure observed in humans (Jensen et al., 2016). However, even monkey may exhibit some substrate-dependence with regard to predicting human PK of AO substrates, as Zhang et al. reported that formation of the AO metabolite of the p38 kinase inhibitor RO1 identified in human was negligible in monkey (Zhang

et al., 2011). Overall, monkey appears likely to be an appropriate species for estimating AO-mediated metabolism and clearance in human and should be considered more reliable than rat or mouse, particularly when AO-mediated metabolism is low in rodent and higher in monkey.

Though some substrate dependence was observed, our *in vitro* data also support prior speculation that guinea pig could serve as a suitable species for estimation of human AO-mediated metabolism (Garattini and Terao, 2012). SSS with guinea pig CL_{int} predicted four of the five compounds within 2-fold of human CL_{int} , and $F_{m,AO}$, E , and biotransformation for these four compounds were similar between human and guinea pig. However, guinea pig metabolism and clearance of BIBX1382 demonstrated a closer resemblance to the other rodent species than to human, and consequently, SSS with guinea pig CL_{int} under-predicted human CL_{int} of BIBX1382 similar to SSS of CL_{int} with rat and mouse. Likewise, though guinea pig SSS accurately predicted human CL_{int} of O⁶-benzylguanine *in vitro*, SSS with guinea pig *in vivo* over-predicted human CL_p 3.9-fold, similar to over-predictions obtained using rat and mouse. *These data indicate that perhaps guinea pig may be used as an initial screening tool for metabolic stability, with the recommendation that potential drug candidates be evaluated in monkey prior to advancing to clinical trials. Notably, when guinea pig exhibits similar metabolism/clearance to rat and mouse in vitro and/or in vivo (especially if different from human in vitro), it may be particularly important to evaluate additional species such as monkey.*

While minipig successfully predicted human *in vivo* CL_p of zaleplon and O⁶-benzylguanine within 2-fold, human zonisporide CL_p was over-predicted ~5-fold. In addition, substrate-dependence of AO metabolism *in vitro* further indicates that caution should be advised with regard to broad use of this species to estimate AO-mediated metabolism in human. Though minipig SSS of *in vitro* CL_{int} predicted human CL_{int} within 3-fold for four of the five compounds evaluated, $F_{m,AO}$ and biotransformation experiments revealed AO-mediated metabolism was not always similar between minipig and human (decreased AO-mediated metabolism of zaleplon and O⁶-benzylguanine in minipig S9 relative to human). Interestingly, NADPH-dependent metabolism of zaleplon in minipig S9 apparently compensated for the decreased AO metabolism, resulting in a similar E between minipig and human. While this apparent compensation effectively permitted prediction of zaleplon human CL_{int} by minipig SSS, this NADPH-dependent compensatory effect was not observed for O⁶-benzylguanine. Furthermore, while an NADPH-dependent mechanism may compensate for low AO metabolism in a hepatic *in vitro* system, this compensatory effect would not be expected in extra-hepatic tissues where AO metabolism might also occur *in vivo*. Interestingly, there was essentially no difference in the IVIVC of zaleplon between human and minipig, though it is not known if zaleplon is subject to extra-hepatic metabolism *in vivo*. While minipig is increasing in popularity as a model species for preclinical toxicology evaluations (Bode et al., 2010; van der Laan et al., 2010), this apparent substrate-dependence in AO vs. P450-mediated metabolite formation poses another cause for concern in the

utility of this species for toxicology when AO metabolism predominates in human. However, MA with the inclusion of minipig was generally successful, particularly with regard to methods employing four species in *in vitro* allometry assessments (CL_p data was not available for a comprehensive assessment of 4-species allometry *in vivo*). Overall, the present data indicate that broad application of a minipig model for human PK of AO substrates is not advisable, though it still may be useful in combination with other preclinical species for multispecies allometry.

Future directions

As our *in vitro* examination of minipig S9 revealed substrate-dependency in AO-mediated metabolism relative to that in human S9, investigations to study *in vitro* versus *in vivo* metabolism of AO substrates in minipig would shed light on the potential to use *in vitro* metabolism data to determine if minipig would be an appropriate species for toxicology assessments. While we evaluated interspecies *in vivo* PK in the present investigations, we did not examine metabolite formation *in vivo*. In addition, as was previously reported by Dalvie et al with regard to metabolism of zoniporide (Dalvie et al., 2013), we observed higher CL_{int} of all five compounds in hepatic S9 of female minipigs relative to male minipig S9. This observation leaves open the question as to whether female minipig may serve as a more useful human PK model than male minipig. Biotransformation experiments and *in vivo* PK assessments in female minipigs will be required to better understand this possibility. Extension of the proposed future investigations concerning minipig to investigations in guinea pig and monkey, of course, would

also serve well to better inform the drug metabolism and disposition community as to the general utility of preclinical species in human PK prediction.

Commentary

A comprehensive assessment of all data presented, including *in vitro* biotransformation, *in vitro* estimation of $F_{m,AO}$ and E, and SSS with both *in vitro* CL_{int} and *in vivo* CL_p support prior postulations that guinea pig and monkey would likely serve as better models of AO-mediated drug clearance in human versus commonly employed nonclinical models such as rat or mouse (Garattini and Terao, 2012; Hutzler et al., 2013; Hutzler et al., 2014a); importantly, no single species should be expected to reflect human clearance of all AO substrates (Choughule et al., 2013b; Hutzler et al., 2013). Moreover, the minipig represents a species to consider when investigating AO metabolism, particularly when employed in multispecies allometry. *Collectively, our data support the need for a multiple species assessment when gauging the intrinsic lability of new chemical entities (NCEs) towards AO metabolism and the projection of that metabolism-mediated drug clearance in human. With regards to human pharmacokinetic predictions, our data support a confidence-inspiring approach towards the scaling of human clearance when nonclinical species metabolism, single-species scaling, and the corresponding IVIVC assessments are all similar between the species employed during preclinical investigations (e.g., rat, guinea pig, and monkey); when these confidence inspiring tenets are not observed,*

the present data would support use of nonhuman primate for the in vitro and in vivo investigations of NCEs. Applications of the methodology presented herein, either as a stand alone or in combination with previously published strategies (Zientek et al., 2010) would likely reduce the risks associated with AO-mediated clearance in clinical trials. While mechanisms behind variable AO activity (*in vitro* and/or *in vivo*) and contributions of *extra-hepatic* metabolism remain important unanswered questions towards the implementation of standardized methods pertaining to AO-mediated drug disposition, the work provided here offers new insight to aid in the appropriate application of preclinical species, thus helping to prevent future clinical failures resulting from unexpected human AO metabolism. Furthermore, the present body of research may in fact be applied to other emerging drug metabolizing enzyme classes by which standardized methodologies (i.e., for P450-mediated drug clearance) also falls short of predicting hepatic metabolism and drug clearance.

REFERENCES

- Adolph EF (1949) Quantitative Relations in the Physiological Constitutions of Mammals. *Science* **109**:579-585.
- Akabane T, Gerst N, Masters JN, and Tamura K (2012) A quantitative approach to hepatic clearance prediction of metabolism by aldehyde oxidase using custom pooled hepatocytes. *Xenobiotica* **42**:863-871.
- Akabane T, Tanaka K, Irie M, Terashita S, and Teramura T (2011) Case report of extensive metabolism by aldehyde oxidase in humans: Pharmacokinetics and metabolite profile of FK3453 in rats, dogs, and humans. *Xenobiotica* **41**:372-384.
- Al-Salmy HS (2001) Individual variation in hepatic aldehyde oxidase activity. *IUBMB Life* **51**:249-253.
- Alfaro JF and Jones JP (2008) Studies on the mechanism of aldehyde oxidase and xanthine oxidase. *J Org Chem* **73**:9469-9472.
- Barr JT and Jones JP (2011) Inhibition of human liver aldehyde oxidase: implications for potential drug-drug interactions. *Drug Metab Dispos* **39**:2381-2386.
- Barr JT, Jones JP, Joswig-Jones CA, and Rock DA (2013) Absolute quantification of aldehyde oxidase protein in human liver using liquid chromatography-tandem mass spectrometry. *Mol Pharm* **10**:3842-3849.
- Beedham C (1985) Molybdenum hydroxylases as drug-metabolizing enzymes. *Drug Metab Rev* **16**:119-156.
- Beedham C, Bruce SE, Critchley DJ, al-Tayib Y, and Rance DJ (1987) Species variation in hepatic aldehyde oxidase activity. *Eur J Drug Metab Pharmacokinet* **12**:307-310.
- Beedham C, Critchley DJ, and Rance DJ (1995) Substrate specificity of human liver aldehyde oxidase toward substituted quinazolines and phthalazines: a comparison with hepatic enzyme from guinea pig, rabbit, and baboon. *Arch Biochem Biophys* **319**:481-490.
- Beedham C, Miceli JJ, and Obach RS (2003) Ziprasidone Metabolism, Aldehyde Oxidase, and Clinical Implications. *Journal of Clinical Psychopharmacology* **23**:229-232.

- Beer B, Clody DE, Mangano R, Levner M, Mayer P, and Barrett JE (1997) A Review of the Preclinical Development of Zaleplon, a Novel Non-Benzodiazepine Hypnotic for the Treatment of Insomnia. *CNS Drug Reviews* **3**:207-224.
- Bode G, Clausing P, Gervais F, Loegsted J, Luft J, Nogues V, and Sims J (2010) The utility of the minipig as an animal model in regulatory toxicology. *J Pharmacol Toxicol Methods* **62**:196-220.
- Bogaards JJ, Bertrand M, Jackson P, Oudshoorn MJ, Weaver RJ, van Bladeren PJ, and Walther B (2000) Determining the best animal model for human cytochrome P450 activities: a comparison of mouse, rat, rabbit, dog, micropig, monkey and man. *Xenobiotica* **30**:1131-1152.
- Boxenbaum H (1980) Interspecies variation in liver weight, hepatic blood flow, and antipyrine intrinsic clearance: extrapolation of data to benzodiazepines and phenytoin. *J Pharmacokinet Biopharm* **8**:165-176.
- Boxenbaum H (1982) Interspecies scaling, allometry, physiological time, and the ground plan of pharmacokinetics. *J Pharmacokinet Biopharm* **10**:201-227.
- Cerny MA (2016) Prevalence of Non-Cytochrome P450-Mediated Metabolism in Food and Drug Administration-Approved Oral and Intravenous Drugs: 2006-2015. *Drug Metab Dispos* **44**:1246-1252.
- Choughule KV, Barr JT, and Jones JP (2013a) Evaluation of Rhesus Monkey and Guinea Pig Hepatic Cytosol Fractions as Models for Human Aldehyde Oxidase. *Drug Metabolism and Disposition* **41**:1852-1858.
- Choughule KV, Barr JT, and Jones JP (2013b) Evaluation of rhesus monkey and guinea pig hepatic cytosol fractions as models for human aldehyde oxidase. *Drug Metab Dispos* **41**:1852-1858.
- Clarke SE, Harrell AW, and Chenery RJ (1995) Role of aldehyde oxidase in the in vitro conversion of famciclovir to penciclovir in human liver. *Drug Metab Dispos* **23**:251-254.
- Coelho C, Foti A, Hartmann T, Santos-Silva T, Leimkuhler S, and Romao MJ (2015) Structural insights into xenobiotic and inhibitor binding to human aldehyde oxidase. *Nat Chem Biol* **11**:779-783.
- Coelho C, Mahro M, Trincao J, Carvalho AT, Ramos MJ, Terao M, Garattini E, Leimkuhler S, and Romao MJ (2012) The first mammalian aldehyde oxidase crystal structure: insights into substrate specificity. *J Biol Chem* **287**:40690-40702.

- Critchley DJ, Rance DJ, and Beedham C (1994) Biotransformation of carbazeran in guinea pig: effect of hydralazine pretreatment. *Xenobiotica* **24**:37-47.
- Dalgaard L (2015) Comparison of minipig, dog, monkey and human drug metabolism and disposition. *J Pharmacol Toxicol Methods* **74**:80-92.
- Dalvie D, Sun H, Xiang C, Hu Q, Jiang Y, and Kang P (2012) Effect of structural variation on aldehyde oxidase-catalyzed oxidation of zoniporide. *Drug Metab Dispos* **40**:1575-1587.
- Dalvie D, Xiang C, Kang P, and Zhou S (2013) Interspecies variation in the metabolism of zoniporide by aldehyde oxidase. *Xenobiotica* **43**:399-408.
- Dalvie D, Zhang C, Chen W, Smolarek T, Obach RS, and Loi CM (2010) Cross-species comparison of the metabolism and excretion of zoniporide: contribution of aldehyde oxidase to interspecies differences. *Drug Metab Dispos* **38**:641-654.
- Dalvie D and Zientek M (2015) Metabolism of xenobiotics by aldehyde oxidase. *Curr Protoc Toxicol* **63**:4 41 41-13.
- Dedrick RL (1973) Animal scale-up. *J Pharmacokinet Biopharm* **1**:435-461.
- Deguchi T, Watanabe N, Kurihara A, Igeta K, Ikenaga H, Fusegawa K, Suzuki N, Murata S, Hirouchi M, Furuta Y, Iwasaki M, Okazaki O, and Izumi T (2011) Human Pharmacokinetic Prediction of UDP-Glucuronosyltransferase Substrates with an Animal Scale-Up Approach. *Drug Metabolism and Disposition* **39**:820-829.
- Deshmukh SV, Durston J, and Shomer NH (2008) Validation of the use of nonnaive surgically catheterized rats for pharmacokinetics studies. *J Am Assoc Lab Anim Sci* **47**:41-45.
- Di L, Feng B, Goosen TC, Lai Y, Steyn SJ, Varma MV, and Obach RS (2013) A Perspective on the Prediction of Drug Pharmacokinetics and Disposition in Drug Research and Development. *Drug Metabolism and Disposition* **41**:1975-1993.
- Di L and Obach RS (2015) Addressing the challenges of low clearance in drug research. *AAPS J* **17**:352-357.
- Diamond S, Boer J, Maduskuie TP, Falahatpisheh N, Li Y, and Yeleswaram S (2010a) Species-Specific Metabolism of SGX523 by Aldehyde Oxidase and the Toxicological Implications. *Drug Metabolism and Disposition* **38**:1277-1285.

- Diamond S, Boer J, Maduskuie TP, Jr., Falahatpisheh N, Li Y, and Yeleswaram S (2010b) Species-specific metabolism of SGX523 by aldehyde oxidase and the toxicological implications. *Drug Metab Dispos* **38**:1277-1285.
- Dittrich C, Greim G, Borner M, Weigang-Köhler K, Huisman H, Amelsberg A, Ehret A, Wanders J, Hanauske A, and Fumoleau P (2002) Phase I and pharmacokinetic study of BIBX 1382 BS, an epidermal growth factor receptor (EGFR) inhibitor, given in a continuous daily oral administration. *European Journal of Cancer* **38**:1072-1080.
- Dolan ME, Chae MY, Pegg AE, Mullen JH, Friedman HS, and Moschel RC (1994) Metabolism of O6-benzylguanine, an inactivator of O6-alkylguanine-DNA alkyltransferase. *Cancer Res* **54**:5123-5130.
- Felts AS, Rodriguez AL, Morrison RD, Venable DF, Manka JT, Bates BS, Blobaum AL, Byers FW, Daniels JS, Niswender CM, Jones CK, Conn PJ, Lindsley CW, and Emmitte KA (2013) Discovery of VU0409106: A negative allosteric modulator of mGlu5 with activity in a mouse model of anxiety. *Bioorg Med Chem Lett* **23**:5779-5785.
- Foti A, Hartmann T, Coelho C, Santos-Silva T, Romao MJ, and Leimkuhler S (2016) Optimization of the Expression of Human Aldehyde Oxidase for Investigations of Single-Nucleotide Polymorphisms. *Drug Metab Dispos* **44**:1277-1285.
- Fu C, Di L, Han X, Soderstrom C, Snyder M, Troutman MD, Obach RS, and Zhang H (2013) Aldehyde oxidase 1 (AOX1) in human liver cytosols: quantitative characterization of AOX1 expression level and activity relationship. *Drug Metab Dispos* **41**:1797-1804.
- Garattini E, Fratelli M, and Terao M (2008) Mammalian aldehyde oxidases: genetics, evolution and biochemistry. *Cell Mol Life Sci* **65**:1019-1048.
- Garattini E and Terao M (2012) The role of aldehyde oxidase in drug metabolism. *Expert Opinion on Drug Metabolism & Toxicology* **8**:487-503.
- Guengerich FP (2001) Common and uncommon cytochrome P450 reactions related to metabolism and chemical toxicity. *Chem Res Toxicol* **14**:611-650.
- Hartmann T, Terao M, Garattini E, Teutloff C, Alfaro JF, Jones JP, and Leimkuhler S (2012) The impact of single nucleotide polymorphisms on human aldehyde oxidase. *Drug Metab Dispos* **40**:856-864.

- Hosea NA, Collard WT, Cole S, Maurer TS, Fang RX, Jones H, Kakar SM, Nakai Y, Smith BJ, Webster R, and Beaumont K (2009) Prediction of Human Pharmacokinetics From Preclinical Information: Comparative Accuracy of Quantitative Prediction Approaches. *The Journal of Clinical Pharmacology* **49**:513-533.
- Hoshino K, Itoh K, Masubuchi A, Adachi M, Asakawa T, Watanabe N, Kosaka T, and Tanaka Y (2007) Cloning, expression, and characterization of male cynomolgus monkey liver aldehyde oxidase. *Biol Pharm Bull* **30**:1191-1198.
- Hu R, Xu C, Shen G, Jain MR, Khor TO, Gopalkrishnan A, Lin W, Reddy B, Chan JY, and Kong AN (2006) Identification of Nrf2-regulated genes induced by chemopreventive isothiocyanate PEITC by oligonucleotide microarray. *Life Sci* **79**:1944-1955.
- Huang DY, Furukawa A, and Ichikawa Y (1999) Molecular cloning of retinal oxidase/aldehyde oxidase cDNAs from rabbit and mouse livers and functional expression of recombinant mouse retinal oxidase cDNA in *Escherichia coli*. *Arch Biochem Biophys* **364**:264-272.
- Huang Y, Li W, Su ZY, and Kong AN (2015) The complexity of the Nrf2 pathway: beyond the antioxidant response. *J Nutr Biochem* **26**:1401-1413.
- Hutzler JM, Cerny MA, Yang YS, Asher C, Wong D, Frederick K, and Gilpin K (2014a) Cynomolgus monkey as a surrogate for human aldehyde oxidase metabolism of the EGFR inhibitor BIBX1382. *Drug Metab Dispos* **42**:1751-1760.
- Hutzler JM, Obach RS, Dalvie D, and Zientek MA (2013) Strategies for a comprehensive understanding of metabolism by aldehyde oxidase. *Expert Opinion on Drug Metabolism & Toxicology* **9**:153-168.
- Hutzler JM, Ring BJ, and Anderson SR (2015) Low-Turnover Drug Molecules: A Current Challenge for Drug Metabolism Scientists. *Drug Metab Dispos* **43**:1917-1928.
- Hutzler JM, Yang Y-S, Albaugh D, Fullenwider CL, Schmenk J, and Fisher MB (2012) Characterization of Aldehyde Oxidase Enzyme Activity in Cryopreserved Human Hepatocytes. *Drug Metabolism and Disposition* **40**:267-275.
- Hutzler JM, Yang Y-S, Brown C, Heyward S, and Moeller T (2014b) Aldehyde Oxidase Activity in Donor-Matched Fresh and Cryopreserved Human Hepatocytes and Assessment of Variability in 75 Donors. *Drug Metabolism and Disposition* **42**:1090-1097.

- Infante JR, Rugg T, Gordon M, Rooney I, Rosen L, Zeh K, Liu R, Burris HA, and Ramanathan RK (2013) Unexpected renal toxicity associated with SGX523, a small molecule inhibitor of MET. *Invest New Drugs* **31**:363-369.
- Itoh K, Yamamura M, Takasaki W, Sasaki T, Masubuchi A, and Tanaka Y (2006) Species differences in enantioselective 2-oxidations of RS-8359, a selective and reversible MAO-A inhibitor, and cinchona alkaloids by aldehyde oxidase. *Biopharm Drug Dispos* **27**:133-139.
- Jensen KG, Jacobsen AM, Bundgaard C, Nilausen DO, Thale Z, Chandrasena G, and Jorgensen M (2016) Lack of exposure in a first-in-man study due to aldehyde oxidase metabolism: Investigated by use of ¹⁴C-microdose, humanized mice, monkey pharmacokinetics and in vitro methods. *Drug Metab Dispos*.
- Johnson C, Stublely-Beedham C, and Stell JG (1984) Elevation of molybdenum hydroxylase levels in rabbit liver after ingestion of phthalazine or its hydroxylated metabolite. *Biochem Pharmacol* **33**:3699-3705.
- Johnson C, Stublely-Beedham C, and Stell JG (1985) Hydralazine: a potent inhibitor of aldehyde oxidase activity in vitro and in vivo. *Biochem Pharmacol* **34**:4251-4256.
- Kawashima K, Hosoi K, Naruke T, Shiba T, Kitamura M, and Watabe T (1999) Aldehyde oxidase-dependent marked species difference in hepatic metabolism of the sedative-hypnotic, zaleplon, between monkeys and rats. *Drug Metab Dispos* **27**:422-428.
- Kaye B, Rance DJ, and Waring L (1985) Oxidative metabolism of carbazepin in vitro by liver cytosol of baboon and man. *Xenobiotica* **15**:237-242.
- Kitamura S, Sugihara K, Nakatani K, Ohta S, Ohhara T, Ninomiya S, Green CE, and Tyson CA (1999) Variation of hepatic methotrexate 7-hydroxylase activity in animals and humans. *IUBMB Life* **48**:607-611.
- Kitamura S, Sugihara K, and Ohta S (2006) Drug-metabolizing ability of molybdenum hydroxylases. *Drug Metab Pharmacokinet* **21**:83-98.
- Klecker RW, Cysyk RL, and Collins JM (2006) Zebularine metabolism by aldehyde oxidase in hepatic cytosol from humans, monkeys, dogs, rats, and mice: influence of sex and inhibitors. *Bioorg Med Chem* **14**:62-66.
- Kola I and Landis J (2004) Can the pharmaceutical industry reduce attrition rates? *Nat Rev Drug Discov* **3**:711-715.

- Kurosaki M, Demontis S, Barzago MM, Garattini E, and Terao M (1999) Molecular cloning of the cDNA coding for mouse aldehyde oxidase: tissue distribution and regulation in vivo by testosterone. *Biochem J* **341 (Pt 1)**:71-80.
- Kurosaki M, Terao M, Barzago MM, Bastone A, Bernardinello D, Salmona M, and Garattini E (2004) The aldehyde oxidase gene cluster in mice and rats. Aldehyde oxidase homologue 3, a novel member of the molybdo-flavoenzyme family with selective expression in the olfactory mucosa. *J Biol Chem* **279**:50482-50498.
- Lake BG, Ball SE, Kao J, Renwick AB, Price RJ, and Scatina JA (2002a) Metabolism of zaleplon by human liver: evidence for involvement of aldehyde oxidase. *Xenobiotica* **32**:835-847.
- Lake BG, Ball SE, Kao J, Renwick AB, Price RJ, and Scatina JA (2002b) Metabolism of zaleplon by human liver: evidence for involvement of aldehyde oxidase. *Xenobiotica* **32**:835-847.
- Li Y, Lai WG, Whitcher-Johnstone A, Busacca CA, Eriksson MC, Lorenz JC, and Tweedie DJ (2012a) Metabolic switching of BILR 355 in the presence of ritonavir. I. Identifying an unexpected disproportionate human metabolite. *Drug Metab Dispos* **40**:1122-1129.
- Li Y, Xu J, Lai WG, Whitcher-Johnstone A, and Tweedie DJ (2012b) Metabolic switching of BILR 355 in the presence of ritonavir. II. Uncovering novel contributions by gut bacteria and aldehyde oxidase. *Drug Metab Dispos* **40**:1130-1137.
- Linder CD, Renaud NA, and Hutzler JM (2009) Is 1-aminobenzotriazole an appropriate in vitro tool as a nonspecific cytochrome P450 inactivator? *Drug Metab Dispos* **37**:10-13.
- Lolkema MP, Bohets HH, Arkenau HT, Lampo A, Barale E, de Jonge MJ, van Doorn L, Hellemans P, de Bono JS, and Eskens FA (2015) The c-Met Tyrosine Kinase Inhibitor JNJ-38877605 Causes Renal Toxicity through Species-Specific Insoluble Metabolite Formation. *Clin Cancer Res* **21**:2297-2304.
- Maeda K, Ohno T, Igarashi S, Yoshimura T, Yamashiro K, and Sakai M (2012) Aldehyde oxidase 1 gene is regulated by Nrf2 pathway. *Gene* **505**:374-378.
- Mahmood I (2007) Application of allometric principles for the prediction of pharmacokinetics in human and veterinary drug development. *Adv Drug Deliv Rev* **59**:1177-1192.
- Mahmood I and Balian JD (1996) Interspecies scaling: predicting clearance of drugs in humans. Three different approaches. *Xenobiotica* **26**:887-895.

- Martignoni M, Groothuis GM, and de Kanter R (2006) Species differences between mouse, rat, dog, monkey and human CYP-mediated drug metabolism, inhibition and induction. *Expert Opin Drug Metab Toxicol* **2**:875-894.
- Moriwaki Y, Yamamoto T, Takahashi S, Tsutsumi Z, and Hada T (2001) Widespread cellular distribution of aldehyde oxidase in human tissues found by immunohistochemistry staining. *Histol Histopathol* **16**:745-753.
- Morrison RD, Blobaum AL, Byers FW, Santomango TS, Bridges TM, Stec D, Brewer KA, Sanchez-Ponce R, Corlew MM, Rush R, Felts AS, Manka J, Bates BS, Venable DF, Rodriguez AL, Jones CK, Niswender CM, Conn PJ, Lindsley CW, Emmitte KA, and Daniels JS (2012) The Role of Aldehyde Oxidase and Xanthine Oxidase in the Biotransformation of a Novel Negative Allosteric Modulator of Metabotropic Glutamate Receptor Subtype 5. *Drug Metabolism and Disposition* **40**:1834-1845.
- Mugford CA and Kedderis GL (1998) Sex-dependent metabolism of xenobiotics. *Drug Metab Rev* **30**:441-498.
- Nagilla R and Ward KW (2004) A comprehensive analysis of the role of correction factors in the allometric predictivity of clearance from rat, dog, and monkey to humans. *J Pharm Sci* **93**:2522-2534.
- Nirogi R, Kandikere V, Palacharla RC, Bhyrapuneni G, Kanamarlapudi VB, Ponnamaneni RK, and Manoharan AK (2014) Identification of a suitable and selective inhibitor towards aldehyde oxidase catalyzed reactions. *Xenobiotica* **44**:197-204.
- Nishimura M and Naito S (2006) Tissue-specific mRNA expression profiles of human phase I metabolizing enzymes except for cytochrome P450 and phase II metabolizing enzymes. *Drug Metab Pharmacokinet* **21**:357-374.
- Obach RS (1999) Prediction of human clearance of twenty-nine drugs from hepatic microsomal intrinsic clearance data: An examination of in vitro half-life approach and nonspecific binding to microsomes. *Drug Metab Dispos* **27**:1350-1359.
- Obach RS (2004) Potent inhibition of human liver aldehyde oxidase by raloxifene. *Drug Metab Dispos* **32**:89-97.
- Obach RS, Baxter JG, Liston TE, Silber BM, Jones BC, Macintyre F, Rance DJ, and Wastall P (1997) The Prediction of Human Pharmacokinetic Parameters from Preclinical and In Vitro Metabolism Data. *Journal of Pharmacology and Experimental Therapeutics* **283**:46-58.

- Obach RS, Huynh P, Allen MC, and Beedham C (2004) Human liver aldehyde oxidase: inhibition by 239 drugs. *J Clin Pharmacol* **44**:7-19.
- Ohkubo M, Sakiyama S, and Fujimura S (1983) Increase of nicotinamide methyltransferase and N1-methyl-nicotinamide oxidase activities in the livers of the rats administered alkylating agents. *Cancer Lett* **21**:175-181.
- Otteneder MB, Knutson CG, Daniels JS, Hashim M, Crews BC, Remmel RP, Wang H, Rizzo C, and Marnett LJ (2006) In vivo oxidative metabolism of a major peroxidation-derived DNA adduct, M1dG. *Proc Natl Acad Sci U S A* **103**:6665-6669.
- Pang KS and Rowland M (1977) Hepatic clearance of drugs. I. Theoretical considerations of a "well-stirred" model and a "parallel tube" model. Influence of hepatic blood flow, plasma and blood cell binding, and the hepatocellular enzymatic activity on hepatic drug clearance. *J Pharmacokinet Biopharm* **5**:625-653.
- Prueksaritanont T, Chu X, Gibson C, Cui D, Yee KL, Ballard J, Cabalu T, and Hochman J (2013) Drug-drug interaction studies: regulatory guidance and an industry perspective. *AAPS J* **15**:629-645.
- Prueksaritanont T, Kuo Y, Tang C, Li C, Qiu Y, Lu B, Strong-Basalyga K, Richards K, Carr B, and Lin JH (2006) In vitro and in vivo CYP3A64 induction and inhibition studies in rhesus monkeys: a preclinical approach for CYP3A-mediated drug interaction studies. *Drug Metab Dispos* **34**:1546-1555.
- Pryde DC, Dalvie D, Hu Q, Jones P, Obach RS, and Tran T-D (2010) Aldehyde Oxidase: An Enzyme of Emerging Importance in Drug Discovery. *Journal of Medicinal Chemistry* **53**:8441-8460.
- Ramanathan S, Jin F, Sharma S, and Kearney BP (2016) Clinical Pharmacokinetic and Pharmacodynamic Profile of Idelalisib. *Clin Pharmacokinet* **55**:33-45.
- Ramirez J, Kim TW, Liu W, Myers JL, Mirkov S, Owzar K, Watson D, Mulkey F, Gamazon ER, Stock W, Undevia S, Innocenti F, and Ratain MJ (2014) A pharmacogenetic study of aldehyde oxidase I in patients treated with XK469. *Pharmacogenet Genomics* **24**:129-132.
- Rane A, Wilkinson GR, and Shand DG (1977) Prediction of hepatic extraction ratio from in vitro measurement of intrinsic clearance. *J Pharmacol Exp Ther* **200**:420-424.
- Rashidi MR, Smith JA, Clarke SE, and Beedham C (1997) In vitro oxidation of famciclovir and 6-deoxypenciclovir by aldehyde oxidase from human, guinea pig, rabbit, and rat liver. *Drug Metab Dispos* **25**:805-813.

- Renwick AB, Ball SE, Tredger JM, Price RJ, Walters DG, Kao J, Scatina JA, and Lake BG (2002) Inhibition of zaleplon metabolism by cimetidine in the human liver: in vitro studies with subcellular fractions and precision-cut liver slices. *Xenobiotica* **32**:849-862.
- Rivera SP, Choi HH, Chapman B, Whitekus MJ, Terao M, Garattini E, and Hankinson O (2005) Identification of aldehyde oxidase 1 and aldehyde oxidase homologue 1 as dioxin-inducible genes. *Toxicology* **207**:401-409.
- Roy SK, Gupta E, and Dolan ME (1995a) Pharmacokinetics of O6-benzylguanine in rats and its metabolism by rat liver microsomes. *Drug Metab Dispos* **23**:1394-1399.
- Roy SK, Korzekwa KR, Gonzalez FJ, Moschel RC, and Dolan ME (1995b) Human liver oxidative metabolism of O6-benzylguanine. *Biochem Pharmacol* **50**:1385-1389.
- Sahi J, Khan KK, and Black CB (2008) Aldehyde oxidase activity and inhibition in hepatocytes and cytosolic fractions from mouse, rat, monkey and human. *Drug Metab Lett* **2**:176-183.
- Sanoh S, Tayama Y, Sugihara K, Kitamura S, and Ohta S (2015) Significance of aldehyde oxidase during drug development: Effects on drug metabolism, pharmacokinetics, toxicity, and efficacy. *Drug Metab Pharmacokinet* **30**:52-63.
- Saretok T, Almersjo O, Biber B, Gustavsson B, and Hasselgren PO (1984) Effects of hydralazine on liver blood flow in normovolemic dogs. *Acta Chir Scand* **150**:1-4.
- Sharma R, Eng H, Walker GS, Barreiro G, Stepan AF, McClure KF, Wolford A, Bonin PD, Cornelius P, and Kalgutkar AS (2011) Oxidative metabolism of a quinoxaline derivative by xanthine oxidase in rodent plasma. *Chem Res Toxicol* **24**:2207-2216.
- Shintani Y, Maruoka S, Gon Y, Koyama D, Yoshida A, Kozu Y, Kuroda K, Takeshita I, Tsuboi E, Soda K, and Hashimoto S (2015) Nuclear factor erythroid 2-related factor 2 (Nrf2) regulates airway epithelial barrier integrity. *Allergol Int* **64 Suppl**:S54-63.
- Smeland E, Fuskevåg OM, Nymann K, Svendsen JS, Olsen R, Lindal S, Bremnes RM, and Aarbakke J (1996) High-dose 7-hydroxymethotrexate: acute toxicity and lethality in a rat model. *Cancer Chemother Pharmacol* **37**:415-422.
- Smith DA and Obach RS (2005) Seeing through the mist: abundance versus percentage. Commentary on metabolites in safety testing. *Drug Metab Dispos* **33**:1409-1417.

- Smith MA, Marinaki AM, Arenas M, Shobowale-Bakre M, Lewis CM, Ansari A, Duley J, and Sanderson JD (2009) Novel pharmacogenetic markers for treatment outcome in azathioprine-treated inflammatory bowel disease. *Aliment Pharmacol Ther* **30**:375-384.
- Sodhi JK, Wong S, Kirkpatrick DS, Liu L, Khojasteh SC, Hop CE, Barr JT, Jones JP, and Halladay JS (2015) A novel reaction mediated by human aldehyde oxidase: amide hydrolysis of GDC-0834. *Drug Metab Dispos* **43**:908-915.
- Strelevitz TJ, Orozco CC, and Obach RS (2012) Hydralazine As a Selective Probe Inactivator of Aldehyde Oxidase in Human Hepatocytes: Estimation of the Contribution of Aldehyde Oxidase to Metabolic Clearance. *Drug Metabolism and Disposition* **40**:1441-1448.
- Sugihara K, Kitamura S, Yamada T, Ohta S, Yamashita K, Yasuda M, and Fujii-Kuriyama Y (2001) Aryl hydrocarbon receptor (AhR)-mediated induction of xanthine oxidase/xanthine dehydrogenase activity by 2,3,7,8-tetrachlorodibenzo-p-dioxin. *Biochem Biophys Res Commun* **281**:1093-1099.
- Svensson CK, Knowlton PW, and Ware JA (1987) Effect of hydralazine on the elimination of antipyrine in the rat. *Pharm Res* **4**:515-518.
- Tang H, Hussain A, Leal M, Mayersohn M, and Fluhler E (2007) Interspecies prediction of human drug clearance based on scaling data from one or two animal species. *Drug Metab Dispos* **35**:1886-1893.
- Tayama Y, Moriyasu A, Sugihara K, Ohta S, and Kitamura S (2007) Developmental changes of aldehyde oxidase in postnatal rat liver. *Drug Metab Pharmacokinet* **22**:119-124.
- Tayama Y, Sugihara K, Sanoh S, Miyake K, Kitamura S, and Ohta S (2012) Developmental changes of aldehyde oxidase activity and protein expression in human liver cytosol. *Drug Metab Pharmacokinet* **27**:543-547.
- Terao M, Kurosaki M, Barzago MM, Fratelli M, Bagnati R, Bastone A, Giudice C, Scanziani E, Mancuso A, Tiveron C, and Garattini E (2009) Role of the molybdoflavoenzyme aldehyde oxidase homolog 2 in the biosynthesis of retinoic acid: generation and characterization of a knockout mouse. *Mol Cell Biol* **29**:357-377.
- Terao M, Kurosaki M, Saltini G, Demontis S, Marini M, Salmona M, and Garattini E (2000) Cloning of the cDNAs coding for two novel molybdo-flavoproteins

- showing high similarity with aldehyde oxidase and xanthine oxidoreductase. *J Biol Chem* **275**:30690-30700.
- Terao M, Romao MJ, Leimkuhler S, Bolis M, Fratelli M, Coelho C, Santos-Silva T, and Garattini E (2016) Structure and function of mammalian aldehyde oxidases. *Arch Toxicol* **90**:753-780.
- Tomita S, Tsujita M, and Ichikawa Y (1993) Retinal oxidase is identical to aldehyde oxidase. *FEBS Lett* **336**:272-274.
- Tracey WR, Allen MC, Frazier DE, Fossa AA, Johnson CG, Marala RB, Knight DR, and Guzman-Perez A (2003) Zoniporide: a potent and selective inhibitor of the human sodium-hydrogen exchanger isoform 1 (NHE-1). *Cardiovasc Drug Rev* **21**:17-32.
- van der Laan JW, Brightwell J, McAnulty P, Ratky J, and Stark C (2010) Regulatory acceptability of the minipig in the development of pharmaceuticals, chemicals and other products. *J Pharmacol Toxicol Methods* **62**:184-195.
- Vila R, Kurosaki M, Barzago MM, Kolek M, Bastone A, Colombo L, Salmona M, Terao M, and Garattini E (2004) Regulation and biochemistry of mouse molybdo-flavoenzymes. The DBA/2 mouse is selectively deficient in the expression of aldehyde oxidase homologues 1 and 2 and represents a unique source for the purification and characterization of aldehyde oxidase. *J Biol Chem* **279**:8668-8683.
- Wienkers LC and Heath TG (2005) Predicting in vivo drug interactions from in vitro drug discovery data. *Nat Rev Drug Discov* **4**:825-833.
- Wilkinson GR (1987) Clearance approaches in pharmacology. *Pharmacol Rev* **39**:1-47.
- Wilkinson GR and Shand DG (1975) Commentary: a physiological approach to hepatic drug clearance. *Clin Pharmacol Ther* **18**:377-390.
- Wolf DL, Metzler CM, Froeschke MO, and Luderer JR (1994) Dose-Related Hepatic Blood Flow Effects Differentiate Nicorandil, Hydralazine, and Isosorbide Dinitrate in Healthy Subjects. *Am J Ther* **1**:150-156.
- Yoshihara S and Tatsumi K (1997) Involvement of growth hormone as a regulating factor in sex differences of mouse hepatic aldehyde oxidase. *Biochem Pharmacol* **53**:1099-1105.

- Yoshimatsu H, Konno Y, Ishii K, Satsukawa M, and Yamashita S (2016) Usefulness of minipigs for predicting human pharmacokinetics: Prediction of distribution volume and plasma clearance. *Drug Metab Pharmacokinet* **31**:73-81.
- Zhang L, Zhang YD, Zhao P, and Huang SM (2009) Predicting drug-drug interactions: an FDA perspective. *AAPS J* **11**:300-306.
- Zhang X, Liu HH, Weller P, Zheng M, Tao W, Wang J, Liao G, Monshouwer M, and Peltz G (2011) In silico and in vitro pharmacogenetics: aldehyde oxidase rapidly metabolizes a p38 kinase inhibitor. *Pharmacogenomics J* **11**:15-24.
- Zhou SF, Liu JP, and Chowbay B (2009) Polymorphism of human cytochrome P450 enzymes and its clinical impact. *Drug Metab Rev* **41**:89-295.
- Zientek M, Jiang Y, Youdim K, and Obach RS (2010) In Vitro-In Vivo Correlation for Intrinsic Clearance for Drugs Metabolized by Human Aldehyde Oxidase. *Drug Metabolism and Disposition* **38**:1322-1327.
- Zientek MA and Youdim K (2015) Reaction phenotyping: advances in the experimental strategies used to characterize the contribution of drug-metabolizing enzymes. *Drug Metab Dispos* **43**:163-181.